Supramolecular Assembly of Amino Acid/Peptide Based Small Molecules and Some Applications

by

Sahnawaz Ahmed

Department of Chemistry

Indian Institute of Technology Guwahati

Guwahati, Assam, 781039

India

A Thesis Submitted in Partial Fulfillment of the

Requirements for the degree of

Doctor of Philosophy

In

Chemistry

IIT Guwahati, April 2017

Dedication

To My Grandparents and Parents

Declaration

I hereby declare that the matter embodied in this thesis is result of investigations carried out by me in the Department of Chemistry, Indian Institute of Technology Guwahati, India, under the guidance of Dr. Debapratim Das. In keeping with the general practice of reporting scientific observations, due acknowledgements have been made wherever the work described is based on the findings of other investigators.

Sahnawaz Ahmed

भारतीय प्रौद्योगिकी संस्थान गुवाहाटी
INDIAN INSTITUTE OF TECHNOLOGY GUWAHATI

Dr. Debapratim Das
Associate Professor
Department of Chemistry
Ph: + 91 361 258 3301
Fax: + 91 361 258 2349
E-mail: ddas@iitg.ernet.in

10th April, 2017.

To whom it may concern .

This is to certified that the thesis entitled **"Supramolecular Assembly of Amino Acid/Peptide Based Small Molecules and Some Applications"** submitted by Sahnawaz Ahmed (Roll No. 126122026) for the award of PhD degree to IIT Guwahati, is absolutely based on his own research work and that neither this thesis nor any part of it has been submitted for any degree/diploma or any academic award anywhere before.

(Dr. Debapratim Das)

Contents

Abstract i
Acknowledgement ii
List of Abbreviations iii

Chapter 1
Introduction
1.1 Prelude 3
1.2 Peptide Based Soft-Materials 3
1.2.1 Peptide Self-Assembly 4
1.2.1.1 Gels and Peptide Based Hydrogels 4
1.2.1.2 Applications of Peptide Hydrogels 9
1.2.2 Supramolecular Assembly via Host-Guest Chemistry 11
1.2.2.1 Cucurbiturils 11
1.2.2.2 Host-Guest Chemistry of CB[5], CB[6] and CB[7] 12
1.2.2.3 Host-Guest Chemistry of CB[8]: The Hetero and Homo-Ternary Complexation 13
1.2.2.4 Supramolecular Polymers using CB[8] 15
1.2.3 Organic Electronics: The Case of Perylenediimides 17
1.2.3.1 Perylenediimides: Semiconducting and Self-Assembly Property 17
1.2.3.2 Self-Assembly of PDI-Peptide Conjugates 18
1.3 Objectives of the Present Thesis 21

Chapter 2
A Peptide-Amphiphile based Hydrogel: Synthesis, Characterization and Self-Assembly Mechanism
2.1 Introduction 25
2.2 Results and Discussion 25
2.3 Conclusions 37
2.4 Experimental section 37
2.4.1 General 37
2.4.2 Synthesis of Compounds 38
2.4.3 Characterization of the Synthesized Compounds 38
2.4.4 Methods 39
2.5 NMR, Mass Spectra 41

Chapter 3
An Amino Acid-Dimer Based Redox Active Supramolecular Polymer using Host Guest Chemistry of Cucurbit[8]uril
3.1 Introduction 51
3.2 Results and Discussion 51
3.3 Conclusions 65
3.4 Experimental Section 65
3.4.1 General 65
3.4.2 Synthesis and Characterization of Compounds 65
3.4.3 Methods 67
3.5 Chromatogram, NMR, Mass Spectra of the Synthesized Compounds 70

Chapter 4
Self-Assembly of a Peptide-Perylenediimide Conjugate: Solvent Directed Tuning of Helicity and Morphology
4.1 Introduction 79
4.2 Results and Discussion 80
4.3 Conclusion 91
4.4 Experimental Section 91
4.4.1 General 91
4.4.2 Synthesis and Characterization of Compounds 92
4.4.3 Methods 94
4.5 NMR and Mass Spectra 96

Chapter 5
Applications of Supramolecular Assemblies
5.1 Introduction 105
5.2 Template Fabrication of Single Walled Silica Nanotubes 105
5.3 Semi-conducting Behavior of Supramolecular Assemblies 110
5.4 Experimental Section 114
5.4.1 Methods 114
Postlude 117
References 119
List of Publications 131

Abstract

The thesis **"Supramolecular Assembly of Amino Acid/Peptide Based Small Molecules and Some Applications"** deals with the understanding of mechanistic details of supramolecular assembly process in amino acid/peptide based molecules to create different soft materials and their utilization.

Chapter 1 is a brief introduction of peptide based soft materials created by supramolecular assembly and applications with up to date literature review.

Chapter 2 describes the rational design, synthesis, and hydrogelation of a peptide amphiphile. The gelation mechanism is studied in detail to understand the supramolecular assembly.

Chapter 3 deals with the formation of a tryptophan based redox active supramolecular polymer using 'ternary' complexation of CB[8]. The formation and reversible transformation of hetero polymer to homo- polymer and vice versa are studied.

Chapter 4 describes the self-assembly of a symmetric conjugate of perylenediimide and PhePhe peptide in different solvent compositions. The kinetic and thermodynamic control over the self-aggregation of the conjugate in different environment is revealed. The formation mechanism of helical nano-fibers and nano-rings in these solvent systems is studied in detail.

Chapter 5 is about applying the soft-materials prepared during these studies. The nano-fibers obatined from the hydrogelator described in Chapter 2 is used as a template to prepare different types of silica nanotubes. The nano-structures obtained from perylenediimide-PhePhe conjugate are tested for their semi-conducting properties in order to utilize them in organic-electronics.

Acknowledgements

First and foremost, praises and thanks to the God, the Almighty, for His showers of blessings throughout my research work to complete the research successfully.

I am extremely grateful to my supervisor Dr. Debapratim Das for his valuable guidance, scholarly inputs, consistent encouragement and unconditional support I received throughout the research work. He is a person with an amicable and positive disposition. He has always made himself available for me whenever and wherever I required. I consider it as a great honour and pleasure to do my research under his guidance and to learn from his research expertise. Thank you Sir, for all your help and support. Besides my supervisor, I would like to give special thanks to my doctoral committee members: Prof. Tharmalingam Punniyamurthy, Prof. Biplab Mondal, Dr. Lal Mohan Kundu for their encouragement, insightful comments, helps and suggestions.

I am grateful to the collaborators for lending me their expertise and intuition to my scientific and technical problems: Dr. Rama Ranjan Bhattacharjee, Dr. Kallol Mahanta and his student, K. N. Amba Sankar (PSG Institute of Advanced Studies, Coimbatore), Dr. Ananya Debnath and her students, Abhinav Srivastava, Arpita Srivastava (IIT Jodhpur).

Words will be too little to express my thanks to my parents SK. Safiuddin Ahmed and Farida Begum for providing me all the affection, encouragement, support and prayers. I am also grateful to my brothers and sister for the love, help and support for me.

I would like to thank Department of Chemistry, IIT Guwahati for all the facilities that were made available to me. I thank Central Instruments Facility, IIT Guwahati for the instrumental facility. I am thankful to IIT Guwahati for financial support.

I am grateful to my past and present lab mates Dr. Julfikar Hassan Mondal, Nibedita Behera, Titli Ghosh, Bapan Pramanik, Nilotpal Singha, Payel Dowari, Basab Kanti Das, Dr. Subhajit Ghosh for their help and support. I would like to thank Dr. Antara Dasgupta, Dr. Md. Palashuddin Sheikh, Dr. Sameer Hussain, Dr. Ashim Paul, Md. Belal, Wajid Ali, Akthar Hussain Malik, Krapa Shankar Kashyap, Suranjan De, Md. Ashraful Haque, Subhankar Panda.

I would like to express my gratitude to all others who are associated with my work directly or indirectly at IIT Guwahati or anywhere else for their help.

LIST OF ABBREVIATIONS

Abbreviations

AFM	Atomic Force Microscopy
ADA	1 –adamantlyamine
ANS	8-anilino-1-naphthalanesulfonic acid
BET	Brunauer-Emmett-Teller
BJH	Barrett-Joyner-Halenda
C-AFM	Conductive Atomic Force Microscopy
CB[*n*]	Cucurbit[*n*]uril
CD	Circular Dichroism
CDs	Cyclodextrins
CT	Charge Transfer
CV	Cyclic Voltammetry
D_{av}	Diffusion Coefficient
DFT	Density Functional Theory
DFTB	Density Functional Tight Binding
DHN	2,6-dihydroxy naphthalene
DLS	Dynamic Light Scattering
DOSY	Diffusion Ordered Spectroscopy
DSC	Differential Scanning Calorimetry
EDX	Energy Dispersive X-ray
EPR	Electron Paramagnetic Resonance
ESI-MS	Electro Spray Ionization-Mass Spectrometry
FESEM	Field Emission Scanning Electron Microscopy
FTIR	Fourier Transform Infrared
G′	Dynamic storage moduli
G″	Dynamic loss moduli
HLB	Hydrophilic-Lipophilic Balance
ITC	Isothermal Titration Calorimetry
MV^{2+}	Methyl Viologen dication
PA	Peptide Amphiphiles
PDI	Perylenediimide
Phe-Phe	Diphenylalanine
SEM	Scanning Electron Microscopy
T_g	Sol-Gel Transition Temperature
TEM	Transmission electron Microscopy
TLC	Thin Layer Chromatography
Trp	Tryptophan
MALDI-TOF	Matrix Assisted Laser Desorption Ionization-Time Of Flight

CHAPTER 1

Introduction

1.1 Prelude

Though the first report on non-covalent interaction appeared in 1873 proposed by Johannes Diderik van der Waals,[1] proper realization of non-covalent chemistry took almost a century. It was Jean-Marie Lehn who finally provided a name to this rapidly expanding area of research, "Supramolecular Chemistry".[2] Since then tremendous effort is made to understand, create and utilize the supramolecular interactions. One prominent and effective approach is to mimic natural systems as they are the treasure house of all sorts of non-covalent interactions utilized to the perfection. Among the bio-molecules, peptides and proteins are the most studied systems. Over the years, the self-assembly of peptides and protein molecules have been studied in detail to utilize these knowledge toward the development of novel synthetic soft-materials. However, we are yet to a situation where one can design and dictate the self-assembly of synthetic molecules. Knowledge in this area can only enhance with more and more examples and studies. With this view, in the present thesis, various peptide or amino acid based small molecules are prepared and their self-assembly mechanism is studied.

1.2 Peptide Based Soft-Materials

The research in the area of peptide based smart and soft materials is increasing due to their applicability in the field of tissue engineering,[3,4] drug delivery,[5,6] sensing,[7] cell imaging,[8] nano fabrication[9-13] *etc.* The usefulness of peptide based materials comes from the fact that the physicochemical characteristics, such as chemical functionality, rheology, morphology, as well as stimuli sensitivity can be fine-tuned for peptides at the molecular level.[14,15] Amino acid based materials not only permit to incorporate the desired chemical functionalities but also offer the possibility of integrating bio-functionality, biocompatibility and biodegradability.

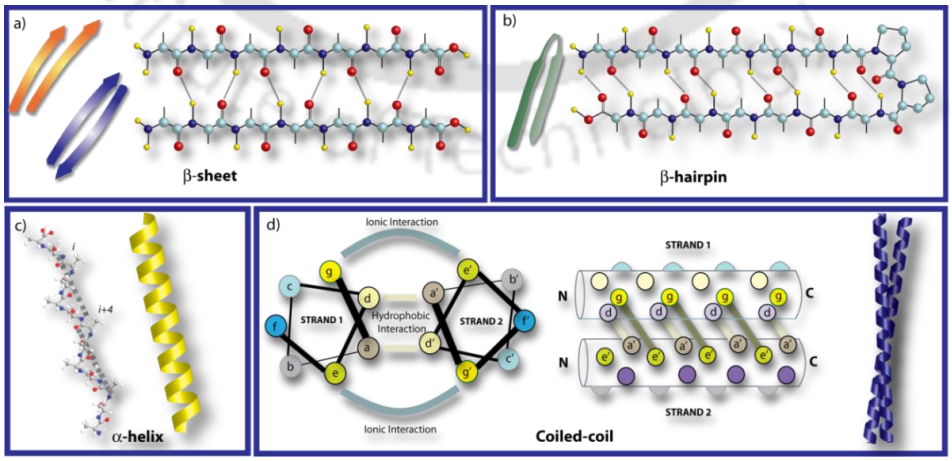

Figure 1.1 Schematic illustration of the molecular self-assembly involved in the formation of different secondary structures of peptides; a) β–sheet, b) β –hairpin, c) α–helix, and d) coiled-coil.[16]

1.2.1 Peptide Self-Assembly

One of the characteristic properties of peptides and proteins is the self-assembly which leads to different secondary structures. The formation of these secondary structures are regulated by appropriate non-covalent interactions such as hydrogen bonding, π–π stacking, salt-bridge, hydrophobic interaction *etc.* The common secondary structures are β–sheet, β–turn, α–helix, coiled-coil *etc.* (Figure 1.1). Utilizing these secondary structural motifs, various peptide based soft-materials such as gels are created. Comprehensive reviews on peptide based hydrogels can be found in references 16-18. In the next section, a brief discussion with representative examples is given on amino acid and peptide based small molecule hydrogelators and some of their applications.

1.2.1.1 Gels and Peptide Based Hydrogels

Gels are three-dimensional, hydrophilic/hydrophobic hierarchical networks capable of immobilizing large amounts of solvents (up to 1000 times of their dry weight). They are made of polymers or small molecules such as peptides that self-assemble into network structures. The nature of the solvent is a crucial factor in the gelation process and based on the type of solvent immobilized gels can be categorized as hydrogel (aqueous) or organogel (organic solvent). The balance between gelator–solvent interactions is determined by the solvent polarity, pH, ionic strength, and temperature. In recent years, the interest in studying gels derived from low molecular mass gelators (supramolecular, or simply molecular gels) has increased drastically. This is not only to understand the fundamental aggregate structures in the gels at different length scales, but also to explore their potential for futuristic technological applications. Gels have been made external stimuli sensitive like light and chemical entities by incorporating a spectroscopically active or a receptor unit as part of the gelator molecule. This makes them suitable for applications such as sensing and actuating. The diversity of gel structural architectures has allowed them to be utilized as templates to prepare novel inorganic superstructures for possible applications in catalysis and separation.

The different secondary conformations of peptides undergo hierarchical self-organization (Figure 1.2) to form various nano structures such as fiber, tube, belt, ribbon, tape.[9-13,19] On many occasions, these nano-structures further entangle together leading to the formation of gels.

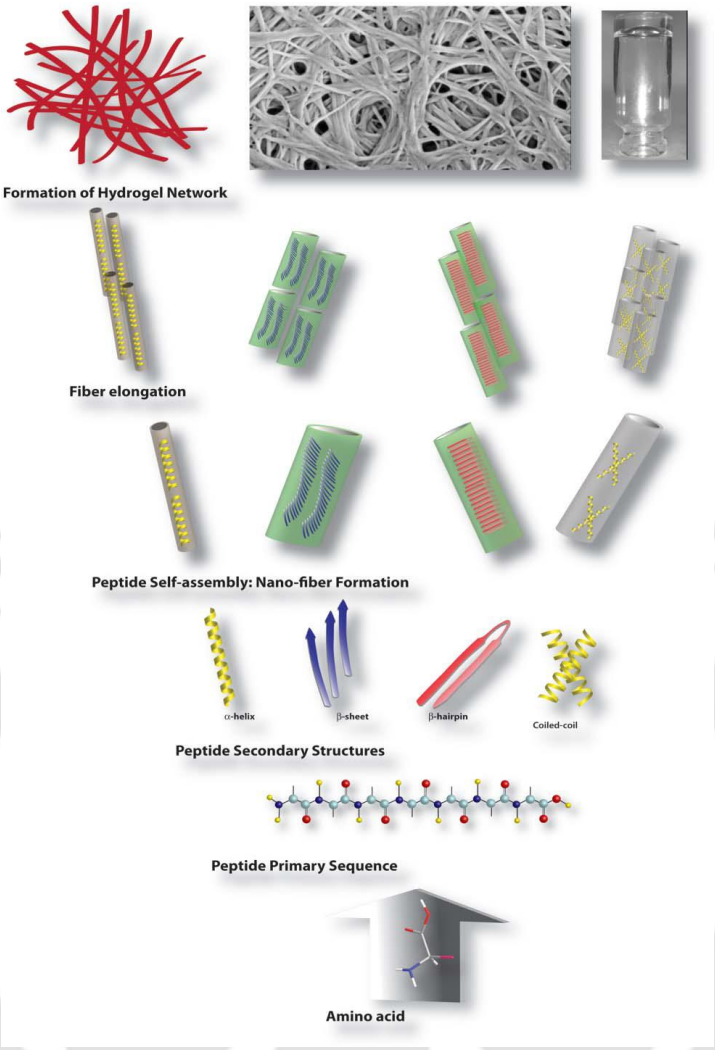

Figure 1.2 Simplified schematic illustrations of the hierarchical self-assembly process involved in the formation of hydrogel from peptide molecules.[16]

Amino acid, Di, Tri-Peptide Based Gelators

First amino acid based hydrogelator was reported by Gortner and Hoffman almost a century ago where dibenzoyl cysteine (**1.1**, Figure 1.3) formed gel in water.[20] The smallest amino acid based hydrogelator studied so far is the cinnamoyl protected phenylalanine (**1.2**).[21] Xu and co-workers were the first to demonstrate the hydrogelation of 'Fmoc' protected single amino acids.[21] They have shown that a mixture of Fmoc-Lysine and Fmoc-Valine can form hydrogel upon systematic basification. The same group reported the stimuli sensitive hydrogelation where Fmoc-Tyrosine phosphate (**1.3**, Figure 1.3) was converted into a hydrogelator (**1.4**) by enzymatic de-phosphorylation to screen the inhibitors for an acid phosphatase thereby, developing an approach which would be useful for reporting enzymatic processes for bio-analytical applications.[22] Janmey *et al.* was the first to find that some Fmoc protected dipeptides, such as, Fmoc-Leu-Asp, Fmoc-Ala-Asp, Fmoc-Ile-Asp (**1.5, 1.6, 1.7**, Figure 1.4) can form

hydrogels. Later, the same group described that the non-charged Phe-Phe analogue, as well as the assembly of other amine-modified analogues: Boc– Phe–Phe–COOH (**1.8**), Z-Phe–Phe–COOH (**1.9**) and Fmoc–Phe– Phe–COOH (**1.10**) peptides could self-assemble into tubular and amyloid-like structures.[23]

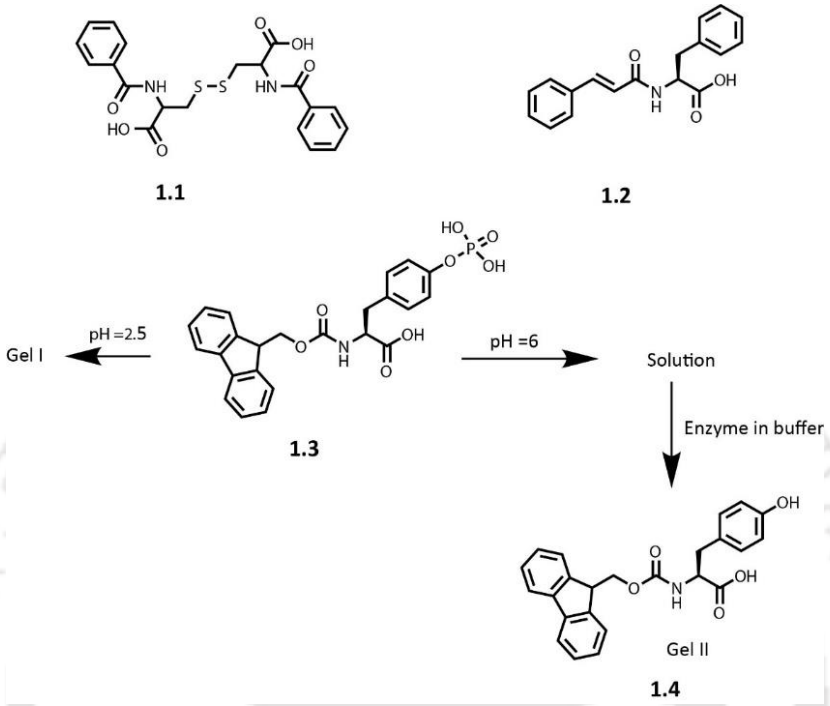

Figure 1.3 Chemical structures of the hydrogelators. Compound **1.3** forms gel under different conditions such as under highly acidic condition and after enzymatic de-phosphorylation.[22]

Since proteolysis is a common drawback for peptide-based therapeutic agents, much attention has been given to design and synthesize non-peptide molecules that mimic the structures and functions of peptides or proteins to achieve desired stability and bioavailability of those molecules.[24] Xu *et al.* developed a new class of supramolecular hydrogels based on dipeptidic mimics that consist of β–amino acids, **1.11** (Figure 1.4) is composed of a α–amino acid (glycine) and a β–amino acid (β^3-alanine) and **1.12** of two β–amino acids (β^3-phenylalanine) with the aim to offer proteolytic resistance to the hydrogels for biomedical applications.[25] Parquette *et al.* reported a di-lysine peptide (Fmoc-KK(NDI)) (**1.13**) conjugate to form a self-assembled hydrogel at low concentrations, composed of uniform 1D nanobelts.[26] The hydrophobic π–π association of both the 'NDI' and 'Fmoc' in this system, is responsible for the β–sheet self-assembly in aqueous media. Banerjee *et al.* reported Boc protected dipeptide as efficient hydrogelator. N-Boc-Leu-Phe (**1.14**), N-Boc-Phe-Leu (**1.15**), N-Boc-Leu-Leu (**1.16**) can form thermo-reversible pH sensitive hydrogels which showed nanofibrillar network with antiparallel β–sheet structure and efficiently adsorbed toxic water-soluble dyes including Rhodamine B, Reactive Blue 4 and Direct Red 80 that are found in industrial waste-water.[27] The same group has reported three self-

assembling pH sensitive tripeptide based hydrogelators with general structure Boc-Phe-X-Phe-OH (where X = Val, Leu, Phe for **1.17**, **1.18** and **1.19** respectively) and used for template synthesis.[28]

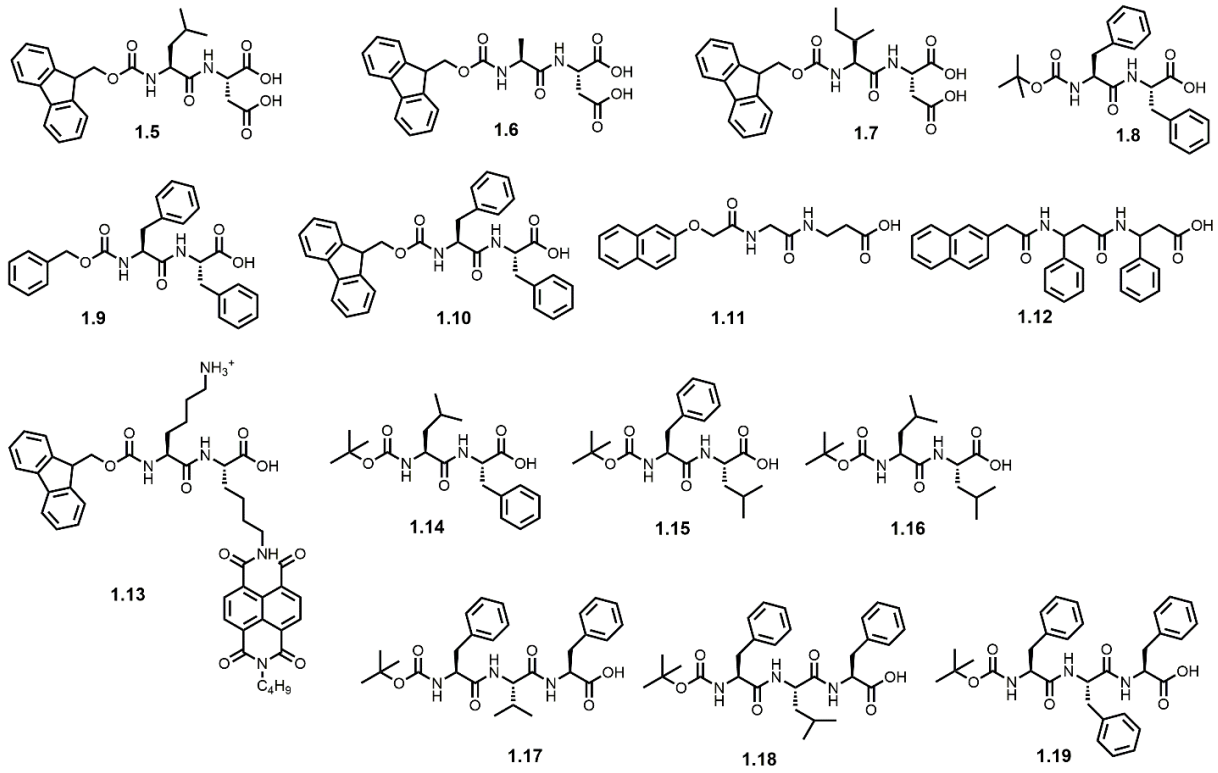

Figure 1.4 Small peptide hydrogelators.

Hydrogels of Peptide Amphiphiles

As hydrophobic and hydrophilic interactions are two major controlling factors for peptide self-assembly, proper balance (hydrophilic lipophilic balance, HLB) between these two factors is extremely important in constructing supramolecular assemblies of peptide based materials. Peptide amphiphiles are one prominent class of gelators owing to the proper HLB present in these molecules. The peptide based amphipathic molecules can broadly be categorized into two main categories (a) amphiphilic peptides, those which are all amino acid peptides and behave like amphiphilic molecules, and (b) lipidated peptide amphiphiles.

Amphiphilic Peptides

This class of peptides are made of amino acids only. These peptides are comprised of both hydrophilic and hydrophobic domains to regulate the proper folding. These amphiphilic peptides can be divided into two subclasses.[29-31] First one is the peptide with alternating polar and hydrophobic residues while the other is a hydrophobic stretch attached to a number of polar amino acids that acts as amphiphilic head group. Schneider *et al.* reported a series of amphiphilic peptides of the first type containing

alternating Val-Lys repeats.[32-34] Deming reported the other type of amphiphilic peptides, where a hydrophobic amino acid stretch was connected to a hydrophilic peptide domain in a diblock or triblock fashion.[29-31,35-39] Highly water soluble polyelectrolytes such as poly(L-lysine) or poly(L-glutamate) were connected to hydrophobic domains such as poly(L-leucine) or poly(L-valine) which formed α–helices or crystalline β–sheets respectively.[40] These polypeptides (**1.20–1.22**, Figure 1.5) formed thermally stable hydrogels at a low concentration (0.25 wt%) in deionized water.[30] Zhao *et al.* reported an interesting amphiphilic peptide capable of forming a self-healing hydrogel consisting of more than 99% water.[41] The 9-residue peptide **1.23** is intramolecularly amphiphilic owing to the presence of a single pair of ionic residues, Lys and Glu, at one end and nonionic residues, Phe, Cys and Phe, at the other end. The peptide adopts stable β–turn and β–sheet structures which self-assemble into hierarchically arranged aggregates. The peptide hydrogel was used to encapsulate and release a model drug pyrene from coated microcrystals to liposomes.

Lipidated Peptides

Different proteins, such as, signal transduction proteins, Ras super-family proteins, have been post-translationally modified by one or two alkyl chains (geranylgeranyl, palmitoyl, farnesyl *etc.*). The attachment of these alkyl chains allow them to anchor the cell membrane.[42] Attaching a hydrophobic tail to a hydrophilic peptide residue generates the hydrophobic interaction region to facilitate the self-assembly process. A large number of lapidated peptides are reported in literature which form hydrogels. Stupp *et al.* have reported a group of asymmetric peptide bolaamhiphiles (**1.24**) which can form self-healing, self-supporting hydrogels at a lower pH and at 0.5 wt% concentration.[43] Das *et al.* reported a positively charged tryptophan containing peptide amphiphile (**1.25**) forming hydrogel with minimum gelation concentration (MGC) of 0.3 wt%.[44] The same group extended their research to cationic lipidated dipeptides (**1.26-1.29**) using tryptophan, phenylalanine and tyrosine as the amino acid residues and found efficient microbial activity and utilizing for controlled release of cytochrome c and vitamin B_{12}.[45-49] Hanabusa *et al.* reported a family of L-lysine-based low-molecular-weight amphiphiles (one representative molecule is shown as **1.30**) with various positively charged terminals (pyridinium and imidazolium derivatives).[50,51] The PAs at low concentration behave like surfactant molecules which self-assemble to form micelles and bilayer structures in a concentration dependent manner. The bilayer structure serves as the basic unit for subsequent hierarchical self-assembly.[44]

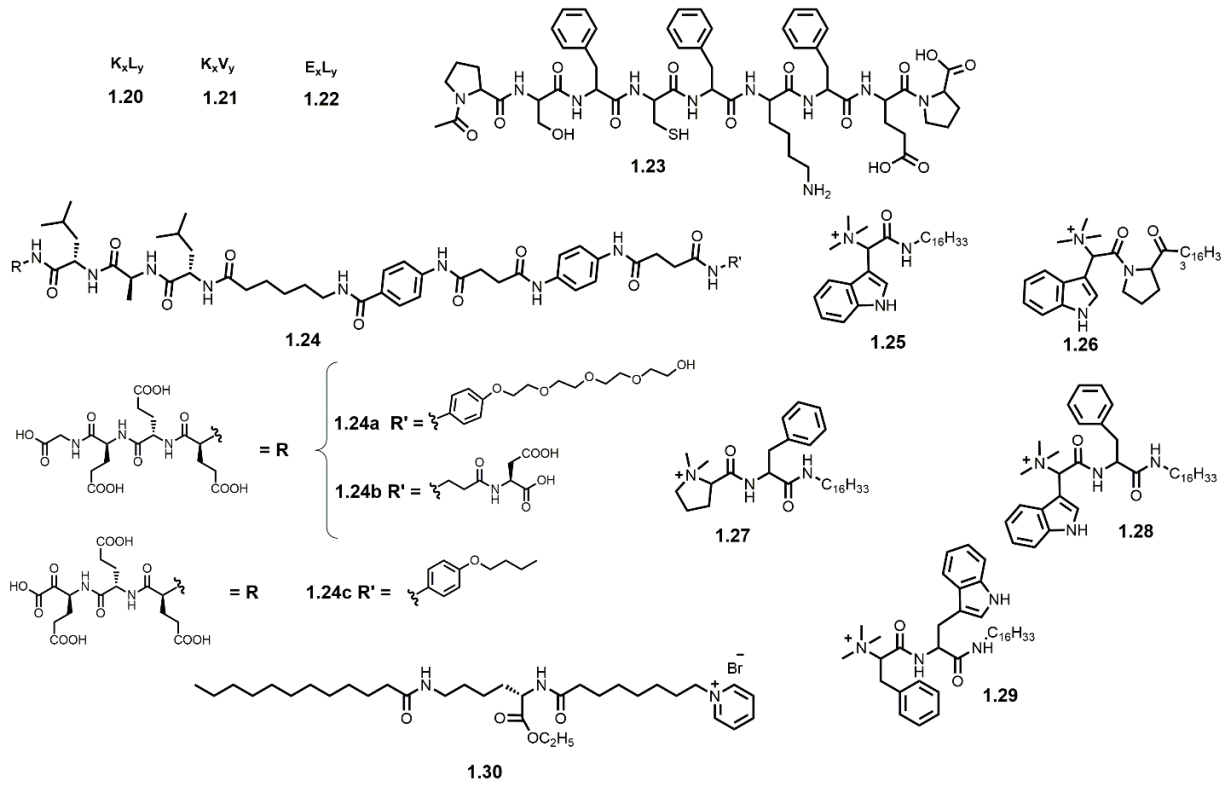

Figure 1.5 Examples of peptide amphiphiles capable of hydrogelation.

1.2.1.2 Applications of Peptide Hydrogels

Peptide hydrogels have wide range of applicability in the field of tissue engineering, drug delivery, as therapeutic agents, template synthesis *etc.* The fibrous network formation, biodegradability, biocompatibility and non-cytotoxic nature of these peptide soft materials have made them an ideal candidate for biomedical applications. On the other hand, the rigidity, stimuli responsiveness and formation of various nanostructures can also be exploited in the material science perspective. In the next section, the uses of peptide hydrogels in biomedical as well as template nano-fabrication is discussed in brief.

Biomedical Application

There is a plethora of examples where peptide based hydrogels have been used for biomedical applications. However, in this section, only a selected examples are discussed. Tissue engineering is ''an interdisciplinary field that applies the principles of engineering and life sciences toward the development of biological substitutes that restore, maintain or improve tissue function or a whole organ''.[52] Considering the advances in biomedical engineering, it is required to fabricate tissues in the laboratory from combinations of engineered extracellular matrices (ECM, ''scaffolds''), cells and biologically active molecules. One of the major challenges of tissue engineering is the need for complex

functionality, as well as both functional and biomechanical stability in laboratory-grown tissues destined for transplantation. In this regard, peptide hydrogels provide a suitable alternative to overcome the challenges. Fmoc-RGD, mimicking the extracellular matrix (ECM) has displayed excellent performance in 3D cell culture using human adult dermal fibroblast cells.[53] Stupp and coworkers have designed peptide amphiphile molecules having bioactive epitopes and obtained exciting results.[54] For example, upon being mixed with cell culture media, the peptides can self-assemble into a three-dimensional network of nanofibers in the presence of calcium ions to afford a hydrogel that can promote neural progenitor cells to differentiate rapidly into neurons.[54] In another example, the doxorubicin loaded hydrogels formed by amphiphilic β–sheet peptide Pro-Asp-$(Phe\text{-}Asp)_5$-Pro showed sustained release profiles over several days.[55] Yang *et al.* reported the first example of a co-delivery hydrogel system based on two complementary anticancer drugs, which might be applied in the cavity after tumor removal for sustained release of anticancer drugs.[56] Das *et al.* reported lipopeptides showing remarkable growth inhibition activity on both Gram positive and Gram-negative bacteria and fungus.[46,49,57,58]

Template Nano-Fabrication

One of the major applications of peptide hydrogels is in the field of bio-mineralization which was pioneered by Stupp *et al.*[59] The nanostructures formed as a result of self-assembly process have successfully been used as templates for the fabrication of nano-materials with proper control of shape, size and dimension. This technique is attractive owing to the specific molecular recognition, simple chemical and biological modification and easy availability for bottom-up fabrication.[60] One of the shortest peptides, diphenylalanine (Phe-Phe) can form nanotube on which metals can be deposited to form electromagnetic coaxial nanowires.[61-71] The Phe-Phe nanotubes have also been used for the fabrication of silicon nanowires that can be used in different applications.[71] In another example , Das *et al.* reported *in situ* synthesis of gold and silver nanoparticles of different shapes using low molecular weight gel template of tryptophan or tyrosine containing peptide amphiphiles in water without using any external reducing or capping agents.[45,57,58,72] Sheet, wire, octahedral and decahedral shaped gold nanocrystals were modulated by the different morphology of the supramolecular gel network.[45] The same group have demonstrated the influence of pristine SWNT in the hydrogelation of amphiphilic dipeptides and developed SWNT nano hybrids with improved mechanical strength. This hybrid can act as scaffold for the superior peroxidase activity of cytochrome c in organic media.[73,74] In another example, template from peptide bolaamphiphile has been used for *in situ* synthesis of Pt nanoparticles which showed catalytic activity toward hydrogenation reactions.[75] Similarly there are number of reports where

peptide hydrogel template have been used successfully for nanofabrication which are beyond the scope of our discussion.

1.2.2 Supramolecular Assembly via Host-Guest Chemistry

Crown ether was the first synthetic macrocyclic host capable of encapsulating guest molecules by non-covalent interaction, discovered by Charles J. Pedersen (Figure 1.6).[76] Active research began toward synthesizing shape- and ion-selective receptors, and throughout the 1980s research in this area gained a rapid pace with emerging concepts such as mechanically-interlocked molecular architectures.[2,77,78] This era produced several macrocyclic structures like cryptands, synthetic hosts, rotaxanes, pseudorotaxanes *etc.* It was Jean-Marie Lehn who finally provided a name to this rapidly expanding area of research, "Supramolecular Chemistry".[2,79] Over the years, supramolecular chemistry and especially the host-guest chemistry have grown as an independent sub-branch of chemistry. Amongst all these supramolecular hosts (Figure 1.6) Cyclodextrins,[80] Calixarenes,[81] Pillararenes,[82,83] and Cucurbiturils[84] are commonly used owing to their strong and selective binding with various guests. However, the present work deals with Cucurbituril (CB) and thus further discussion about synthetic macrocyclic hosts is centered on Cucurbiturils.

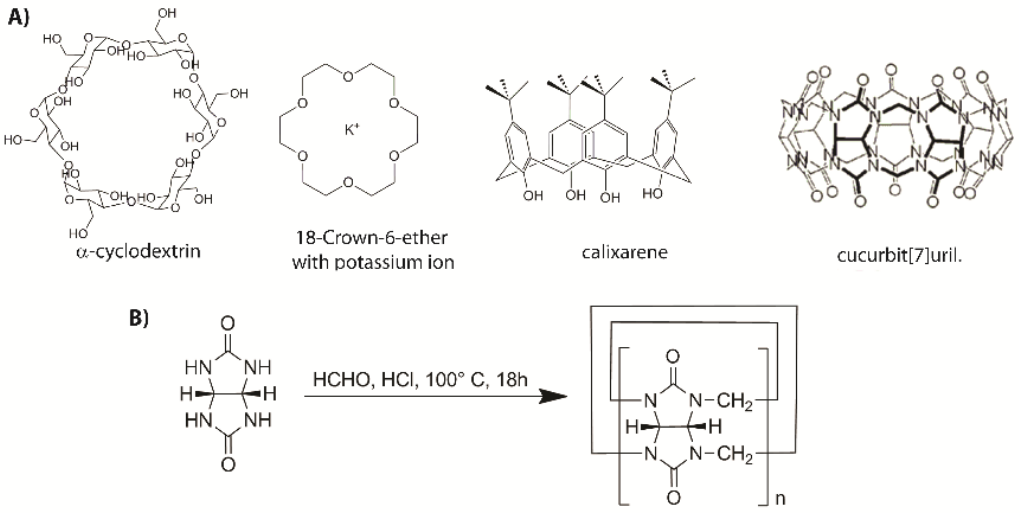

Figure 1.6 A) Various synthetic macrocyclic hosts and B) synthesis of CB[*n*].

1.2.2.1 Cucurbiturils

Brief History and Synthesis

Among the common synthetic receptors, Cyclodextrins (CDs) are commercially available and are industrially important. But they have several limitations such as low affinity and selectivity. These limitations are overcome by a relatively new family of synthetic macrocyclic host, Cucurbit[*n*]uril (CB[*n*],

Figure 1.6).[84-86] The association constants (K_a) of their host-guest complexes are found to be several orders of magnitude higher than CDs in aqueous system.[84,86] The highest K_a recorded so far is 3×10^{15} M^{-1} for CB[7] binding with ferrocene derivatives, reaching that of the well-known avidin–biotin complex.[87] In 1981 Mock *et al.* confirmed the macrocyclic structure having six glycoluril units with twelve methylene bridges (CB[6]) and named it "cucurbituril" owing to its resemblance of a pumpkin, a prominent member of the Cucurbitaceae family.[88] It was synthesized (Figure 1.6) by condensation reaction of glycoluril and formaldehyde in concentrated HCl based on first report published by Behrend in 1905.[89]

The research groups of Kim and Day almost 20 years later, performed the same reaction under milder and kinetically controlled conditions and reported the crystal structures of three other members of the cucurbituril family (CB[5,7,8]).[90,91] Day *et al.* in 2002 and Isaacs *et al.* in 2005 reported the crystal structure of CB[10] (as the CB[5]@CB[10] complex) and (cucurbit[5]uril-free CB[10]) respectively[92,93] whereas those of CB[9] and CB[11] are yet to be isolated.

Structure and Properties

Like cyclodextrins, the various CB[*n*] have a common depth (*c*) (9.1 Å), while their equatorial widths (*b*), annular widths (*a*), and cavity volumes vary systematically with increasing number of glycoluril units present (Table 1.1). The structural rigidity and thermal stability make CB[*n*] a better choice over CDs but the main limitation associated with CB[n] is its solubility in water. CB[6] and CB[8] are almost insoluble in water whereas CB[5], CB[7] have modest solubility in water (Table 1.1).[84,85,94]

Table 1.1 Dimension and physical properties of CB[*n*]

CB[*n*]	M_r	a[Å][a]	b[Å][a]	c[Å][a]	V[Å^3]	S_{water} (mM)	Stability [°C]	pK_a
CB[5]	830	2.4[85]	4.4[85]	9.1[85]	82[85]	20-30[85]	>420[85]	
CB[6]	996	3.9[85]	5.8[85]	9.1[85]	164[85]	0.018[94]	425[95]	3.02[96]
CB[7]	1163	5.4[85]	7.3[85]	9.1[85]	279[85]	20-30[85]	370[85]	
CB[8]	1329	6.9[85]	8.8[85]	9.1[85]	479[85]	<0.01[85]	>420[85]	
CB[10][b]	1661	9.0-11.0	10.7-12.6	9.1	-	-	-	-

[a]The values quoted for a, b, and c for CB[*n*] take into account the van der Walls radii of the relevant atoms. [b]Determined from the X-ray structure of CB[5]@CB[10] complex.[84]

1.2.2.2 Host-Guest Chemistry of CB[5], CB[6] and CB[7]

The rigid hydrophobic cavity and two hydrophilic portals make CB[*n*] an interesting host for a plenty of molecules. Some excellent reviews are available in the literature covering all the different types of molecules tested as probable guests for CB[*n*].[84-86,97-99] The binding of CB[*n*] with different guest molecules primarily occur involving two different supramolecular interactions, ion-dipole interaction at

the portal region as well as hydrophobic interaction inside the cavity. CB[5] can encapsulate small molecules such as N_2 in the cavity and binds cations such as NH_4^+ and Pb^{2+} strongly at the portals. Two NH_4^+ ions can completely seal both the openings of CB[5].[85,96,100-102] Among the various types of guests studied for binding with CB[*n*], positively charged organic species were found to be most preferred.[84] CB[6] forms especially stable complexes with protonated diaminoalkanes ($^+NH_3(CH_2)_n NH_3^+$, n = 4-7, Ka> 10^5 M^{-1}, Figure 1.7) while protonated aromatic amines such as *p*-methylbenzylamine (Ka~ 3×10^5 M^{-1}) binds with CB[6] relatively lesser affinity.[86] CB[6] has the ability to encapsulate neutral molecules such as tetrahydrofuran, Xe, diethylether, and benzene in aqueous solution.[84,85] CB[6] can also bind alkali-metal, alkaline-earth, transition-metal, and lanthanide cations.[85,86,96,100-104] CB[7] forms complexes with larger guest molecules like, 2,6-bis(4,5-dihydro-1*H*-imidazol-2-yl)naphthalene (BDIN, **1.41,** Figure 1.7).[85] It binds protonated adamantylamine (**1.37**, Figure 1.7) as well as methyl viologen dication (*N*,*N*'-dimethyl-4,4'- bipyridinium, MV^{2+}(**1.38,** Figure 1.7) in a 1:1 ratio.[85] Neutral molecules such as ferrocene and carborane get easily encapsulated in CB[7] in aqueous solution. A variety of dyes, ionic liquids, neurotransmitters *etc.* also form inclusion complexes with CB[6] and CB[7]. Apart from all these guests mentioned above, plenty of other guests were found to bind with CB[6] and CB[7], discussion of which is beyond the limit of this section.

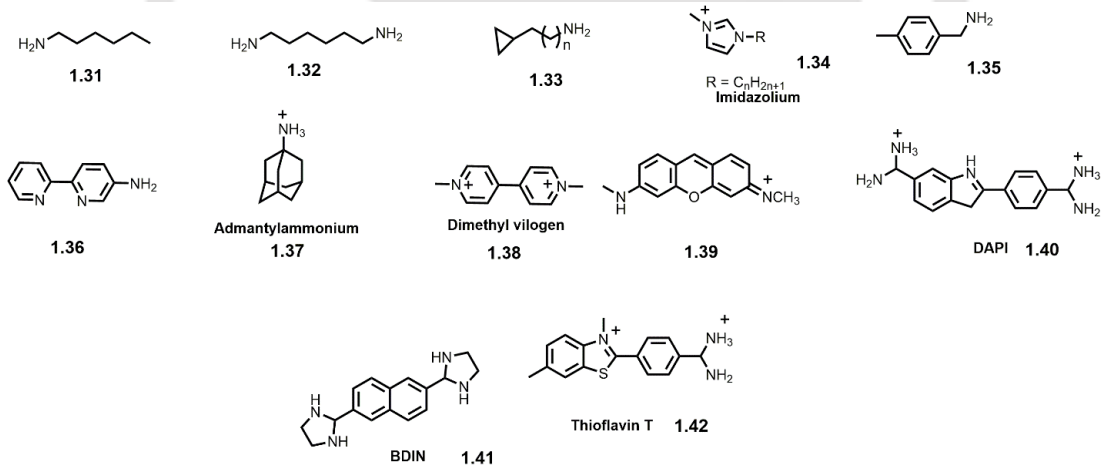

Figure 1.7 Various types of charged organic species as guests for CB[6] and CB[7].

1.2.2.3 Host-Guest Chemistry of CB[8]: The Hetero and Homo-Ternary Complexation

Unlike the other common hosts, CB[8] has the unique ability to encapsulate two guest molecules simultaneously in its cavity and acts as "molecular handcuff". The larger cavity volume (Table 1.1) of CB[8] compared to other members of the family allows it to accommodate two guests inside it's hydrophobic cavity.[84] Typically an electron deficient molecule like MV^{2+} binds to CB[8] as the first guest as shown in figure 1.8 to form a binary complex. On addition of an electron rich donor, like 2,6-

dihydroxynaphthalene (DHN), the binary complex MV@CB[8] incorporates DHN through charge transfer (CT) complexation and forms a hetero-ternary complex, MV-DHN@CB[8] (Figure 1.8). The ternary complexation can be studied using UV-visible spectroscopy by the appearance of a CT band as well as by the formation of an intense colored solution (Figure 1.9). The binding can be analyzed by Isothermal Titration Calorimetry (ITC), NMR, fluorescence spectroscopy and by ESI-MS. Kim *et al.* and Urbach *et al.* have shown that aromatic amino acids such as tryptophan, tyrosine, and phenylalanine also form such ternary complexes with tryptophan showing the highest bonding affinity.[105,106] It is worth mentioning that peptide with tryptophan at N terminal binds with more strongly than tryptophan in any other position.[106] Peptides with the N-terminal sequences like Trp-Gly-Gly and Phe-Gly-Gly could form dimers inside the CB[8] cavity.[107] Kim *et al.* reported the ability of CB[8] to form hetero ternary complex in aqueous media.[108] The one electron reduction product of MV^{2+} *i.e.*, the cation radical $MV^{+\cdot}$ can form a 2:1 homo-ternary complex with CB[8].[109] The dimerization constant of $MV^{+\cdot}$ in the presence of CB[8] is estimated to be 2×10^7 M^{-1}, which is about 10^5 times higher than that of $MV^{+\cdot}$ alone in aqueous media.

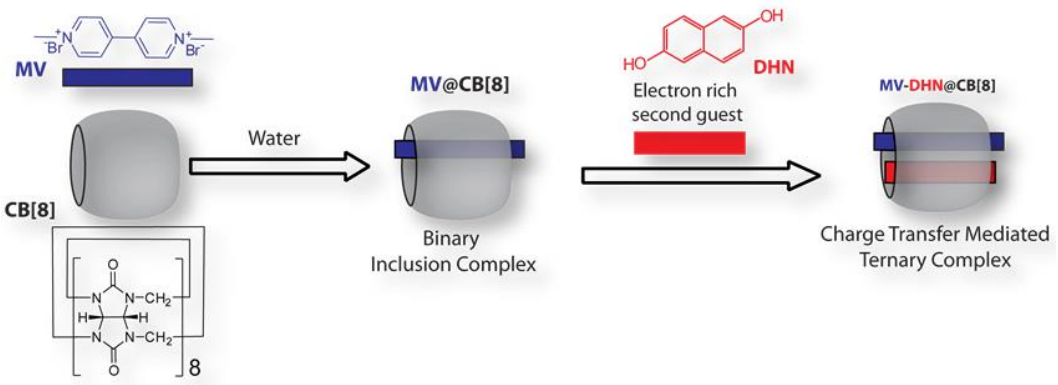

Figure 1.8 Pictorial presentation of the formation of MV-DHN@CB[8] ternary complex

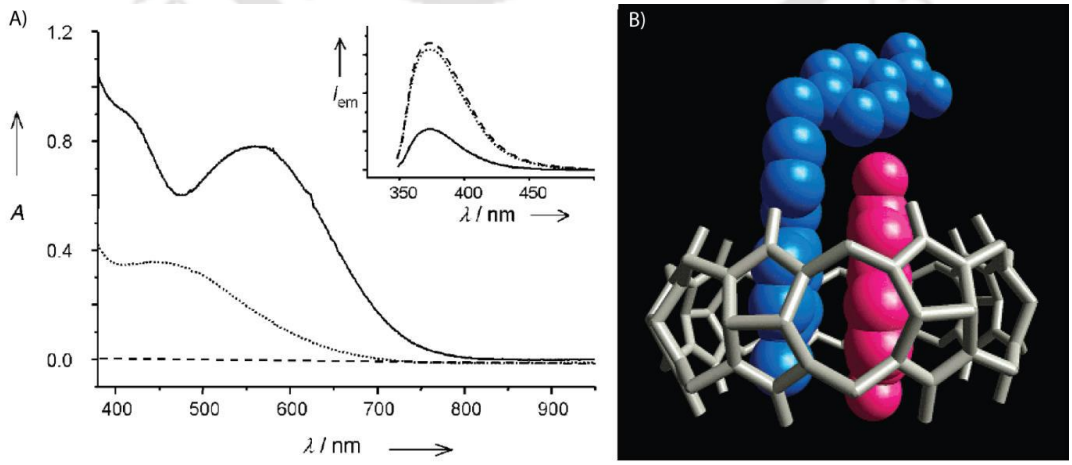

Figure 1.9 A) Absorption and emission (inset) spectra obtained in H_2O of DHN (dashed line), a 1:1 mixture of DHN and MV (dotted line), and DHN-MV@CB[8] (solid line). B) Crystal structure of 1:1:1 complex of DHN (magenta)-a MV containing molecule (blue)-CB[8](magenta).[108]

1.2.2.4 Supramolecular Polymers using CB[8]

The unique ternary complexation of CB[8], has been used in several occasions to construct supramolecular polymers in aqueous system.[110-124] Below is a brief discussion on some of the supramolecular polymers created using host guest chemistry of CB[8].

AB di-block and ABA tri-block copolymers were reported by Scherman *et al.* using the ternary complexation of CB[8], a viologen containing and a naphthalene functionalized polymer (Figure 1.10).[110] ABA triblock copolymer was formed when NpPEG (**1.43**, Figure1.10) was added to an aqueous solution of 2:1 CB[8]@MVdimer. Two different polymers were supramolecularly conjugated using the ternary complexation to create a linear polymer (Figure 1.10).[111]

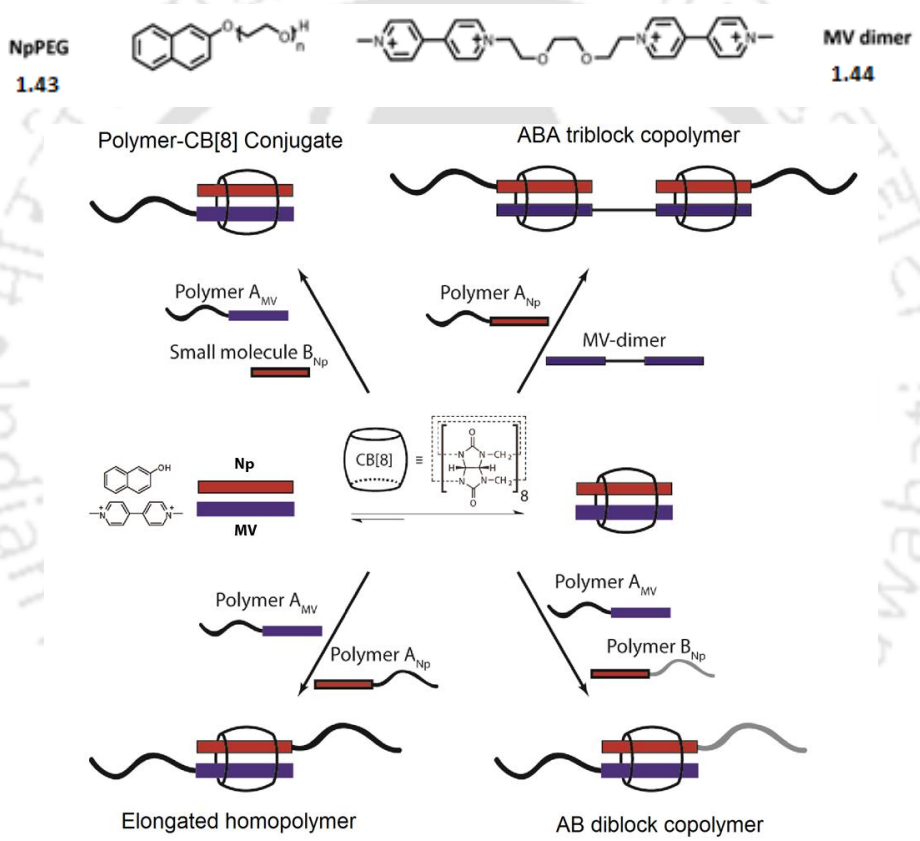

Figure 1.10 Variety of polymeric structures can be formed in aqueous medium via host-guest interaction of CB[8] by interconnecting complementary end-groups such as electron-rich 2-naphthol (Np) and electron deficient methyl viologen (MV) attached onto polymers.[110,111]

The same group reported the formation of a cross-linked three-dimensional polymer using the same 1:1:1 ternary complexation strategy.[112] In this report, multivalent polymeric scaffolds of relatively low molecular weight (M_n<40 kDa), bearing either MV or Np functionality pendant from the polymer backbone were utilized to develop a cross-linked gel.[112]

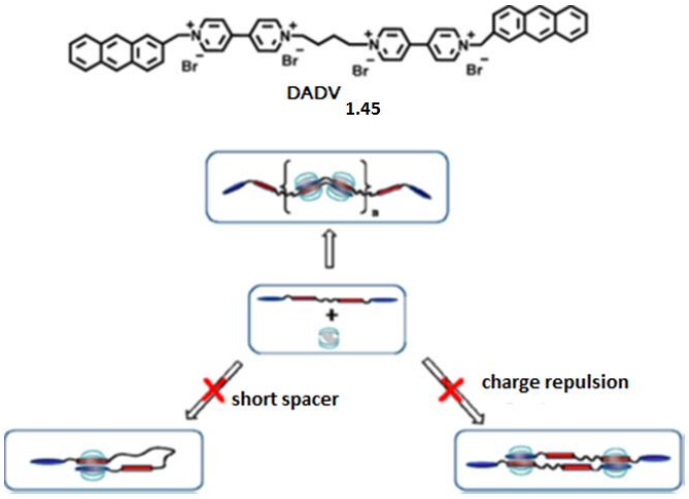

Figure 1.11 Supramolecular linear polymer constructed using the host-enhanced charge-transfer interaction of DADV (**1.45**) inside the cavity of CB[8]. The 1:1 cyclic species can be inhibited because of the short spacer, and 2:2 cyclic species can be prevented by the charge repulsion between viologen moieties.[113]

Zhang *et al.* reported a series of supramolecular linear as well as hyperbranched polymers based on ternary complexation.[113-123]The group reported an anthracene–viologen–viologen–anthracene (DADV, **1.45**, Figure 1.11), an ABBA-type monomer, and the supramolecular polymer was fabricated through the host-enhanced charge-transfer interaction.[113] Scherman *et al.* used the same strategy for the construction of photo-controlled CB[8]-mediated supramolecular polymer of azobenzene-containing monomers.[124] In another report, Zhang *et al.* used host enhanced π–π interaction to prepare hyperbranched supramolecular polymer. BTNI (**1.46**, Figure 1.12), a tri-arm monomer having one naphthalene moiety in each arm formed a dendrimer like supramolecular polymer in presence of CB[8] via homo-ternary complexation.[122] Similarly, a number of different supramolecular polymers using CB[8] are reported in literature and a comprehensive review can be found in reference no. 125.

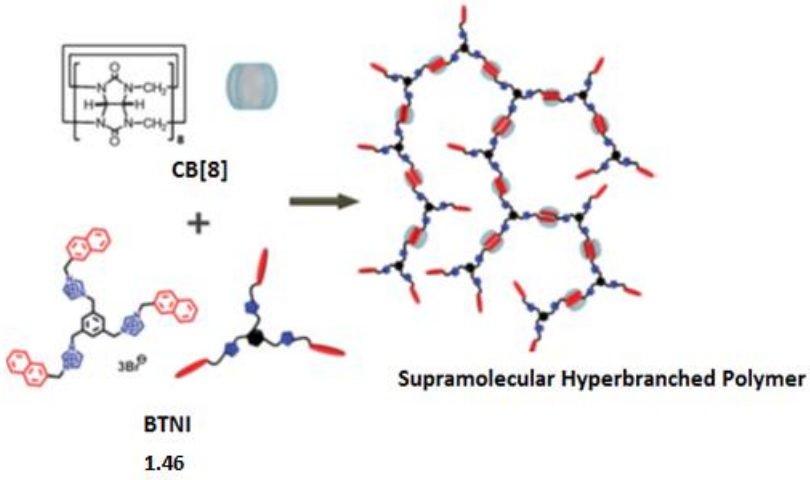

Figure 1.12 Illustration of the formation of supramolecular hyperbranched polymers using host CB[8] induced π–π interaction.[122]

1.2.3 Organic Electronics: The Case of Perylenediimides

Organic electronics is a branch of materials science dealing with the design, synthesis, characterization, and application of organic small molecules or polymers that show desirable electronic properties. In contrast to traditional inorganic conducting materials, organic electronic materials are constructed from organic small molecules or polymers. One of the most prominent benefits of organic electronics is their potential low cost compared to traditional inorganic electronics.[126,127] Polyaniline, the earliest reported organic conductive material, was reported by Henry Letheby in 1862. In 1960s, a derivative of tetraiodopyrrole was reported to show high conductivity of 1 S/cm.[128] The 2000 Nobel Prize in Chemistry was awarded to Alan J. Heeger, Alan G. MacDiarmid, and Hideki Shirakawa jointly for their work on conductive polymers.[129] Organic semiconductors are π–bonded molecules or polymers made up by carbon and hydrogen atoms and sometime with heteroatoms such nitrogen, sulfur and oxygen. They exist in form of molecular crystals or amorphous thin films. In general, they are electrical insulators but become semiconducting when charges are either injected from appropriate electrodes, upon doping or by photoexcitation. In this context, arylenediimides, such as perylenediimides (PDI, Figure 1.13) were found to be n-type semiconductors and are quite extensively studied to create new organic-electronic devices. Below is a concise discussion about the recent studies involving PDI-based molecules and their self-assembly and semiconducting behavior.

1.2.3.1 Perylenediimides: Semiconducting and Self-Assembly Property

Perylenediimide (PDI) semiconductors have been among the most intensively studied semiconductor materials. In recent years, the preparation of PDI-based n-type organic semiconductors with good OFET performance has achieved great advancement.

Desired chemical and physical properties of PDIs are heavily dependent on the functionalization at the imide N,N′ positions, the 1, 6, 7, 12 positions of the perylene core (also known as "bay" positions), and even at the 2, 5, 8, 11 positions (so-called "ortho-" positions) (Figure 1.13).[130-140]

In general, the substitution at the two imide positions has little or no effect on the electronic property of PDIs (*e.g.,* energy levels, redox potentials), thus resulting in no significant change of the molecular absorption or emission features.[141] On the contrary, substitution at the bay positions often significantly changes the optical and electronic properties, especially when electron-donating moieties are attached.[142] The orbital energy shifting, in combination with the disturbance of the planar π-conjugation, can explain such performance changes.[142] Change in molecular planarity affects the solubility of PDI molecules and at the same time, the significantly twisted π- conjugation weakens the π–π stacking interaction. The core of PDIs is a planar π-conjugated system, prone to π–π stacking into

crystal aggregates with an interlayer distance of ca. 3.4 Å (similar to that in graphite).[134] The aggregation behavior of PDIs can be monitored in situ by monitoring relevant UV–vis absorption spectra. Monomeric PDI molecules in solution usually have three characteristic vibronic absorption peaks around 400–550 nm for the lowest energy electronic transitions (arising from 0-0, 0-1, and 0-2 transitions). For monomeric species the ratio of $A_{0\text{-}0}$ to $A_{0\text{-}1}$ is about 1.7 whereas for fully aggregated state it is 0.8.[143-146] A red-shift in absorption peaks are often observed for molecular aggregation.[147,148] In addition, the transformation from isolated PDI molecules into condensed phase is often accompanied by significant fluorescence quenching. Interestingly, the molecular stacking conformation in 1D nanostructures can be readily demonstrated by polarized fluorescence spectroscopy due to their optically uniaxial property along the π–π stacking axis.[149]

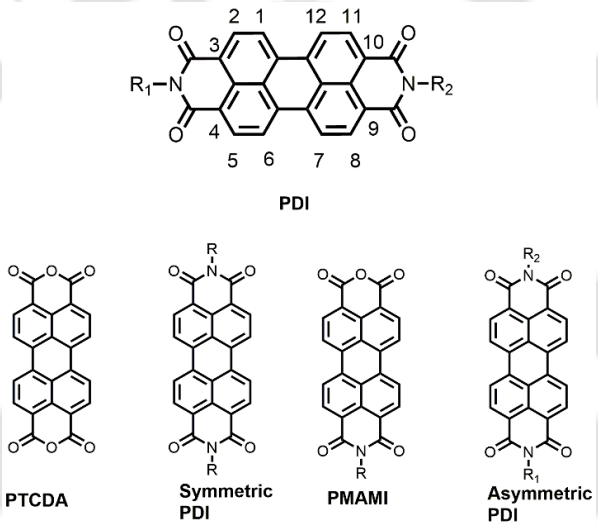

Figure 1.13 Fundamental chemical structures of PDI with the numbering of the positions in the ring system, PTCDA (Perylene tetracorboxylic dianhydride), symmetric, asymmetric N,N′-PDIs and most common precursors PMAMI (Perylene monoanhydride monoimide).

1.2.3.2 Self-assembly of PDI – Peptide Conjugates

Characteristic molecular assemblies involving weaker noncovalent interactions often end up with stable thermodynamically controlled assembly whereas kinetically controlled molecular assemblies are rarely achieved as it demands strong and complex interplay of multiple noncovalent interactions. Rybtchinski group reported one such fascinating kinetically controlled self-assembly of **1.47** and **1.48** in aqueous medium.[150] These amphiphiles showed pathway dependent assembly to various nano-morphologies which evolved in a stepwise manner. In another example lysine-functionalized tetrachloro PDI (**1.49**, **1.50,** Figure 1.14) were shown to organize into controllable nanostructures with tunable dimensions.[151] H-bonding driven self-assembly was also reported where supramolecular helices of PDIs containing chiral amino acids were realized (**1.51**, **1.52,** Figure 1.14).[152] Clockwise and anti-

clockwise supramolecular helices were induced by L and D phenylalanine respectively. The hydrogen bonding induced helical superstructures were strongly dependent on external stimuli such as, solvent polarity, concentration and temperature. In another work, PDIs appended with alanine or lysine as imide substituents, were coupled to Newkome type dendrimers acting as hydrophilic groups to obtain water soluble chiral PDIs.[153] Jin and coworkers designed a series of PDIs to obtain a liquid crystalline ordering.[154] Compound **1.53** resulted in crystalline π -stacks with highly ordered columnar smectic phase at room temperature. Extending further on the similar strategy the same group reported non racemic chiral main-chain PDI polymers via acyclic diene metathesis polymerization.[155]

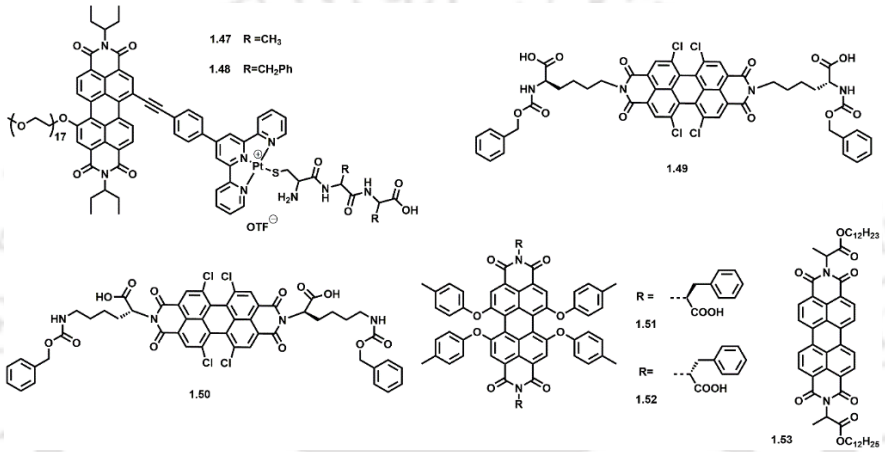

Figure 1.14 Chemical Structures of some Peptide PDI conjugates.

Amino acid or peptide-perylene gels are also reported in the literature. Zang and co-workers reported a pH-triggered hydrogelation route enabling the fabrication of **1.54** (Figure 1.15) molecule into well-defined 1D nanobelts.[156] Self-assembly was triggered through lowering the pH of aqueous trimethylamine (TEA) solutions (pH ≈ 9.0) of **1.54** by the addition of hydrochloric acid. On varying the amino acid functional groups, uniform 1D nanofibers of amino-acid functionalized PDIs (**1.55**, **1.56**, and **1.57**, but not **1.58**; Figure 1.15) were fabricated. Both fromed viscous aqueous solutions (pH ≈ 10) and xerogels through moderately adjusting the solution pH by glucono-δ-lactone (slowly hydrolyzing to gluconic acid).[157] Such 1D self-assembly is dominated by synergistic π–π stacking, H-bonding, and hydrophobic/hydrophilic interactions irrespective of the methods and the carboxylic acid side chains used.[156,157] A similar self-assembly strategy was applied to a series of tetra-carboxylic acid-substituted PDI derivatives, **1.59** and **1.60** (Figure 1.15). These PDI molecules are water-soluble in part due to the twisted perylene cores: irregular 1D nanofibers can be successfully fabricated from co-assembly of **1.59** and **1.60** using a mole ratio of 1:4 upon lowering the pH of aqueous solution to the optimum level. Similarly, Malik *et al.* reported the hydrogelation of D/L aspartic acid appended PDI (**1.61**, **1.62**, Figure 1.15).[158] Aqueous solution of the compounds **1.61** and **1.62** formed reversible gel which is controlled by

pH. Under acidic condition (pH 4) both formed gel and with increasing pH the gel turned into sol. FESEM image shows helical fibers with opposite helicity. Compound **1.61** forms right handed whereas compound **1.62** forms left handed helical fibers.

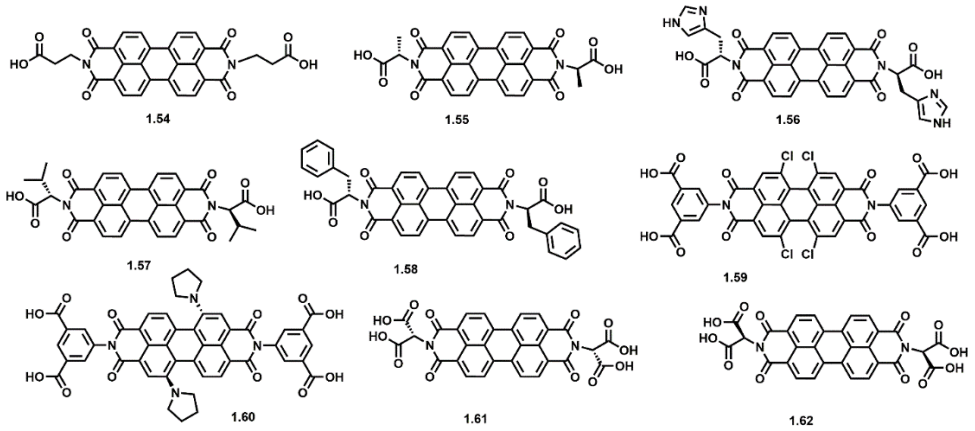

Figure 1.15 Chemical Structures of some Peptide PDI conjugate

Though biomolecular interfaces have already started getting attention in electronic devices, peptides are yet to be exploited properly.[159] A number of related studies by means of natural materials highlight the prospective of this methodology to create new properties and applications.[160-162] However, it still remains a difficult task to fabricate nanowires or other types of 1D nanostructures with well-defined morphology and molecular arrangement.[163] The main difficulty lies in the fact that a successful 1D fabrication demands a correlation between the self-assembling kinetics or thermodynamics and the molecular design and engineering. This, in turn usually requires a strong interplay between chemical synthesis, materials fabrication and physical characterization.[163]

Though several PDI-amino acid or peptide conjugates have been reported, not much attention have been payed to correlate the semiconducting behavior of the nano-morphologies generated by their assembly and the self-assembly process. In one of the few reports, Li *et al.* have designed and synthesised CBZ-lysine-functionalized tetrachloroperylenediimides (**1.49** and **1.50**, Figure 1.14).[151] Interestingly, with varying solvent polarity, and sample concentration, compound **1.49** could self-assemble to achieve different nano-architectures such as nanosphere, nanowire, nanobelt, and nanosheet, which were found to have different degree of molecular ordering (Figure 1.16). These nanowires (Figure 1.16a), nanobelts (Figure 1.16b), nanosheets (Figure 1.16c) and nanotubes (Figure 1.16d) exhibited an average conductivity of the order of magnitude 10^{-3}, 10^{-2} and 10^{-6} Scm^{-1} respectively.

It is worth mentioning that the ordered structure of such n-type semiconductors is an essential requirement to improve the performance. In this regard, natural materials such as DNA-based polymers,

peptides, proteins have successfully been used as insulating gate dielectric layers in FETs.[160-162] However, peptide based semiconductors is a new approach and a very limited number of such materials have so far been prepared and actually tested for OFETs and other organic electronic devices. Peptide sequences adapted from natural proteins capable of self-assembly can easily be coupled with organic semiconductor moieties by proper synthetic protocol development. The inherent self-assembling property of the peptide sequence will lead to the desired ordered nano-structures which presumably enhance the performance of these semiconducting materials.

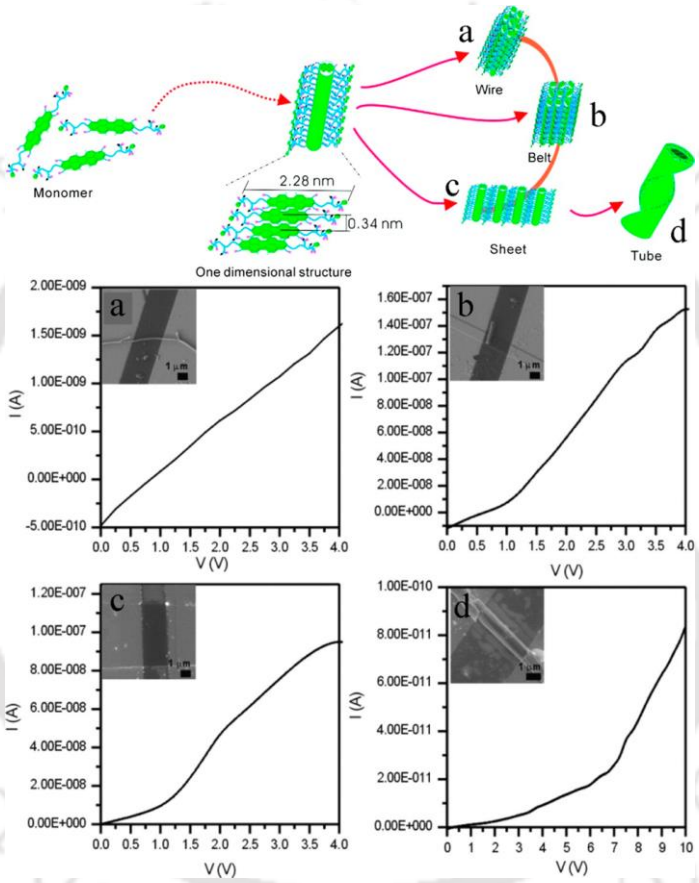

Figure 1.16 Concentration-dependent self-assembly of PDI (**1.49**, Figure 1.14) molecules from 45% H_2O/acetone mixtures when tuning the concentration of **1.49** in acetone from a) 100 μM, b) 300 μM, c) 800 μM to d) 1 mM, and the effect of morphologies (a, nanowire; b, nanobelt; c, nanosheet; d, nanotube) on the I–V curves. The inset is a photograph of the corresponding device.[151]

1.3 Objectives of the Present Thesis

As discussed in the previous sections, amino-acids and peptide based small molecules have the intrinsic tendency to self-assemble and these self-assemblies can be utilized for various applications. A plethora of studies have so far been performed to understand the assembly mechanisms and the overall conclusion of these studies is that, every system has its own pathway to form the self-assembly. The

understanding of the secondary structural motifs of peptides and their hierarchical self-assembly processes opened up the possibility to design, synthesize and modulate the properties of self-assembling peptides. Today formation of gels by a synthetic peptide is no longer a serendipitous observation but to a certain extent a rational approach to create a platform where the properties of the self-assembled structures can be fine-tuned with the help of external stimuli. Though the success to failure ratio in this context is not extremely high, yet the understanding of the molecular interactions and the requirement for such interactions, has certainly helped in designing such materials. In the present work, three different systems were chosen and the very basic idea behind the work is to get fundamental insight into the self-assembly mechanism of these amino acid/peptide based system.

Chapter 2. A Peptide-Amphiphile based Hydrogel: Synthesis, Characterization and Self-Assembly Mechanism

A Lysine based peptide amphiphile (PA) is rationally designed and synthesized. The PA showed efficient hydrogelation behavior. The work depicted here is a methodical study to reveal the self-assembly mechanism of the PA.

Chapter 3. An Amino Acid-Dimer Based Redox Active Supramolecular Polymer using Host Guest Chemistry of Cucurbit[8]uril

Using ternary complexation of CB[8], a tryptophan based supramolecular redox active polymer is prepared and its formation mechanism is investigated in detail. The supramolecular hetero-polymer can reversibly be transformed to a homo-polymer using a simple reduction/oxidation reaction couple.

Chapter 4. Self-Assembly of a Peptide-Perylenediimide Conjugate: Solvent Directed Tuning of Helicity and Morphology

A symmetrical Phe-Phe-peptide-PDI conjugate is exposed to different solvent compositions with varying THF-water ratio and the difference in the self-assembly mechanism is investigated in these media. Interestingly, the conjugate formed a helical nano-fiber via a kinetically controlled assembly mechanism in THF. However, in 10% THF in water, the morphology changed to nano-rings and the formation of the rings is found to be thermodynamically controlled.

Chapter 5. Applications of supramolecular Assemblies

In this section of the thesis, the obtained self-assemblies from the previous sections are used for two different application, A) the nano-fibers of the PA in Chapter 2 is used as a template to synthesize hollow silica nano-tubes and B) the semiconducting behavior of the different morphologies obtained in Chapter 4 is analyzed to get a correlation between the conductivity and the assembly mechanism.

Chapter 2

A Peptide-Amphiphile based Hydrogel: Synthesis, Characterization and Self-Assembly Mechanism

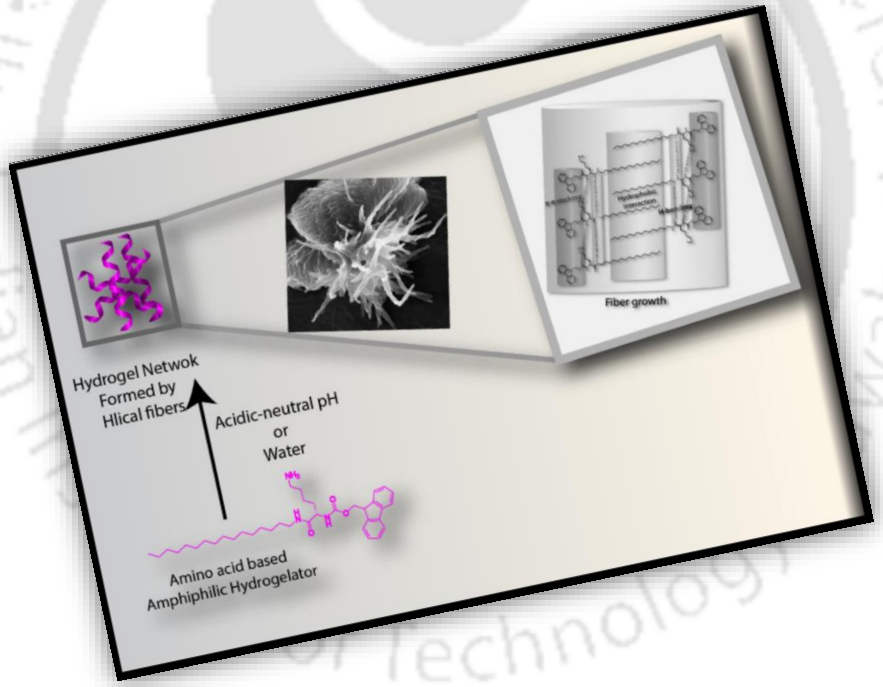

2.1 Introduction

Among the peptide based hydrogelators, peptide amphiphiles (PA) are one of the major categories which demonstrate efficient self-assembly owing to the appropriate hydrophilic-lipophilic balance (HLB) within the molecular architectures.[16,164,165] Numerous PAs have been exemplified in recent literature to show efficacious self-assembly and utilized for various applications such as tissue engineering, delivery vehicle, antibacterial agents, nano-fabrication *etc.*[44,45,50,59,166-171] As discussed in Chapter 1, amphiphilic peptides are more commonly found in literature as efficient hydrogelators whereas the number of lipidated peptide amphiphiles is somewhat limited. Moreover, most of these lipidated amphiphiles are found to form supramolecular gels only in presence of some organic solvents or at a particular pH.[59,169,170] Only a few such molecules have been reported to show hydrogelation in plain water which is essential for their biological uses.[44,168]

Appropriate balance between all the supramolecular forces is the prime requirement for the self-assembly in a particular solvent.[14,15] Hydrogen bonds, one key parameter controlling the assembly process, loses their strength in aqueous system while hydrophobic interaction becomes most important in such environment.[172,173] Thus HLB comes into prominence while designing the lipidated peptide amphiphile as a hydrogelator. Proper HLB leads to enough solubility of the molecule to get dissolved in water and allow the other forces act in a concentration dependent fashion. The primary to tertiary assembly of a PA in water generally follows the order of micelles/bilayer-fibers and finally the gel network in a hierarchical fashion.[14,15] The presence of chiral centers often gets transformed into supramolecular chirality in this hierarchical process.[14-16]

In this chapter the rational design, synthesis and hydrogelation of a simple lysine containing peptide amphiphile **2.1** (Scheme 2.1) is described along with the mechanistic details of gelation.

2.2 Results and Discussion

It has been reported that Fmoc-protected glycine containing a C_{18} chain forms organogel and twisted nano-fiber like structures.[174] Based on these observations, it was reasoned that decrease in the hydrophobicity and inclusion of a hydrophilic group may allow sufficient solubility to this molecule in aqueous environment. A simple lysine based amphiphile **2.1** (Scheme 2.1) was designed. A C_{16} hydrophobic tail, functionalities capable of forming hydrogen bond (NH and carbonyl group) as well as an aromatic π–electron system in the form of fluorenyl group in the molecule would be adequate to provide enough supramolecular interactions. Appropriate solubility of the molecule is an essential criteria in order to self-organize and thus in our design, a hydrophilic group in the form of a free amine of the lysine side chain is incorporated which may allow to solubilize the molecule in water as well as

keep the proper HLB to self-assemble. The presence of the free amine group is also on purpose to incorporate pH sensitivity of the self-assembly. When dissolved in plain water at 1 % w/v (16.92 mM) concentration by slow heating to 60 °C, PA **2.1** formed a slightly hazy solution which upon slow cooling to room temperature formed a self-supporting opaque hydrogel. In order to establish the hydrogelation mechanism, four structurally similar compounds were also synthesized (**2.2**-**2.5**, scheme 2.1). In case of **2.2** and **2.3**, the tail lengths were varied by changing the tail to C_{14} and C_{12} respectively. Compound **2.4** is the ester analog of compound **2.1** while compound **2.5** was synthesized using the D-lysine isomer to get the D-analog of compound **2.1**.

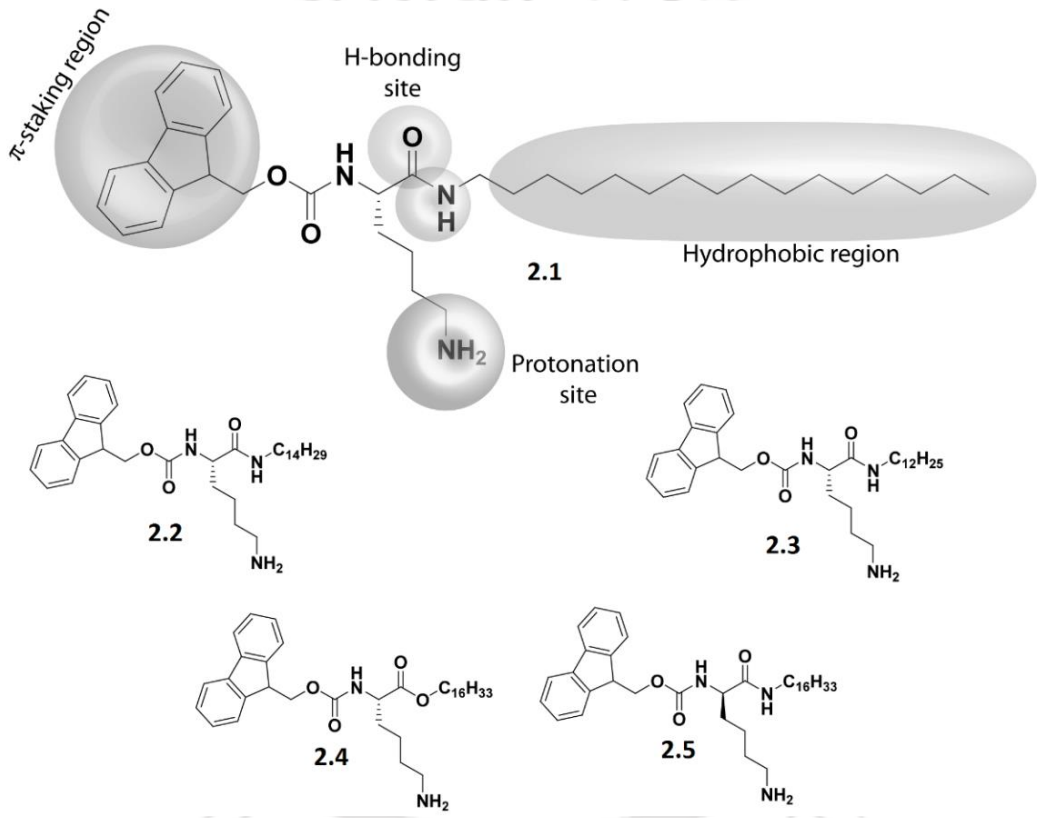

Scheme 2.1 Chemical structures of the synthesized compounds.

The hydrogel was found to be stable at room temperature over a period of more than six months. The sol-gel transition temperature (T_g) was observed to be 47 °C which closely matched with the DSC data (Figure 2.1). A sharp peak was observed in the forward scan of DSC indicating the T_g at 47.3 °C. In accordance with the previously reported results, the T_g increased with increase in gelator concentration.[44,170]

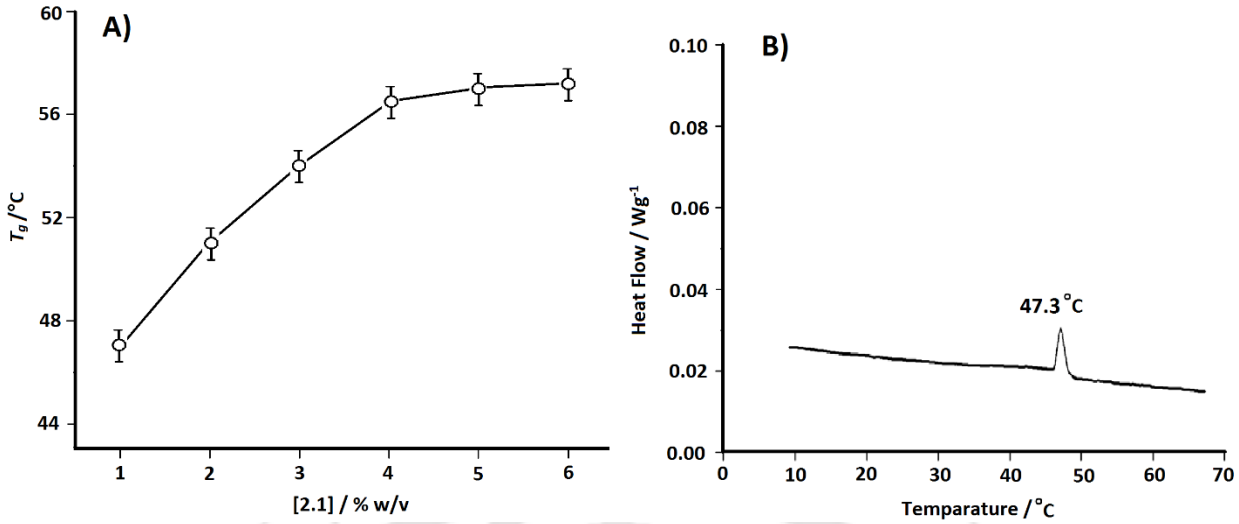

Figure 2.1 A) Plot of T_g against gelator concentration (in plain water) and B) DSC thermogram of hydrogel of **2.1** (1 % w/v) in plain water.

To find the mechanical strength of the hydrogel, the rheological behavior was monitored with varying angular frequency at a constant strain (Figure 2.2A). Linear viscoelastic frequency sweep response of the hydrogel of **2.1** (1 % w/v) exhibited a weak frequency dependence from 0.2 to 100 rad s^{-1} where G′ (dynamic storage moduli) dominating G″ (loss moduli), suggesting the high elasticity leading to a strong hydrogel.

Interestingly, compound **2.1** also formed gel in aqueous mixtures of different organic solvents (methanol, dimethylsulphoxide, dimethylformamide, acetonitrile, and dioxane) at 1 % w/v concentration. Unlike the pure aqueous system, in all those mixed solvent systems except in methanol the gels were observed to be transparent (Figure 2.2B).

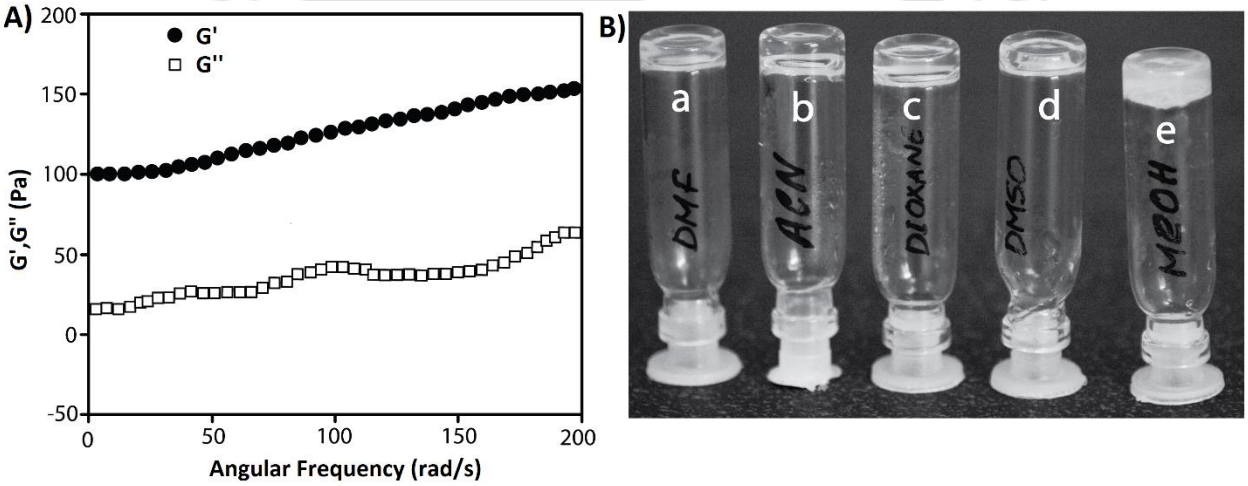

Figure 2.2 A) Dynamic rheology (frequency sweep) of PA **2.1** (1 % w/v) and B) Photographs of gels formed by 1 % w/v **2.1** in a) 30% water in DMF; b) 50% water in acetonitrile; c) 45% water in dioxane; d) 30% water in DMSO; e) 50% water in methanol.

The presence of the free amine at lysine side chain of **2.1** it allowed the molecule to solubilize in water as well as provided the pH sensitivity of the gelation process. Compound **2.1** formed hydrogel in 20 mM buffers of pH 1-8 at 1 % w/v concentration but failed to solubilize above pH 8. The pH sensitive aggregation can be explained based on the protonation of the free amine which remain in the ammonium state even in plain water and thus provides the solubility of the molecule in the pH range of 1-8. Above that pH, the amine group gets deprotonated which reduces its solubility at this condition. As the pH dependency was established, the pH responsive gelation of **2.1** was explored. A 3 % w/v hydrogel of **2.1** in 1 mL 20 mM buffer at pH 1 was prepared and at the top of the gel, a 50 μL of 3M sodium hydroxide solution was placed (Figure 2.3). After six hours, the gel melted to a suspension and the pH of the system was observed to be 9. pH of the suspension was then adjusted to 2 by adding concentrated hydrochloric acid. The acidic suspension was then heated slowly to 60 °C and allowed to come to room temperature. The suspension neither got solubilized at elevated temperature nor did form hydrogel upon cooling.

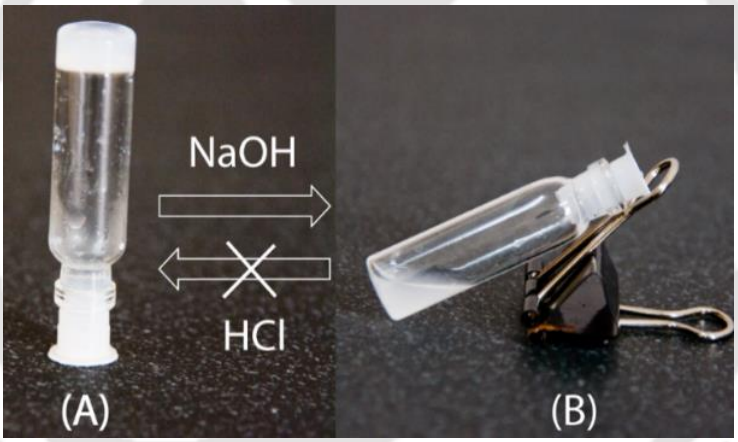

Figure 2.3 Photographs of pH dependent gelation of **2.1**: A) Hydrogel of **2.1** (3% wt/vol) at pH 1 and B) the gel transformed into a sol after addition of 3 M NaOH solution.

The observation can be explained in terms of the removal of "Fmoc" group under basic condition which leads to phase separation and irreversibility of the hydrogelation process.[175,176] To prove the deprotection of "Fmoc" group, thin layer chromatography (TLC) behavior and ESI-MS of the sample after the NaOH treatment were checked. TLC of this sample showed disappearance of the parent compound (**2.1**) and the appearance of another major compound with a lower retention factor along with a UV active spot at the solvent front (Figure 2.4C). The ESI-MS measurement of the material showed (Figure 2.4A, B) the mass of the deprotected product which clarifies the assumption.

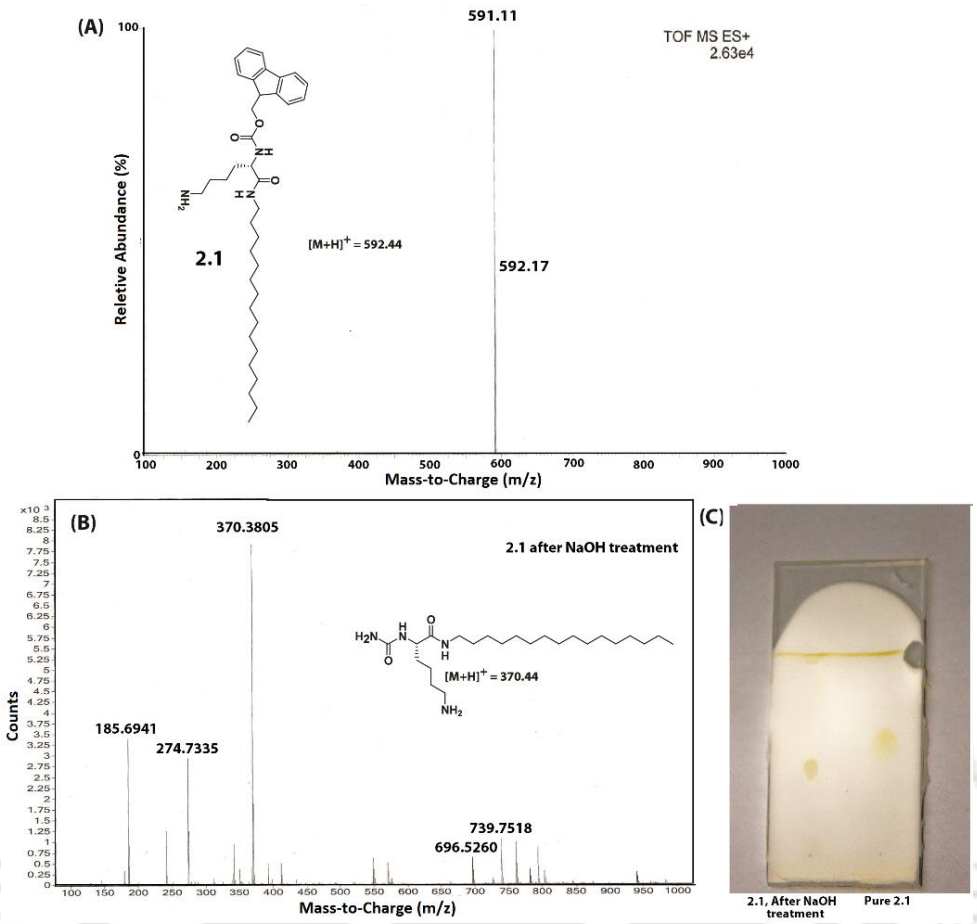

Figure 2.4 ESI-MS spectrum of the hydrogel of **2.1** A) before and B) after treating it with NaOH solution. C) TLC behavior of compound **2.1** before and after the NaOH treatment (Solvent system: 12% MeOH in DCM, spots developed by prolonged treatment with iodine vapor).

The peptide amphiphile **2.1** was designed to attain sufficient hydrophobicity which may favor the self-aggregation. In order to decipher the role of hydrophobicity in the hydrogelation process, two more analogues **2.2** and **2.3** with altered hydrophobic characters were synthesized. Although compound **2.2** could immobilize water to form hydrogel at a higher concentration above 3 % w/v, compound **2.3** failed to form any self-supporting gel in plain water. The observation was found to be similar when the experiment was repeated with a buffer of pH 1. The fall in the hydrophobic character significantly alters the HLB of the molecule and consequently the self-aggregation could not be achieved.

The presence of the hydrophobic interaction is also prominent from the emission spectra of a hydrophobic probe 8-anilino-1-naphthalenesulfonic acid (ANS) with varying concentration of the gelator (Figure 2.5). Due to slight haziness at higher concentration in aqueous medium, the experiment was performed in 1:1 water-acetonitrile medium as the gelator can also form gel in this solvent system at 1 % w/v concentration. As the concentration of the gelator increased, the intensity of the emission

peak showed a steady enhancement accompanied by a blue shift in the maxima from 508 to 495 nm (Figure 2.5A). Such luminescence behavior of ANS indicated the existence of a hydrophobic environment.[44,50] Moreover, the dependence of the emission intensity at 495 nm with the gelator concentration showed some interesting features (Figure 2.5B). At a very low concentration below 5×10^{-4} % w/v the intensity was similar to that of only ANS in the system indicating that the gelator molecules were in monomeric form and no aggregation occurring at that concentration range. Above that concentration, the intensity increased steadily up to 2.5×10^{-3} % w/v and no further change was observed till 2.5×10^{-2} % w/v. Another inflection point was noted at this concentration. This pattern in the intensity at this concentration range indicates two distinct self-aggregation processes happening in this concentration range. It may be presumed that the initial inflection point at 2.5×10^{-3} % w/v signifies the primary aggregation leading to formation of the micelles/bilayer whereas the second inflection point at 2.5×10^{-2} % w/v is caused by the secondary aggregation and signifies the formation of fibers at this concentration.

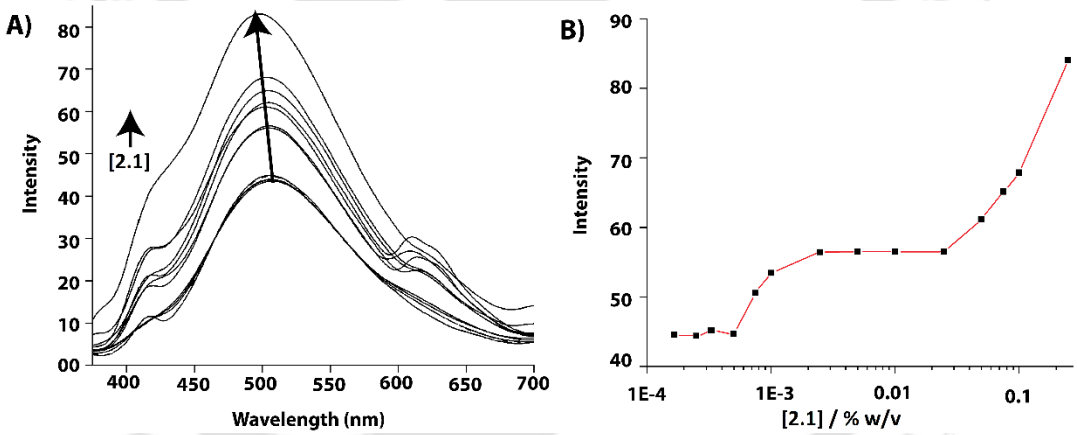

Figure 2.5 A) Fluorescence spectra of ANS (1×10^{-5} M) with increasing concentration of **2.1** in 1:1 water/acetonitrile at RT (λ_{ex} = 365 nm). B) Dependence of fluorescence intensity of ANS on gelator concentration.

Further to understand the role of hydrophobicity, the emission spectra of pyrene in the aqueous solution of **2.1** were recorded. The overlaid spectra in figure 2.6 showed an initial decrease in intensity of the pyrene emission peaks with increase in concentration of the gelator. Above 0.025 % w/v concentration of **2.1** a red shifted peak at 470 nm appeared along with the distortion of the original fine emission structure of pyrene. The intensity of the peak at 470 nm increased with concomitant increase in the gelator concentration. This new peak at 470 nm signifies the appearance of the pyrene excimer.[177] With increase in concentration of the **2.1**, micellar aggregate forms. Further increase in concentration probably leads to the hierarchical self-assembly process and fiber formation starts. The probe molecules may get incorporated in these fibers and hence the local concentration increases. With increase in the

fiber concentration, the local concentration of pyrene molecules reaches a value where they could dimerize to show the excimer band.[44] These data along with the chain length dependency of the gelation process clearly signifies the role of hydrophobicity in the self-assembly process.

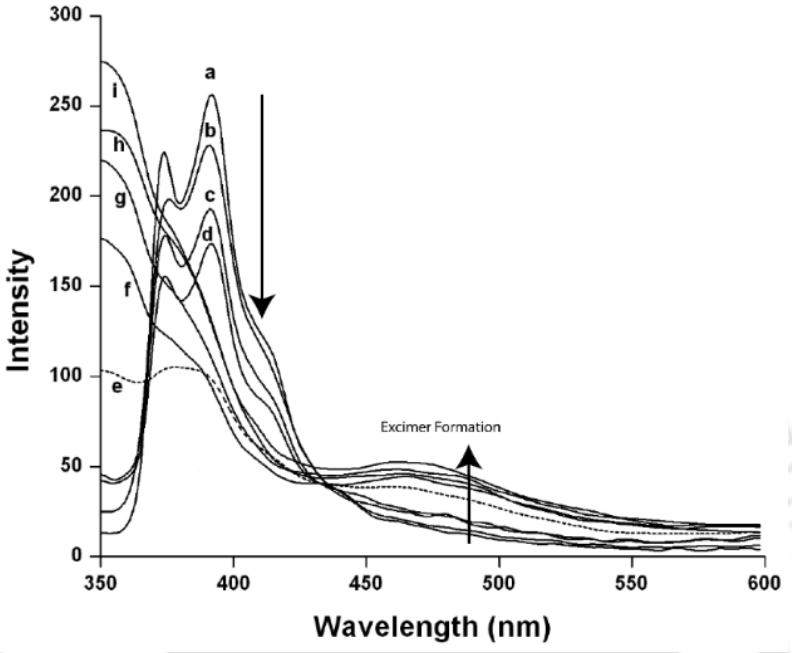

Figure 2.6 Luminescence spectra of pyrene (1×10^{-7} M) in aqueous solutions of various concentration of **2.1** at RT (λ_{ex} =337 nm). [**2.1**] (% w/v): a) 0.0025; b) 0.005; c) 0.0075; d) 0.01; e) 0.025; f) 0.05; g) 0.075; h) 0.1; i) 0.25.

The presence of amide *NH* in the molecule along with the carbonyl oxygen allows the possibility of hydrogen bonding among the gelator molecules during the self-aggregation process. To confirm the role of the amide *NH*, another molecule (**2.4**, scheme 2.1) was synthesized where the hydrogen bond donor *"NH"* is replaced by an ester linkage. In accord to our expectation, this analogue precipitated from the warm solution upon cooling to room temperature even at a concentration of 0.05 % w/v. The presence of the amide group facilitates the hydrogen bonding process with the neighboring molecules via *NH* in case of **2.1**. The absence of such hydrogen bond donor in **2.4** makes it unsuccessful for the self-aggregation process. The involvement of the hydrogen bonds is also prominent from the IR spectra (Figure 2.7) of the powder gelator and the lyophilized hydrogel. A unique *NH* band, centered at around 3437 cm^{-1}, was observed for solid compound **2.1**, which is typically involved in hydrogen bonding interactions. In the xerogel, the peak shifted to 3395 cm^{-1}, which indicates a greater extent of hydrogen bonding interactions. The carbonyl peaks of the carbamate and the amide appeared at 1696 cm^{-1} and 1643 cm^{-1} respectively in the powder gelator and both were shifted to a lower wavenumber upon gelation (1676 cm^{-1} and 1626 cm^{-1} respectively). The shift in the peak positions clearly point out the involvement of the hydrogen bonding by both carbonyl groups.

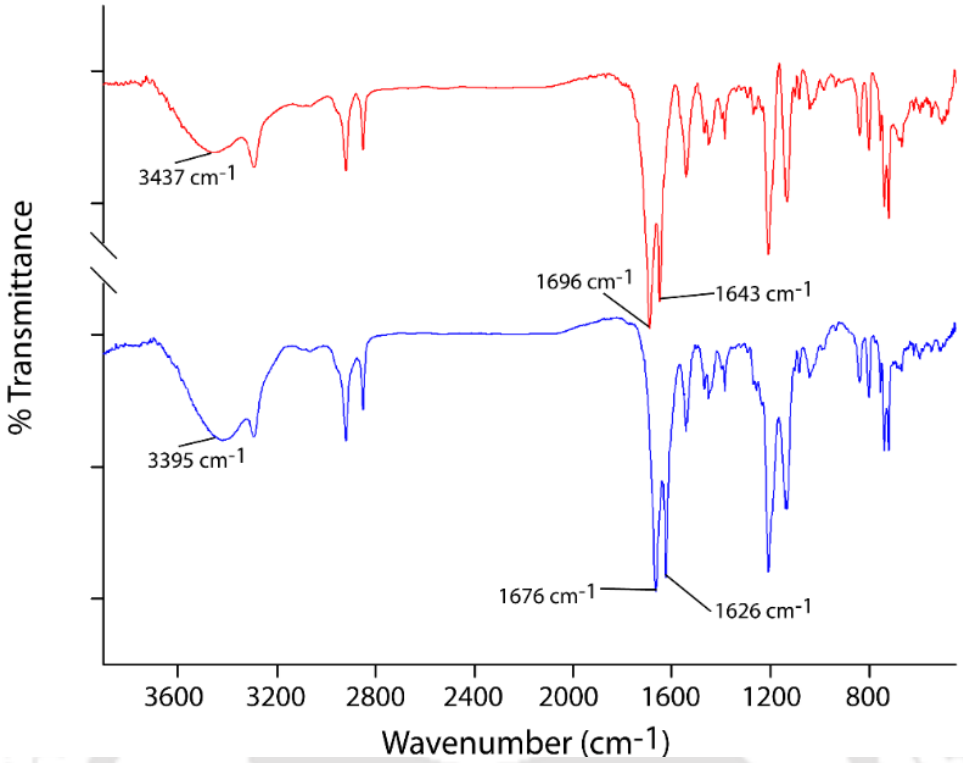

Figure 2.7 IR spectra of the powder gelator **2.1** (Red) and the lyophilized 1 % w/v gel of **2.1** in plain water (Blue).

The overlaid spectra of the temperature dependent ^{1}H NMR of 1 % w/v **2.1** in D_2O shows a downfield shift of the aromatic proton signals with increase in temperature (Figure 2.8A). At lower temperature the system remains in the gel state which involves the interaction between the aromatic rings of neighboring molecules. At elevated temperature, the system gets enough heat to break the aromatic stacks and thus the protons from the π–rings shift downfield.[44]

The presence of the stacking can be further understood from the concentration dependent fluorescence spectra of the gelator (Figure 2.8B). At a lower concentration the emission spectra followed the pattern of 'Fmoc' group showing two peaks at 307 and 311 nm along with a broad phosphorescence peak centered at 458 nm. Initial increase in the concentration of the gelator led to the increase in the intensity of the fluorescence peaks whereas the phosphorescence peak diminished.[178,179] At 0.05 % w/v concentration, the well-structured emission abated and a red shifted structure-less peak with single emission maxima at 315 nm appeared, which further red shifted to 326 nm with increase in concentration. Along with the red shift, another peak appeared at 425 nm. The red shifted peak signifies the stacking of the fluorenyl groups in the system. The extra emission band at 425 nm could be attributed to the excited dimer (excimer) emission.[177,179] Interestingly, the red shift of the emission band started at a concentration of 0.05 % w/v which is close to the concentration at which the pyrene-excimer

started appearing (0.025% w/v) and could be attributed to the commencement of the hierarchical self-assembly and presumably the fibers start forming at this concentration.[44,179]

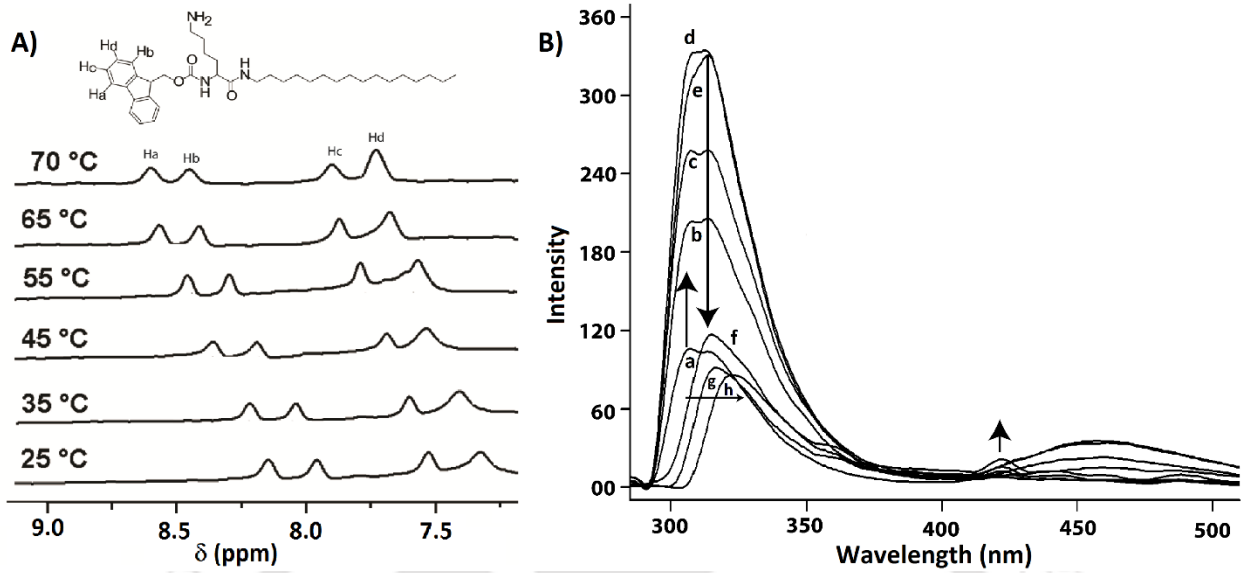

Figure 2.8 A) Temperature dependent shifts of the aromatic protons of **2.1** in the ^{1}H NMR spectra of the hydrogel of **2.1** in D_2O. B) Fluorescence spectra of **2.1** in plain water at RT (λ_{ex} = 265 nm). [**2.1**] (% w/v): a) 0.0001; b) 0.0005; c) 0.001; d) 0.005; e) 0.01; f) 0.05; g) 0.1; h) 0.5.

The concentration dependent circular dichroism spectra of **2.1** in water reveal some useful information on the molecular arrangement of **2.1** in the hydrogel (Figure 2.9A). The negative cotton effect at 220 nm and 264 nm indicate the super-helical arrangements of the amino acid residue which influence the helical orientation of the fluorenyl groups.[179,180] At a higher concentration (0.5 % w/v), both the bands disappeared and three new bands appeared at 238 nm, 288 nm and 305 nm. The peaks at 288 nm and 305 nm are the characteristic signature of 'Fmoc' containing gelator but the red shifted peak at 238 nm is unprecedented in such systems.[179,180] A plausible explanation could be the formation of the fibers at this concentration. This is also supported by the formation of excimer in case of pyrene and the fluorenyl moiety around this concentration. As the network formation has started, the chirality generated by the system is now quite different than its precursor assembly. Nevertheless this phenomenon could be addressed only after detailed study in future. The CD spectra of similar experiment with **2.5** (*i.e.* D analog of the gelator) provided exactly the mirror images (Figure 2.9B) of what observed in case of compound **2.1**, which indicates the influence of the supramolecular chirality and presence of superhelical arrangement in opposite direction in case of the D analog.

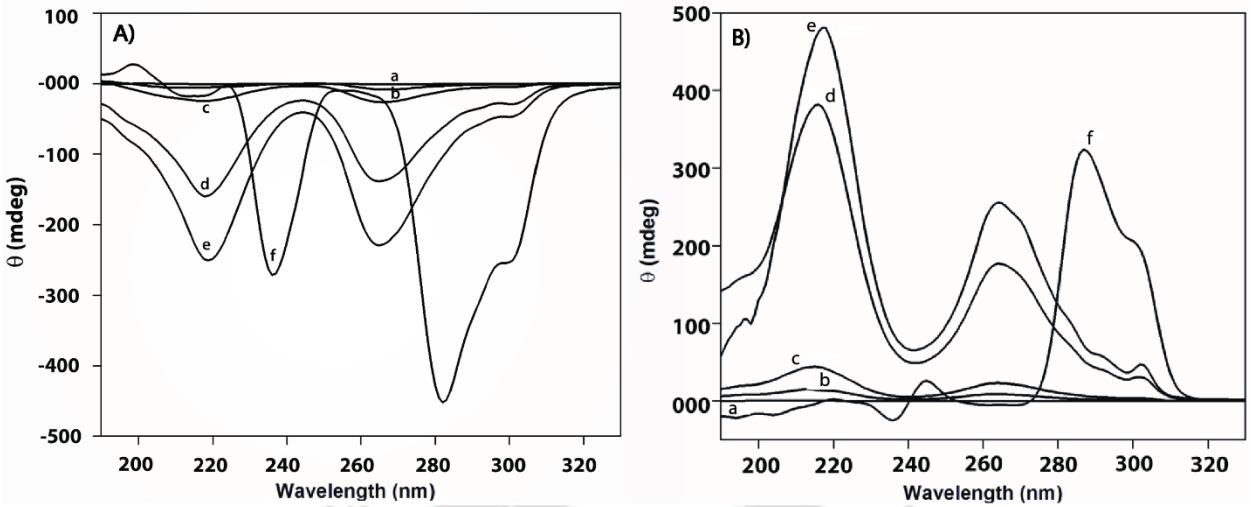

Figure 2.9 A) CD spectra of **2.1** and B) CD spectra of **2.5** in plain water at RT. [**2.1**, **2.5**] (% w/v): a) 0.001; b) 0.005; c) 0.01; d) 0.05; e) 0.1; f) 0.5.

The FESEM images of the dried hydrogel of **2.1** shows network of left-handed helical nano-fibers of 3-5 μm length (Figure 2.10). These long fibers are having a diameter of 30-40 nm. Similarly right handed helical fibers were found in case of the D-analogue **2.5**. Similar helical fibers were also observed in the AFM image of the hydrogel (Figure 2.11). The helicity of the fibers are generated from the presence of the lysine residue and as observed in the circular dichroism, it induces the helical orientation at the fluorenyl moiety which subsequently gets transferred into supramolecular helicity. Interestingly when equimolar mixture of **2.1** and **2.5** was investigated for the gelation, no such aggregation was observed and the FESEM image of the dried sample showed no specific structural element (data not shown).The concentration dependent FESEM images show interesting features (Figure 2.10C-F). At a sub-gel concentration (0.1 % w/v), thin fibers were observed but no helical nature was detected (Figure 2.10C). When the concentration was increased to 3 % w/v, the fibers were much thicker than that at MGC (Figure 2.10D). Interestingly figure 2.10E shows a probable overlap of two thinner fibers which depicts the hierarchical assembly process involved. The FESEM images of all the mixed solvent gels show different types of fibrous networks. Similarly, the helical nature was found to be intact in the methanol and acetonitrile systems whereas in case of DMSO, DMF, and dioxane normal fibers were observed (Figure 2.12).

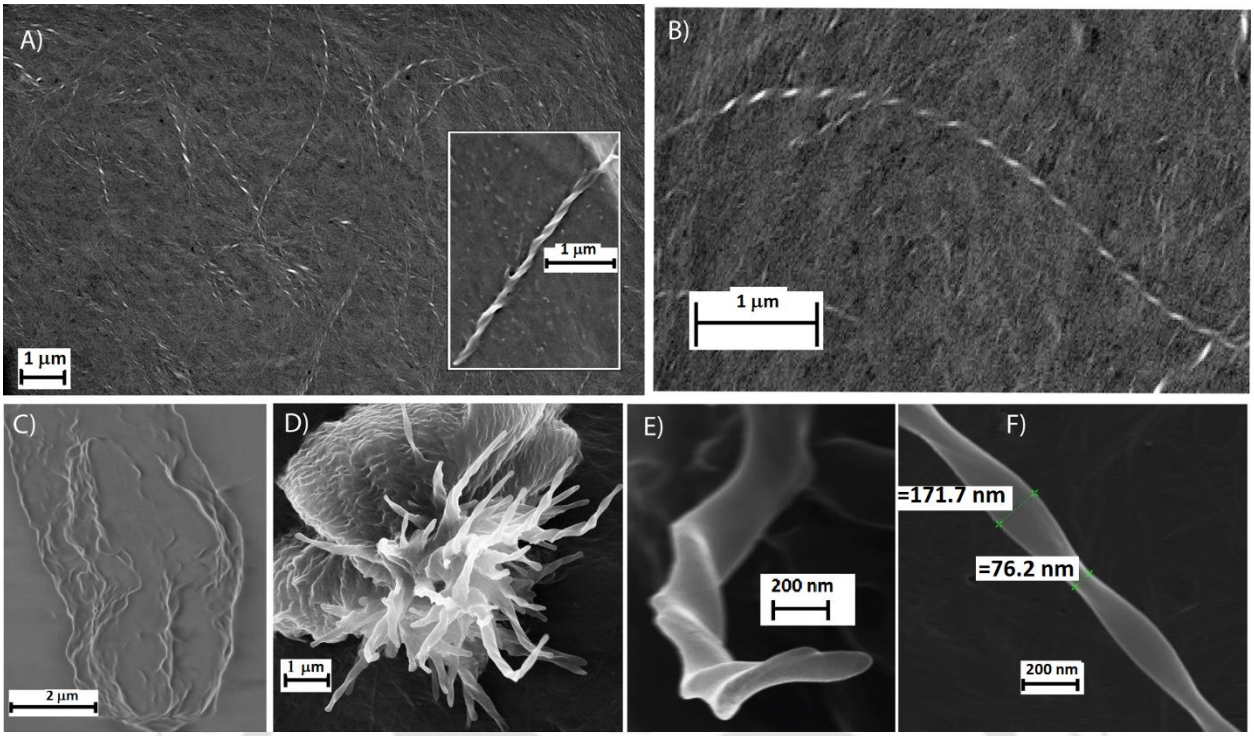

Figure 2.10 FESEM images of hydrogels of **2.1** in plain water A) (1% w/v) showing left-handed helical fibers. Inset: right handed helical fibers obtained from hydrogel of **2.5** (1% w/v) in plain water. B) Magnified view of one fiber from A). C) At 0.1% w/v. (D–F). At 3% w/v. E) Closer view of one of the helical fibers showing the hierarchical overlapping of two fibers to generate a thicker fiber. F) Closer view of one such helical fibers showing the different diameters of the fiber at different positions owing to the helical nature.

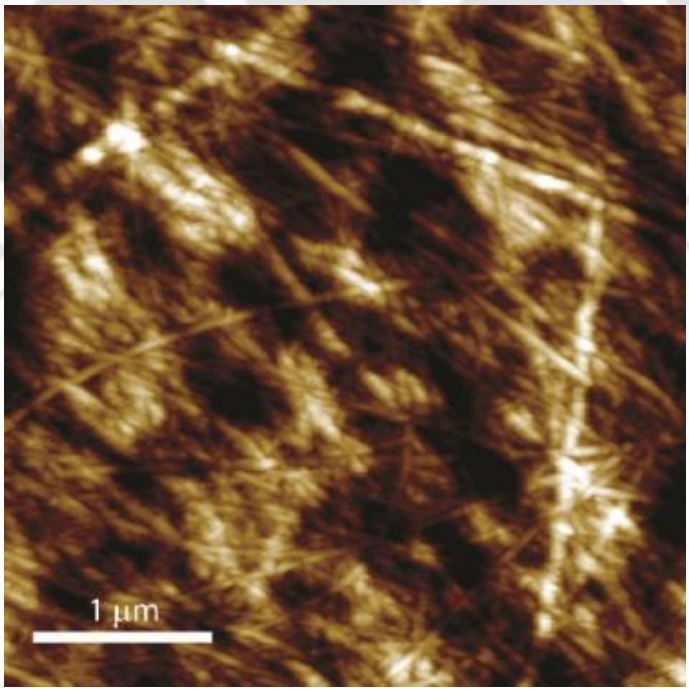

Figure 2.11 AFM image of the 1 % w/v hydrogel of **2.1**

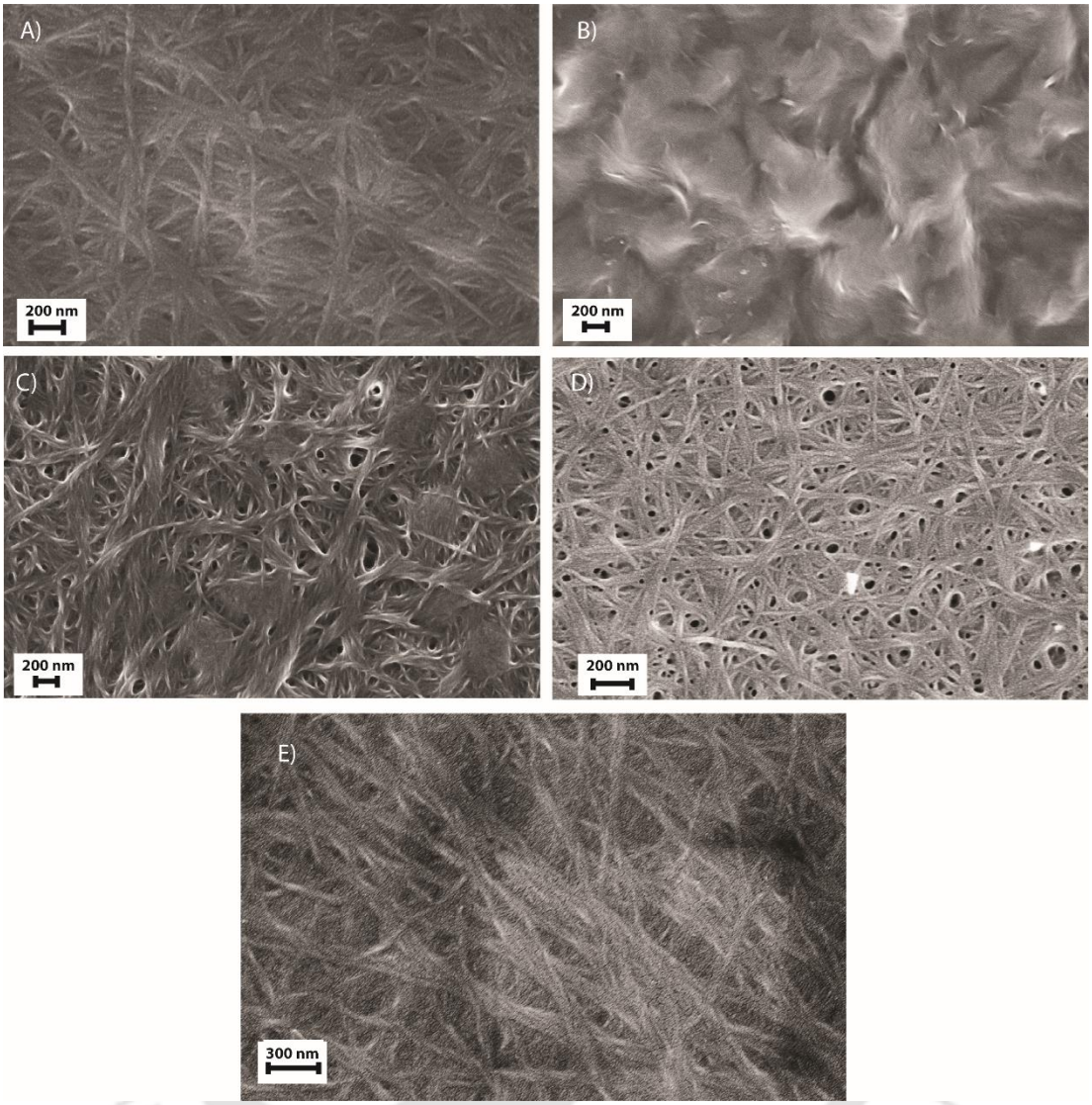

Figure 2.12 FESEM image of the dried gel of **2.1** (1 % w/v) in A) 30% water in DMSO; B) 30% water in DMF; C) 50% water in methanol; D) 45% water in dioxane; E) 50% water in acetonitrile.

Results of the spectroscopic and microscopic experiments lead to the conclusion that the PA self-assemble in water in a hierarchical fashion. The concentration dependent formation of bilayers to fibers and finally to the fibrous network are assisted by hydrogen bonding, π–π stacking and hydrophobic interactions as expected for the designed molecule. Based on these inferences a plausible mechanism is proposed for the self-assembly of PA **2.1** in water (Figure 2.13). The helicity of the fibers are generated owing to the supramolecular helicity induced by the chiral lysine residue at the fluorenyl groups in the stacking process and hence with elongation of the fiber, it twists along the long axis of the fiber. The presence of opposite handed helical fibers in the hydrogels of the two enantiomers as well as the observation of no gelation in case of mixture of the enantiomers strongly supports this hypothesis.

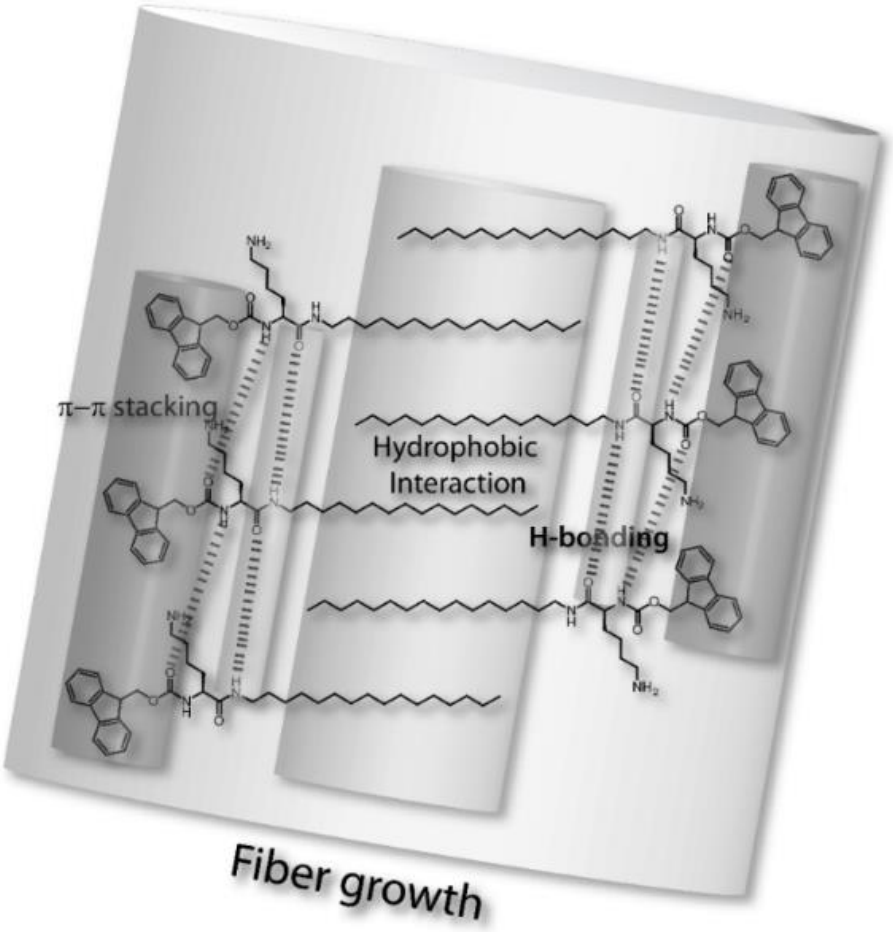

Figure 2.13 Schematic representation of the possible fiber formation mechanism in the hydrogel of **2.1**.

2.3 Conclusions

The work has successfully demonstrated the rational design and hydrogelation of a simple lysine based peptide amphiphile. The hydrogelation is responsive to the change in pH and the molecule is also able to immobilize a variety of aqueous mixtures of organic solvents. Structural elucidation of the hydrogel has revealed the presence of hydrophobic interaction, π–π stacking and H-bonding in the self-assembly process. The chirality in the molecule has influenced the formation of helical nano-fibers with appropriate handedness.

2.4 Experimental Section

2.4.1 General

All the chemicals and solvents were purchased from Sigma-Aldrich or Spectrochem, India. ^{1}H NMR spectra were recorded by using an Oxford AS400 (Varian) spectrometer. ESI-MS was performed by using

a Q-tof-Micro Quadrupole mass spectrophotometer (Micromass). SEM, FESEM, AFM and TEM images were taken using LEO1430VP, SIGMA ZEISS, Agilent 5500, and JEOL JEM-2100 microscopes respectively. Emission spectra were recorded by using an Agilent Cary-Eclipse luminescence spectrometer. CD experiments were performed by using a Jasco J-600C spectropolarimeter. Rheology was measured using Paar Physica Modular Compact Rheometer (MCR 301, Austria). IR spectra and DSC were recorded on Nicolet is10 from Thermoscientific and Q-20 from TA instruments respectively.

2.4.2 Synthesis of Compounds

All the compounds were synthesized using the same synthetic protocol. Typically, 1 eq. of (L/D) Fmoc-Lys(Boc)OH was coupled with the corresponding amine or alcohol (1.2 eq.) in dichloromethane (DCM) using 1.2 eq. HBTU, 2.4 eq. triethylamine and 1.2 eq. HOBT for 24h. The reaction mixture was then washed with brine and the organic layer was dried over anhydrous sodium sulfate. The organic layer was filtered and concentrated on a rotory evaporator to get the crude coupled product. It was then subjected to Boc-deprotection by trifluoroacetic acid (TFA, 4 equiv.) in dry DCM. After 2 h of stirring, solvents were removed by using a rotary evaporator and the mixture was taken up in ethyl acetate (EtOAc). The EtOAc phase was washed thoroughly with aqueous 10% sodium carbonate solution followed by brine to neutrality. The organic phase was dried over anhydrous sodium sulfate and concentrated. The crude mixture was subjected to column chromatography on a 60-120 mesh silica gel column using methanol/dichloromethane as the eluent.

2.4.3 Characterization of the synthesized compounds

L-(5-Amino-1-hexadecylcarbamoyl-pentyl)-carbamic acid 9H-fluoren-9-ylmethyl ester (2.1): Yield: 42% (after two steps); R_f = 0.58 (10% MeOH in DCM);^{1}H NMR (400 MHz, $CDCl_3$): δ = 0.83-0.87 (t, J = 7.2 Hz, 3H), 1.23 (br, 28H), 1.37 (br, 2H), 1.59 (br, 2H), 1.81 (br, 2H), 2.95 (br, 2H), 3.20 (br, 2H), 4.12 (m, 1H), 4.42 (br, 1H), 4.66 (br, 2H), 7.28 (t, J = 7.6 Hz, 2H), 7.37 (t, J = 7.6 Hz, 2H), 7.55 (d, J = 7.6 Hz, 2H), 7.75 (d, J = 7.6 Hz, 2H) ppm; ^{13}C NMR (400 MHz, $CDCl_3$): δ = 172.14, 156.81, 143.86, 141.86, 127.88, 127.23, 127.11, 120.07, 67.30, 54.77, 54.76, 45.95, 39.84, 32.08, 31.98, 29.88-29.48 (m), 27.10, 22.85, 22.44, 14.28 ppm; MS (ESI): *m/z* calcd. for $C_{37}H_{57}N_3O_3$: 591.44; found 592.40 [M+H$^+$].

(5-Amino-1-tetradecylcarbamoyl-pentyl)-carbamic acid 9H-fluoren-9-ylmethyl ester (2.2): Yield: 43% (after two steps); R_f = 0.54 (10% MeOH in DCM);^{1}H NMR (400 MHz, $CDCl_3$): δ = 0.83-0.86 (t, J = 7.2 Hz, 3H), 1.22 (br, 24H), 1.35 (br, 2H), 1.57 (br, 2H), 1.84 (br, 2H), 2.93 (br, 2H), 3.24 (br, 2H), 4.18 (m, 1H), 4.40 (br, 1H), 4.71 (br, 2H), 7.22 (t, J = 7.6 Hz, 2H), 7.33 (t, J = 7.6 Hz, 2H), 7.51 (d, J = 7.6 Hz, 2H), 7.70 (d, J = 7.6 Hz, 2H) ppm; ^{13}C NMR (400 MHz, $CDCl_3$): δ = 172.11, 156.84, 143.56, 141.78, 127.46, 127.25, 127.11,

125.43, 67.35, 54.97, 54.66, 45.05, 39.24, 32.48, 31.65, 29.63-29.35 (m), 27.13, 22.43, 22.24, 14.14 ppm; MS (ESI): *m/z* calcd. for $C_{35}H_{53}N_3O_3$: 563.40; found 564.38 [M+H$^+$].

(5-Amino-1-dodecylcarbamoyl-pentyl)-carbamic acid 9H-fluoren-9-ylmethyl ester (2.3): Yield: 46% (after two steps); R_f = 0.50 (10% MeOH in DCM); ^{1}H NMR (400 MHz, $CDCl_3$): δ = 0.827-0.861 (t, J = 7.2 Hz, 3H), 1.168 (br, 20H), 1.38 (br, 2H), 1.57 (br, 2H), 1.69 (br, 2H), 2.91 (br, 2H), 3.11 (br, 2H), 4.09 (m, 1H), 4.27 (br, 1H), 4.70 (br, 2H), 7.24 (t, J = 7.6 Hz, 2H), 7.33 (t, J = 7.6 Hz, 2H), 7.51 (d, J = 7.6 Hz, 2H), 7.70 (d, J = 7.6 Hz, 2H) ppm; ^{13}C NMR (400 MHz, $CDCl_3$): δ = 172.00, 156.88, 143.87, 141.43, 127.97, 127.29, 127.09, 120.18, 67.43, 54.66, 54.56, 45.67, 39.32, 32.01, 31.78, 29.55-29.68 (m), 27.13, 22.88, 22.35, 14.31 ppm; MS (ESI): *m/z* calcd. for $C_{33}H_{49}N_3O_3$: 535.37; found 536.23 [M+H$^+$].

6-Amino-2-(9H-fluoren-9-ylmethoxycarbonylamino)-hexanoic acid hexadecyl ester (2.4): Yield: 54% (after two steps); R_f = 0.55 (10% MeOH in DCM); ^{1}H NMR (400 MHz, $CDCl_3$): δ = 0.83-0.87 (t, J = 7.2 Hz, 3H), 1.18 (br, 28H), 1.36 (br, 2H), 1.56 (br, 2H), 1.73 (br, 2H), 3.09 (br, 2H), 3.20 (br, 2H), 4.09 (m, 1H), 4.27 (br, 1H), 4.70 (br, 2H), 7.24 (t, J = 7.6 Hz, 2H), 7.33 (t, J = 7.6 Hz, 2H), 7.51 (d, J = 7.6 Hz, 2H), 7.70 (d, J = 7.6 Hz, 2H) ppm; ^{13}C NMR (400 MHz, $CDCl_3$): δ = 172.00, 156.88, 143.87, 141.43, 127.97, 127.29, 127.09, 120.18, 67.43, 54.66, 54.56, 45.67, 39.32, 32.01, 31.78, 29.55-29.68 (m), 27.13, 22.88, 22.35, 14.31 ppm; MS (ESI): *m/z* calcd. for $C_{37}H_{56}N_2O_4$: 592.42; found 593.45 [M+H$^+$].

D-(5-Amino-1-hexadecylcarbamoyl-pentyl)-carbamic acid 9H-fluoren-9-ylmethyl ester (2.5): Yield: 38% (after two steps); R_f = 0.58 (10% MeOH in DCM); ^{1}H NMR (400 MHz, $CDCl_3$): δ = 0.84-0.87 (t, J = 7.2 Hz, 3H), 1.21 (br, 28H), 1.36 (br, 2H), 1.57 (br, 2H), 1.81 (br, 2H), 2.95 (br, 2H), 3.20 (br, 2H), 4.12 (m, 1H), 4.42 (br, 1H), 4.66 (br, 2H), 7.27 (t, J = 7.6 Hz, 2H), 7.35 (t, J = 7.6 Hz, 2H), 7.51 (d, J = 7.6 Hz, 2H), 7.80 (d, J = 7.6 Hz, 2H) ppm; ^{13}C NMR (400 MHz, $CDCl_3$): δ = 172.21, 156.62, 143.54, 141.46, 127.45, 127.23, 127.01, 120.09, 67.35, 54.74, 54.65, 45.44, 39.64, 32.18, 31.78, 29.68-29.28 (m), 27.12, 22.65, 22.34, 14.29 ppm; MS (ESI): *m/z* calcd. for $C_{37}H_{57}N_3O_3$: 591.44; found 592.38 [M+H$^+$].

2.4.4 Methods

Preparation of the Hydrogel

In a typical experiment, 10 mg of **2.1** was dissolved in 1 mL of HPLC grade water by slow heating to 60°C in a glass vial with i.d. of 10 mm. The vial was allowed to cool to room temperature without any disturbance. After three hours, an opaque gel was obtained which did not flow downward upon inversion of the glass vial.

Determination of Sol-Gel Transition Temperature (T_g)

T_g was determined using vial inversion method. Typically a capped glass vial with i.d. of 10 mm containing the hydrogel was placed in a thermo-controlled oil bath and the temperature was increased

at 1°C min^{-1} rate. The free flow of the hydrogel was checked by inverting the vial. The temperature at which the gel started flowing down upon inversion was noted. Here, T_g is defined as the temperature (±0.5 °C) at which the hydrogel melts and begins to flow out of the vial. The experiments were performed in duplicate. The T_g of the hydrogel of **2.1** (1 % w/v) was also determined using differential scanning calorimetry (DSC, TA Instruments, Model Q100). Both the heating rate was 10 °C/min over 10 to 68 °C.

Fluorescence Spectroscopy

Fluorescence spectra of both ANS and Pyrene were taken with increase in concentration of the gelator. For Pyrene, the probe was dissolved in water by overnight stirring followed by sonication for 3 h and finally filtered. All the experimental solutions were prepared by using this aqueous solution of pyrene. The fluorescence spectra of these solutions containing varying concentration of the gelator were recorded in the 350-600 nm range (λ_{ex} = 337 nm). In case of ANS, the experiments were carried out in 1:1 water-acetonitrile mixture owing to the haziness of the pure aqueous solutions at higher concentrations. As PA **2.1** forms efficient transparent gel in 1:1 water-acetonitrile mixture, we decided to carry out the experiments in this system. A stock (0.01 M) of ANS was prepared in the solvent mixture (1:1 water-acetonitrile) and 5 μL of the stock was added to the experimental solutions (5 mL) containing varying concentration of the gelator to reach the effective concentration of 1×10^{-5} M. The fluorescence spectra of these solutions containing varying amounts of the gelator were recorded in the 375-700 nm range (λ_{ex} = 365 nm). All the experiments were carried out at room temperature. In case of the fluorescence of the fluorenyl group contained in the gelator molecule, the dependence of the emission spectra was determined for varying concentration of the gelator. The solutions were excited at λ_{ex} = 275 nm and the emission spectra were recorded over the range 285-510 nm. In all fluorescence experiments, mission and excitation slit widths were set at 5 and 10 nm, respectively.

NMR Spectroscopy

^{1}H, ^{13}C spectra were recorded in deuterated Chloroform ($CDCl_3$ at 298 K and processed with standard 1D software. For temperature dependent ^{1}H NMR, heavy water (D_2O) was used.

Circular Dichroism (CD) Spectroscopy

The CD spectra of aqueous solutions of **2.1** at various concentrations were recorded by using a 1.2 mL quartz cuvette of 0.5-mm path length with a Jasco J-600C spectropolarimeter at RT. Spectra were collected at 1-nm intervals and 1-nm bandwidth from 190 to 350 nm with 1-s signal averaging time, with three-times scans for averaging. All spectra were corrected by subtracting the baseline.

Fourier Transformed Infrared (FTIR) Spectroscopy

KBr pellets were prepared using the samples (gelator, lyophilized gel) and the spectra were recorded on a Nicolet is10 spectrometer. The baseline was subtracted from the obtained absorbance intensity in each case.

Rheology

Oscillating rheology was used to quantify the final mechanical properties of the peptide amphiphile hydrogel. For the study, 2 ml of hydrogel was utilized. A 50 mm cone plate with a 1° angle configuration was used and the temperature was set constant at 25 °C. Storage (G′) and loss (G″) moduli were measured at 0.1% strain with true gap 0.097 mm.

SEM, FESEM, and AFM sample preparation

For the hydrogel, a small portion of the gel (various concentrations) was casted on a glass plate and air dried for two days before the experiments.

2.5 NMR and Mass spectra of the synthesized compounds

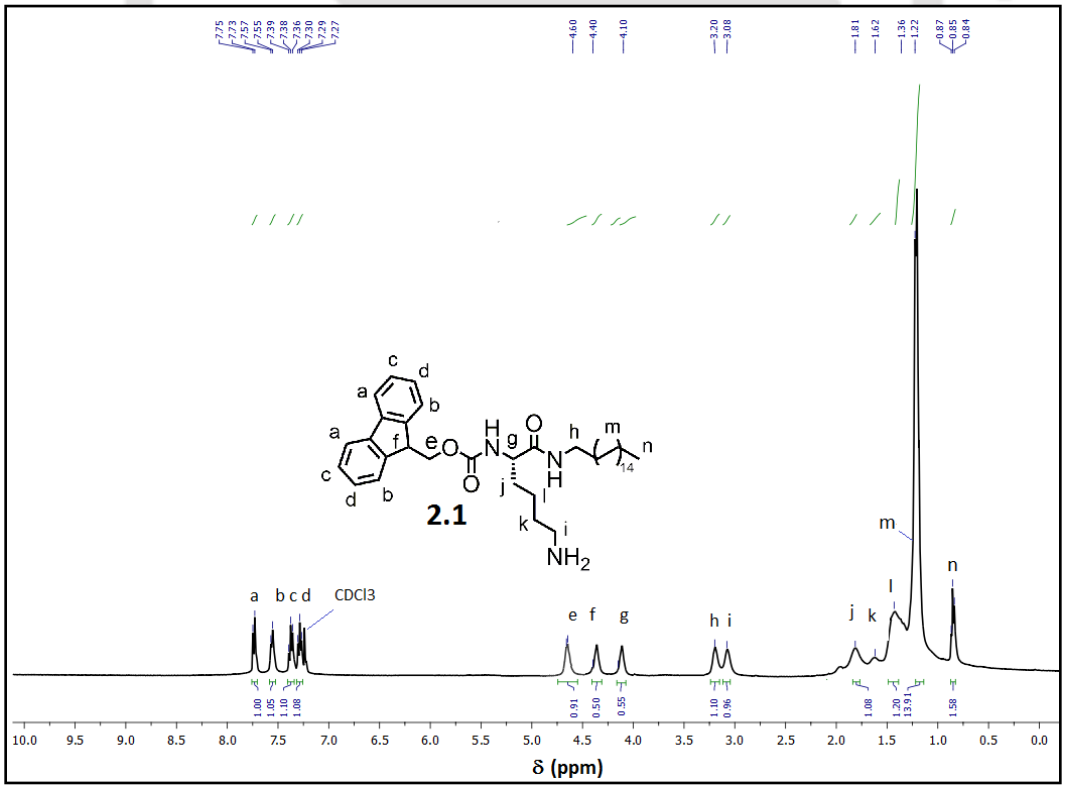

^{1}H NMR spectrum of Compound **2.1**

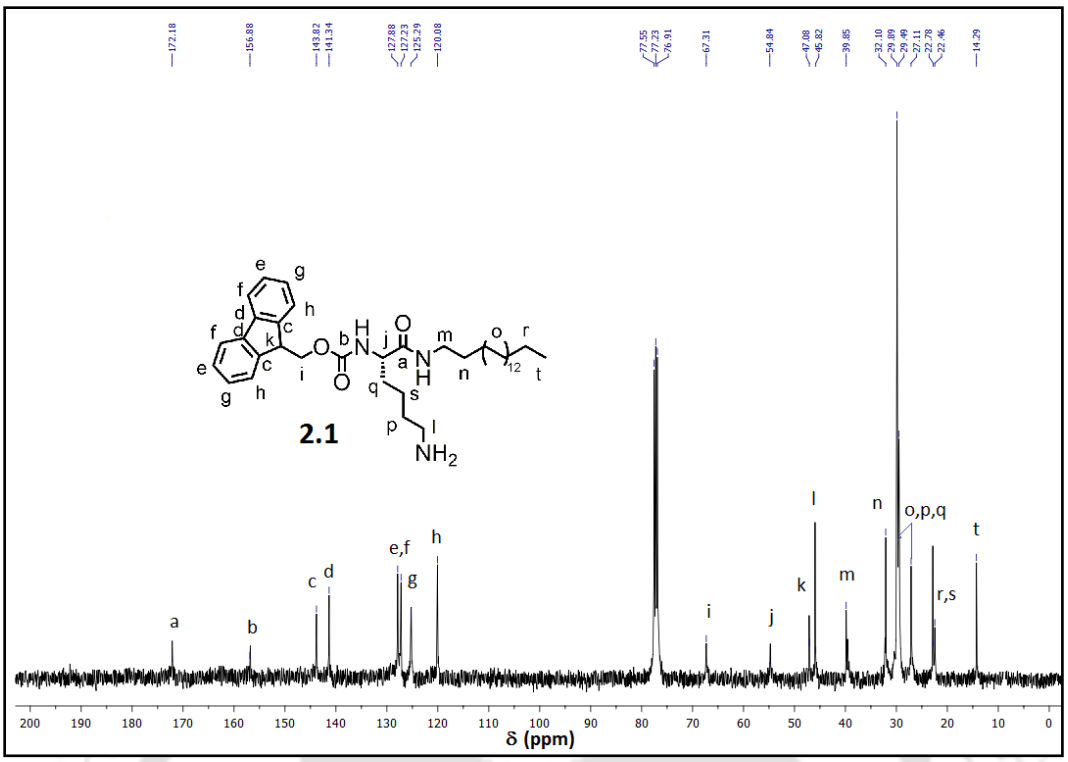

^{13}C NMR spectrum of Compound **2.1**

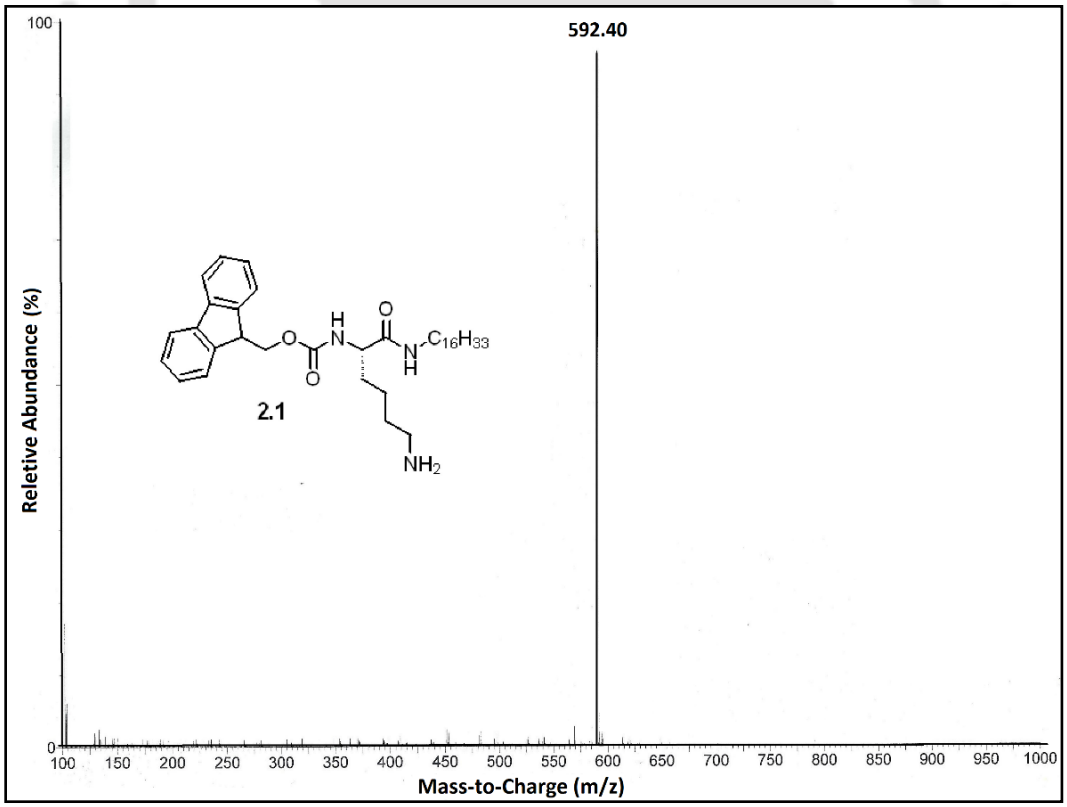

ESI-MS of Compound **2.1**

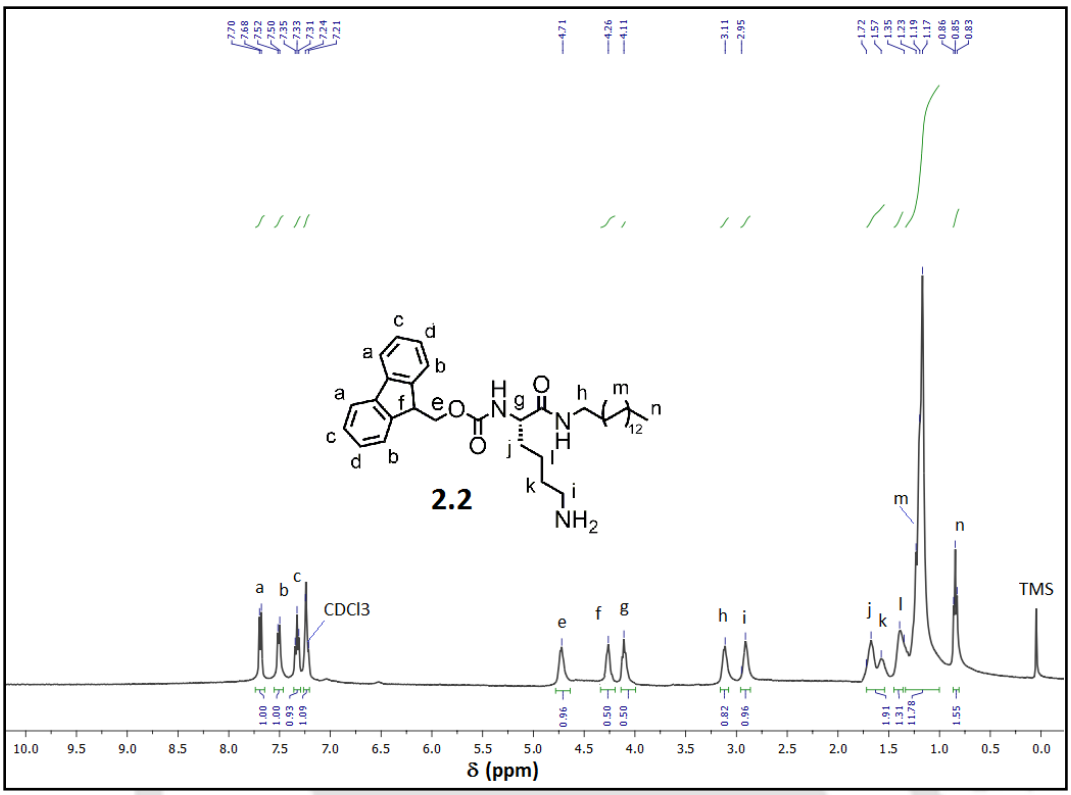

[1]H NMR spectrum of Compound **2.2**

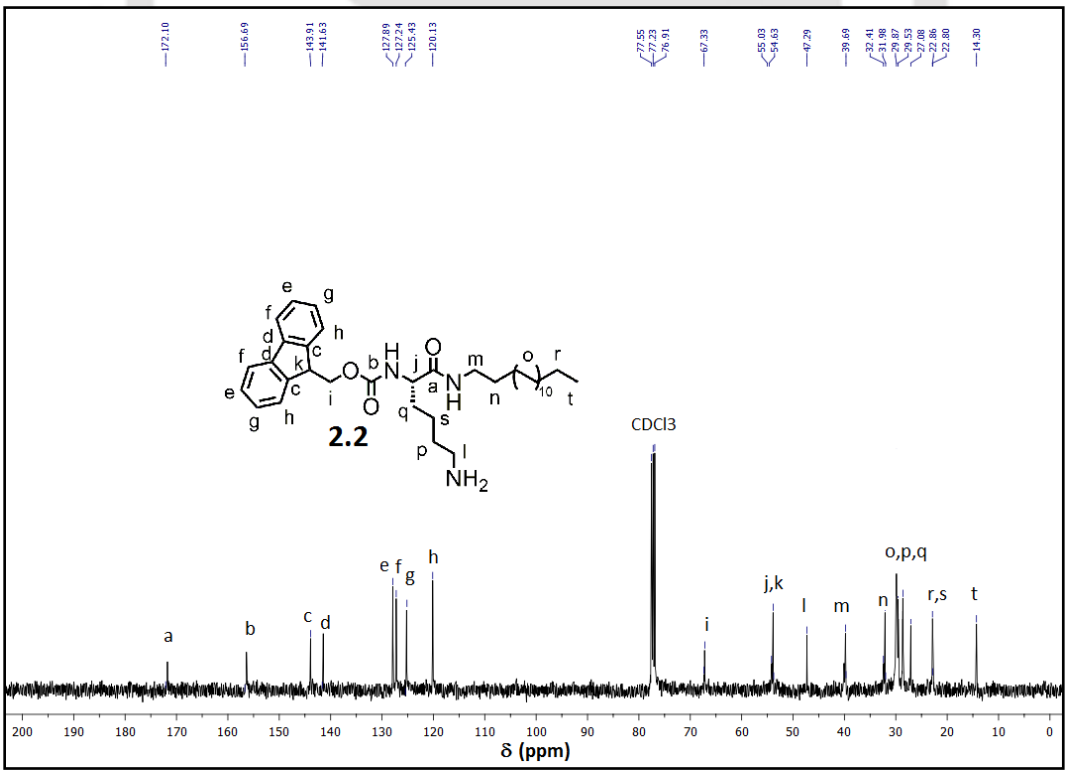

[13]C NMR spectrum of Compound **2.2**

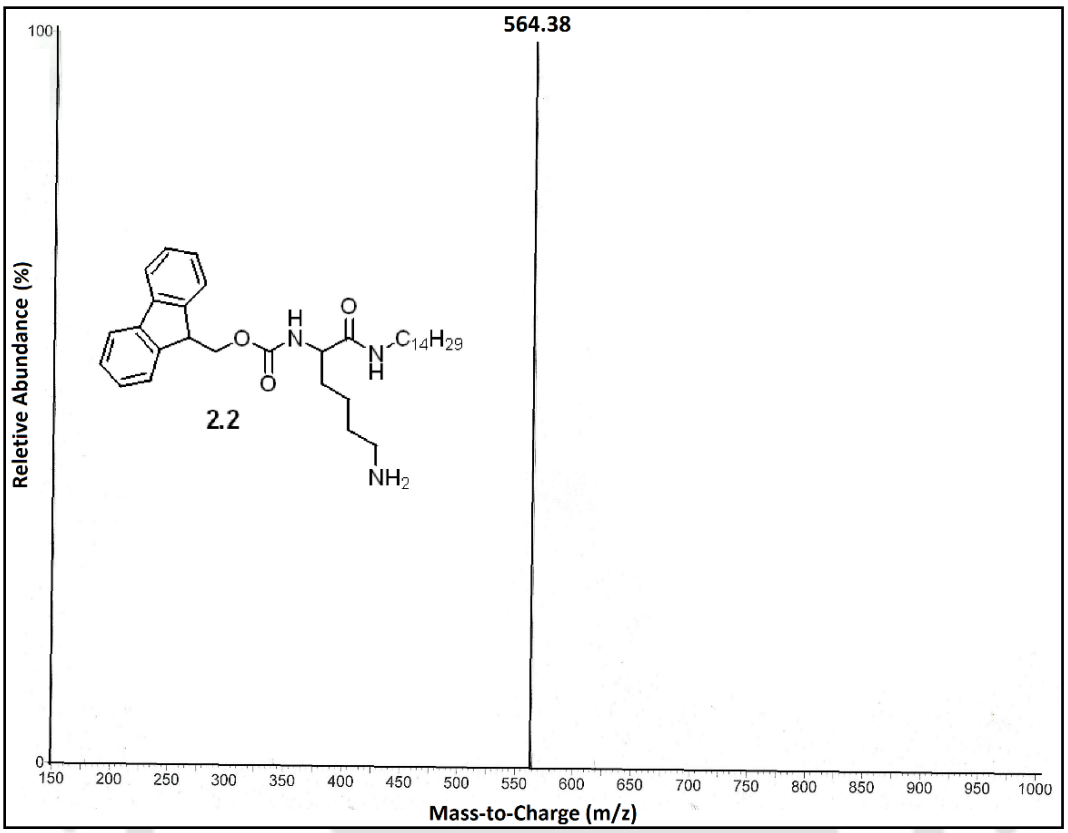

ESI-MS of Compound **2.2**

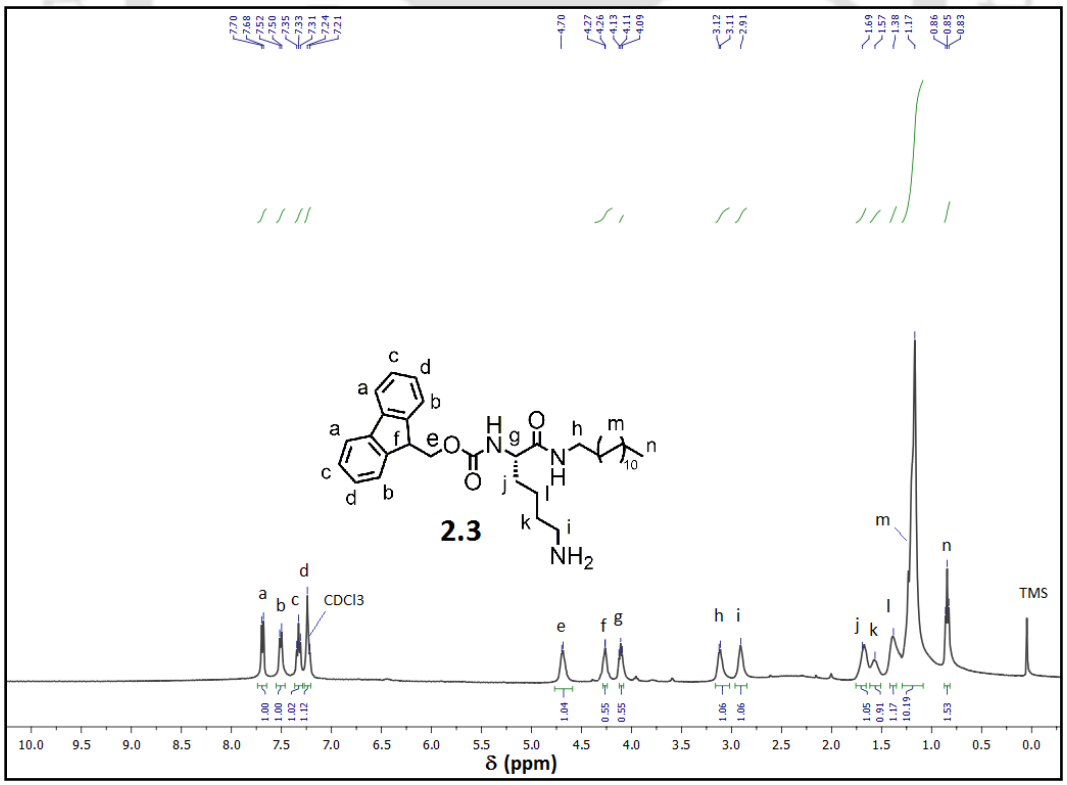

^{1}H NMR spectrum of Compound **2.3**

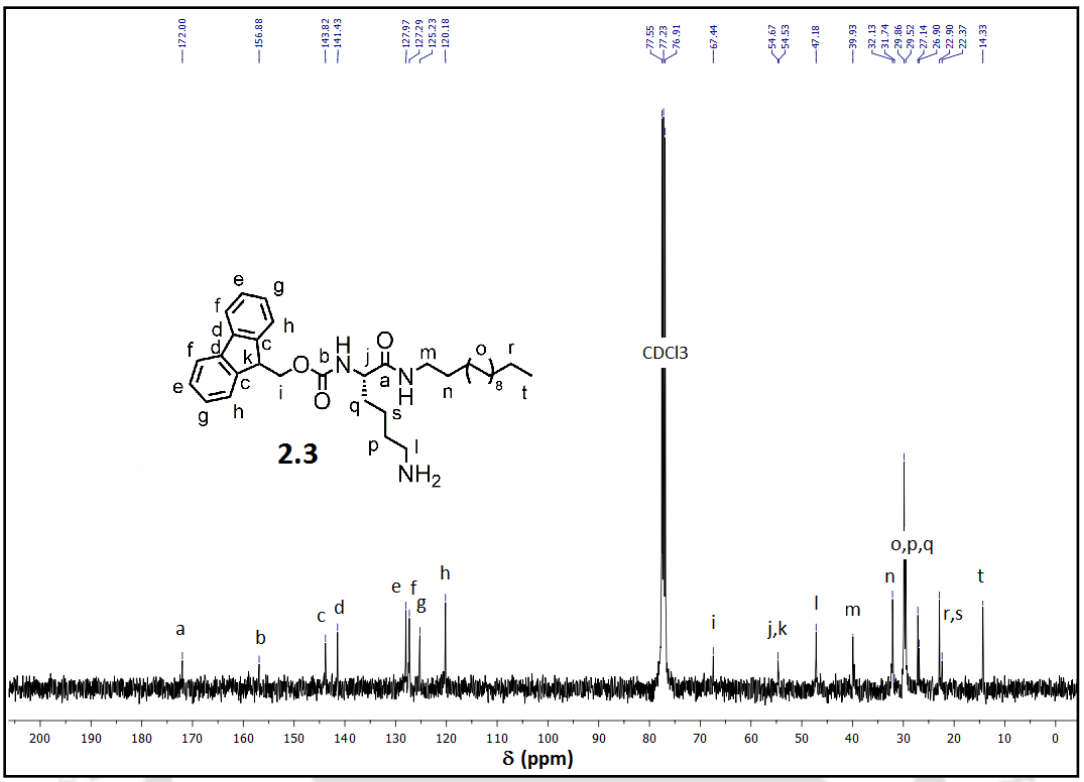

^{13}C NMR spectrum of Compound **2.3**

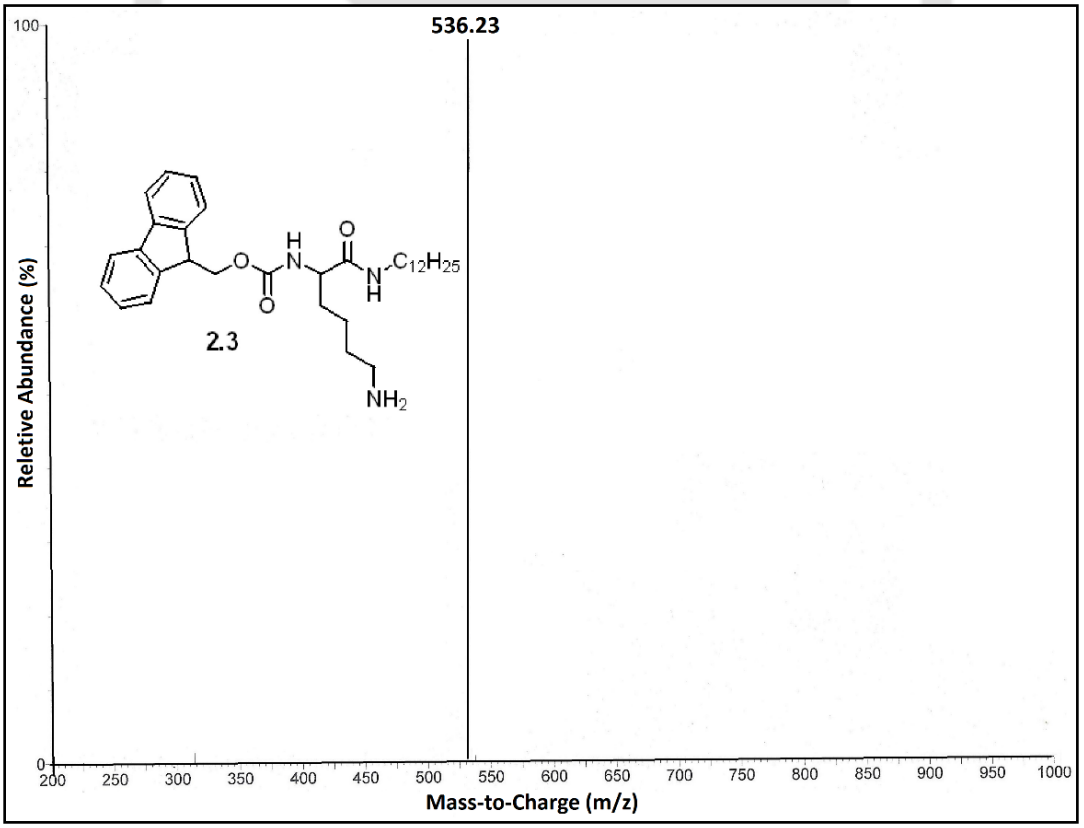

ESI-MS of Compound **2.3**

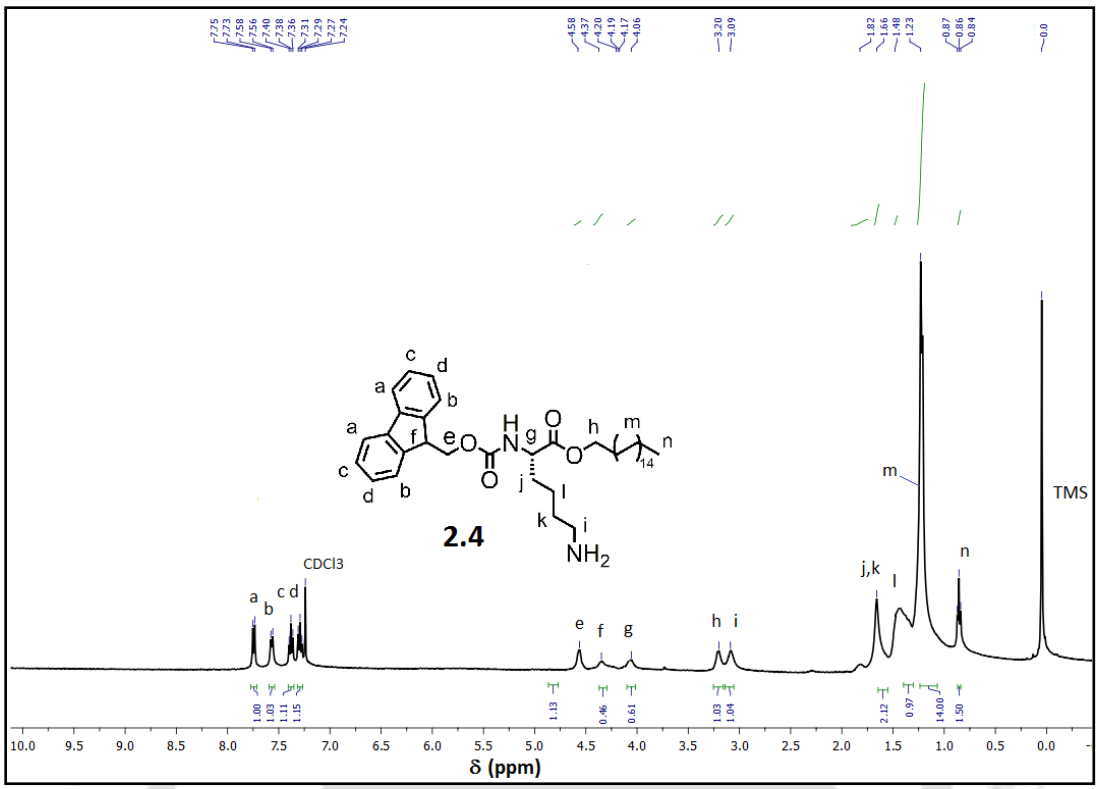

^{1}H NMR spectrum of Compound **2.4**

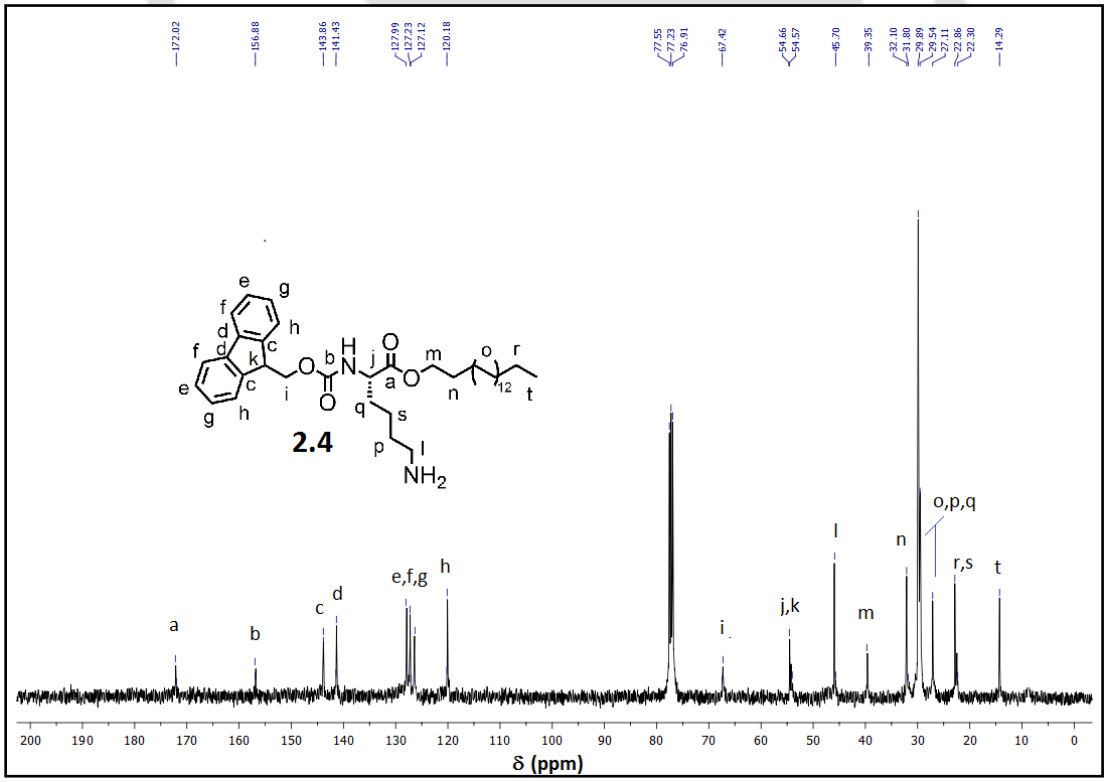

^{13}C NMR spectrum of Compound **2.4**

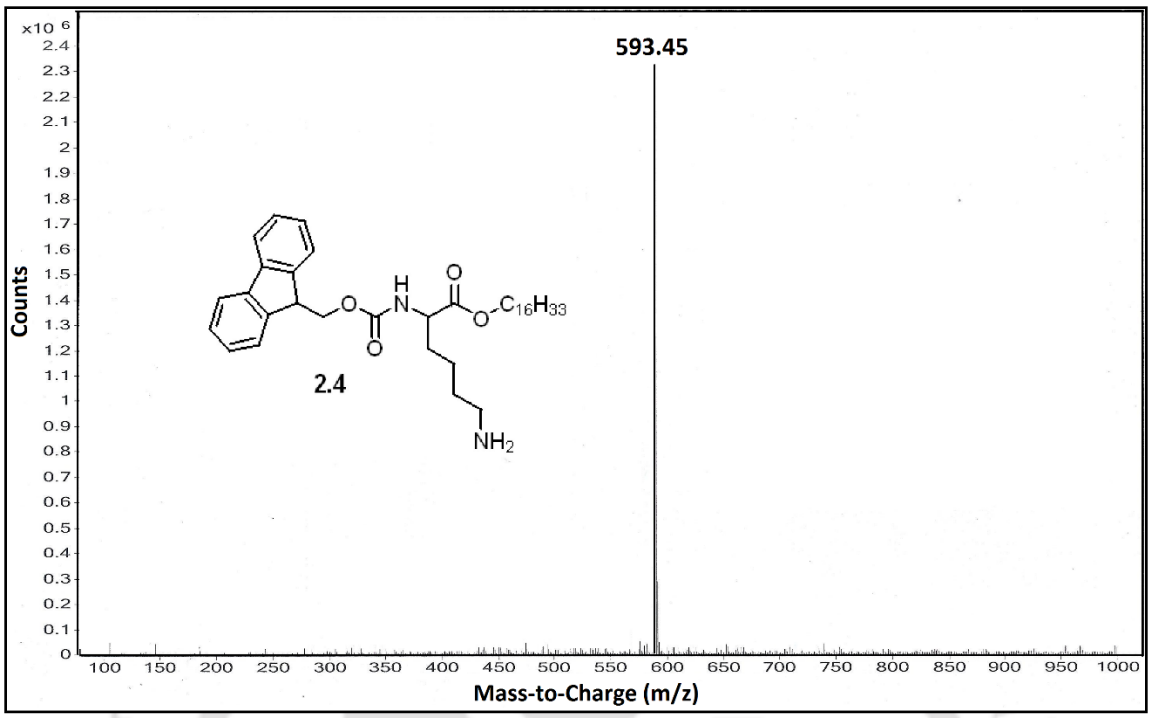

ESI-MS of Compound **2.4**

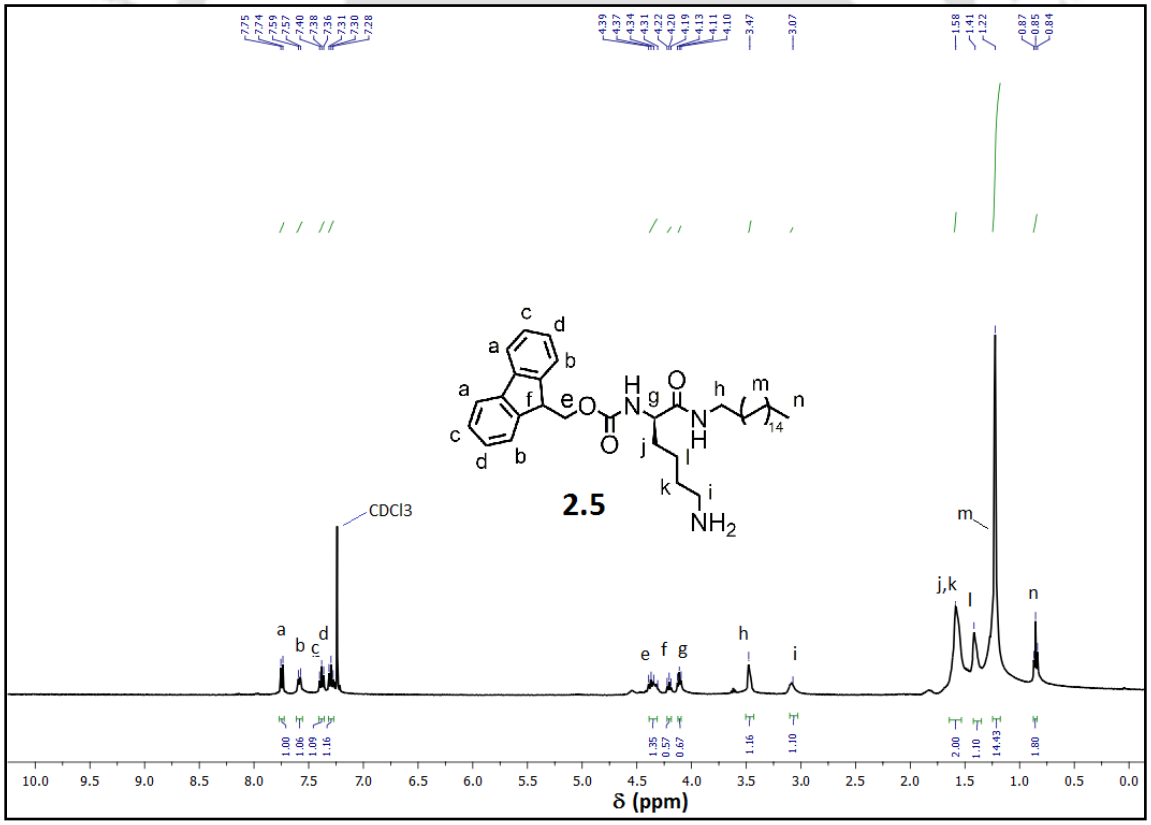

^{1}H NMR spectrum of Compound **2.5**

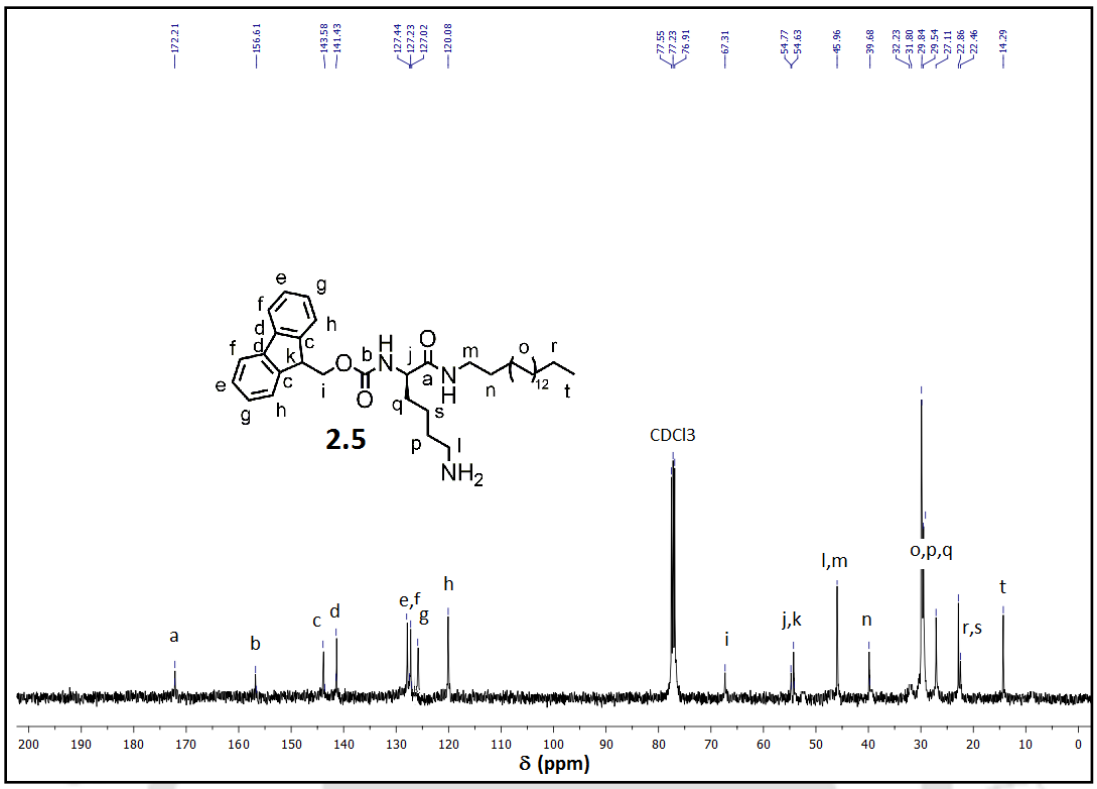

^{13}C NMR spectrum of Compound **2.5**

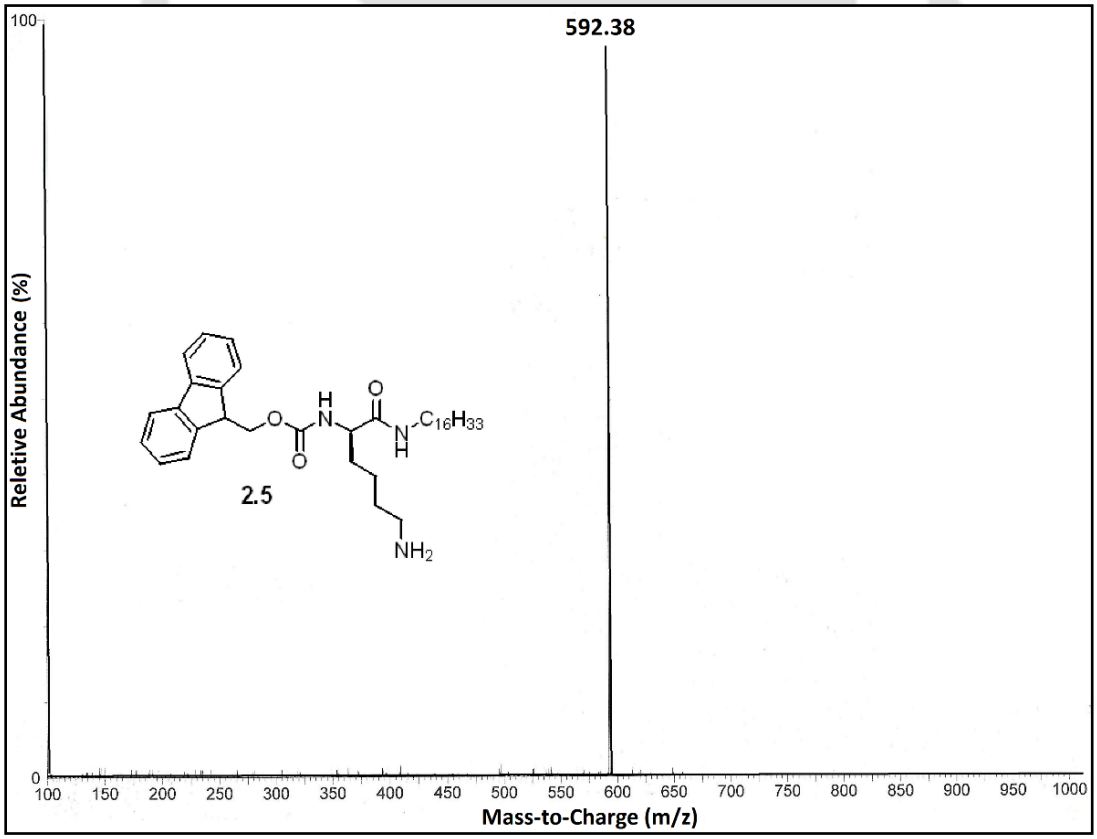

ESI-MS of Compound **2.5**

Chapter 3

An Amino Acid-Dimer Based Redox Active Supramolecular Polymer using Host Guest Chemistry of Cucurbit[8]uril

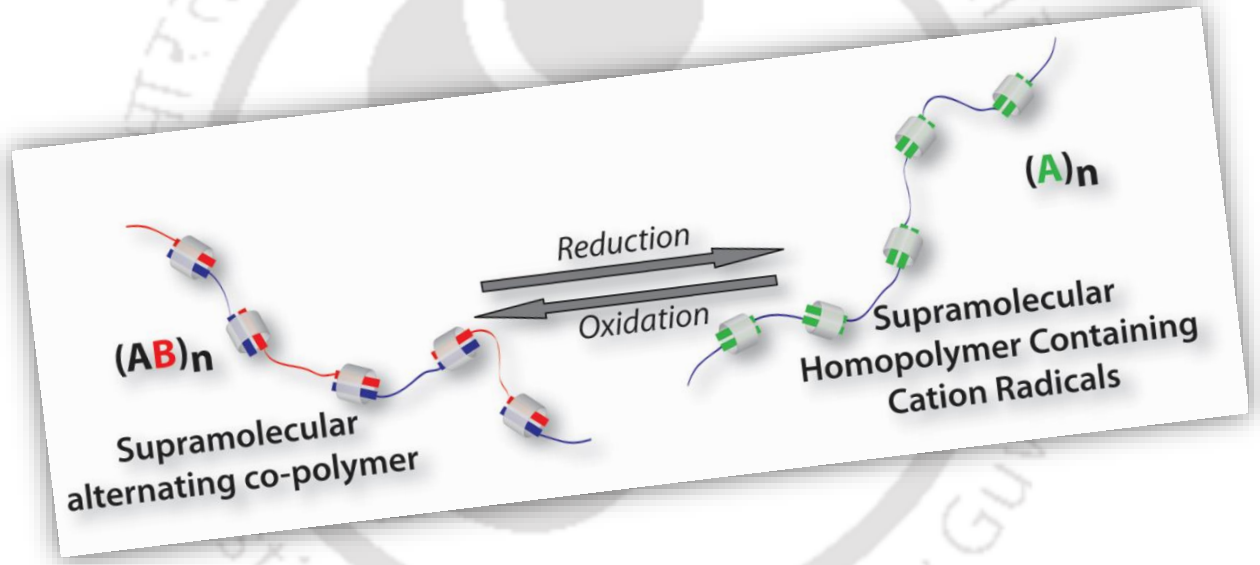

3.1 Introduction

As discussed in Chapter 1, CB[*n*] is a family of macrocyclic receptors well-known for their high recognition binding selectivity toward variety of guests.[84-86,125] CB[8], a larger member of the CB[*n*] family has shown the unique ability to encapsulate two guests simultaneously inside it's cavity thus acting as a "supramolecular handcuff".[86,111] This ternary complexation has been successfully utilized to construct various supramolecular soft-materials and for other applications as well.[86,108,125,181-186] Supramolecular polymers and polymer conjugates are also reported using the CB[8] chemistry.[113,115,124,187-190]

Amino acids are a class of molecules providing ample opportunities to modulate the hierarchical assembly to form desired nano-structures.[16,59,191] Variety of side chain functionalities, presence of hydrogen bond donor and acceptors, aromatic rings to form $\pi-\pi$ stacking are the key components of amino acids and molecules made by combining these amino acids (peptides or related molecules) that are utilized to prepare various self-assembled nano-structures.[10,48,192,193] These amino acid linked supramolecular polymers have gained considerable attention owing to their bio-compatibility and application toward drug delivery and tissue engineering.[16,59,191,194,195] These polymeric materials are in general prepared exploiting the intrinsic self-assembling characteristics of the amino acid building blocks.[16,59,191,194,195] Supramolecular polymers from short peptide monomers via synthetic macrocyclic hosts are important as they carry the benefits like stimuli responsiveness of host-guest chemistry as well as the versatility and bioavailability of peptide mimetic molecules. Though there are some recent reports describing such type of polymeric materials, further examples will certainly open up the possibility of practical usage of these materials.[117,196,197]

Supramolecular polymers reported in the literature are commonly either homo-polymers where the same monomer unit is connected through non-covalent interactions or copolymers wherein two different monomeric units are linked together in a repetitive manner. In this work, for the first time such reversible conversion of these alternating copolymers to a homo-polymer within the same system is described.

3.2 Results and Discussion

Viologens (Scheme 3.1A) are well known for their electrochromic behaviour and form radical cations upon reduction.[117,198] It has been mentioned in the chapter 1, that a hetero-ternary complex by CB[8] involving viologen as the first guest can be transformed to a homo-ternary complex upon reduction of the viologen unit (Scheme 3.1A).[109] Two units of viologen-radical cations are able to form 2:1 complex with CB[8] with a high binding constant ($2\times10^7\ M^{-1}$).[199] This phenomenon has been utilized on several

occasions to construct stimuli responsive materials.[199-202] It is worth mentioning that, among the natural amino acids, tryptophan (Trp) shows the highest affinity to form ternary complexes with CB[8] in presence of a first guest like viologen[106] and the efficiency of the ternary complexation has been observed to increase when Trp is situated at the N-terminal of a peptide.[107] In order to prepare the supramolecular copolymer, two different molecules were designed and synthesized. Compound **3.1** is a molecule containing Trp at both ends of the molecule which act as the second guest for CB[8] while compound **3.2** contains two viologen units at its two ends (Scheme 3.1B). Compound **3.2** binds with CB[8] in a 1:2 ratio to form a **3.2**@CB[8] complex. The average binding constant was found to be $(2.02 \pm 0.2) \times 10^6$ M^{-1} from ITC measurements (Figure 3.1 and Table 3.1). In case of the ITC data analysis, it was assumed that the sites are non-interacting and thereby treating each binding event as independent of other binding events. The binding was further confirmed by ^{1}H NMR (Figure 3.2). The up-field shift of the viologen protons indicate the encapsulation of viologen units inside CB[8] cavity. Single diffusion coefficient of 2.82×10^{-10} m^2s^{-1} as observed in the DOSY experiment also confirms the formation of inclusion complex (Table 3.2).

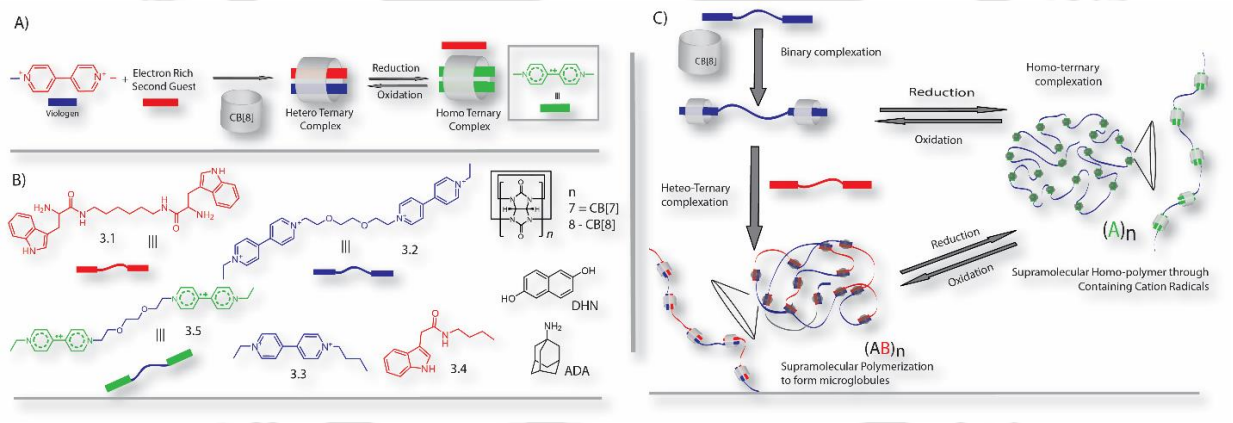

Scheme 3.1 A) Redox controlled homo- and hetero-ternary complexation by CB[8]; B) Chemical structures of the compounds synthesized or used for this study; C) Pictorial presentation of the formation and redox controlled reversible transformation of the supramolecular (AB)n type copolymer to (A)n type homo-polymer.

As expected, when tested, tryptophan formed a 2:1 complex with **3.2**@CB[8] (1:2), obtained from the ITC experiment (Figure 3.1C and Table 3.1). This complexation is also evident from the UV-Vis and fluorescence spectra. Tryptophan in presence of **3.2**@CB[8] formed CT band centred at 420 nm (Figure 3.3A) whereas tryptophan alone with other combination did not show any CT band. Similarly the drastic decrease in fluorescence intensity of tryptophan in presence of **3.2**@CB[8] (Figure 3.3B) and the up-field shift of the aromatic protons of tryptophan in presence of compound **3.2**@CB[8] (Figure 3.3C) also confirmed the encapsulation of tryptophan inside the cavity of CB[8].

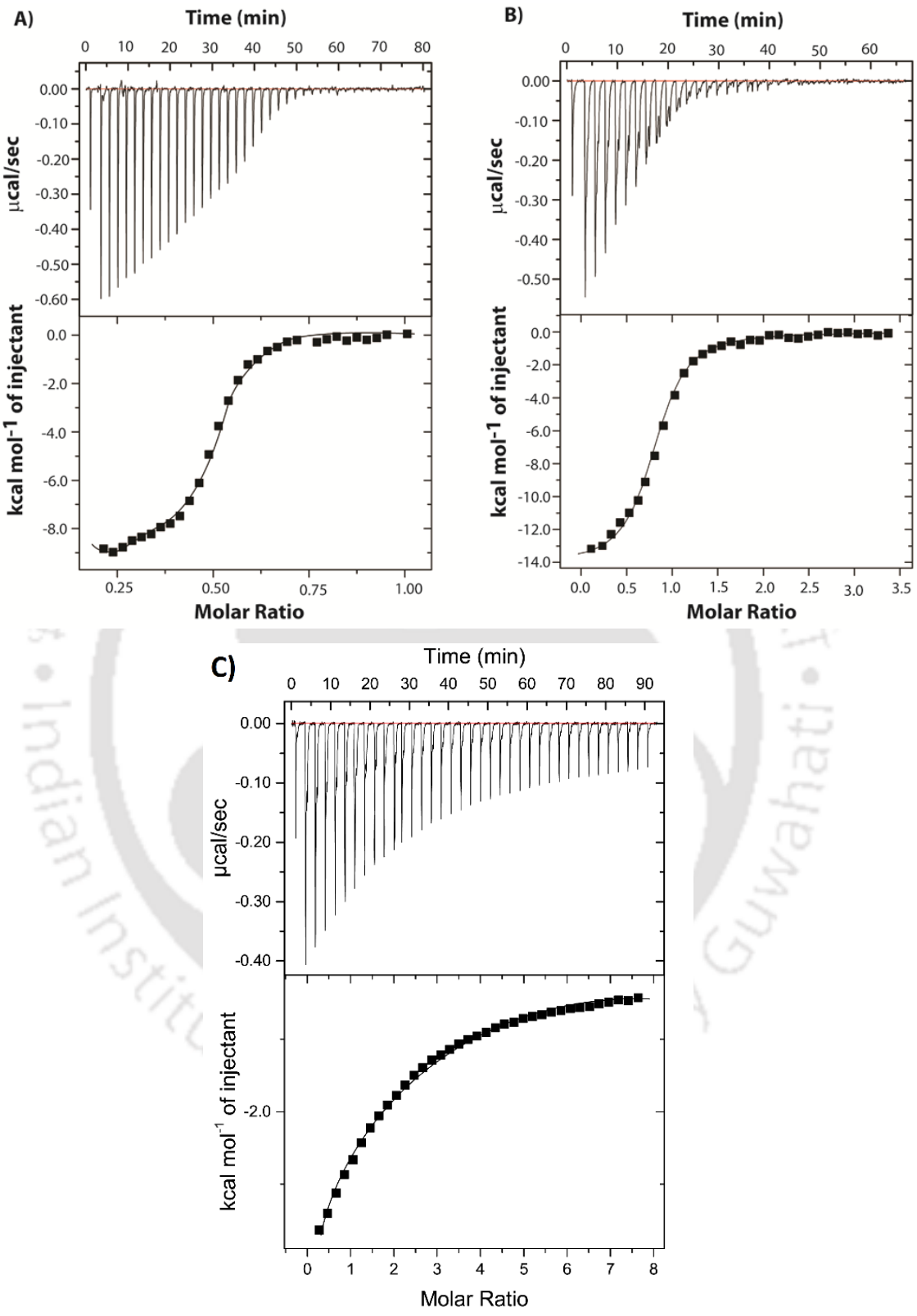

Figure 3.1 Thermograms (top) and binding isotherms (bottom) of A) CB[8] with **3.2**; B) **3.2**@CB[8] (1:2) with **3.1** and C) Tryptophan with **3.2**@CB[8] (2:1).

Table 3.1. Solution binding constants and related thermodynamic parameters obtained from ITC experiments.

System titrated	Titrant	N (sites)	K_a (M^{-1})	ΔH (cal/mol)	ΔS (cal/mol/deg)
CB[8]	**3.2**	0.486 ± 0.0026	(2.02 ± 0.201) × 10^6	-9259 ± 78.02	-2.21
3.2-CB[8] (1:2)	**3.1**	0.94 ± 0.0011	(5.12 ± 0.348) × 10^5	-13640 ± 145.1	-19.60
3.2-CB[8] (1:2)	Trp	2.08 ± 0.034	(1.07 ± 0.266) × 10^4	-6453± 1393	-3.21

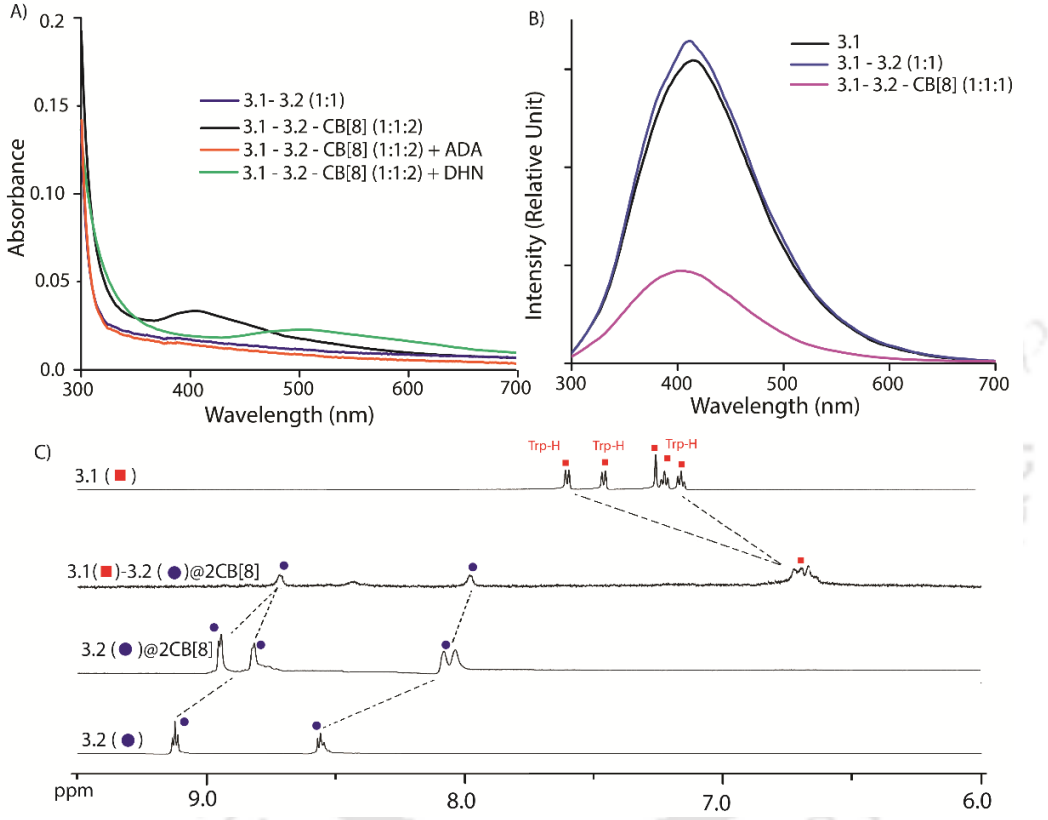

Figure 3.2 A) UV-Visible spectra of different compositions of **3.1**, **3.2** and CB[8] showing the formation of CT complex; B) Fluorescence spectra of **3.1** in absence and presence of **3.2** and CB[8]; C) NMR signals of the aromatic protons of different composition of **3.1**, **3.2** and CB[8].

Next, the possibility of formation of supramolecular polymer in the aqueous mixture of **3.1**, **3.2** and CB[8] (1:1:2) was examined. ITC experiment reveals a binding constant of (5.12 ± 0.35) × 10^5 M^{-1} between **3.1** and **3.2**@CB[8] (1:2) complex (Figure 3.1 and Table 3.1). Hence, the overall binding constant obtained is in the range of 10^{11} M^{-2} for **3.1**-**3.2** with CB[8]. Absorption spectra reveals the ternary complexation between tryptophan units of **3.1** and the viologen units of **3.2** inside CB[8] cavity as the CT band appeared at ~420 nm only when all three components were present (Figure 3.2A).[186] The up-field shifts of the aromatic protons of both viologen and Trp units in ^{1}H NMR spectra is a clear indication of the

ternary complexation (Figure 3.2C). The sudden fall of fluorescence intensity of **3.1** in presence of **3.2**@CB[8] (1:2) also supported the formation of the ternary inclusion complex (Figure 3.2B).[203]

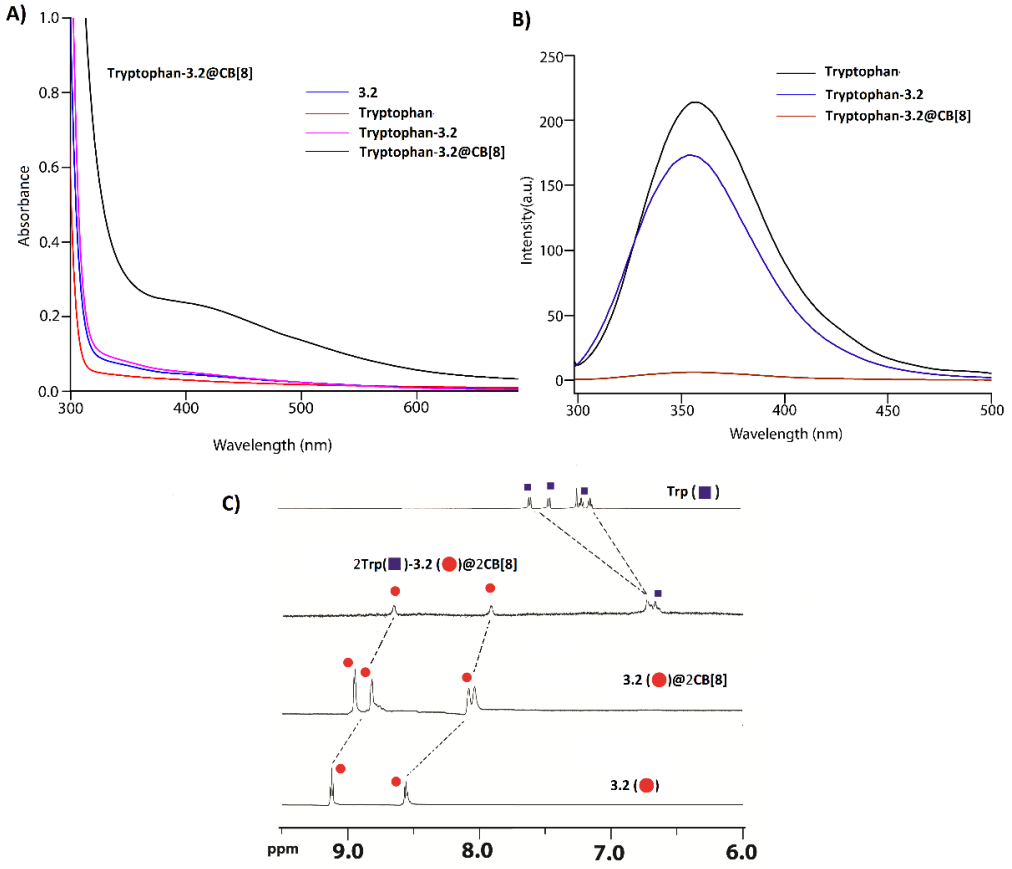

Figure 3.3 A) UV-Visible spectra of different compositions of Tryptophan, **3.2** and CB[8] showing the formation of CT complex; B) Fluorescence spectra of tryptophan in absence and presence of **3.2** and CB[8]; C) NMR signals of the aromatic protons of different composition of Tryptophan, **3.2** and CB[8].

A clear indication toward the formation of a polymeric species was obtained from the DLS measurements. Substantial scattering intensity of large sized polymer even at a concentration of 0.5 mM was observed (Figure 3.4A). With further increase in concentration, the solution became turbid and finally, the particles precipitated. The hydrodynamic diameter distribution was centred at 230 nm and no measurable distribution was observed with smaller particles. Notably, in the case of control experiments with other different combinations of **3.1**, **3.2**, and CB[8], only a negligible (~0.1%) distribution of very small particles (1-2 nm) were observed which may arise from the presence of CB[8] (Figure 3.4B). The formation of well distributed polymeric material was further supported by the FESEM and AFM images where large spherical aggregates were observed which can be termed as micro-globules (Figure 3.5). The size distribution of these micro-globules ranged 150-250 nm which closely matches with the DLS data. It is worth mentioning that the possibility of forming smaller aggregates

cannot be ignored as the building blocks contain relatively flexible linkers. However, the observed data point toward the major population of larger aggregates (polymeric species) and a very minute and non-measurable population of such smaller aggregates may also be present in the system.

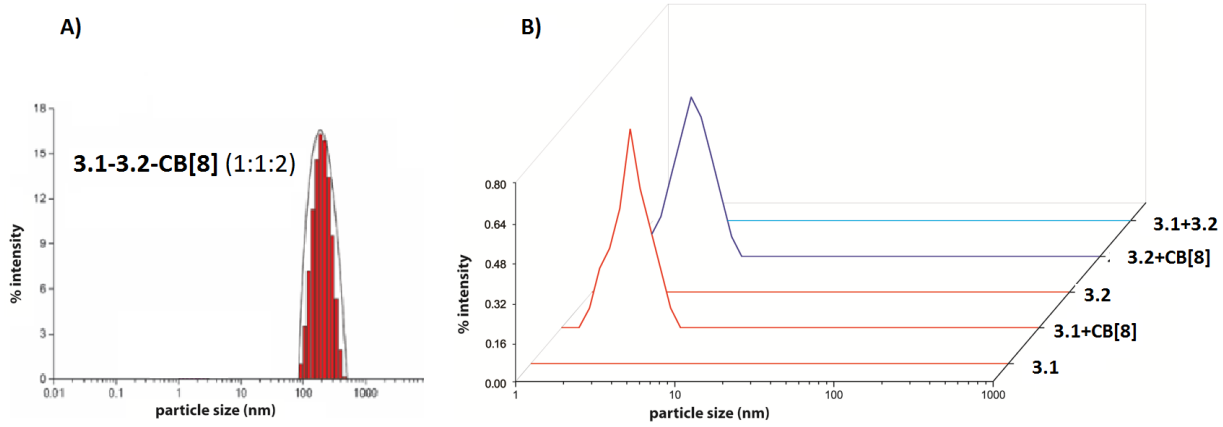

Figure 3.4 A) Intensity weighted distribution of particles obtained from DLS for **3.1**-**3.2**-CB[8] (1:1:2). B) DLS profile of the solutions of **3.1** and **3.2** in absence and presence of CB[8] showing extremely negligible distributions without CB[8].

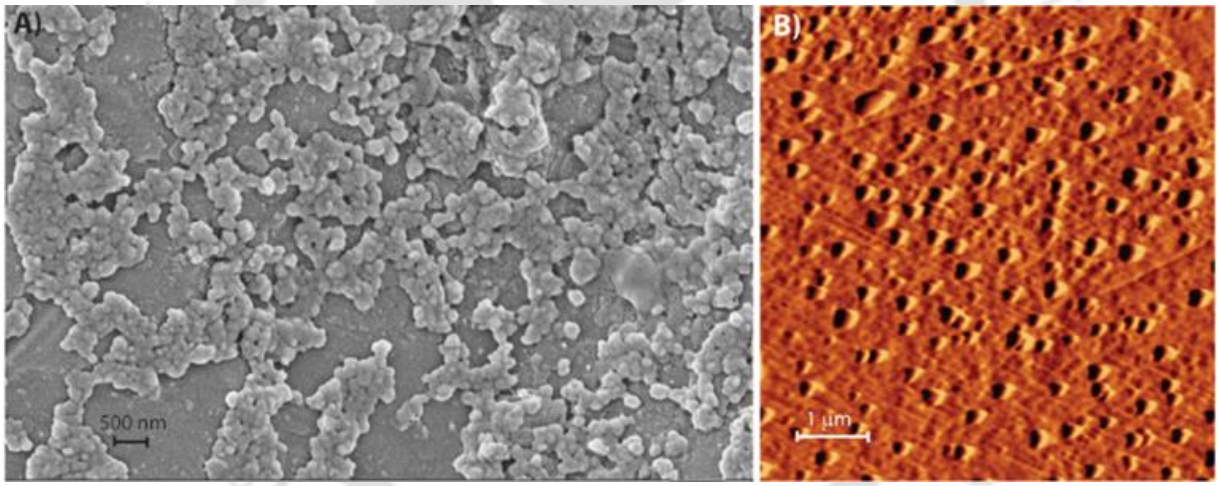

Figure 3.5 A) FESEM and B) AFM images of the **3.1**–**3.2**–CB[8] (1:1:2) supramolecular alternating copolymer.

DOSY technique has been utilized efficiently to evaluate the degree of polymerization in case of similar supramolecular polymers.[115,203-205] For a spherical molecule, the diffusion coefficient (*D*) can be correlated to its hydrodynamic radius (*R*) following Stokes-Einstein equation (equation 3.1) where k_B, *T*, and η represents Boltzmann's constant, absolute temperature, and viscosity respectively. For two spherical molecules in the system, equation 3.1 can be modified as equation 3.2. Equation 3.3 relates volume (*V*) of a sphere to its radius. Hence, the ratio of the diffusion coefficients for two spherical entities in the same system is inversely proportional to the cube root of their volumes or their molecular weight (MW) as shown in equation 3.4.

$$D = \frac{k_B T}{6\pi\eta R} \quad (3.1)$$

$$\frac{D_1}{D_2} = \frac{R_2}{R_1} \quad (3.2)$$

$$V = \frac{4}{3}\pi R^3 \quad (3.3)$$

$$\frac{D_1}{D_2} = \sqrt[3]{\frac{V_2}{V_1}} = \sqrt[3]{\frac{MW_2}{MW_1}} \quad (3.4)$$

The average diffusion coefficients (D_{av}) of **3.1**, **3.2** and CB[8] were found to be 4.31 × 10^{-10} m^2s^{-1}, 4.09 ×10^{-10} m^2s^{-1} and 2.91 × 10^{-10} m^2s^{-1} respectively when measured separately (Table 3.2). However, they showed a single D_{av} (0.54 × 10^{-10} m^2s^{-1}) when mixed together in 1:1:2 ratio (Table 3.2). The single diffusion coefficient can be attributed to the fact that majorly a single type of aggregate is present in the solution. The significant decrease in D_{av} value implies that large polymeric aggregates have formed. The degree of polymerization was determined assuming a hydrodynamically spherical aggregate formation. In this regard, a 1:1:1 mixture of **3.3**, **3.4** and CB[8] was prepared to form a ternary complex of **3.3**-**3.4**@CB[8]. This small ternary complex can be considered as the monomeric repeat unit of the polymer and can be used as a monomeric standard.[115] The ternary complexation of **3.3**, **3.4** in presence of CB[8] was confirmed by the emission spectra (Figure 3.6).

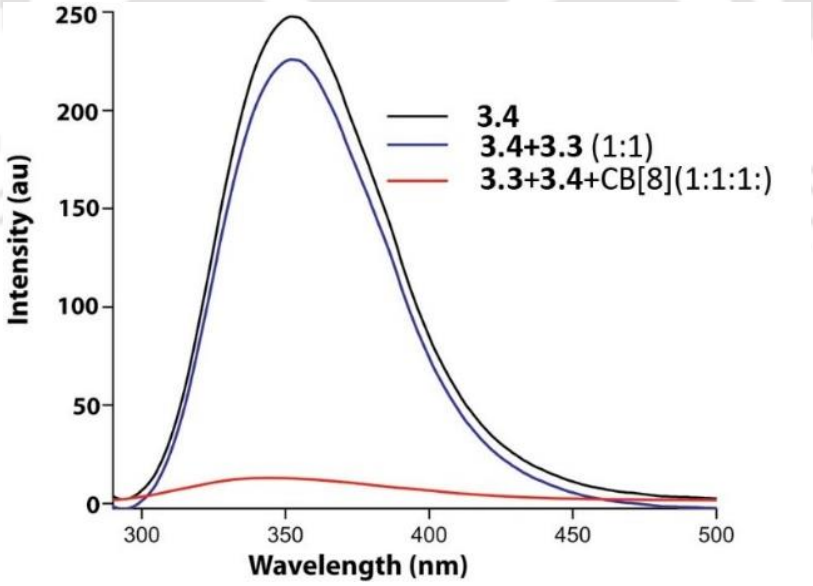

Figure 3.6 Emission spectra of aqueous solutions of various compositions of **3.3**, **3.4** and CB[8] showing the significant quenching of Tryptophan fluorescence upon formation of the ternary complex of **3.3**-**3.4**@CB[8]; [**3.3**] = 0.5mM. [**3.4**] = 0.5 mM, [CB[8]] = 0.5 mM (λ_{ex}= 279nm).

The diffusion coefficient of **3.3**-**3.4**@CB[8] was determined as 2.72 × 10^{-10} m^2s^{-1} (Table 3.2). Following equation 3.4, the average size of the supramolecular polymer was calculated to be 128 times that of the

monomeric standard. Though the calculation is purely an approximation, it undoubtedly confirms the supramolecular polymerization. At this point, it is worth mentioning that no significant evidence was found in favor of polymerization between **3.2** and CB[8] in spectroscopic, microscopic, or DLS experiments when **3.2** and CB[8] were mixed together in 1:2 ratio at this concentration range. This ruled out the probability of formation of polymer through homo-ternary complexation by viologen units of **3.2**.

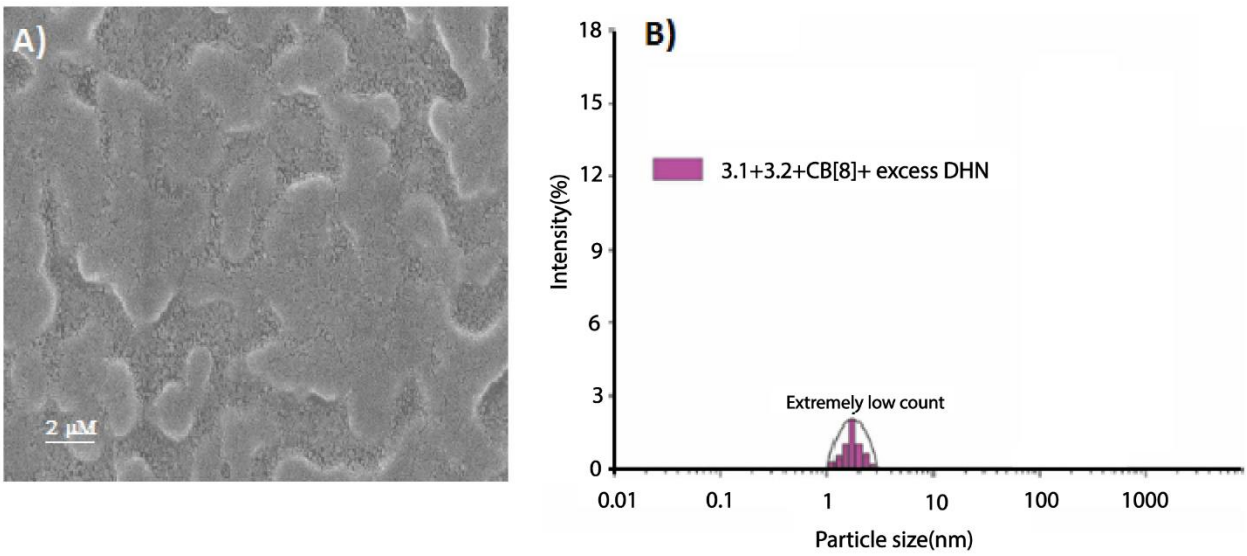

Figure 3.7 A) FESEM image and B) DLS profile of the homo-polymer after DHN Treatment.

The co-polymer was further tested for its stimuli responsiveness. A stronger second guest in the form of DHN (Scheme 3.1) allowed to break the polymer as it replaces the Trp units of **3.1** to form a DHN-**3.2**@CB[8] (2:1:2) ternary complex.[186] In the absorption spectra, the original CT band from viologen-Trp complex disappeared and a new CT band appeared with a shift in the λ_{max} (Figure 3.2A). The new CT band can be attributed to the viologen-DHN complex inside CB[8] cavity. However, no particular morphology was found in the microscopic images and only a very small size distribution centred at ~ 2 nm with extremely low count was observed in DLS measurements (Figure 3.7). Similar breakdown of the supramolecular copolymer was also observed when 1-adamantylamine (ADA, Scheme 3.1) was added to the polymer solution. Being a stronger and larger guest than viologen and tryptophan, it replaces both the guests from the inclusion complexes. The disappearance of the CT band in the UV visible spectra (Figure 3.2) and recovery of the tryptophan fluorescence upon addition of these two molecules separately signifies the collapse of the polymer.

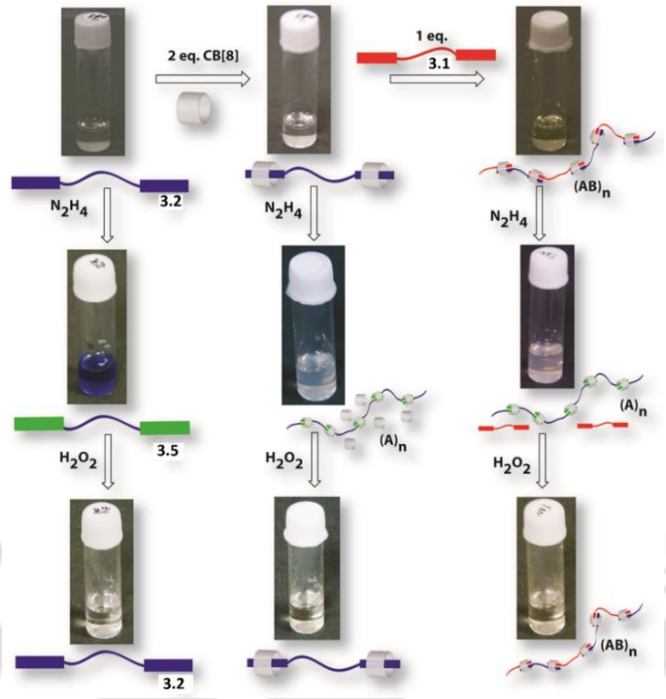

Figure 3.8 Photographs showing color changes of different compositions and pictorial illustrations of the corresponding compositions. [**3.2**] = 0.5 mM.

As mentioned earlier, the reduction of the viologen produces radical cations which can form homo-ternary complex with CB[8] (Scheme 3.1A).[109,199-202] The formation of this complex possibly can lead to a completely different kind of polymer in this particular case where the radical cation **3.5** (Scheme 3.1B) can polymerize to form (**3.5**@CB[8])$_n$ (Scheme 3.1C). When treated with hydrazine, a slightly bluish orange colour generated (Figure 3.8) in the aqueous solution of **3.1**-**3.2**@CB[8] (1:1:2) indicating the formation of viologen radical cations. The radical cations were characterized by the appearance of the signature bands at 385 nm, 580 nm, 910 nm and 1058 nm in the absorption spectrum (Figure 3.9A).[109,199,200] Particle size analysis of this solution resulted in various size distributions (centred at ~1.7 nm, ~66.2 nm, ~ 227.4 nm, ~ 550 nm, ~900 nm, Figure 3.9B) immediately after the reduction. After incubation for 6 h under complete inert condition, the system got stabilized with a prominent distribution centred at ~950 nm (Figure 3.9C).

Interestingly, treatment of this solution with H_2O_2 and incubation for 2 h (to remove all the air bubbles formed), brought back the original pale orange colour (Figure 3.8) and the stable smaller size distribution in DLS experiment (Figure 3.9D). The slightly smaller sizes obtained after the redox cycle may be attributed to the error inherent to DLS measurements. Moreover, the new bands generated in the UV-visible spectra (Figure 3.9A) disappeared and the profile returned back to the original nature with small decrease in the absorbance values owing to the dilution effect. The microscopic images at

these two stages showed micro-globules of 900-1000 nm (Figure 3.10) range in case of hydrazine hydrate treated solution whereas the average size of the micro-globules were of ~ 150 nm for the H_2O_2 treated solution (Figure 3.9D).

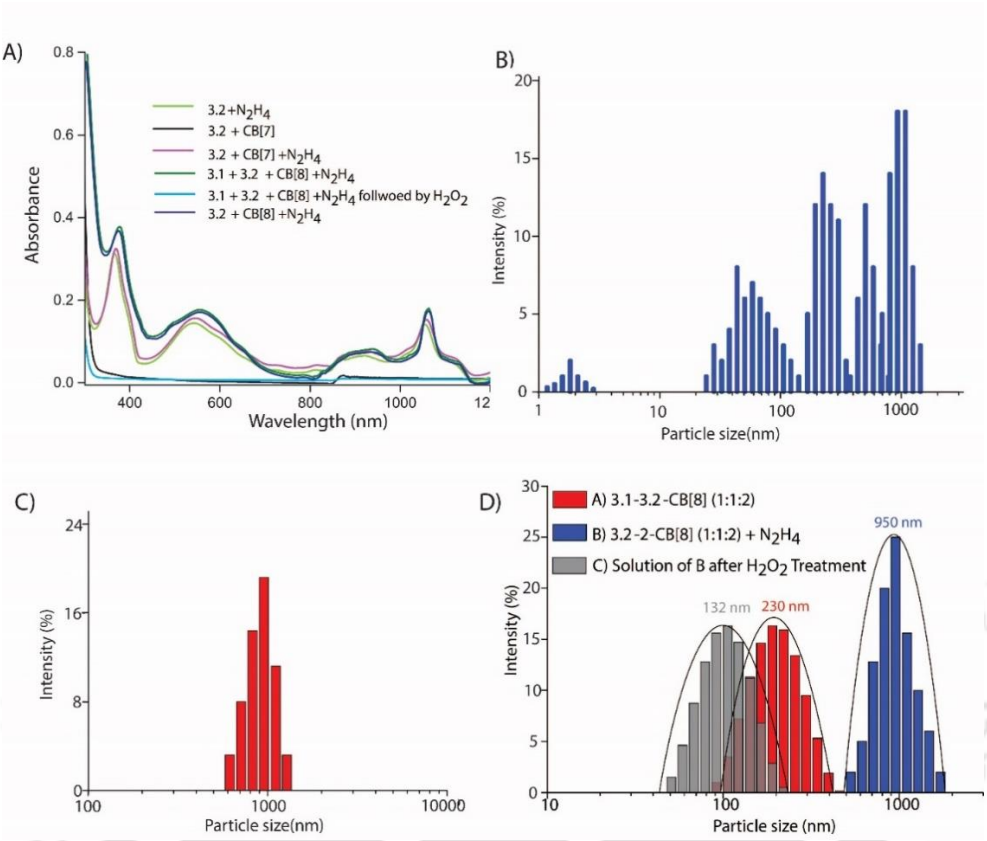

Figure 3.9 A) Absorption spectra of **3.2** in different combinations with **3.1**, hydrazine, CB[8] and CB[7]; **B)** intensity weighted distribution of particle sizes of the homo-polymer, immediately after the hydrazine hydrate addition; C) DLS profile of the solution of **3.1**-**3.2**@2CB[8] (1:1:2) 6 h after the hydrazine hydrate treatment D) intensity weighted distribution of particle sizes of the homo-polymer, after 6 h of reduction by hydrazine hydrate and finally re-oxidation by H_2O_2.

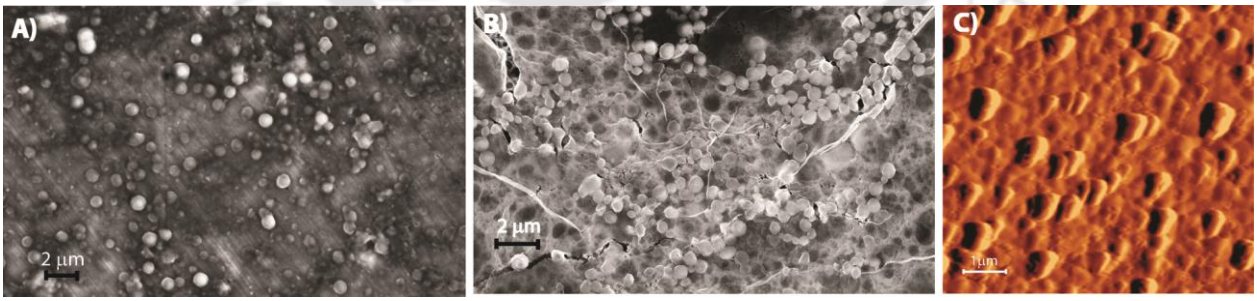

Figure 3.10 FESEM images of hydrazine hydrate treated solutions of A) **3.1**–**3.2**@CB[8] (1:1:2), and B) **3.1**@CB[8] (1:2). C) AFM image of **3.1**–**3.2**@CB[8] (1:1:2).

Introduction of a reducing agent like hydrazine hydrate produced viologen radical cations 3.5 (Scheme 3.1B) which leads to de-complexation of the hetero-ternary system and eventually disrupted the copolymer 3.1-3.2@CB[8] (1:1:2). As viologen radical cations have the ability to form dimers inside CB[8],

the radical cation 3.5 formed $(3.5@CB[8])_n$ within the same solution which led to a new polymer of $(A)_n$ type (Scheme 3.1C). Upon oxidation, the radical cations reverted back to the di-cationic state and thus regenerated the original copolymer. To further analyze the dimerization of the viologen radical cation units inside CB[8] cavity, the absorption spectra of reduced 3.2 in absence and presence of CB[7] (Scheme 3.1) were checked. All the peaks shifted to lower wavelengths in both cases (Figure 3.9A). Having smaller cavity size, CB[7] cannot accommodate two guests but is capable of binding viologen radical cations strongly and thus in presence of CB[7], the viologen cation radicals cannot dimerize.[206] In presence of CB[8], the bathochromic shifts of the absorption peaks indicate the dimerization process. This shift of the absorption peaks upon dimerization of the radical cations is a well-established phenomenon and strongly supports the formation of homo-polymer in the present case in presence of CB[8].

In order to establish this hypothesis, a 1:2 mixture of **3.2** and CB[8] was subjected to similar hydrazine/H_2O_2 treatments. The colourless solution of the mixture immediately turned bluish upon addition of hydrazine hydrate (Figure 3.8) and showed characteristic absorption features of the radical cation formation (Figure 3.9A) similar to the case of copolymer. The FESEM image of this system showed similar sized micro-globules as found in case of hydrazine hydrate treated **3.1**-**3.2**@CB[8] (1:1:2) system (Figure 3.10B).

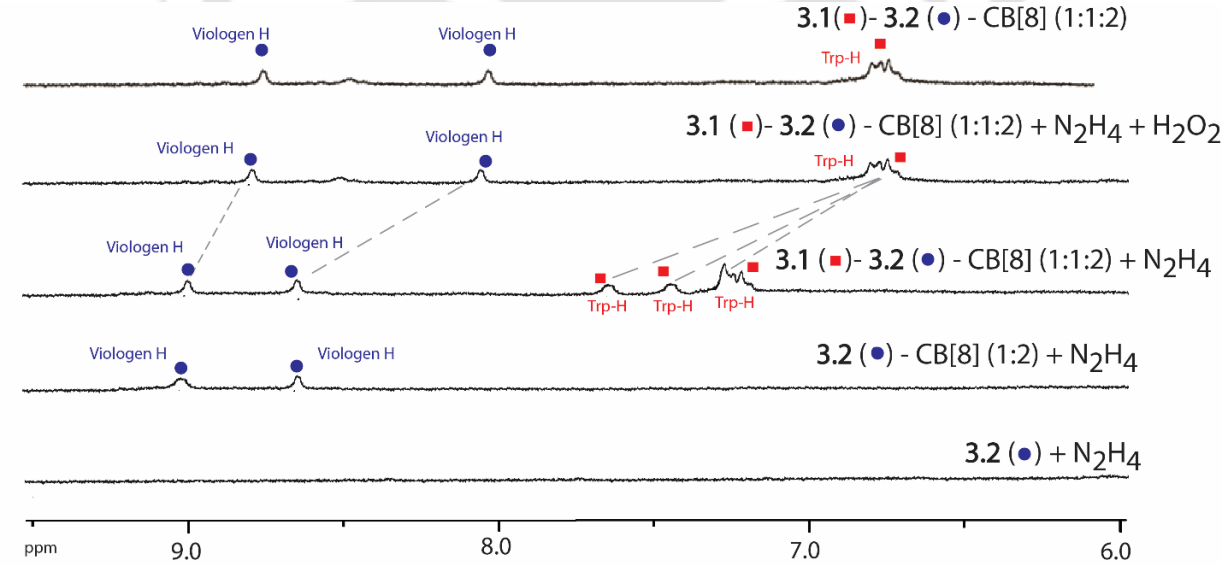

Figure 3.11 ^{1}H NMR spectra (aromatic region) of hydrazine hydrate treated different compositions of **3.1**, **3.2**, and CB[8] at room temperature in D_2O.

Both, **3.1**-**3.2**@CB[8] (1:1:2) and **3.2**@CB[8](1:2) were treated with hydrazine hydrate and subjected to ^{1}H NMR analysis separately. ^{1}H NMR spectra of both systems showed clear evidences in favour of homo-ternary complexation (Figure 3.11). Reduction of the copolymer system (**3.1**-**3.2**@CB[8] (1:1:2)) resulted

in a broadening (presumably due to paramagnetic nature of the radical cation) of the aromatic signals. A down-field shift of the tryptophan protons to its native positions (as in free **3.1**) indicates the release of compound **3.1** from CB[8]. The aromatic protons from the viologen units also showed down-field shifts but remained slightly up-field shifted compared to its unbound state (as in free **3.2**). Similar small down-field shift of the viologen protons were also observed in case of hydrazine hydrate treated solution of **3.2**@CB[8](1:2) system. Introduction of H_2O_2 in these systems re-generated their respective original spectral features (Figure 3.11). Interestingly, under reduced condition, the aromatic protons of compound **3.2** in absence of CB[8] (i.e. compound **3.5**) were shifted outside the normal NMR frame (Figure 3.11). These observations are very much in agreement with the previous reports from Kim and Sun about the homo-ternary complexation of viologen radical cations inside CB[8].[109,199,200]

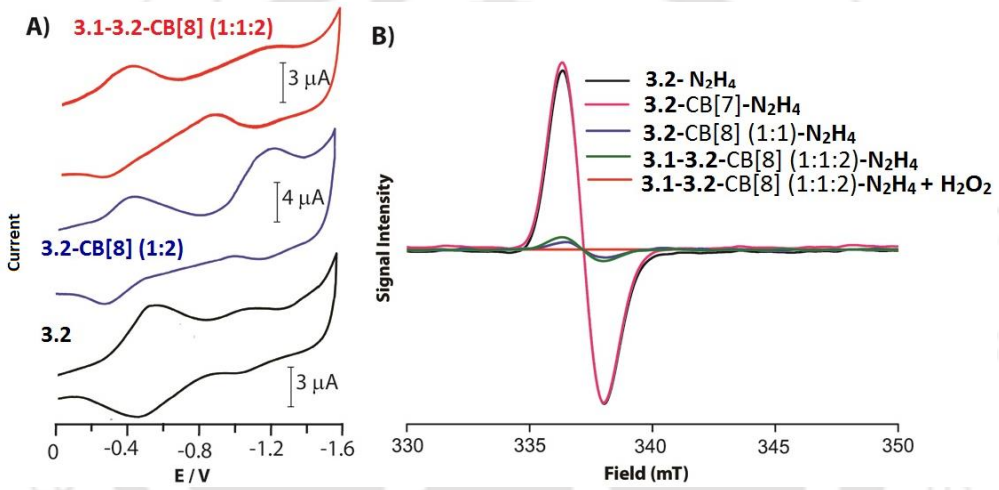

Figure 3.12 A) Cyclic voltammograms at the scan rate of 0.1 V s^{-1} (in pH 7 phosphate buffer), and B) EPR spectra of various compositions of **3.1**, **3.2** and CB[8] at room temperature. [**3.1**], [**3.2**] and CB[8] for both experiments were maintained at 0.25, 0.25 and 0.5 mM.

In order to further ascertain the homo-ternary complexation in both cases, the electrochemical behaviour of **3.2** was analysed. Compound **3.2** exhibited two one-electron reduction waves on CV as shown in figure 3.12A. The waves at -0.48 V and -1.05 V correspond to the reduction of viologen dication to radical cation and radical cation to the neutral species respectively. In presence of CB[8], the peak potentials shifted to -0.35 V and -1.23 V. This pattern fits properly with the literature reports about dimerization of viologen radical cations inside CB[8] cavity.[109,199,200] A similar electrochemical behaviour was also observed in case of **3.1**-**3.2**@CB[8] (1:1:2) indicating the ternary complexation by two viologen radical cations in this case as well.

EPR measurements of various compositions led to a further conclusive result. After reduction of **3.2** to make **3.5**, a strong signal attributed to the viologen radical cation was detected (Figure 3.12B). In order to ascertain that the signal correspond to the monomeric viologen cations, EPR was measured in

presence of 2 equivalents CB[7] which prevents the radical cations from dimerization.[206] Very similar intensities were observed in both cases signifying the presence of primarily the free viologen radical cations in the system. Same reduction product in presence of CB[8] resulted in a very weak signal (~ 24 fold decrease in signal strength as estimated from the integration value). The drastic diminution in the paramagnetic behaviour can be attributed to the dimerization of the radical cations inside the CB[8] cavity.[207] The minor signal can presumably be attributed to the contribution from a thermal population of un-complexed radical cations. Extremely low signal was also observed in case of hydrazine hydrate treated solution of the co-polymer (**3.1**-**3.2**@CB[8] (1:1:2)) signifying the formation of the homo-ternary complex in this case as well.

The formation of the homo-polymer was confirmed by DOSY. Two different diffusion coefficients were observed in case of hydrazine hydrate treated copolymer (**3.1**-**3.2**@CB[8] (1:1:2)). The tryptophan dimer (**3.1**) showed a higher diffusion coefficient than both **3.5** and CB[8] whereas **3.5** and CB[8] had similar D_{av} values (Table 3.1). Notably, no other diffusion coefficients were detected for **3.5** or CB[8] which along with the absence of any quantifiable distribution of smaller sized particles in DLS analysis of this sample ruled out the formation of cyclic or smaller aggregates in measurable quantity. The results indicated the breakdown of the hetero-ternary complex and formation of homo-polymeric system. Similar diffusion coefficients for **3.5** and CB[8] was also observed in case of hydrazine hydrate treated **3.2**@CB[8](1:2). The degree of polymerization for the homo-polymer ((**3.5**@CB[8])$_n$) in both cases were determined by measuring the D_{av} of the hydrazine hydrate treated **3.3**@CB[8] and utilizing equation 3.4. It was found to be ~328, which also justifies the much larger size of the micro-globules produced by (**3.5**@CB[8])$_n$. These results have confirmed the formation of homo-polymers in both systems.

Table 3.2 Diffusion coefficients obtained from DOSY spectroscopy.

Sample (0.25 mM for guests)	D_{av}[a] (10^{-10} m^2s^{-1})	Degree of polymerization
3.1	4.31	-
3.2	4.09	-
CB[8]	2.91	-
3.3	4.25	-
3.4	4.38	-
3.1-**3.2**-CB[8] (1:1:2)	0.54	127
3.3-**3.4**-CB[8] (1:1:1)	2.72	-
3.1-**3.2**-CB[8] (1:1:2)+ N_2H_4	0.38	354
3.2-CB[8] (1:2)	2.82	-
3.3-CB[8] (1:2) + N_2H_4	2.69	-
3.2-CB[8] (1:2) + N_2H_4 (*ie.* **3.5**@CB[8] (1:2))	0.39	328

[a] only the diffusion coefficients for the complexes mentioned in case of multiple D_{av} values in the same sample.

The experimental results evidently proved the formation of a homo-polymer in both systems upon reduction with hydrazine. In case of 3.1-3.2@CB[8] (1:1:2) this homo-polymer reverted back to the copolymer when treated with H_2O_2. Both the transformations can easily be identified by their distinct colour changes (Figure 3.8). However, like in the case of copolymer, though no detectable evidence in favour of cyclic dimer/trimer formation by 3.5@CB[8] was found, there is still a possibility of a very minute amount of such smaller aggregates may also be present in the system.

It is interesting to know whether this reversible transformations can be achieved in a repetitive manner. In order to test the possibility of controlling this process, DLS experiments were carried out as significantly different sized micro-globules formed by the two polymers. A solution of the co-polymer (**3.1**-**3.2**@CB[8] (1:1:2)) was treated with hydrazine hydrate and the particle sizes were measured. The same solution was further treated with H_2O_2 and subjected to DLS measurement. This process was repeated several times. As shown in figure 3.13, the reversible transformation of these two different types of polymers could be achieved for at least up to four cycles.

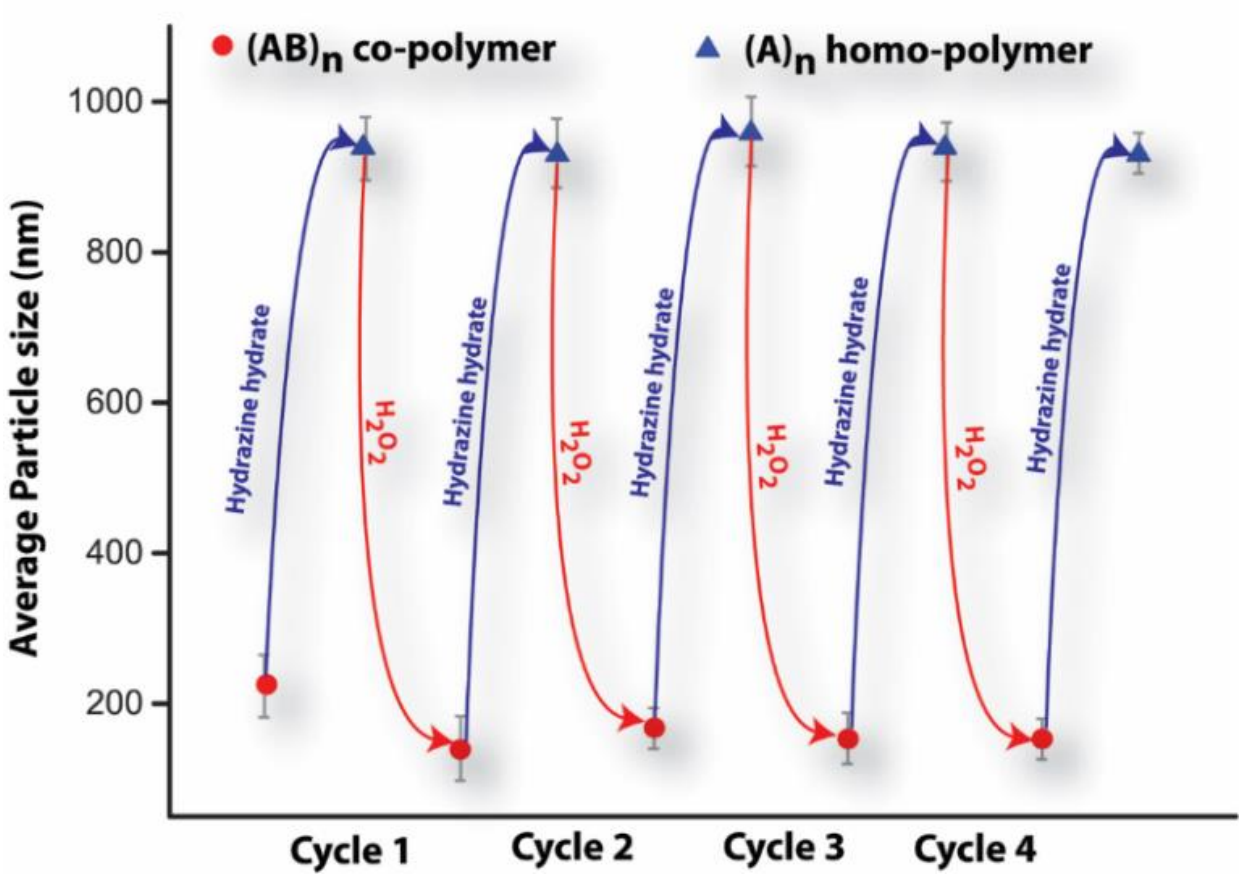

Figure 3.13 Reversible transformation cycles of an $(AB)_n$ alternating copolymer to an $(A)_n$ homo-polymer by consecutive treatments with hydrazine hydrate and H_2O_2. Data were taken from the average particle sizes obtained from DLS measurements after each transformation. After the addition of hydrazine hydrate, the samples were incubated at room temperature under a complete argon atmosphere for 6 h prior to measurements. For H_2O_2 treated samples, the measurements were done after 2 h of incubation at room temperature.

3.3 Conclusion

In summary, the work has demonstrated the formation of a supramolecular copolymer of $(AB)_n$ type using the hetero-ternary complexation of CB[8] in aqueous medium. The supramolecular copolymer forms uniform sized micro-globules and are sensitive to stronger guests of CB[8]. The one electron reduction of viologen units of compound **3.2** leads to the formation of a supramolecular polymer of $(A)_n$ type in the same system. Notably, the supramolecular homo-polymer is made of radical cations and the co-polymer to homo-polymer formation is reversible in nature. The reversible transformation can be repeated for several cycles. These supramolecular polymers will certainly open up the possibility to use these material toward applications involving stimuli responsiveness, radical chemistry, and in conductive polymers.

3.4 Experimental section

3.4.1 General

All the chemicals and reagents used were obtained from Sigma-Aldrich (USA) and used without further purification. All solvents were procured from Merck, India and Spectrochem, India. To prepare samples, Milli-Q water with a conductivity of less than 2 $\mu S \cdot cm^{-1}$ was used. ^{1}H NMR, ^{13}C NMR, diffusion-ordered spectroscopy (DOSY) were recorded either on a Bruker Ascend 600 MHz (Bruker, Coventry, UK) or on an Oxford AS400 (Varian) spectrometer. ESI-MS was measured using a Q-tof-Micro Quadrupole mass spectrophotometer (Micromass). FESEM and AFM images were taken using SIGMA ZEISS and Agilent 5500 microscopes respectively. Cyclic voltammetric experiments were carried out with a CHI680C Amp Booster from CH Instruments Inc.

3.4.2 Synthesis and Characterization of Compounds

2-amino-N-(6-(2-amino-3-(1H-indol-2-yl)propanamido)hexyl)-3-(1H-indol-3-yl)propanamide (3.1): To a stirring solution of 1,6-diaminohexane (0.3 g, 2.6 mmol) in dichloromethane (DCM), Boc-Trp-OH (2g, 6.6 mmol) was added and the temperature was maintained around 0°C using an ice-bath; followed by the successive addition of EDC.HCl (1.25g, 6.6 mmol), DIPEA (2.1g, 16.2 mmol) and HOBT (0.89 g, 6.6 mmol). The reaction mixture was brought to room temperature and stirred for 24 h. It was then washed with saturated $NaHCO_3$ solution (twice), 10% citric acid solution (twice), again with saturated $NaHCO_3$ and finally with brine. The reaction mixture was then extracted with DCM. The organic phase was dried over anhydrous Na_2SO_4, filtered and the solvent was removed on a rotary evaporator. The crude mixture was subjected to column chromatography on a 60-120 mesh silica gel column using ethyl acetate/hexane as the mobile phase (yield: 75%). The product obtained was then

subjected to deprotection of the Boc group by trifluoroacetic acid (TFA, 2 ml) containing 1% triethylsilane (TES). After 2 h of stirring, solvents were removed on a rotary evaporator followed by precipitation from diethyl ether. The precipitate was washed with dry diethyl ether several times. The solid was then dried under vacuum, dissolved in water and lyophilized. The purity of the sample was checked by HPLC, NMR and ESI-MS techniques (yield: 65%).^{1}H NMR (600 MHz, D_2O): δ = 7.59-7.58 (d, *J* = 7.8 Hz, 2H), 7.45-7.44 (d, *J* = 8.4 Hz, 2H), 7.25 (s, 2H), 7.22-7.20 (t, *J* = 7.2 Hz, 2H) , 7.16-7.13 (t, *J* = 7.2 Hz, 2H), 4.13-4.11 (t, *J* = 6 Hz, 2H), 3.37-3.27 (m, 4H), 3.06-3.04(m, 2H), 2.80-2.78 (m, 2H), 0.95-0.92 (m, 4H), 0.61-0.59 (m, 4H) ppm. ^{13}C NMR (100 MHz, D_2O): δ = 169.20, 136.19, 126.69, 125.06, 122.33, 118.27, 115.59, 112.03, 106.78, 54.09, 39.49, 30.04, 27.09, 25.09 ppm; HRMS (ESI) *m/z* calcd. for $C_{28}H_{36}N_6O_2$: 488.2978; found 489.2972 [M+H$^+$].

1′,1′′-((ethane-1,2-diylbis(oxy)-2,1-diyl))bis(1-ethyl-[4,4′-bipyridine]-1,1′-diium)dibromide dichloride (3.2): A mixture of 1,2-bis(2-chloroethoxy)ethane (1.6 g, 8.6 mmol) and 4,4′-dipyridyl (4.7 g, 30.1 mmol) in 15 ml DMF was heated at 110°C with constant stirring for 24 h. After cooling, diethyl ether was added to the mixture to get a brown precipitate. The solid was filtered and washed several times with diethyl ether and dried under reduced pressure. The solid was taken in 20 ml MeOH-acetonitrile mixture (3:7) and excess ethyl bromide was added. The reaction mixture was refluxed for 24 h when extra ethyl bromide was added time to time. The solvent was removed under reduced pressure and the material washed with diethyl ether several times and finally dried under reduced pressure to get the pure product (yield: 39%). ^{1}H NMR (600 MHz, D_2O): δ = 9.12-9.10 (t, *J* = 7.2 Hz, 8H), 8.55-8.53 (t, *J* = 6.6 Hz, 8H), 4.91-4.86 (q, *J* = 9.2 Hz, 4H), 4.76-4.74 (t, *J* = 7.8 Hz, 4H), 4.07 (t, *J* = 6.0 Hz, 4H), 3.67 (s, 4H), 1.69-1.66 (t, *J* = 7.2 Hz, 6H) ppm. ^{13}C NMR (100 MHz, D_2O): δ = 150.71, 150.07, 146.31, 145.62, 127.66, 127.46, 70.45, 69.25, 61.77, 58.18, 16.35 ppm. HRMS (ESI) *m/z* calcd. for $C_{30}H_{38}Br_3N_4O_2$: 727.0524; found 725.0521 [M+Br-2Cl]$^+$.

1-butyl-1'-ethyl-[4,4'-bipyridine]-1,1'-diium bromide (3.3): 4, 4′-dipyridyl (2g, 12.8 mmol) was dissolved in DCM followed by the addition of excess ethyl bromide (11 g, 101 mmol) and continuous stirring at room temperature for 24 h. The yellow precipitate was filtered and washed with diethyl ether several times before drying it under reduced pressure to get mono-ethylviologen (yield: 73%). The yellow product was dissolved in 20 ml MeOH-acetonitrile mixture (3:7) and to it n-butyl bromide (2.6 g 18.9 mmol) was added. The reaction mixture was refluxed for 24 h when extra ethyl bromide was added time to time. The solvents were removed under reduced pressure and the solid was suspended in diethyl ether and filtered. The solid was washed several times with diethyl ether and dried under reduced pressure to get the yellow colored title compound. (yield: 68%).^{1}H NMR (400 MHz, D_2O): δ =

9.15-9.12 (t, *J* = 6.4 Hz, 4H), 8.56-8.53 (t, *J* = 6.4 Hz, 4H), 4.77-4.72 (merged with solvent peak, 2H), 4.54 - 4.48 (t, *J* = 6.0 Hz, 2H), 2.11-2.03 (m, 2H), 1.73-1.69 (t, *J* = 7.6 Hz, 3H), 1.46-1.37 (m, 2H), 0.99-0.95 (t, *J* = 7.2Hz, 3H) ppm. ^{13}C NMR (100 MHz, D_2O): δ = 150.19, 145.09, 127.26, 62.24, 57.90, 32.83, 19.01, 15.87, 12.66 ppm. HRMS (ESI) *m/z* calcd. for $C_{16}H_{22}N_{22}$: 121.0886; found 121.0884 $[M -2Br]^{2+.}$

2-amino-N-butyl-3-(1H-indol-3-yl)propanamide (3.4): Boc-Trp-OH (0.5 g, 1.64 mmol), HOBt (0.083 mg, 1.8 mmol), HBTU (0.685 g, 1.8 mmol), were dissolved in DCM. Triethylamine (343 µL, 2.47 mmol) was added to the mixture and stirred vigorously. Finally, *n*-butylamine (326.5 µL, 3.28 mmol) was added. The reaction mixture was allowed to stir for 24 h. The reaction mixture was diluted with DCM and washed with brine. The organic layers were combined together and dried over anhydrous sodium sulfate and filtered. The solvent was removed on a rotary evaporator. The residue was further treated with TFA containing 1% TES for 2h. TFA was removed under reduced pressure and the mixture was subjected to column chromatography on a 60-120 mesh silica gel column. The pure product obtained as an oily liquid after eluting the column with 5% MeOH-DCM solvent mixture. (yield: 47%).^{1}H NMR (600 MHz, D_2O): δ = 7.62-7.60 (d, *J* = 8.4 Hz, 1H), 7.52-7.51 (d, *J* = 7.8 Hz, 1H), 7.27 (s, 1H), 7.26-7.24 (t, *J* = 6 Hz, 1H), 7.19-7.16 (t, *J* = 7.2 Hz, 1H) , 4.17-4.14 (t, *J* = 8.4 Hz, 1H), 3.39-3.29 (m, 2H), 3.11-3.08 (t, *J* = 6.6 Hz, 1H), 2.92-2.87 (m, 1H), 1.12-1.09 (m, 2H), 0.94-0.87 (m, 2H), 0.74-.72 (t, *J* = 7.2 Hz, 3H) ppm. ^{13}C NMR (100 MHz, D_2O): δ = 169.03, 136.53, 126.74, 125.11, 122.19, 119.56, 118.26, 112.10, 106.72, 54.04, 38.13, 30.09, 27.12, 19.25, 13.02 ppm. HRMS (ESI) *m/z* calcd. for $C_{15}H_{21}N_3O$: 259.1763; found 260.1766 $[M+H]^+$.

Cucurbit[8]uril (CB[8]): Cucurbit[8]uril (CB[8]) was synthesized by following previously published protocol.[91] ^{1}H NMR (600 MHz, $D_2O/CF_3CO_2D/D_2SO_4$ (1:1:0.15)): δ = 4.25 (d, 16H), 5.55 (s, 16H), 5.86 (d, 16H) ppm; MS (ESI): *m/z* 1461.41 $(CB[8] + Cs)^+$.

3.4.3 Methods

Sample preparation

In a volumetric flask (10 mL), compound **3.1**, **3.2**, and CB[8] were taken in deionized water in a way to maintain the appropriate concentrations of **3.1**, **3.2** and CB[8] (for the preparation of the co-polymer, the concentrations were maintained at 0.5 mM, 0.5 mM and 1 mM respectively (1:1:2)). The mixtures were sonicated for 1 hour and kept undisturbed at 298 K for one day (in case of the ternary complexations, a pale orange colour developed). These solutions were used for further experiments. For hydrazine hydrate treated samples, proper care was taken to keep the system and the environment inert and hence argon was flushed wherever applicable. After the reduction under argon atmosphere, the samples were incubated for 6 h under argon at room temperature before measurements. For H_2O_2

treated samples, all the measurements were per-formed after two hours of incubation time to remove all the air bubbles generated during the process.

NMR Spectroscopy

^{1}H, ^{13}C, and DOSY NMR spectra were recorded in heavy water (D_2O) at 298 K and processed with standard 1D and 2D DOSY softwares. Wherever necessary, the NMRs were appropriately water suppressed for clarity.

Dynamic Light Scattering (DLS)

The particle sizes of the samples were measured at 298 K on a Zetasizer Nano ZS90 from Malvern using a 632.8 nm He–Ne laser. Prior to measurements, the samples were filtered through appropriate filters to remove dust particles if any. For hydrazine hydrate treated samples, the medium was de-gassed with argon for 1 h prior to preparing the samples. The cuvettes were flushed with argon before and after adding the samples. The measurements were done immediately after adding hydrazine hydrate to the cuvettes.

Isothermal Titration Calorimetry (ITC)

The binding constant, stoichiometry and thermodynamic parameters for the inclusion of guests in CB[8] were determined by isothermal titration calorimetry using a Nano-ITC instrument from MicroCal. For **3.2** and CB[8] system, CB[8] solution (0.05 mM) was titrated with 1 mM solution of compound **3.2** (injection volume of 0.5 μL). For **3.1** vs **3.2**@CB[8] (1:2) or tryptophan vs **3.2**@CB[8](1:2) systems, **3.2**@CB[8] (1:2, 0.1 mM) was titrated with 2 mM solutions of compound **3.1** or of tryptophan (injection volume of 1 μL). For every experiment, the temperature was fixed at 298 K. The first data point was omitted from the data set for curve fitting. All solutions were prepared in buffer (10 mM phosphate, pH 7) and degassed prior to titration. Heats of dilution were checked by titration of the guest into a buffer solution and subtracted from the normalized enthalpies. The data were fitted to a theoretical titration curve by one set of sites binding model using a software supplied by Microcal.

FESEM and AFM

FESEM and AFM samples were prepared by casting a drop of dilute sample solution on aluminium foil coated glass slide (for FESEM) and glass slide (for AFM) and dried under ambient conditions for overnight. For hydrazine hydrate treated samples, proper care was taken to create an inert atmosphere inside a closed chamber connected with inlet and outlets for passing argon gas. Argon was flushed thoroughly to remove all the air before casting the reduced samples and the samples were dried at normal pressure while argon was passed through the chamber throughout the drying process. The samples were kept under argon till they were placed to the instruments.

UV-Visible and Fluorescence spectroscopy

UV-visible and fluorescence spectra were recorded on a Lambda 750 (Perkin Elmer) and Cary Eclipse (Agilent) spectrophotometers respectively. For hydrazine hydrate treated samples, proper care was taken to keep the environment inert by flushing argon into the chamber as well as in the cuvettes before and after adding the samples.

Cyclic Voltammetry (CV)

Cyclic voltammetric experiments were carried out with a CHI680C Amp Booster from CH Instruments Inc. having a glassy carbon working electrode, a Pt counter electrode, and an Ag/AgCl reference electrode. Glassy carbon and platinum working electrodes were customarily polished with 0.05 μm alumina prior to use. Before each experiment, the solutions were deoxygenated by passing nitrogen gas, and an inert atmosphere was maintained during the experiments. As a reference, the electrochemistry of dimethylviologen was measured under similar working conditions, and a satisfactory result was obtained (data not shown).

Electron Paramagnetic Resonance (EPR) spectroscopy

EPR measurements were performed on a JES-FA200 instrument from JEOL. Prior to the addition of the reducing agent, all the samples were degassed by purging argon gas for 30 mins. After the addition of hydrazine hydrate, Argon was flushed thoroughly and the sample tubes were sealed properly in order to prevent any oxidation.

3.4 Chromatogram, NMR and Mass spectra of the synthesized compounds

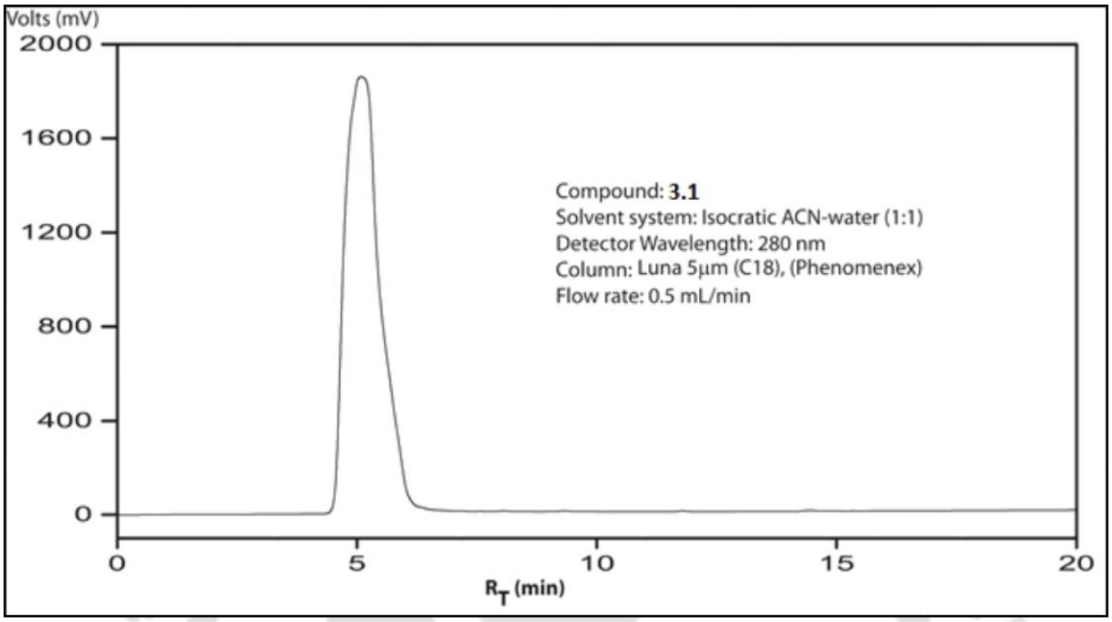

Chromatogram of purified Compound **3.1**

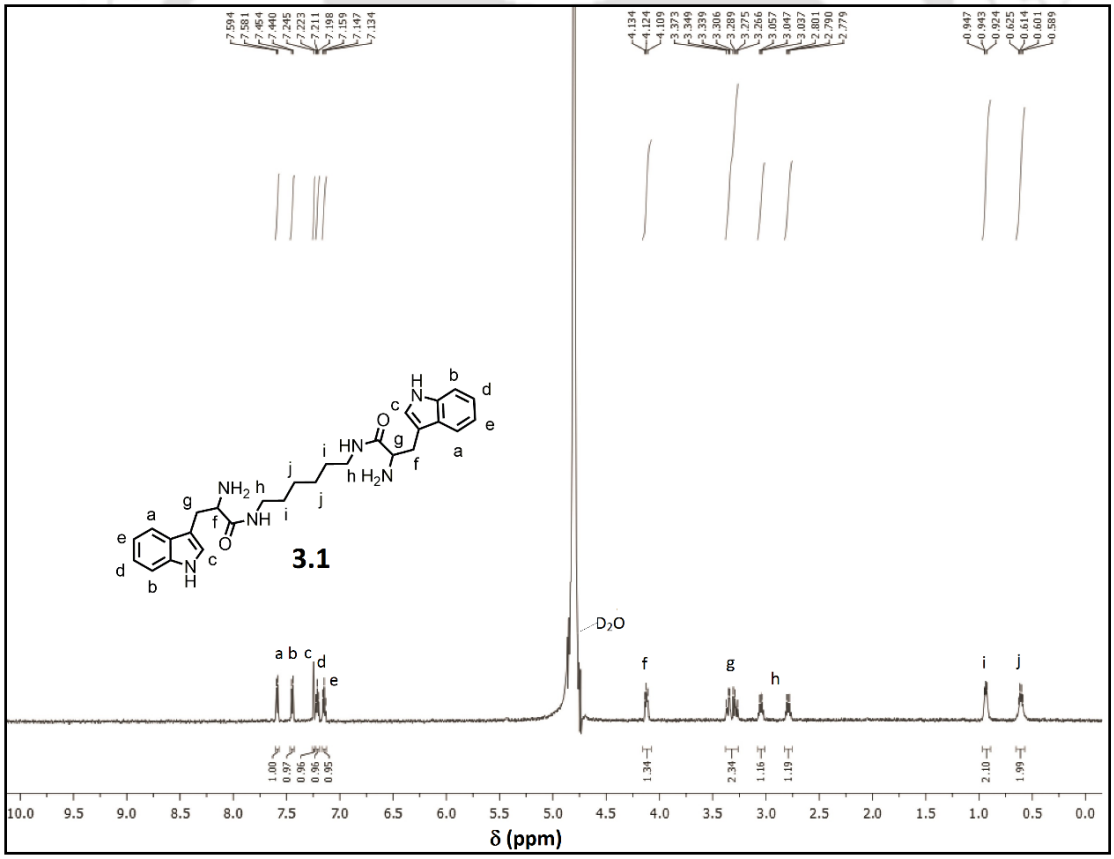

^{1}H NMR spectrum of Compound **3.1**

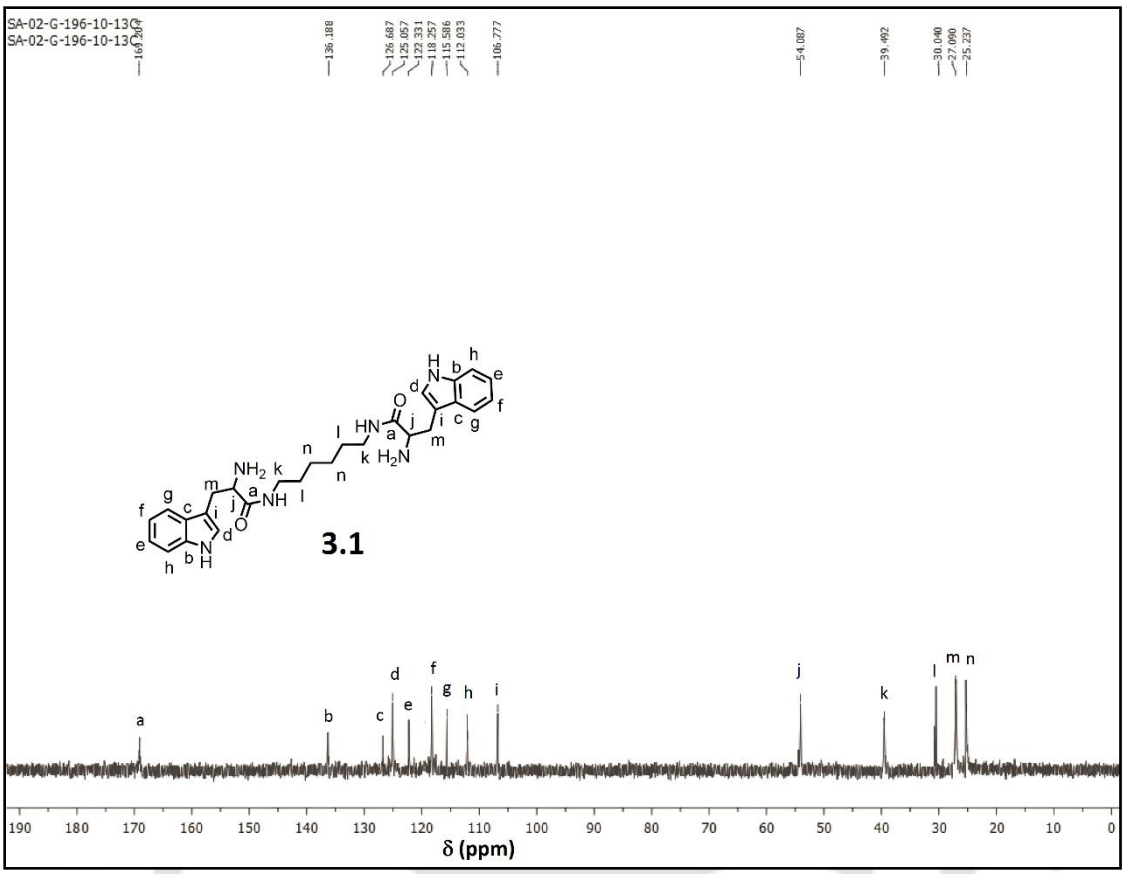

^{13}C NMR spectrum of Compound **3.1**

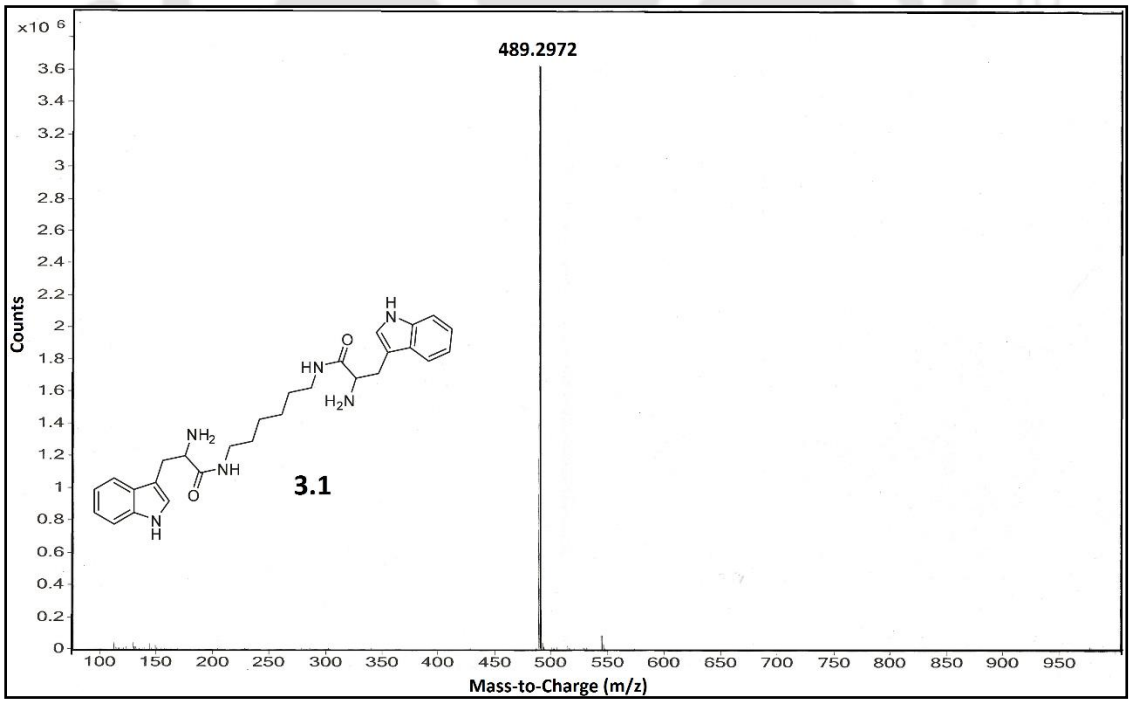

ESI-MS of Compound **3.1**

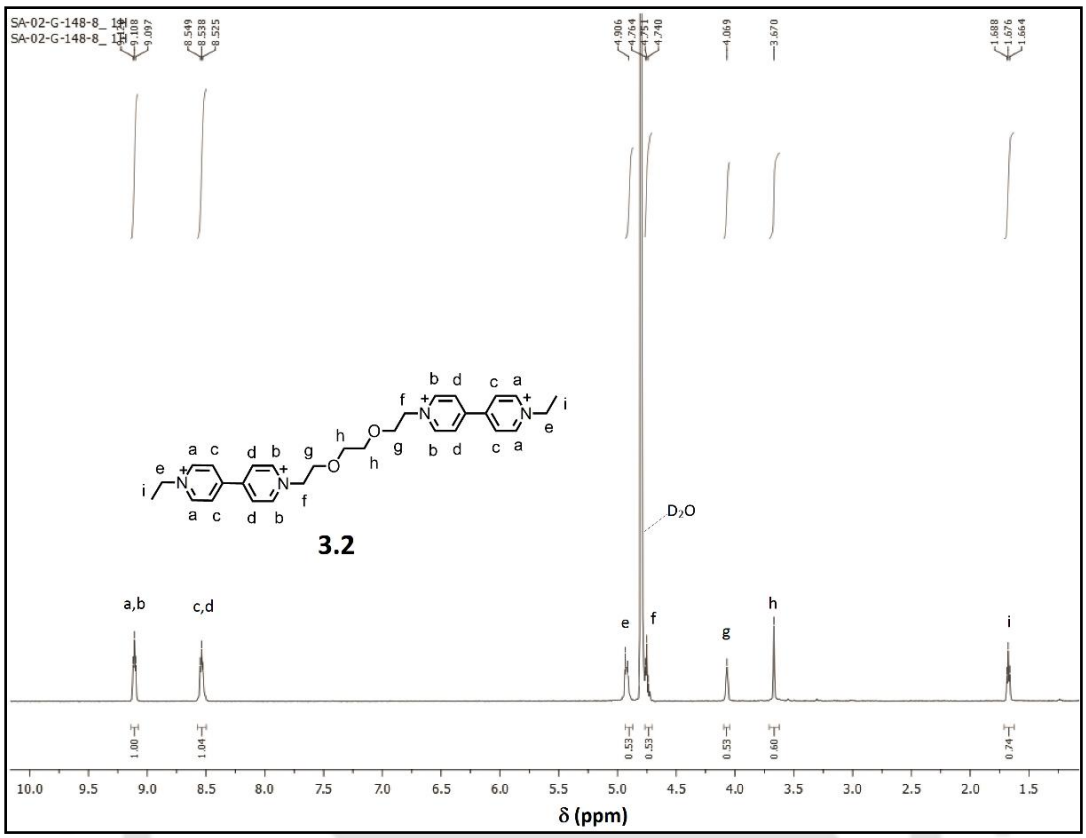

^{1}H NMR spectrum of Compound **3.2**

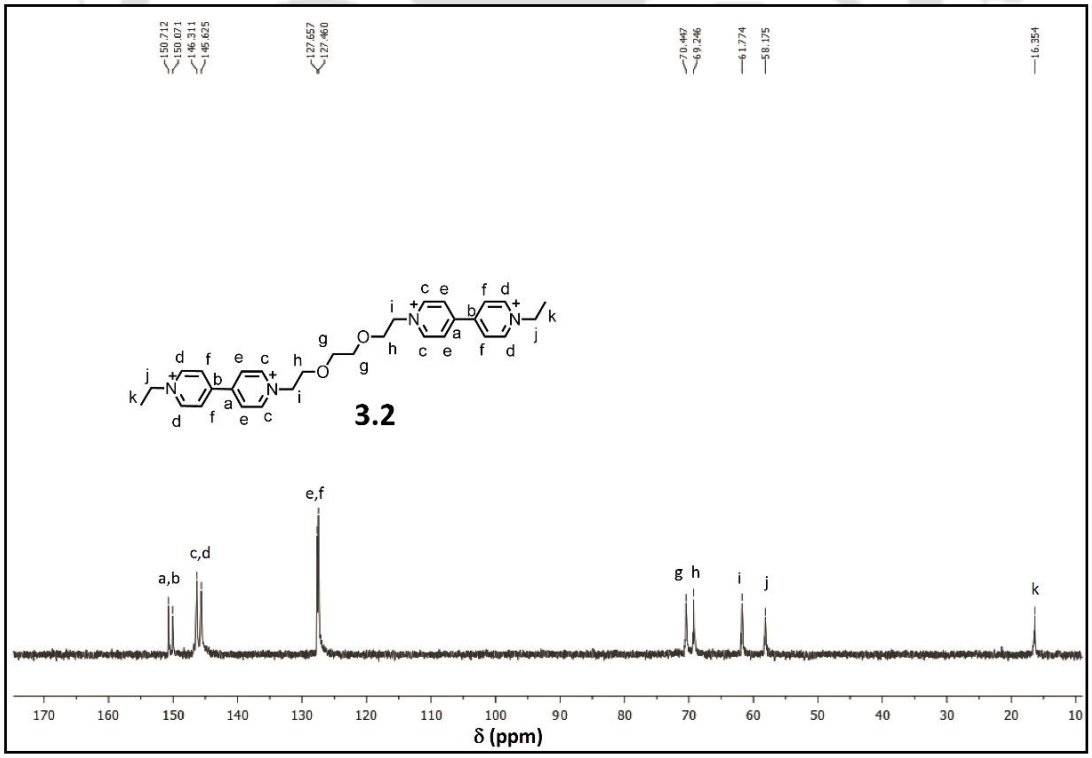

^{13}C NMR spectrum of Compound **3.2**

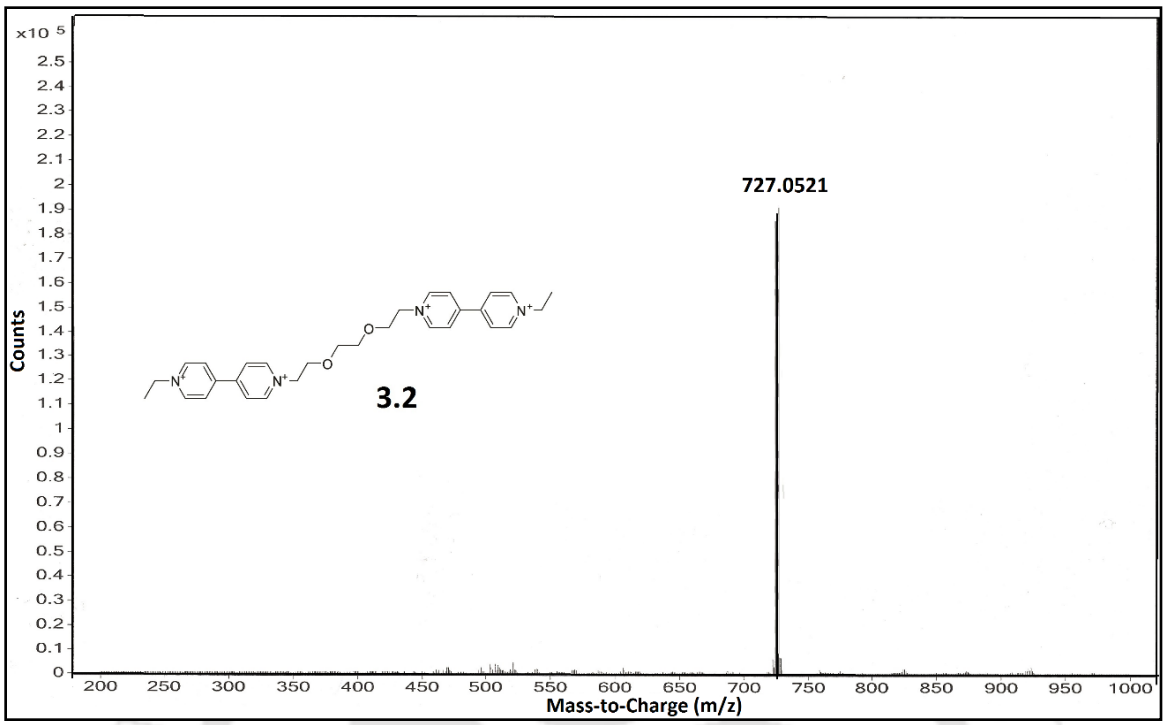

ESI-MS of Compound **3.2**

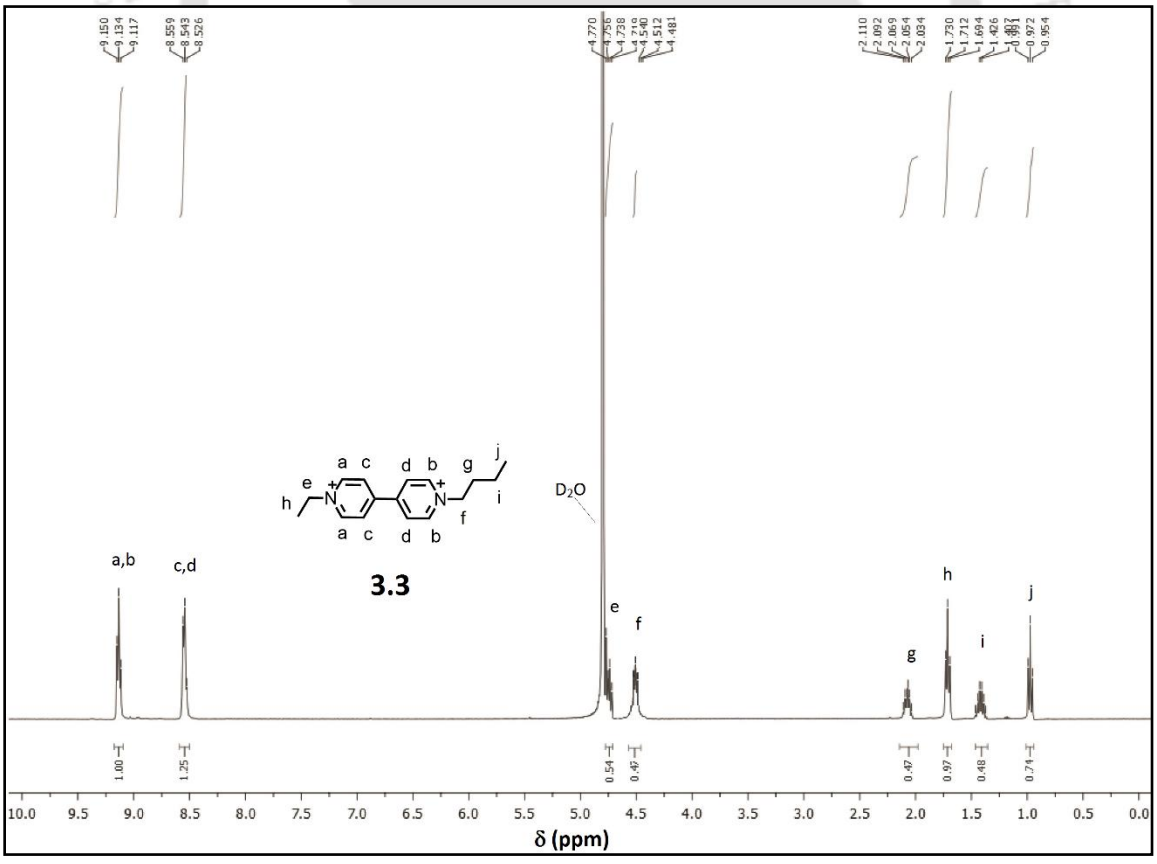

^{1}H NMR spectrum of Compound **3.3**

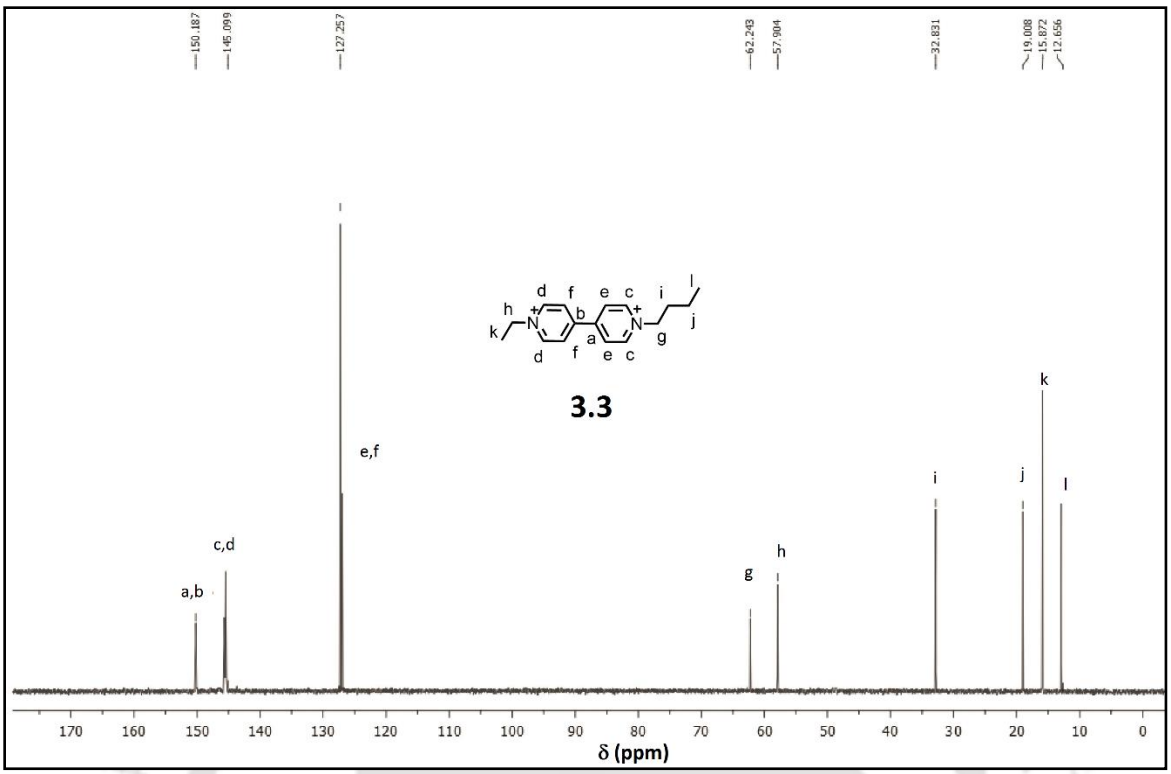

^{13}C NMR spectrum of Compound **3.3**

ESI-MS of Compound **3.3**

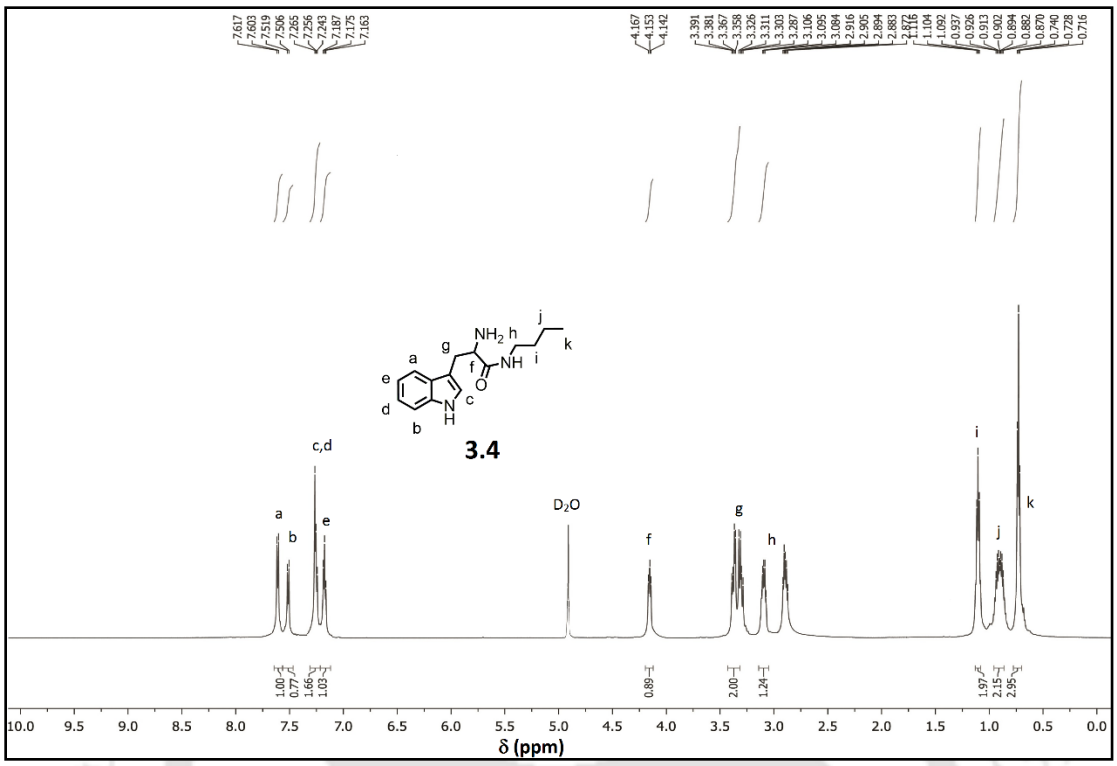

^{1}H NMR spectrum of Compound **3.4**

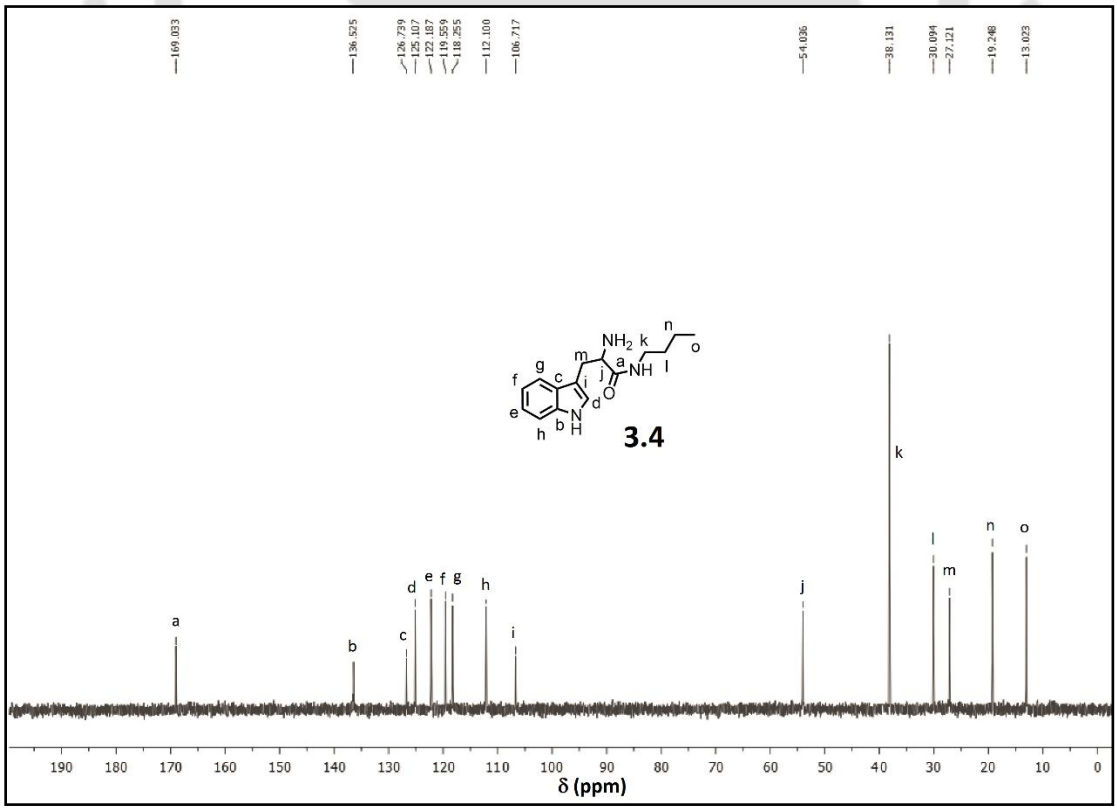

^{13}C NMR spectrum of Compound **3.4**

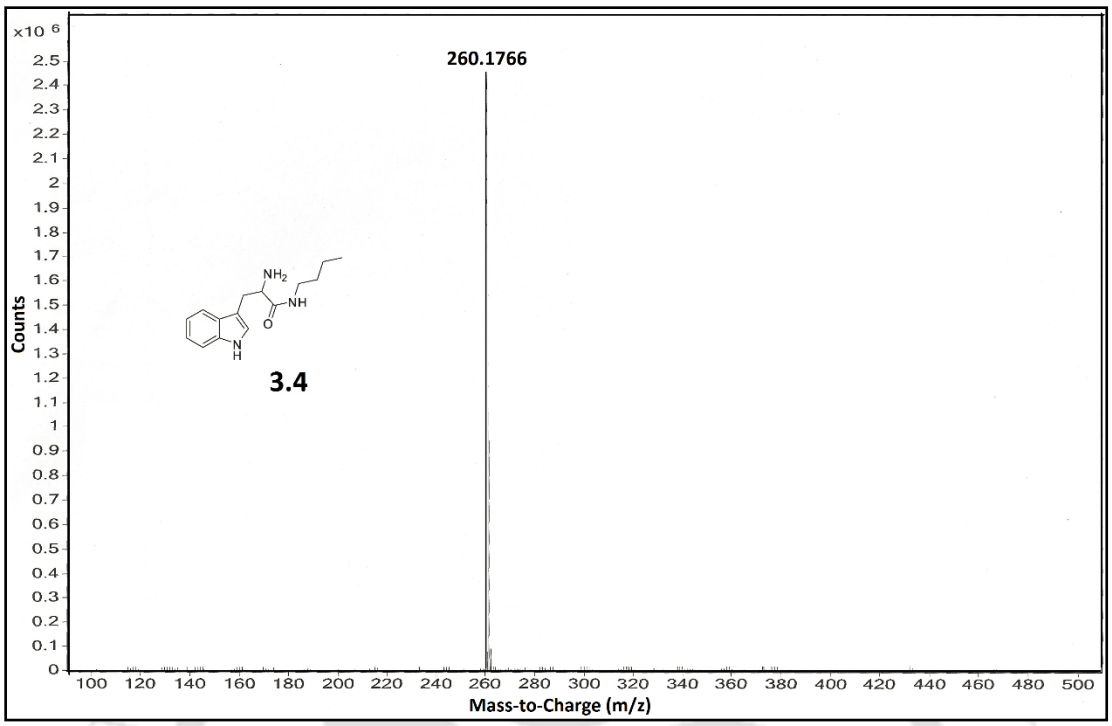

ESI-MS of Compound **3.4**

Chapter 4

Self-Assembly of a Peptide-Perylenediimide Conjugate: Solvent Directed Tuning of Helicity and Morphology

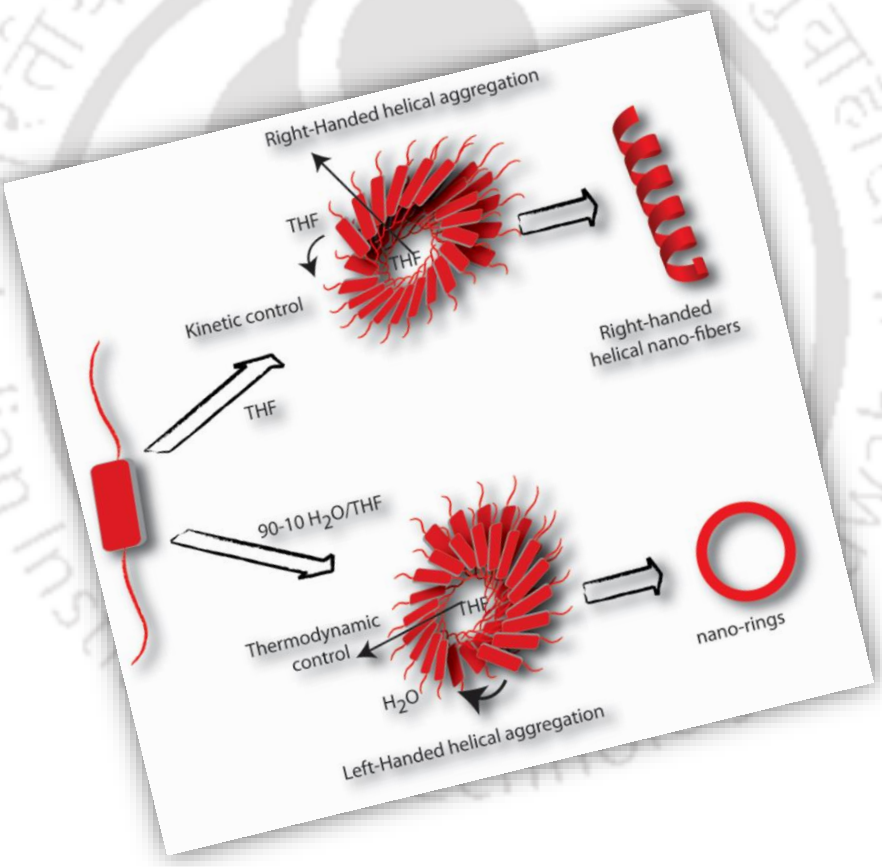

4.1 Introduction

There is a growing interest in systems capable of assembling into helical arrangements with precise shape and size in nanometer regime.[208-213] However, the supramolecular chirality imposed by the chiral center of the monomer on hierarchically organized morphology in solution as well as on surfaces is an extremely multifaceted phenomenon. The growth of such self-assembled systems are influenced by various associated parameters such as solvent, temperature, pH, *etc.*[214-217] Minor alteration in these parameters often lead to dramatic changes in the supramolecular helicity and consequently to the super structure. Understanding the thermodynamic and kinetic control of these self-organization processes is therefore of utmost importance in order to fabricate and fine tune the nanostructures of these self-organized highly functional systems.

In this context, amino acids and peptides are one of the major natural sources of chirality and have been utilized substantially to construct such supramolecular helical structures in recent past.[193,218-220] One of the shortest peptide sequence which attracted considerable attention of supramolecular chemists in the recent past is diphenylalanine (PhePhe). This short peptide from the core of Amyloid β peptide self-assembling sequences, was identified through a methodical reductionist approach envisioned to find the minimum recognition motif for self-assembly.[62] Interestingly, subtle modifications in the chemical structure of the Phe-Phe derivative or minute changes in the experimental conditions are adequate to attain different nanostructures.[60,63,221-223] On the other hand, helical nanostructures created by π–systems are of particular interest due to their potential applications in organic electronic devices.[134,224,225] One such extended π–conjugated ring system discussed in chapter 1, is Perylenediimide (PDI). It was envisioned that the conjugation of "PhePhe" motif with PDI core will lead to a helical assembly owing to the presence of chiral amino acids as well as a π–stacking unit in the form of PDI. Investigation on the factors influencing the formation and fine tuning of the helical nano-aggregates will certainly be of tremendous importance to gain control over such assemblies.

In this chapter, the aggregation behavior of a symmetrical conjugate of "PhePhe" motif and PDI core (**FFPDIFF**, Figure 4.1A) has been reported. The self-assembly, nanostructure and formation mechanism were studied in tetrahydrofuran (THF) with varying ratio of water. The terminal "PhePhe" dipeptide units provide the supramolecular chirality while the planner symmetrical PDI core is responsible for the π–π stacking. The combination of these two factors led to the formation of helical nano-fibers in THF while in presence of higher percentage of water, not only the handedness changed but also the morphology shifted to nano-rings. The detailed study has revealed the kinetic and thermodynamic control of the self-assembly processes in different conditions.

4.2 Result and Discussion

The morphologies of **FFPDIFF** in THF-water mixed solvents (with different volume ratios at a concentration of 10 μM) were examined by field emission scanning electron microscopy (FESEM). Network of high aspect ratio (3-10 μm) right-handed helical fibers were observed in THF (Figure 4.1B). In a THF-water binary system with high amount of water (90%, above which difficult to solubilize), nano-rings with 150-250 nm diameter were obtained (Figure 4.1C). Interestingly, in 50% THF, both fiber and nano-ring like morphologies were observed (Figure 4.1D). Notably, formation of loop in the fibers to generate rings was also observed at places. Similar morphologies were also found from transmission electron microscope images (Figure 4.2).

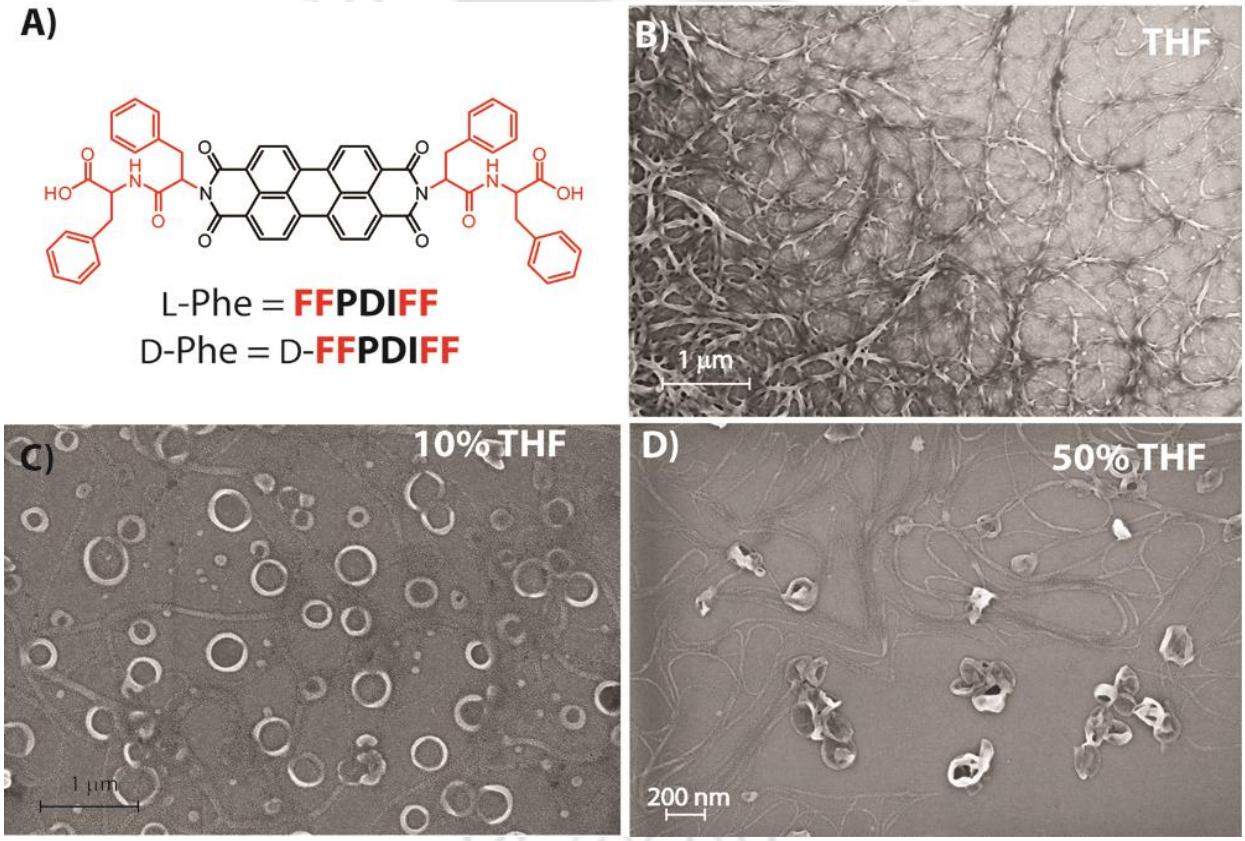

Figure 4.1 A) Molecular structure of **FFPDIFF**; FESEM images of **FFPDIFF** nanostructures obtained from THF/water mixed solvents (10 μM) with different volume ratios of B) THF; C) 10% THF and D) 50% THF. All measurements were carried out after 72 h of mixing.

To understand the aggregation of **FFPDIFF** in these solvent systems, UV-Vis absorption, emission and CD spectra were recorded at various solvent compositions. The UV-vis absorption spectrum of **FFPDIFF** in THF exhibited three characteristic vibronic bands at 517, 482 and 460 nm which are attributed to the 0-0, 0-1 and 0-2 vibrational transitions respectively (Figure 4.3A and B).[156,214-217,226,227] Ratio of the

absorption corresponding to the 0-0, 0-1 transitions obtained (A_{0-0}/A_{0-1} = 1.44) was far lesser than the same for monomeric species (1.72 at a concentration of 0.1 μM, Figure 4.4) and higher than the standard value of fully aggregated state (>0.8) suggesting that the molecules were in partial aggregated state.[143-146] The partial aggregation was also supported by the broadening of the signals in the excitation spectra (Figure 4.5). With gradual increase in water content, a consistent red shift accompanied with decrease in absorbance was recorded for all these transitions.

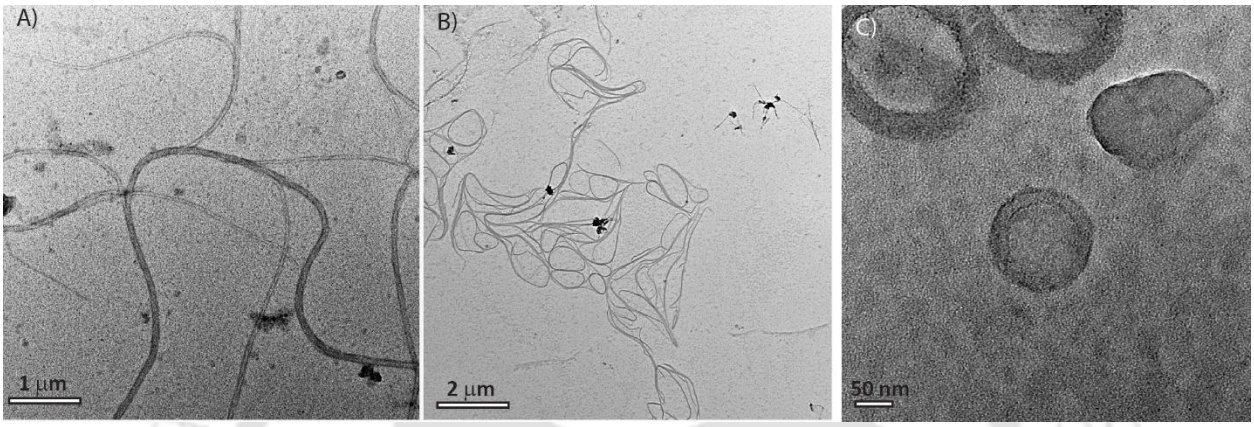

Figure 4.2 TEM micrographs of nanostructures formed by **FFPDIFF** in different THF-water compositions (1 μM) at room temperature. A) THF; B) 50% THF; C) 10% THF. All measurements were carried out with 72 h matured samples.

Below 20% THF, a drastic change was observed in the absorption spectra as the fine structure was lost and a new shoulder appeared at ~ 550 nm which is typically a sign of co-facial π–π stacking.[143-146,214] In 10% THF, A_{0-0}/A_{0-1} value dropped to 0.77 which signifies fully aggregated state of molecules in this system.[143-146] The bathochromic shift of the absorption maxima, broadening of peaks along with the appearance of peak at 550 nm indicate the presence of well-defined J-type aggregates.[214,217,228] The formation of J-aggregates was further supported by emission spectra as shown in figure 4.3D. In THF, the emission spectrum is the mirror image of corresponding absorption spectrum with a maxima at 533 nm (Stokes shift of 15 nm). With increase in water content, a bathochromic shift accompanied by quenching of the emission was observed indicating the onset of aggregation. Below 20% THF, the emission is completely lost and a new band appeared at 610 nm. Further information about the aggregation obtained from the appearance of structure-less broad band centered at ~ 540 nm in the excitation spectra collected at 620 nm (Figure 4.5C).

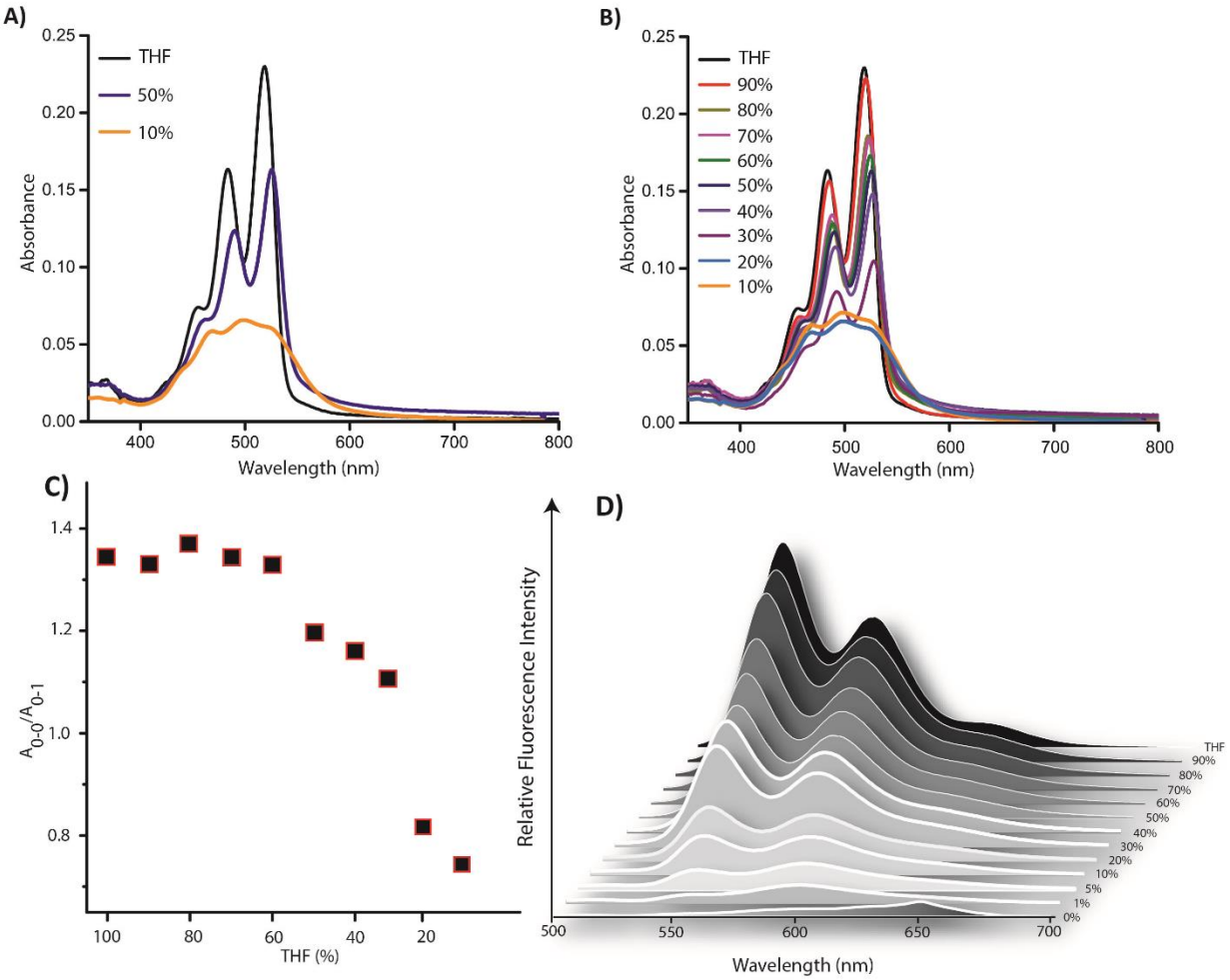

Figure 4.3 A) and B) UV-Visible spectra and C) Absorption ratio of the 0-0 and 0-1 transition at different THF content; D) emission spectra of **FFPDIFF** in different volume ratio of THF/water (10 μM) under ambient condition. All measurements were carried out after 72 h of mixing.

The circular dichroism (CD) data showed intense cotton effects for **FFPDIFF** in 10% THF. As shown in figure 4.6A, the CD spectrum showed a bisignate CD signal with a positive signal at 482 nm and negative signals at 522 and 550 nm (crossover at 502 nm). The bisignate CD signal observed in this case indicates aggregated arrangement of FFPDIFF where the transition dipoles are oriented in a helical manner.[217,229,230] The positive/negative bisignate signal with increasing wavelength suggests that compound **FFPDIFF** adopted a left-handed helical arrangement in this solvent composition.[217,229,230] Similar CD signals, though comparatively lower in intensity, were observed in case of 50% THF.

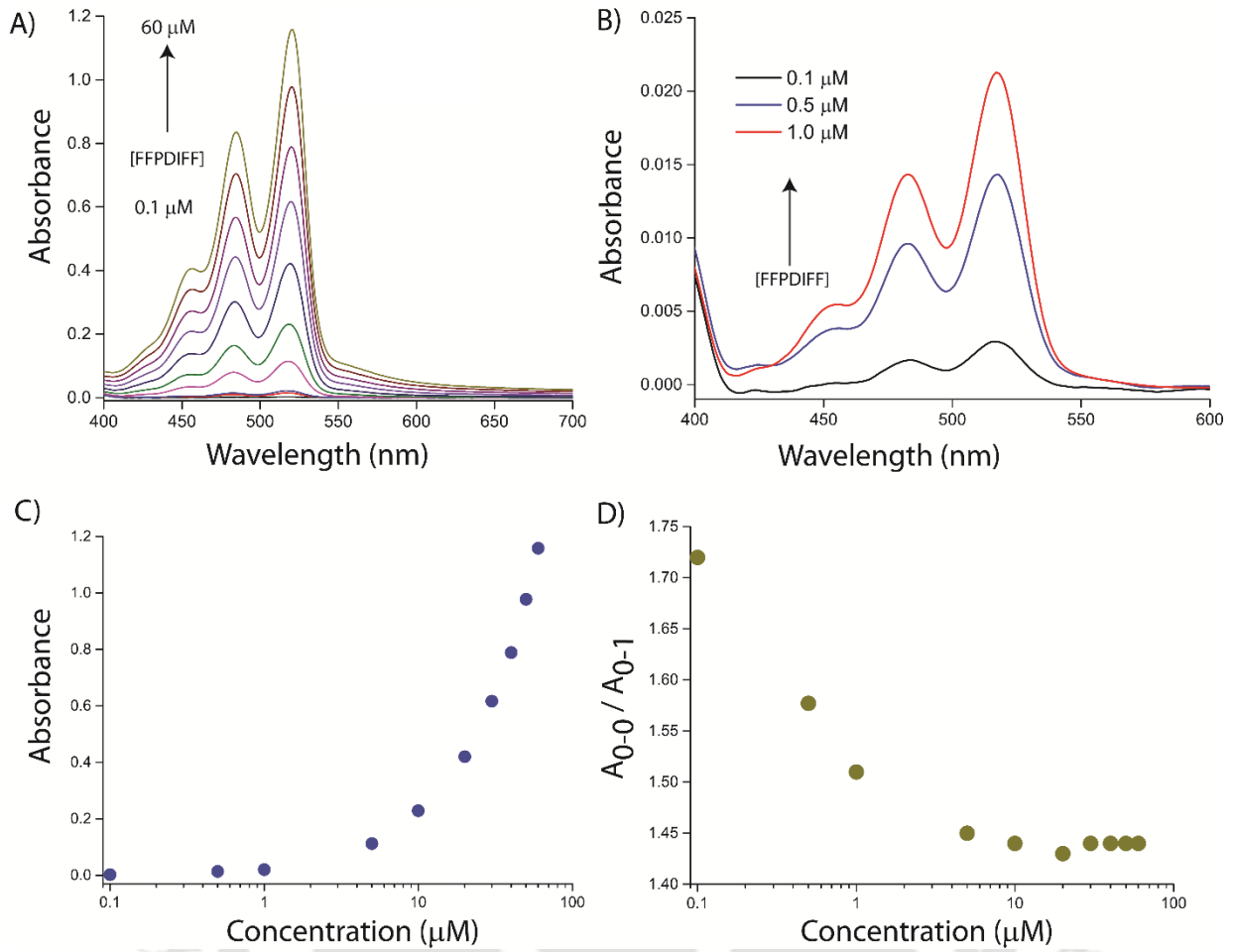

Figure 4.4 (A-B) Concentration dependent UV-Vis absorption spectra of **FFPDIFF** in THF; (C) dependence of the $A_{0\text{-}0}$ transition and (D) $A_{0\text{-}0}/A_{0\text{-}1}$ on concentration of **FFPDIFF** in THF. All measurements were carried out with 72 h matured samples at room temperature.

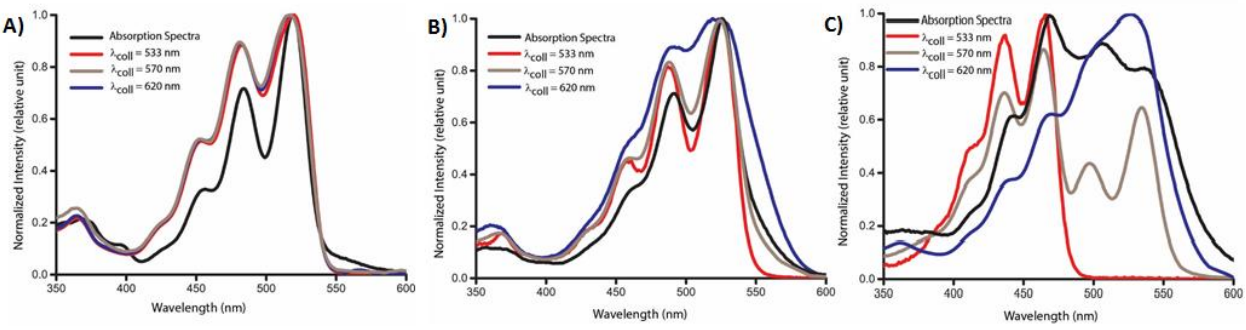

Figure 4.5 Excitation spectra overlaid with the corresponding UV-Vis spectra of **FFPDIFF** in A) THF; B) 50% THF; C) 10% THF. In all cases the concentration of **FFPDIFF** is 10 μM.

Interestingly, in THF, though the crossover point remains the same, negative to positive bisignate signals were observed along with decrease in intensity. The reversal of the positive and negative signals indicates the change in the helicity from left-handed to right handedness. Notably, this is consistent with the right handed helical fibers obtained from THF (Figure 4.1B). The D-analogue (D-**FFPDIFF**) of the

compound, with D-PhePhe units, showed the mirror image CD signals in each case (Figure 4.6B). The morphologies were also consistent with the CD-signals as left-handed helical fibers were formed in THF (Figure 4.6C) while in 10% THF, nano-rings (Figure 4.6D) were observed.

To investigate the self-assembly mechanism in these solvent systems, time-dependent UV-Vis and CD spectra of **FFPDIFF** in different THF-water compositions were recorded (Figure 4.7). Interestingly, in case of 10% THF, initially a low intensity bisignate signal was observed. The intensity was drastically enhanced over a period of 24 h and a clear bisignate CD signal with a positive peak at 482 nm and negative signals at 522 and 550 nm were observed (with a crossover at 502 nm). Similarly, in the UV-Vis spectra, the absorption ratio of the 0-0 and 0-1 transitions was observed to be ~1.30 initially. The ratio dropped to 1.1 within a period of 6 h. The absorption ratio dropped further to 0.77 after 24 h and remained unchanged after that. The decrease in the absorption ratio was accompanied with a broadening of the spectra. The saturation value of 0.77 is similar to the aged sample as shown in figure 4.3A and 4.3B. The observed results suggest that, even at the nucleation stage, **FFPDIFF** adopted a left-handed helical arrangement and the nucleation was a kinetically controlled process. With time, the aggregation proceeds in a thermodynamically controlled fashion.[214,217]

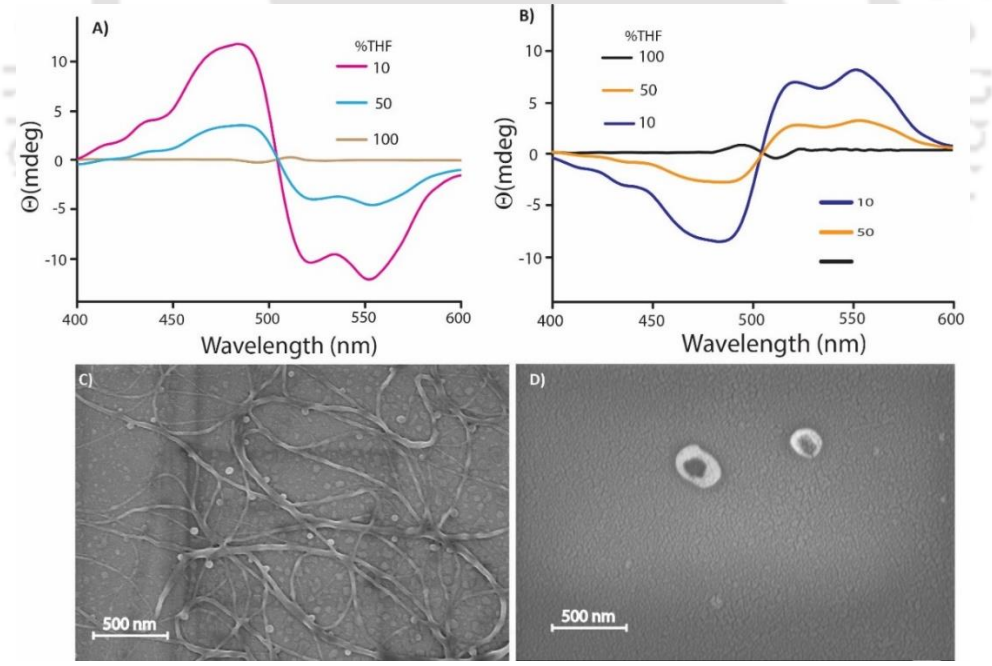

Figure 4.6 CD spectra of **FFPDIFF** in different volume ratio of THF/water (10 μM) under ambient condition. A) For L and B) For D analogue of **FFPDIFF**. FESEM image of D-FFPDIFF in C) THF; D) 10% THF/water.

The thermodynamic control was further elucidated by recording the FESEM images at different time intervals (Figure 4.8A-C). At initial stage (0 h), though no clear morphology could be found, after 6 h, some aggregated structures could be observed. In case of the 12 h aged sample, the formation of ring

like structures started appearing. After 24 h, the morphology was very similar to that shown in figure 4.1B and uniform nano-rings were found all over the surface.

However, in THF, neither did the absorption nor did the $A_{0\text{-}0}/A_{0\text{-}1}$ ratio (remained constant at 1.44) change with time up to 72 h (Figure 4.7A). Similarly, no observable change was monitored in the CD signal over a period of 72 h (Figure 4.7B). The morphology study showed right-handed helical fibers from the very initial stage and did not change with time. These observations signify that the aggregation in THF, takes place in a kinetically controlled process.[217]

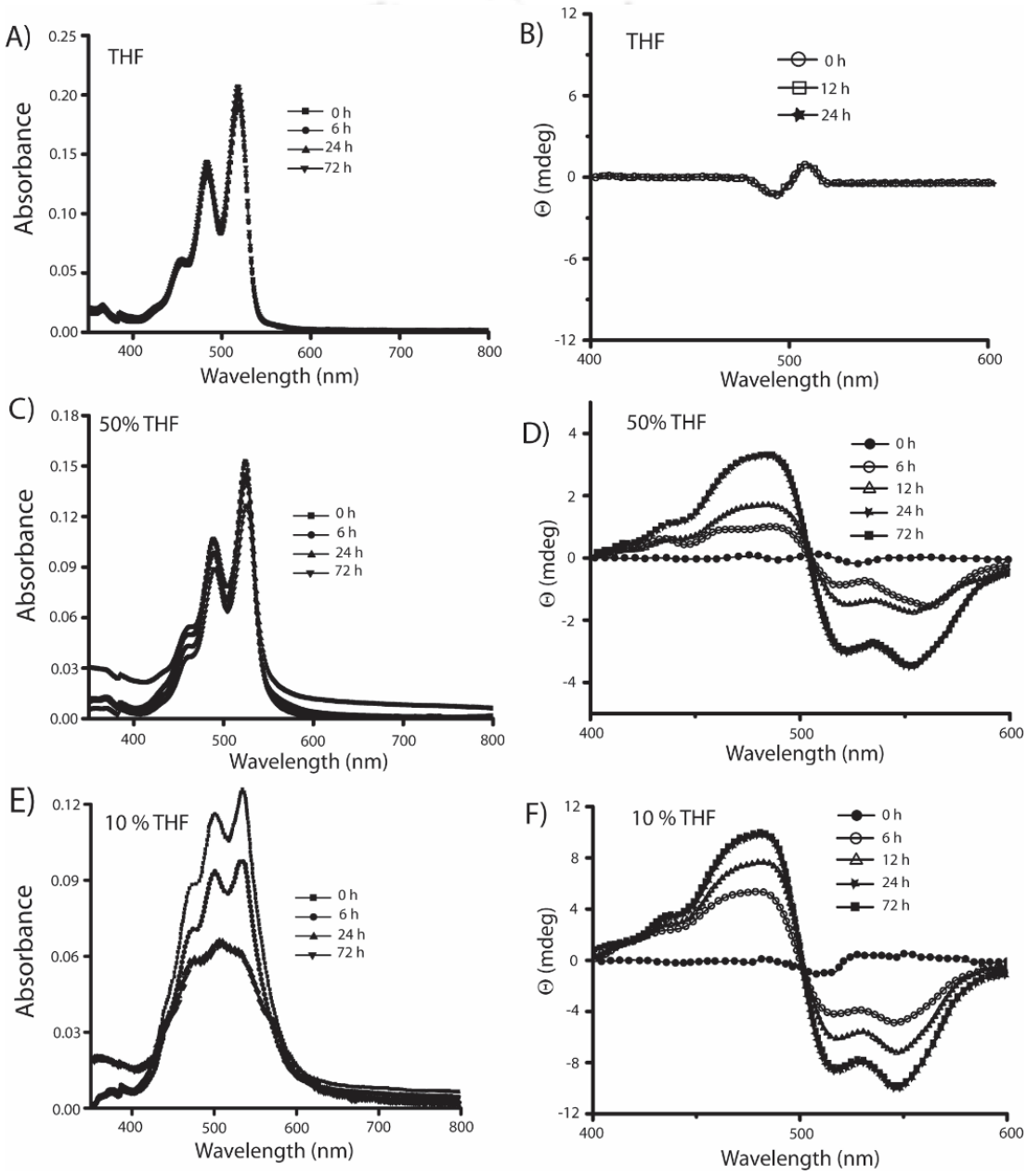

Figure 4.7 Time dependent (A, C, E) UV-Visible and (B, D, F) CD spectra of **FFPDIFF** (10 μM) in THF, 50% THF and 10% THF mixed solvent systems respectively.

The case of 50% THF system was also similar to that of the 10% THF. The UV-Vis spectra showed a decrease in absorption with time. The absorption ratio for the 0-0 and 0-1 transitions dropped from 1.33 to a saturation value of 1.21 within 24 h suggesting maximum aggregation after this time. Interestingly the system showed a weak cotton effect at the initial state having multiple bisignate signals with crossover points at 482 nm and 521 nm. However, after 6 h, the pattern changed to that of 10% THF system showing a bisignate signal with positive and negative peaks at 482 and 550 nm respectively. The positive/negative pattern indicates the formation of left-handed helical aggregates which matches with the CD signal of the matured samples (Figure 4.6A). The intensity of the signals increased with time but after 24 h no change was observed. Unlike the case of 10% THF, the time dependent FESEM study of 50% THF system showed (Figure 4.8D-F) fiber like structures at the initial stage (0 h) while both fiber as well as nano-rings were found after 12 h. After 24h, the morphology was predominantly filled with nano-rings with occasional appearance of fibrous structures which was similar to that of the 72 h aged sample (Figure 4.1D).

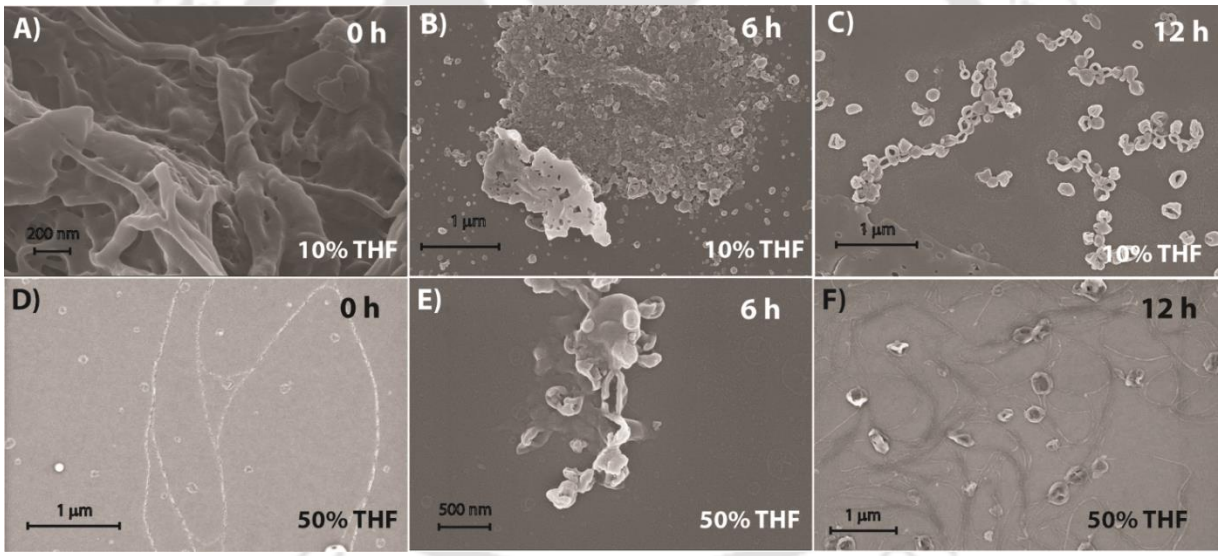

Figure 4.8 FESEM images of **FFPDIFF** nanostructures obtained from 10% THF (A-C) and 50% THF (D-F) mixed solvents (10 µM) at different time intervals.

To further consolidate the kinetic and thermodynamic control over the self-assembly of **FFPDIFF** in different solvent systems, temperature dependent UV-Visible and CD spectra were recorded (Figure 4.9). Absorption and CD spectra recorded for **FFPDIFF** in THF between 25 and 55 °C showed no noticeable change during the heating and cooling cycles supporting the kinetic control over the assembly. Notably, in the case of 10% THF, both absorption and CD signals showed significant changes as a function of temperature. The absorption increased with increase in temperature followed by a reversal of the $A_{0\text{-}0}$ and $A_{0\text{-}1}$ ratio. In case of CD signals, the intensity decreased with temperature as can

be seen in figure 4.9. On cooling, both the spectral features restored back to their initial positions. The dependence of both absorption and CD signals on temperature strongly support the thermodynamic nature of the assembly.[231,232] In the case of 50% THF, somewhat mixed responses were obtained. Both, absorption and CD signals showed slight changes as the absorption increased with temperature while the CD intensity decreased. However, the observed changes were much lower compared to that of the case of 10% THF system. The minor changes observed in this case may presumably due to the fact that both thermodynamic and kinetic factors control the assembly in this case which supports the appearance of mixed morphology in this case.

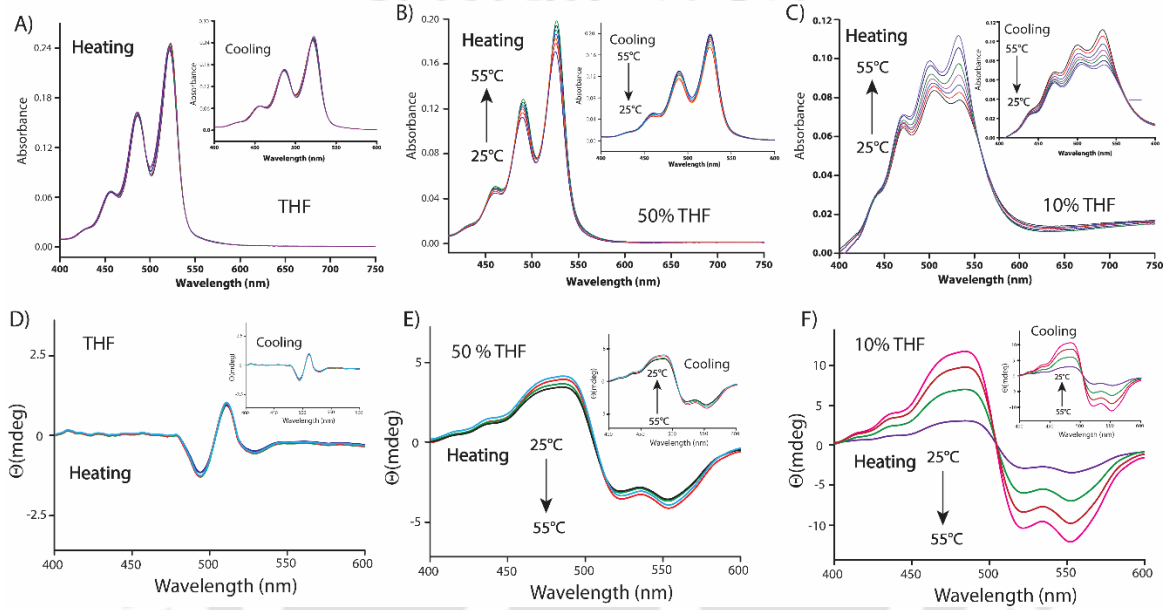

Figure 4.9 Temperature dependent UV-Visible (A-C) and CD (D-F) spectra of 10 μM solutions of **FFPDIFF** in different THF-water compositions.

To further elucidate the self-assembly mechanism, ^{1}H NMR and IR spectra of the matured samples were recorded. In deuterated THF (THF-d_8), the aromatic and the amide protons appeared as sharp peaks which broadened considerably in presence of D_2O (Figure 4.10A). In 50% THF-d_8, a clear upfield shift of the aromatic protons arising from PDI core was observed. Interestingly, the phenylalanine protons showed two broad signals, one down-field shifted while the other slightly upfield shifted. With further increase in D_2O, i.e. 10% THF-d_8, these two sets of protons were further separated as one of them moved to higher chemical shift value while the other showed upfield shift. Though it is possible that these split signals arise from two different "Phe" protons on each sides of the PDI core, the close proximity and similar chemical equivalence of these two "Phe" groups (as they appear at the same chemical shift values in case of THF-d_8) make this possibility very unlikely. On the other hand, two different signals may arise from the "Phe" protons of two different sides of the PDI core if the environments are different

around these two sides. To understand the situation, IR spectra were recorded for these samples. As shown in figure 4.10B, the sample from THF showed three clear carbonyl stretching frequencies at 1639 cm^{-1} (imide), 1718 cm^{-1} (amide) and 1777 cm^{-1} (carboxylic acid).[227,233] As the water content enhanced, not only the intensity for the amide band decreased dramatically, the signal split in to two. The new signals arising from the amide bonds appear at 1708 cm^{-1} and 1728 cm^{-1} in case of 50% THF. In 10% THF, further shifts were observed and the bands appeared at 1702 cm^{-1} and 1731 cm^{-1}. The splitting of the amide signal signifies the presence of two different types of amides in the system. This phenomenon indicates that in 10% THF, the molecules are aggregated unsymmetrically.

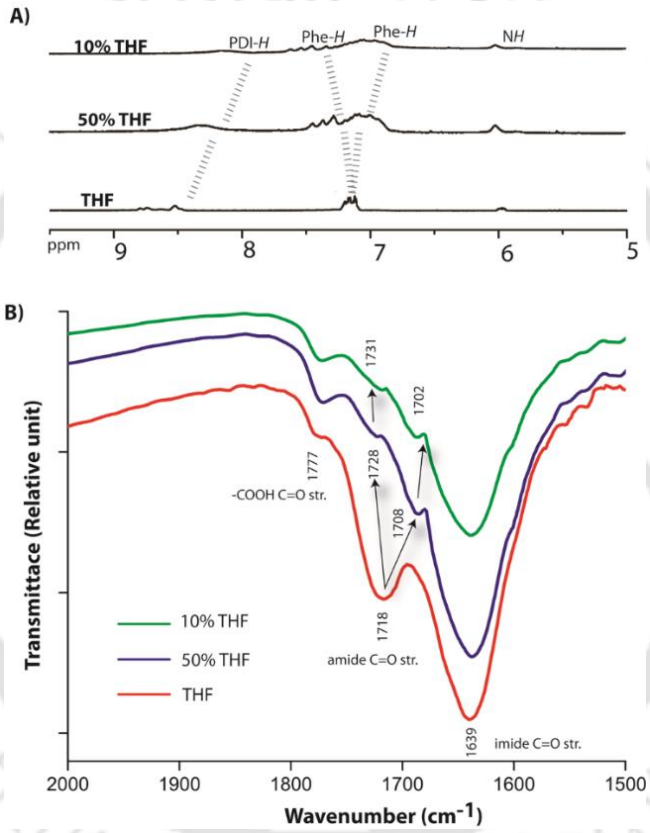

Figure 4.10 A) ^{1}H NMR (aromatic region) spectra and B) IR (carbonyl region) of **FFPDIFF** (10 μM) from different THF-water compositions.

DFT calculations were performed to find out the energetically favorable mechanism of the self-assembly. Three initial configurations of PDIs were chosen based on relative orientations of "PhePhe" units (Figure 4.11). These were geometry optimized to obtain the energetically most favorable structure (Table 4.1, for final energies of optimized structures). The most stable configuration formed the nucleus of the aggregates. Figure 4.12 shows how the optimized stable geometries can be stacked to form helical aggregates as proposed in scheme 4.1. The helical aggregate can form a nano-ring due to the

attractive depletion energy of the expelled water from the core (where the THF molecules reside) which can be accommodated within the bulk-water near the "PhePhe" groups at outer rim of the nano-rings. Thus the inner and outer "PhePhe" groups are differentially solubilized in THF and bulk water respectively to provide an energetically favorable condition.

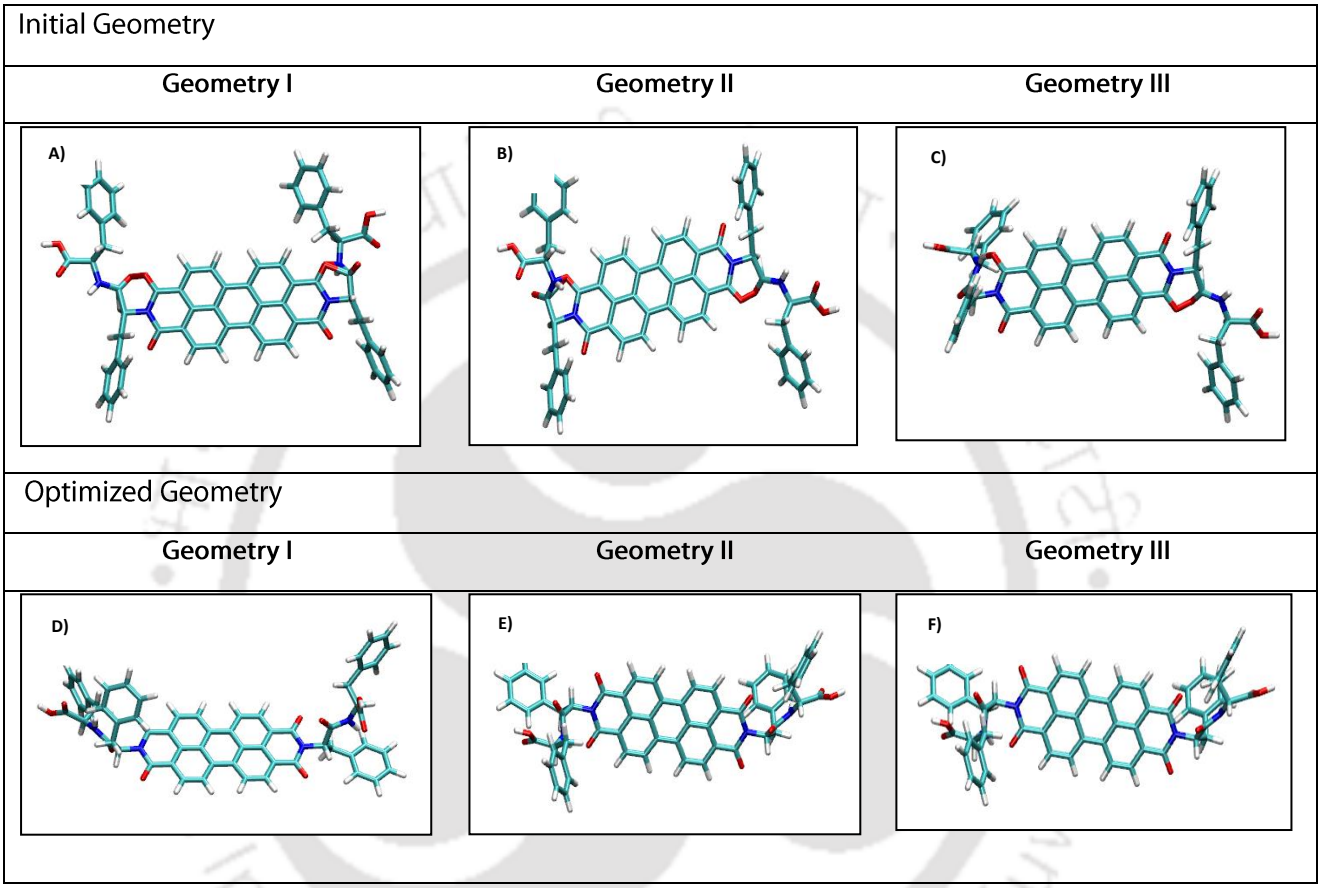

Figure 4.11 Three configurations of **FFPDIFF** molecule. (A)-(C) The initial geometries, (D)-(F) the optimized geometries respective to (A)-(C).

Table 4.1 Final energies of the optimized structures of the three configurations. The energies are expressed in atomic units (a.u.).

Geometry I	Geometry II	Geometry III
-3284.3365	-3284.3358	-3284.3357

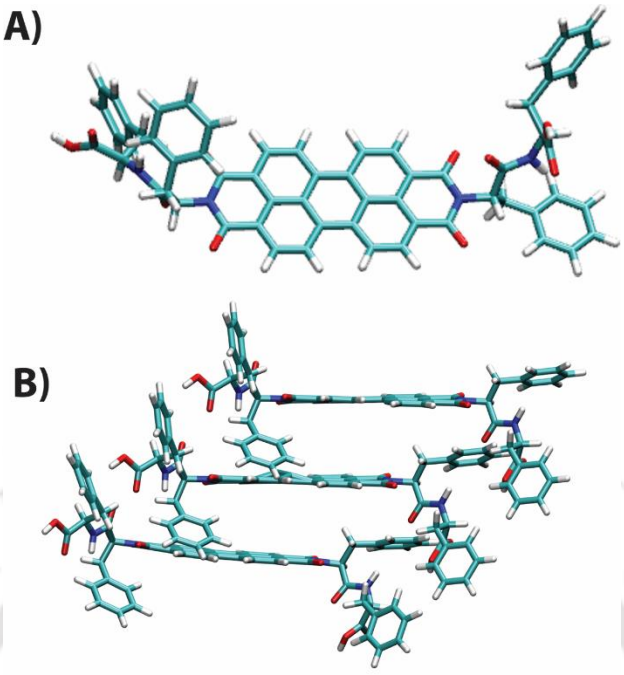

Figure 4.12 A) Energy minimized optimum geometry and B) stacking arrangement of **FFPDIFF** molecule along the Z axis.

Based on the presented data and theoretical calculations, it is now possible to summarize the detailed mechanism of the self-assembly processes involved. **FFPDIFF** is sparingly soluble in water (< 0.1 μM) but shows moderate solubility in THF (~ 0.1 mM) and thus THF can be termed as a good solvent and likewise, water as poor solvent for **FFPDIFF**. However, even in THF, the molecules form kinetically controlled aggregate. The molecules, owing to the presence of chiral residues, form right-handed helical nano-fibers (Scheme 4.1). In presence of a poor solvent like water, the self-assembly occurs dominantly in a thermodynamically controlled fashion. In this case (10% THF), the nucleation of J-type aggregates at the initial stage is a kinetically controlled process and leads to a left-handed helical nuclei. The nuclei further grow with time and the growth of the nuclei is thermodynamically driven. Following the kinetically controlled nucleation, owing to the 'sergeant and soldiers rule', the helicity of the assembly remained left-handed.[234] As the nuclei grow, in case of 10% THF, the THF molecules presumably tend to form an inner core where the "PhePhe" units of one side of the stack get easily solubilized. Being the poor solvent as well as more in number, water molecules tend to come out of this core region, keeping THF within the core in order to increase entropy where depletion energy plays a role. Therefore, the solubilization of the "PhePhe" units are different in the outer and inner rims of the nano-rings. This explains the presence of two types of Phenyl groups as well as two different amide signals in IR spectra. This differential solubility in turn creates a critical hydro-dynamic radius to chain length which does not allow the chain to grow along the long axis but forms the ring.

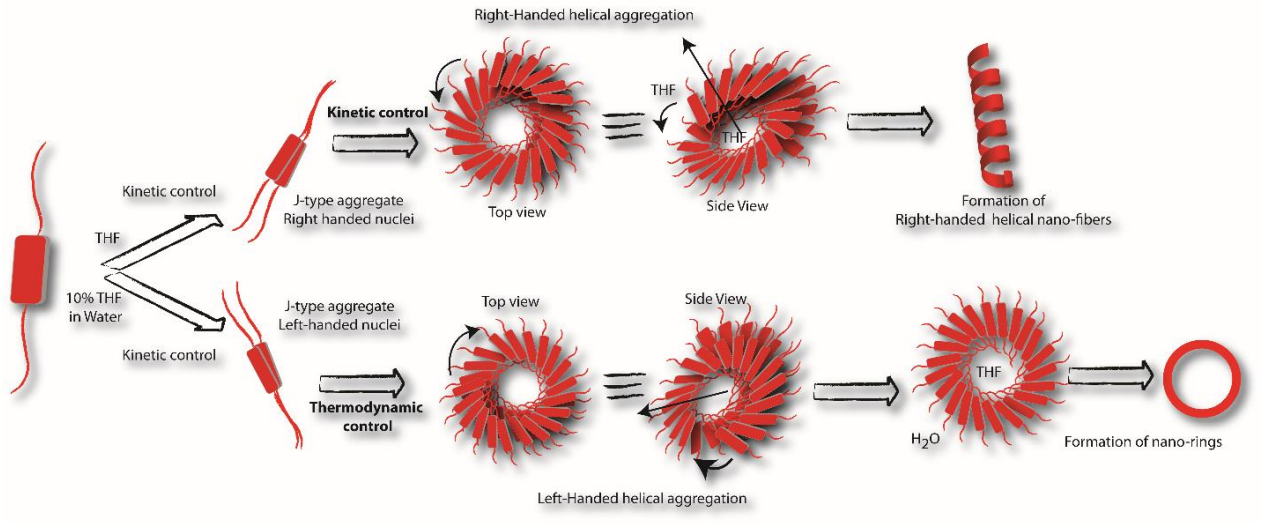

Scheme 4.1 Schematic presentation of the thermodynamic and kinetic control of the self-assembly process of **FFPDIFF** in different solvent composition to show the formation mechanism for helical nano-fibers and nano-rings.

4.3 Conclusion

The mechanistic detail of the solvent controlled self-assembly of a peptide-PDI conjugate in the form of **FFPDIFF** has been revealed. The observed experimental results combined with theoretical calculations show that, in THF, **FFPDIFF** forms kinetically controlled right-handed helical nano-fibers. In presence of high percentage of water, i.e. in 10% THF, the initial nucleation is kinetically controlled and a left-handed helical nuclei is formed, which grows further in a thermo-dynamically controlled manner. A differential solubilization of the "PhePhe" motif on two sides of the fiber leads to the proper curvature which allow the formation of the nano-rings.

4.4 Experimental Section

4.4.1 General

All the chemicals and reagents used were obtained from Sigma-Aldrich (USA) and used without further purification. All solvents were procured from Merck, India and Spectrochem, India. To prepare samples, Milli-Q water with a conductivity of less than 2 μS cm^{-1} was used. ^{1}H NMR, ^{13}C NMR spectra were recorded on either a Bruker Ascend 600 MHz (Bruker, Coventry, UK) or an Oxford AS400 (Varian) spectrometer. ESI-MS spectra were recorded using a Q-Tof-Micro Quadrupole mass spectrometer (Micro-mass). MALDI-TOF was measured on a Bruker Autoflex Speed mass spectrometer.

4.4.2 Synthesis and Characterization of Compounds

FFPDIFF and **D-FFPDIFF** were prepared following scheme 4.2 starting from L- and D- phenylalanine respectively.

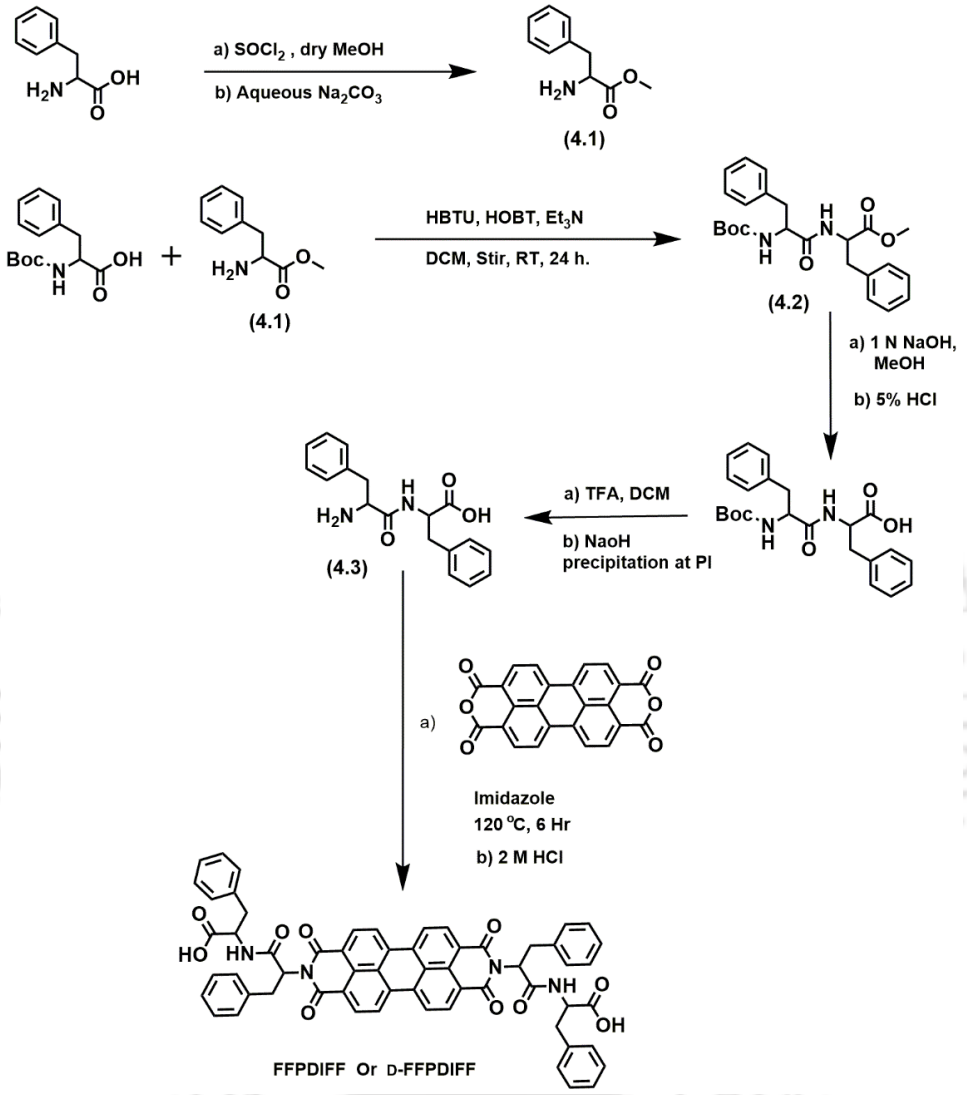

Scheme 4.2 Synthetic route for compound **FFPDIFF** and **D-FFPDIFF**.

Methylphenylananinate (4.1): 1 g (6.06 mmol, 1 equiv.) phenylalanine was dissolved in 15 ml dry methanol and placed in an ice bath. To this solution, 3 ml of freshly distilled thionyl chloride was added dropwise with stirring over a period of 15 mins. The reaction mixture was then allowed to come to room temperature and stirred overnight. After that, solvents were removed under reduced pressure and saturated aqueous Na_2CO_3 solution was added to neutralize. The methyl ester of phenylalanine was extracted with dichloromethane (DCM) and washed with brine. The organic layer was dried over anhydrous Na_2SO_4 followed by removal of the solvent under reduced pressure to get an oily product

with 94% yield. ^{1}H NMR ($CDCl_3$, 600 MHz): δ = 7.36 – 7.22 (m, 5H), 3.79 – 3.77 (t, *J* = 6.0 Hz, 1H), 3.75 (s, 3H), 3.15 – 3.11 (dd, 1H), 2.92 – 2.87 (dd, 1H) ppm. ^{13}C NMR ($CDCl_3$, 150 MHz): δ = 167.13, 135.03, 129.77, 129.21, 127.77, 55.60, 50.83, 39.72 ppm. Mass (ESI-MS): *m/z* calcd. for $C_{10}H_{13}NO_2$: 179.0946, found 180.1026 $[M + H]^+$.

Methyl (tert-butoxycorbonyl)phenylalaninephenylalaninate (4.2): 0.895 g (5 mmol, 1equiv. compound **4.1** was coupled with 1.59 g (6 mmol, 1.2 equiv.) Boc-Phe-OH in DCM using 2.274 g (6 mmol, 1.2 equiv.) HBTU, 1.214 g (12 mmol, equiv.) trimethylamine and 0.81 g (6 mmol, 1.2 equiv.) HOBT for 24 h. The reaction mixture was then washed with brine and the organic layer was dried over anhydrous Na_2SO_4 and filtered. The solvent was removed under reduced pressure to get a white crude product. The crude mixture was subjected to column chromatography on a 60-120 mesh silica gel column using ethylacetate/hexane as the eluent to yield the title compound. Yield: 77%. ^{1}H NMR ($CDCl_3$, 600 MHz): δ = 7.30-7.27 (t, *J* = 9.0 Hz, 2H), 7.24-7.22 (m, 4H), 7.19-7.18 (d, *J* = 6.0 Hz, 2H), 6.98-6.97 (d, *J* = 6.0 Hz, 2H), 6.27 (br, 1H), 4.94 (br, 1H), 4.78 (br, 1H), 4.3 (br, 1H), 3.67 (s, 3H), 3.06-3.01 (m, 4H), 1.4 (s, 9H) ppm. ^{13}C NMR ($CDCl_3$, 150 MHz): δ = 171.42, 170.95, 155.30, 136.61, 135.72, 129.34, 129.21, 128.53, 128.48, 127.03, 126.84, 79.98, 55.60, 53.29, 52.17, 38.36, 37.93, 28.22 ppm. Mass (ESI-MS): *m/z* calcd. for $C_{24}H_{30}N_2O_5$: 426.2155, found 427.2253 $[M+H]^+$.

Phenylalaninephenylalanine (4.3): Compound **4.2** was subjected to ester hydrolysis. For that, 1.5 g (3.5 mmol) of **4.2** was dissolved in methanol and to it 15 ml of 1 N NaOH solution was added and refluxed with stirring overnight. Methanol was then evaporated and 5% HCl was added to bring the system to pH 2 to get a white precipitate. The white product was extracted with DCM and dried over anhydrous Na_2SO_4, filtered and the filtrate was concentrated under reduced pressure. It was then subjected to Boc-deprotection by a 15 ml of 2:1 trifluoroacetic acid (TFA) – DCM mixture. After 2 h of stirring, solvents were removed under reduced pressure. To the residue, dry diethyl ether was added, a white ppt. appeared which was washed with dry ether repeatedly to get a white solid as trifluoroacetate salt of diphenylalanine. The solid was dissolved in water and the pH was adjusted to its isoelectric point (PI) to get free diphenylalanine (**4.3**) with overall yield 80%. ^{1}H NMR (DMSO-d_6, 600 MHz): δ = 7.17-7.04 (m, 10H), 4.45-4.43 (t, *J* = 6.0 Hz, 1H), 3.76-3.74 (t, *J* = 6.0 Hz, 1H), 3.06-3.01 (m, 1H), 2.96-2.84 (m, 2H), 2.64-2.55 (m, 1H) ppm. ^{13}C NMR (DMSO-d_6, 150 MHz): δ = 172.64, 157.70, 137.64, 136.42, 129.40, 129.27, 128.27, 128.09, 126.61, 126.35, 54.75, 53.61, 37.28, 37.00 ppm. Mass (ESI-MS): *m/z* calcd. For $C_{18}H_{20}N_2O_3$: 312.1474, found 313.1591 $[M+H]^+$.

FFPDIFF or D-FFPDIFF: 0.3 g (0.77 mmol, 1 eqv. perylenetetracarboxylic dianhydride (PTCDA), 0.5 g (1.62 mmol, 2.1 equiv.) compound **4.3** and imidazole 2.08 g (30.8 mmol, 40 equiv.) were mixed in a round

bottom flask. Argon was purged for 15 minutes before heating the mixture at 120 °C for 6 h. The reaction mixture was cooled to 90 °C. Water was then added to the reaction mixture with the protection of argon and the reaction was continued for another 1 h. The reaction was cooled to room temperature and it was filtered to remove the trace amount of unreacted PTCDA. The solution was then acidified with 2M HCl solution to pH 3, the precipitate was collected by centrifugation and washed thoroughly with water until the filtrate become neutral. The solid was suspended in 20 ml water, frozen in liquid nitrogen and lyophilized to get the desired final compound with 61% yield. ^{1}H NMR (DMSO-d_6, 400 MHz): δ = 8.45-8.25 (m, 8H), 7.28-7.08 (m, 20H), 5.84-5.82 (t, J = 4.0 Hz, 2H), 4.46 (s, 2H), 3.70-3.67 (dd, 2H), 3.09-3.12 (dd, 2H), 2.94-2.92 (dd, 2H), 2.84-2.81 (m, 2H) ppm. ^{13}C NMR (DMSO-d_6, 150 MHz): δ = 173.26, 168.85, 162.51, 138.04, 133.94, 131.34, 129.47, 129.19, 128.45, 128.30, 126.59, 125.56, 123.96, 122.90, 55.26, 54.45, 36.40, 34.19 ppm. Mass (MALDI-TOF, DHB matrix): *m/z* calcd. for $C_{60}H_{44}N_4O_{10}$: 980.3057, found 980.8560 $[M]^+$.

4.4.3 Methods

Sample Preparation

All the samples were prepared in Class-A volumetric flasks by weighing appropriate amount of the compound and dissolving in the corresponding premixed solvent mixtures. Unless otherwise mentioned, all the working solution were kept undisturbed for at 72 h prior to perform any experiment.

NMR Spectroscopy

^{1}H, ^{13}C spectra were recorded in deuterated Chloroform ($CDCl_3$), dimethyl sulfoxide (DMSO-d_6), Tetrahydrofuran (THF-d_8) and heavy water (D_2O) at 298 K and processed with standard 1D software. Whenever necessary, the NMR spectra were appropriately water suppressed for clarity.

UV-Visible and Fluorescence Spectroscopy

UV-Visible and fluorescence spectra were recorded on a Lambda 750 (Perkin Elmer) and a Cary Eclipse (Agilent) spectrophotometers respectively.

Circular Dichroism (CD) Spectroscopy

The CD spectra of all the samples were recorded by using a 1.2 mL quartz cuvette of 0.5-mm path length with a Jasco J-1500 spectropolarimeter at RT. Spectra were collected at a scan rate 200 nmS^{-1} and 2-nm bandwidth from 190 to 600 nm with three-times scans for averaging. Before running the sample the solvent was run to correct baseline.

Fourier Transformed Infrared (FTIR) Spectroscopy

The 72 h aged solutions of FFPDIFF were freeze-dried. KBr pellets were prepared by mixing the freeze-dried samples and oven dried KBr. The spectra were recorded on a Nicolet is10 spectrometer. The baseline was subtracted from the obtained absorbance intensity in each case.

FESEM

FESEM samples were prepared by casting a drop of dilute solution on a silicon wafer and air dried for at least 1 day. The samples with desired solvent compositions were prepared and incubated for at least 72 hrs before casting on the silicon wafer. For time dependent morphology analyses, samples were drop casted at the specified times. FESEM images were taken using a SIGMA ZEISS microscope.

TEM

A 5 μL very dilute solution of the sample was casted on the carbon coated copper grid (300 mesh Cu grid with thick carbon film from Pacific Grid Tech, USA) and allowed to air dry for 2 minutes and then the excess sample was bloated with a tissue paper. The grid was then air dried for 1 day. The samples with desired solvent compositions were prepared and incubated for at least 3 days before casting on the grid. TEM images were taken in JEOL JEM-2100 microscopes.

Computational details for geometry optimization of FFPDIFF molecules

Geometry optimization of FFPDIFF was performed using density functional theory (DFT) provided by DMol3 code[235,236] using Gaussian09 software.[237] Three initial structures (Figure 4.11A-C) were optimized using semi-empirical method AM1[238] with zero differential overlap (ZDO) basis sets. The optimized geometries obtained from semi-empirical calculations were further optimized using UB3LYP [239-241] and 6-31G9(d) basis sets which are shown in figure 4.11D-F. On comparing the energies of these configurations, geometry (D, Figure 4.11) was found to be energetically favorable (also shown in Figure 4.12A) than the other two. Since electronic structure calculation of PDI dimer is intractable using DFT due to its complex large structure, density-functional tight binding (DFTB)[242,243] method was used to calculate the energy of the dimer with different rotation angles. The calculations in DFTB were performed within DFT framework using either Slater-Koster integrals or from reference structures from DFT calculations. The binding energies of the dimers were calculated from the difference in energies between the dimer and the two monomers. The dimer with a rotation angle -55.20 degree was found to have the lowest binding energy (-10.81 kcal/mol) in compare to the dimers with other angles of rotation. This conformation can lead to a left handed stacking through significant π–π interactions. Moreover, inter-motif OH··O distances between carboxyl group of the side chain and amide oxygen of PDI are within a hydrogen bond distance. Thus, this configuration of the dimer can act as a motif to the thermodynamically stable nano-rings. Figure 4.12B shows the stacking arrangement of FFPDIFF molecules along z axis in order to form the nucleus of the J-type aggregates. This result matched well with our experimental findings where the **FFPDIFF** molecules stacked in the thermodynamically controlled structure to form nano-rings.

4.5 NMR and Mass Spectra of Synthesized Compounds

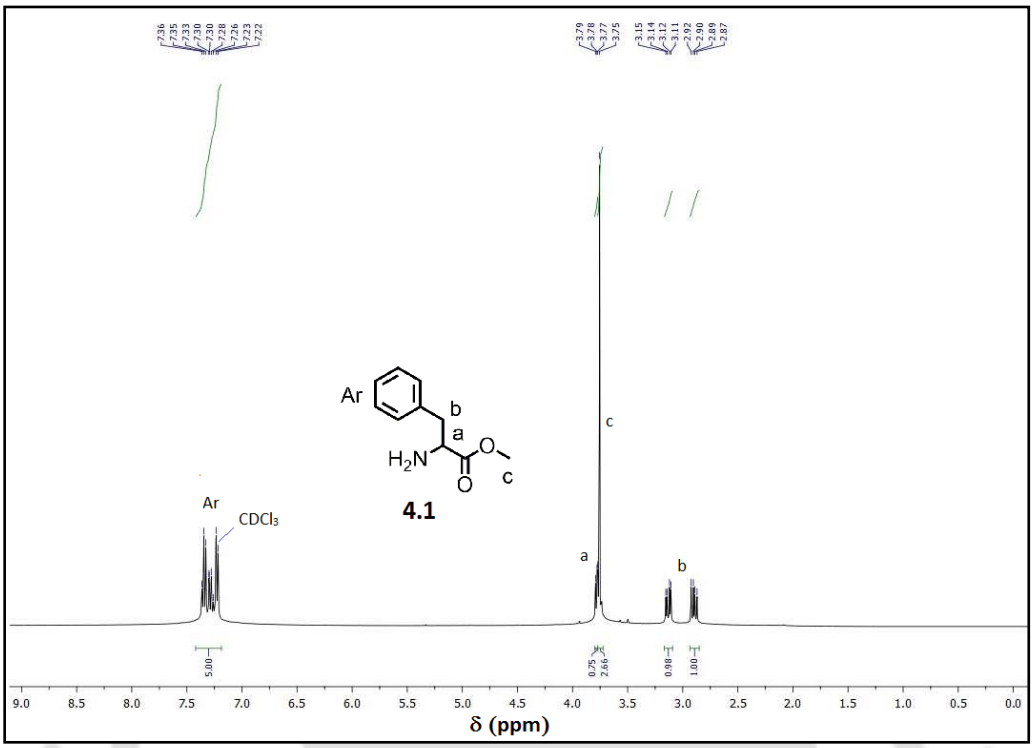

^{1}H NMR spectrum of **4.1**

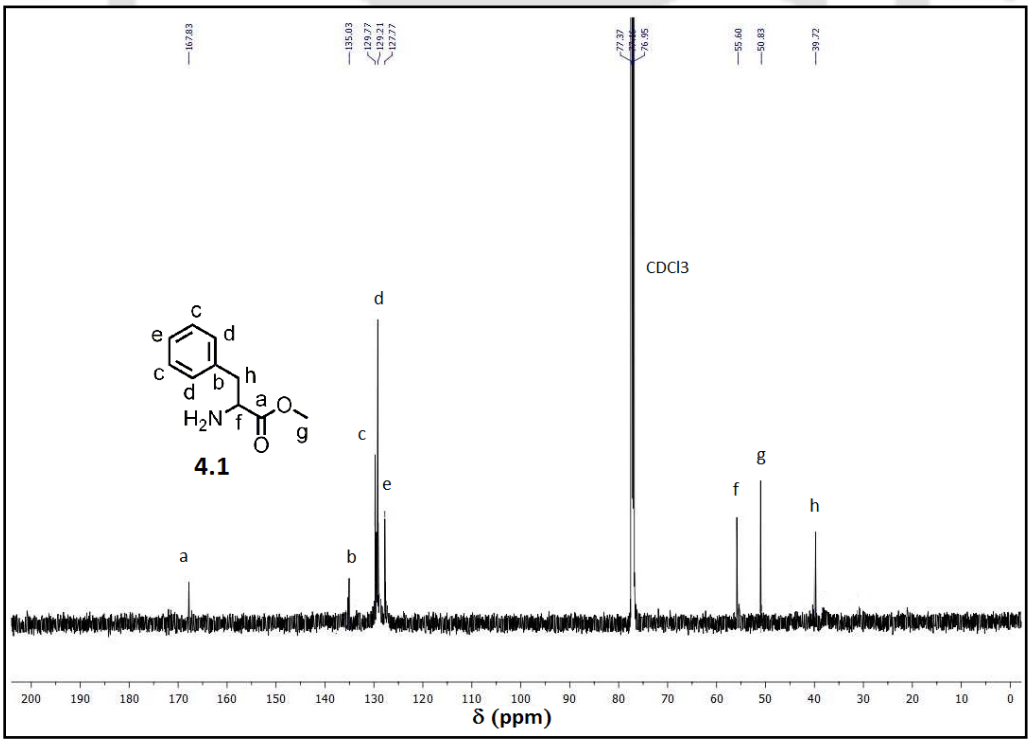

^{13}C NMR spectrum of Compound **4.1**

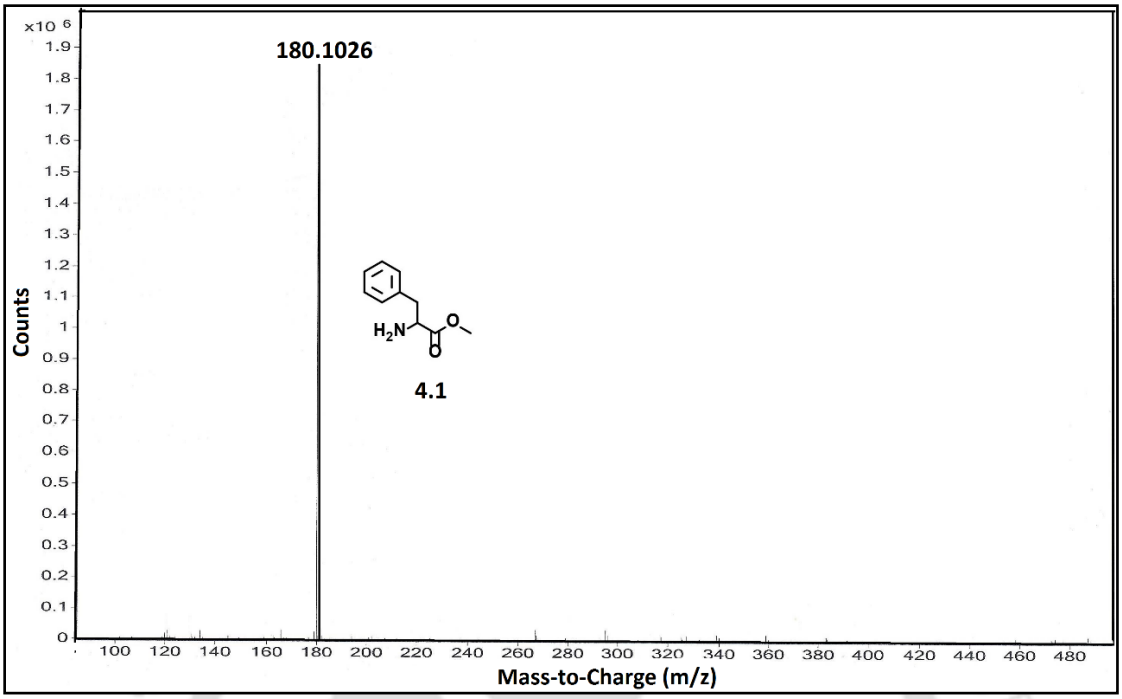

ESI-MS of Compound **4.1**

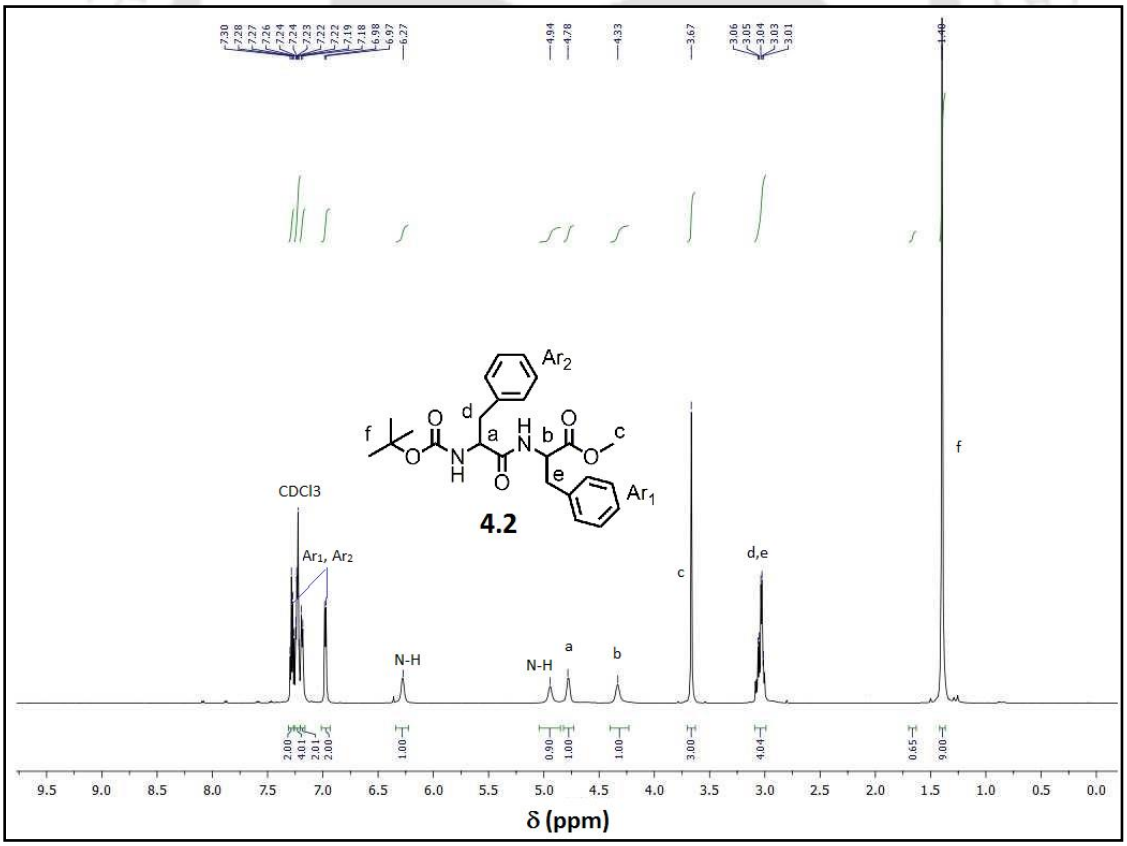

^{1}H NMR spectrum of Compound **4.2**

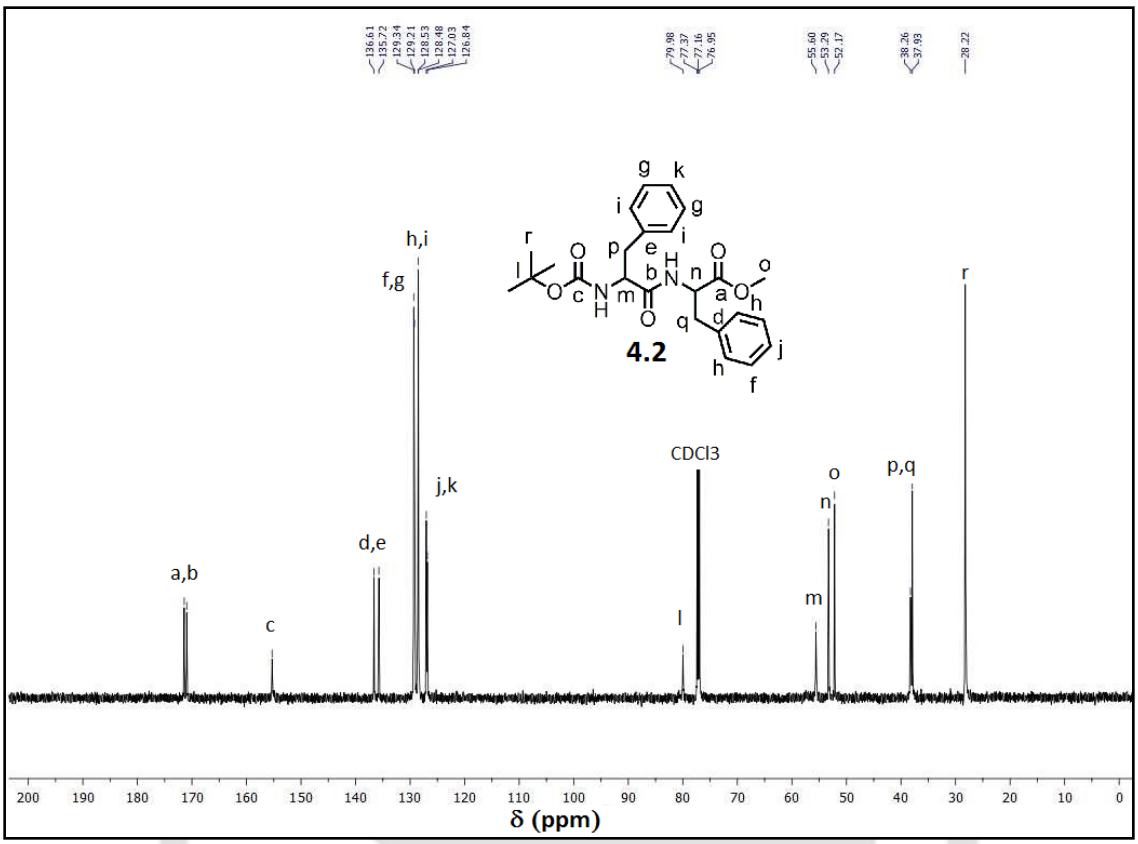

^{13}C NMR spectrum of Compound **4.2**

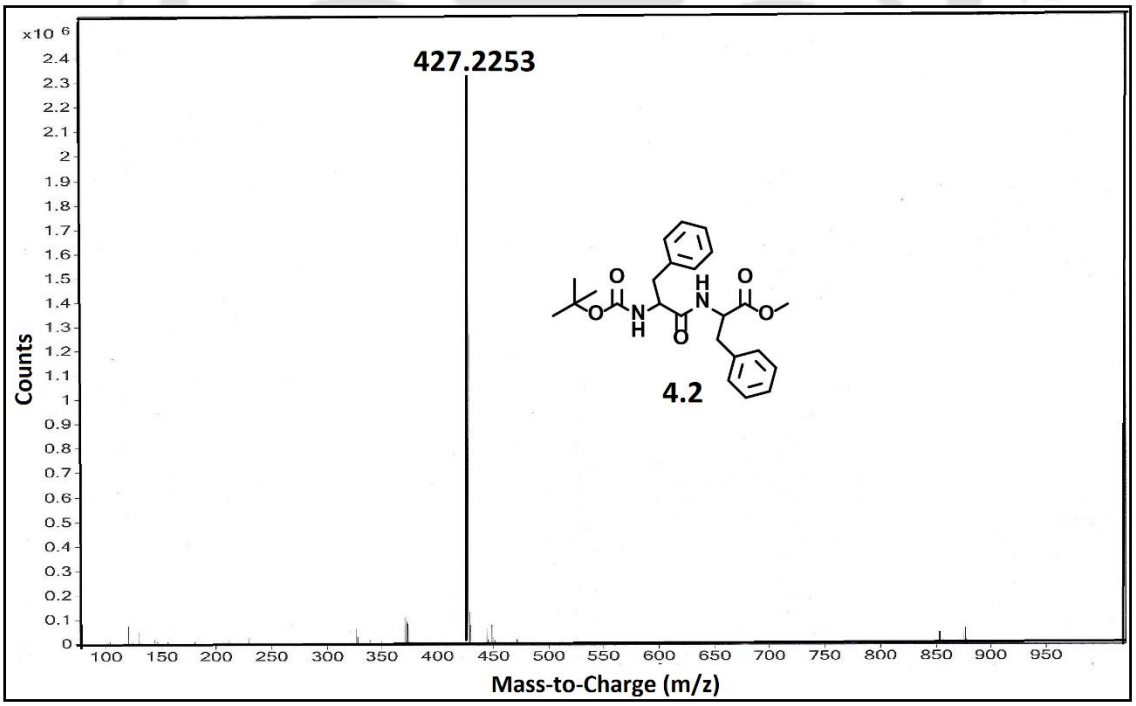

ESI-MS of Compound **4.2**

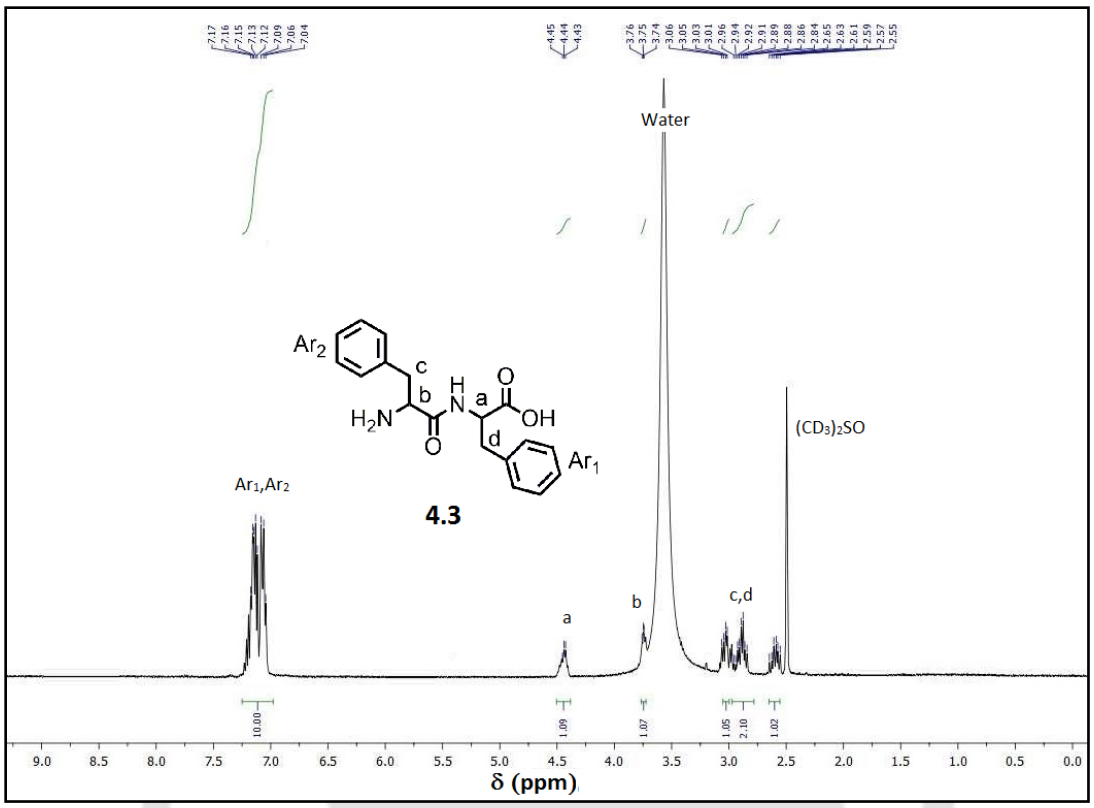

^{1}H NMR spectrum of Compound **4.3**

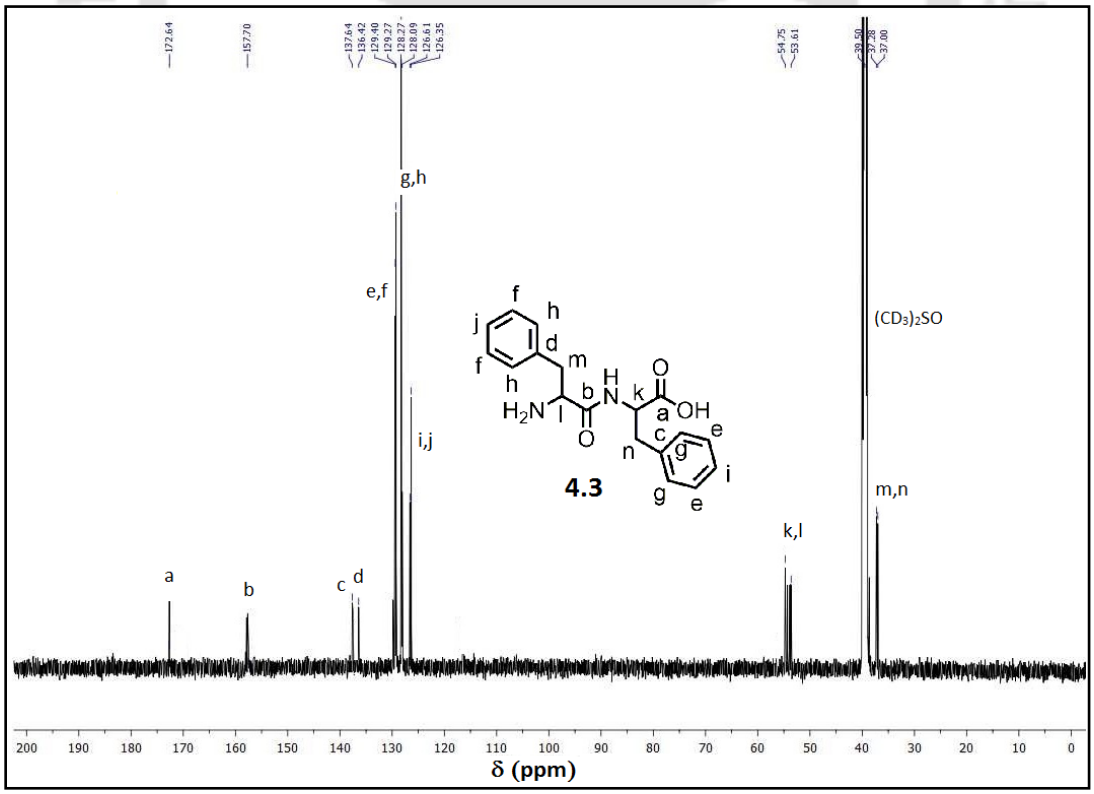

^{13}C NMR spectrum of Compound **4.3**

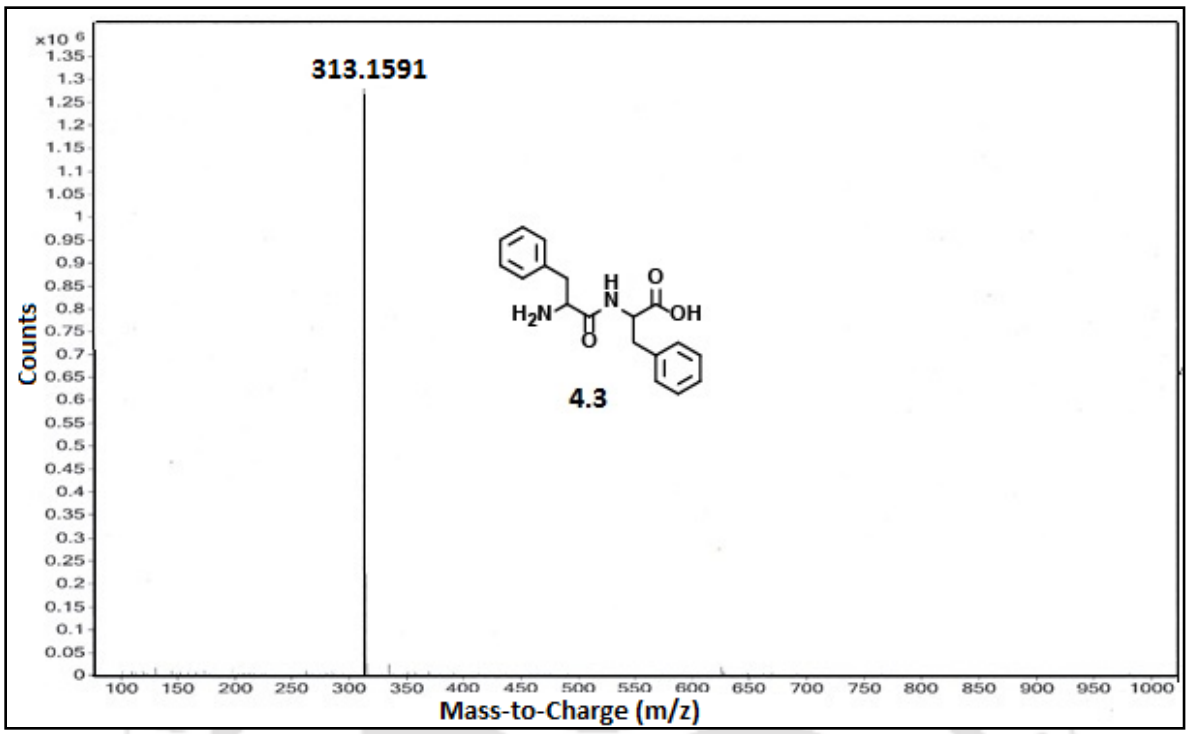

ESI-MS of Compound **4.3**

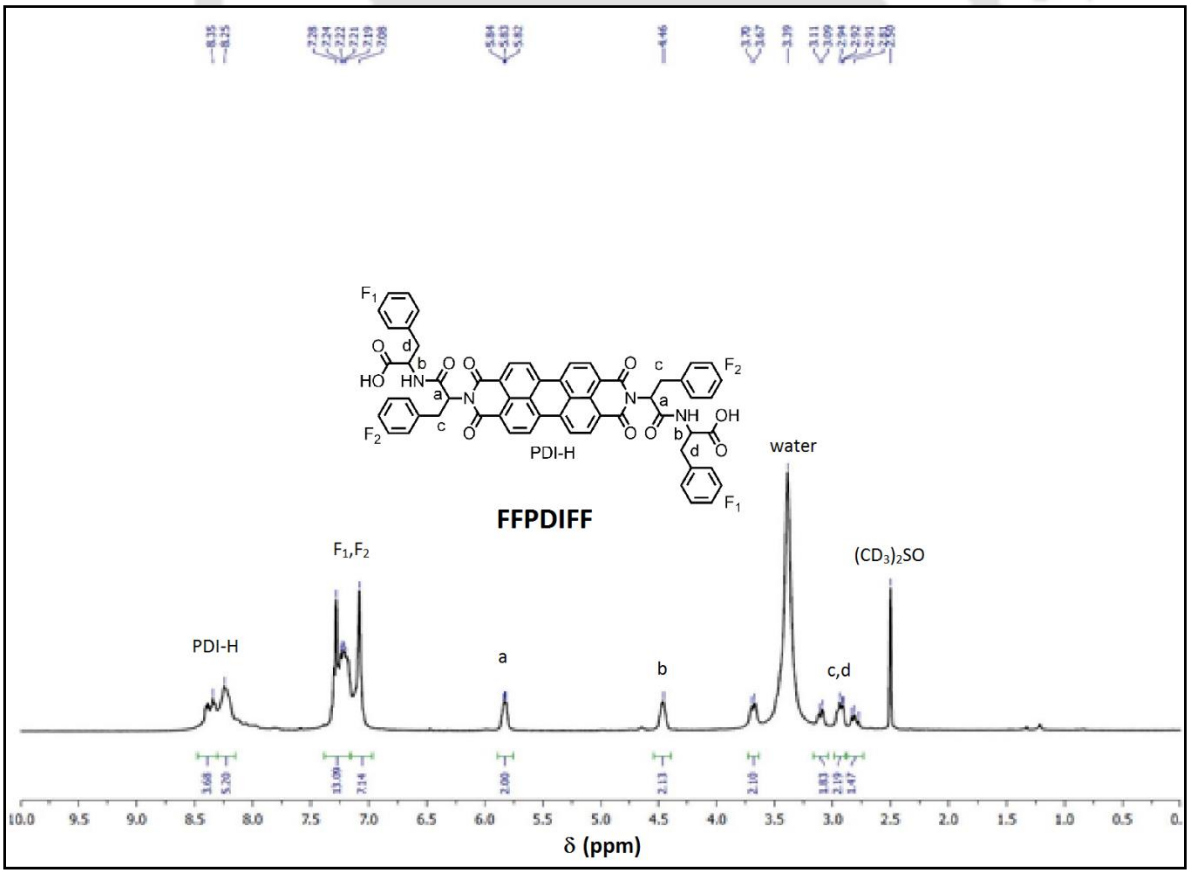

^{1}H NMR spectrum of **FFPDIFF**

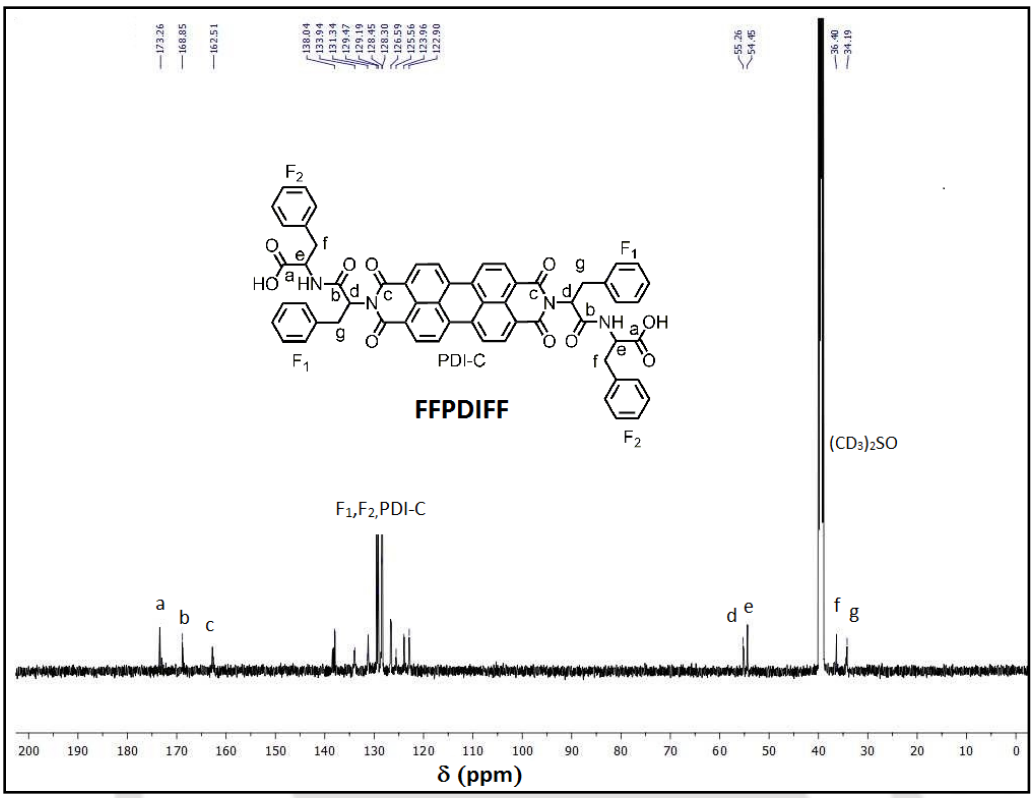

^{13}C NMR spectrum of **FFPDIFF**.

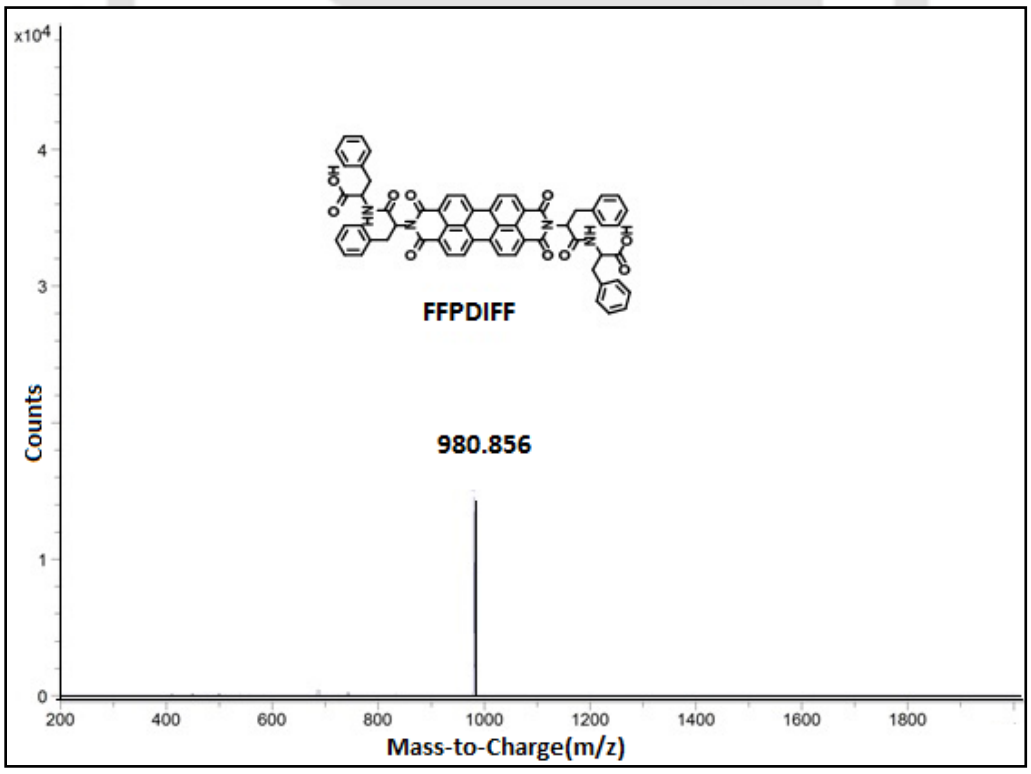

MALDI-TOF spectrum of **FFPDIFF**.

Chapter 5

Applications of supramolecular Assemblies

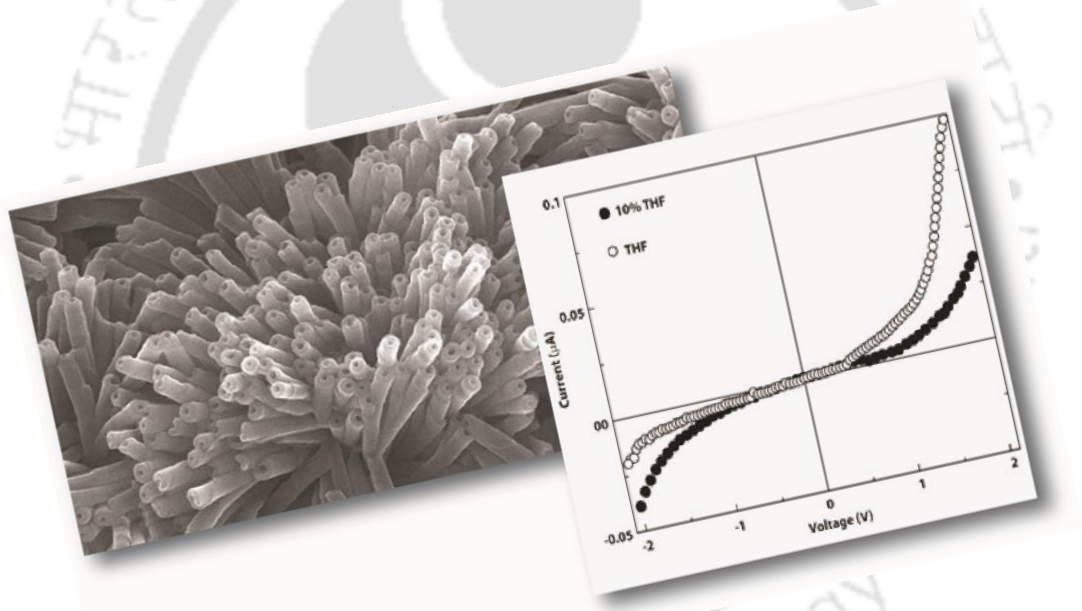

5.1 Introduction

The main aim of synthesizing or preparing a material is always to utilize them for a successful and important application. The soft-aggregates reported in previous chapters are no exception. The helical nano-fibers obtained from the PA-hydrogel reported in Chapter 1 has been utilized as a template for synthesis of silica nanotubes. Similarly, the nano-structures obtained from the self-assembly of **FFPDIFF** has been tested for their semi-conducting behavior for possible applications in organic-electronics. This chapter is about the applicability of these supramolecularly assembled materials for A) Template synthesis and B) Semiconducting Materials.

5.2 Template Fabrication of Single Walled Silica Nanotubes

Nano-tubes made of various materials such as carbon, gold, silver, silica, other metals, polymers have fetched a great deal of interest because of their remarkable physicochemical properties and potential wide ranging applicability.[244-247] Silica is one of the most studied materials to produce nano-tubes because of its inert nature, and ease of surface functionalization.[248-251] Moreover the mesoporous nature of such silica nano-tubes make them an extremely important candidate for industrial use as catalyst support. Among the various methods available for the production of nano-tubes, the template method has been proven to be versatile and inexpensive technique.[252] Nevertheless, template synthesis of silica relies on the organogels or alumina templates and only a few hydrogel based synthesis have been reported.[253-255] Moreover, the hydrogel template synthesis also require an external hydrolyzing agent, an organic solvent or control over the pH of the system. In addition, maintaining uniform length and size of the silica nano-tubes using hydrogel template is a difficult task and not many reports are available in literature.

The nano-fibers obtained from the lysine based hydrogelator (**2.1**) reported in Chapter 1 has been used as a template to create uniform silica nano-tubes with different surface functionalization. In the next sections, the synthesis and characterization of these silica-nanotubes is discussed in detail.

Characterization of the Silica-Nanotubes

The SEM and FESEM images have shown extremely uniform long hollow tubes with open ends (Figure 5.1). The so formed silica nano-tubes are more than few micrometers in length with ~10 nm of inner diameter. The size closely matches with the length of the nano-fibers obtained from the hydrogel of **2.1** at this concentration but surprisingly the diameters are smaller than the template. To further confirm the diameter of the silica nano-tubes, the TEM images of the silica nano-tubes have been taken. The TEM image (Figure 5.1D) of the nano-tubes evidently shows single wall structure with uniform diameter of ~ 10 nm. In order to find the role of aging on the shape and size of the nano-tubes, the samples were

aged for three days before calcination but no changes were observed in the microscopic images. The Energy-Dispersive X-ray (EDX) spectrum (Figure 5.1C) of the nano-tubes clearly shows the presence of silicon and oxygen as the major constituent of the nano-fibers. The IR spectra (Figure 5.2) of the silica nano-tube during the synthesis shows the appearance of the Si-O-Si asymmetric band stretching at 1100 cm^{-1} and a Si-OH stretching at 3440 cm^{-1} along with the characteristic bands of the gelator. After calcination, all the peaks related to the gelator disappeared leaving the characteristic bands of the silica nano-tube indicating the complete removal of the template.

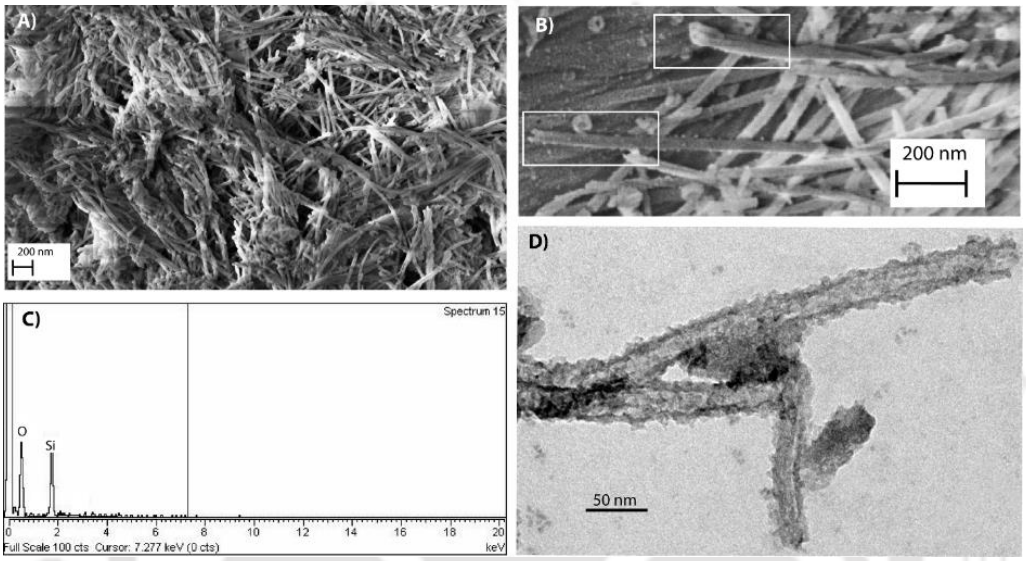

Figure 5.1 A) SEM image of the silica nanotubes; B) FESEM image of silica nanotubes showing the open end of the fibers; C) EDX spectrum of the silica nanotubes; D) TEM image of the silica nanotubes.

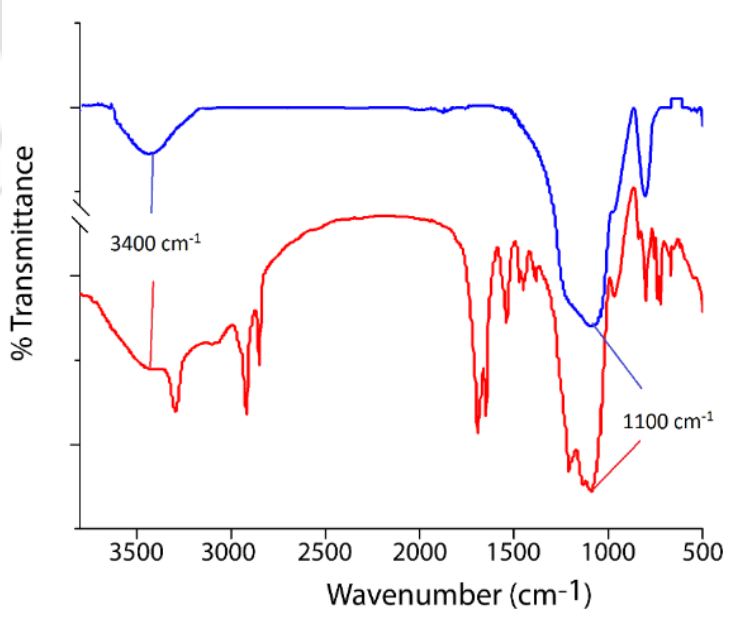

Figure 5.2 IR spectra of the silica nanotubes during its formation (Red) and after calcination (Blue).

Porosity of the Silica Nanotubes

The specific surface areas and pore size distributions of the single walled silica nanotubes have been measured by nitrogen adsorption and desorption measurements. The N_2 adsorption-desorption isotherms of the silica nano-tubes can be classified into type IV hysteresis loop (Figure 5.3A), indicating the mesoporous nature. The BET surface has been calculated from N_2 adsorption/desorption isotherms and found to be 356 m^2/g and the pore volume as 0.6557 cm^3/g. Although the pore size distribution curve (Figure 5.3B) has showed a peak at 5.9 nm, the distribution is somewhat wide in nature and the range closely matches with the diameter of the nano-tubes observed from microscopic images.

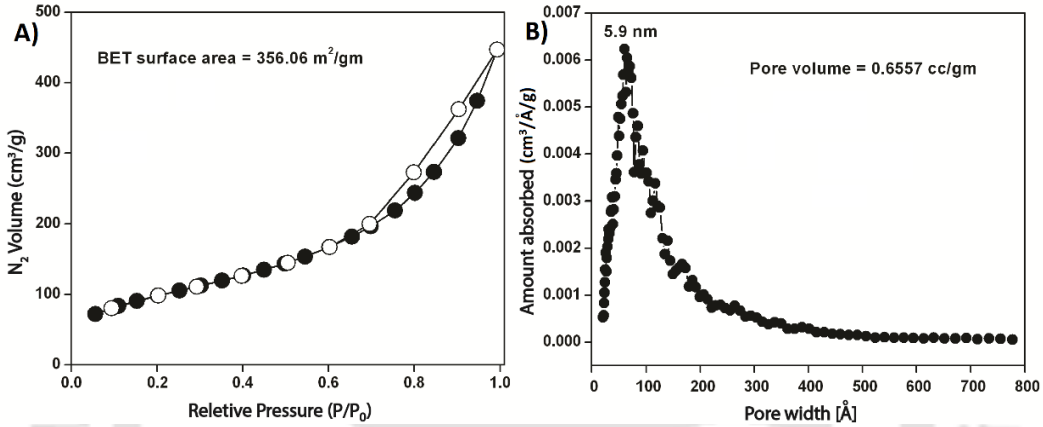

Figure 5.3 A) Nitrogen adsorption–desorption isotherms of silica nanotubes and B) pore size distribution.

Mechanism of Silica Nanotube formation

A possible mechanism of the silica nano-tube formation is pictorially presented in Figure 5.4. When tetraethylorthosilicate (TEOS) or similar silica precursor is mixed with the aqueous solution of **2.1**, initially the gelator forms the fibers with free amines at the surface. These amine groups serve as the nucleation point and the TEOS molecules get deposited on the fibers followed by hydrolysis by the amines. The hydrolysis and aging slowly allows the formation of the silica which coats the nano-fibers. At the final step, the organic residues are removed during calcination leaving the silica nano-tubes. As the TEOS is present during the hierarchical fiber formation process, the nucleation by the free amines started at an early stage of the fibers when the thickness of the fibers was somewhat lesser than the actual fibers at this concentration (1 % w/v). Thus the helical nature could not be transformed to the silica tubes as evident from the concentration dependent FESEM study of the hydrogel which shows no helical nature of the fibers at a lower concentration (Figure 2.10C, Chapter 2). This is also supported by the fact that the nature, shape and sizes of the silica nano-tubes were similar when the experiment was repeated at a higher gelator concentration (3 % w/v) where the thickness of the fibers is even higher than that at MGC (Figure 2.10D, Chapter 2). An attempt to add TEOS after the gel formation failed as the

addition of TEOS followed by heating and subsequent cooling to room temperature did not allow the reversible formation of the fibers and hydrogel.

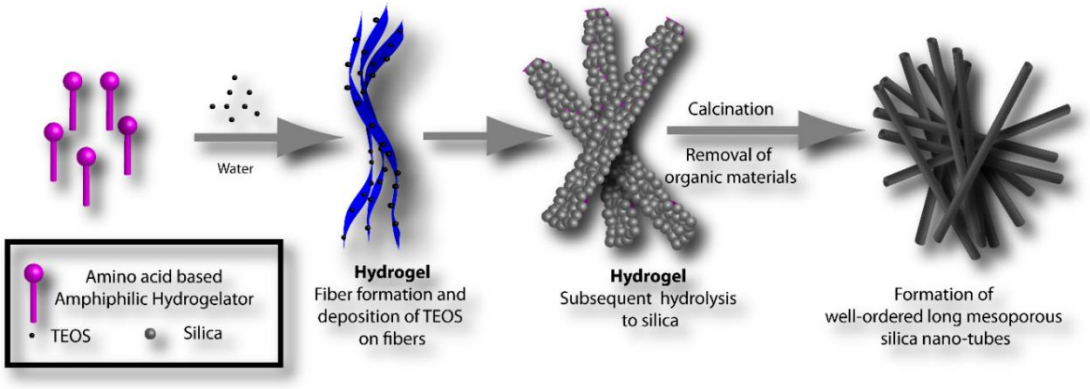

Figure 5.4 Pictorial presentation of the possible mechanism of silica nanotube formation.

Hydrophilic and Hydrophobic Silica Nanotubes

The above discussed template technique was further extended to the fabrication of silica nanotubes having hydrophilic (amine functionalized) and hydrophobic (long alkyl chain functionalized) surface. For that 3-aminopropyltriethoxysilane (APTES) and octadecyltrimethoxysilane (ODTMS) were used as precursors for hydrophilic and hydrophobic silica nanotubes respectively. The procedure and the mechanism is the same as discussed earlier. These nanotubes were characterized using SEM, IR, and N_2 adsorption desorption techniques.

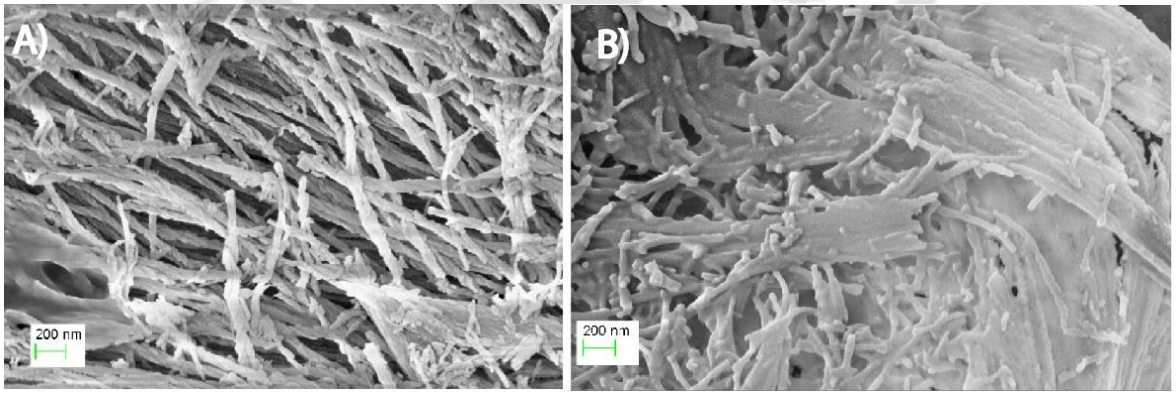

Figure 5.5 SEM images of A) hydrophilic B) hydrophobic silica nanotube

SEM images (Figure 5.5) of both types of materials, have shown tubular structure with high aspect ratio. Figure 5.6 shows the overlaid FTIR spectra of both types of silica nanotubes. The peaks at 1086 cm^{-1} and 803 cm^{-1} (Figure 5.6A, for hydrophilic silica nanotubes) can be attributed to the asymmetric and

symmetric stretching vibrations for Si-O-Si respectively.[256,257] These two bands for the hydrophobic silica nanotube arise at 1090 cm^{-1} and 800 cm^{-1} (Figure 5.6B). Peaks at 2920 cm^{-1}, 2850 cm^{-1} (for hydrophilic) and 2925 cm^{-1}, 2854 cm^{-1} (for hydrophobic) are for the asymmetric and symmetric stretching vibration modes of $-CH_2$ respectively. The peak at 1634 cm^{-1} (Figure 5.6A) can be ascribed for the bending vibration of aliphatic amine (N-H) group which is absent for hydrophobic silica nanotubes (Figure 5.6B). This implies the presence of aliphatic amine group in the hydrophilic silica nanotube. The characteristic band at about 3440 cm^{-1} is responsible for the Si–OH stretching vibration which cannot be clearly distinguished for the stretching vibration of aliphatic amine (N-H).

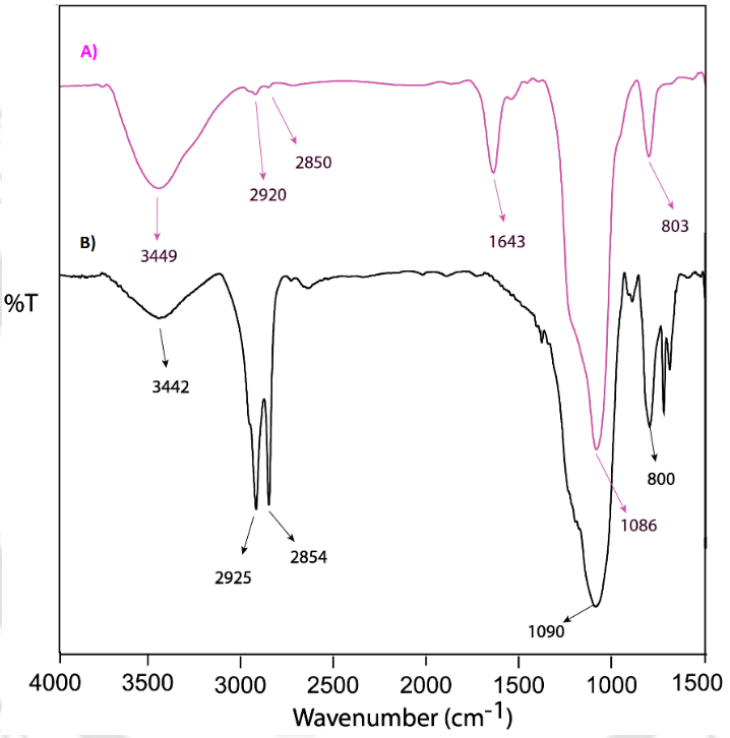

Figure 5.6 Overlaid IR spectra for A) (Pink) Hydrophilic silica nanotubes, B) (Black) Hydrophobic nanotubes.

The N_2 adsorption-desorption isotherms of the hydrophilic silica nano-tubes (Figure 5.7A) has shown behavior similar to the un-functionalized silica nanotubes (obtained when TEOS used as precursor). Hydrophilic silica nano-tubes shows type IV isotherm with a hysteresis loop which is characteristic of mesoporous material. The BET surface area has been calculated to be 219.652 m^2/g which is lower than the un-functionalized silica nanotubes. Using BJH pore size distribution (adsorption), the pore radius and pore volume are found to be 3.2 nm and 2.6 cm^3/g respectively for hydrophilic silica nanotubes (Figure 5.7B). On the other hand, the hydrophobic silica nanotubes have shown different type of isotherm (Figure 5.7C) with surface area 1.035 m^2/g which is very low compared to the hydrophilic silica

nanotubes. This may be because of the blocking phenomena.[258] The pore radius and pore volume have been found to be 1.51 nm and 0.003 cm^3/g respectively for hydrophobic silica nanotubes (Figure 5.7D).

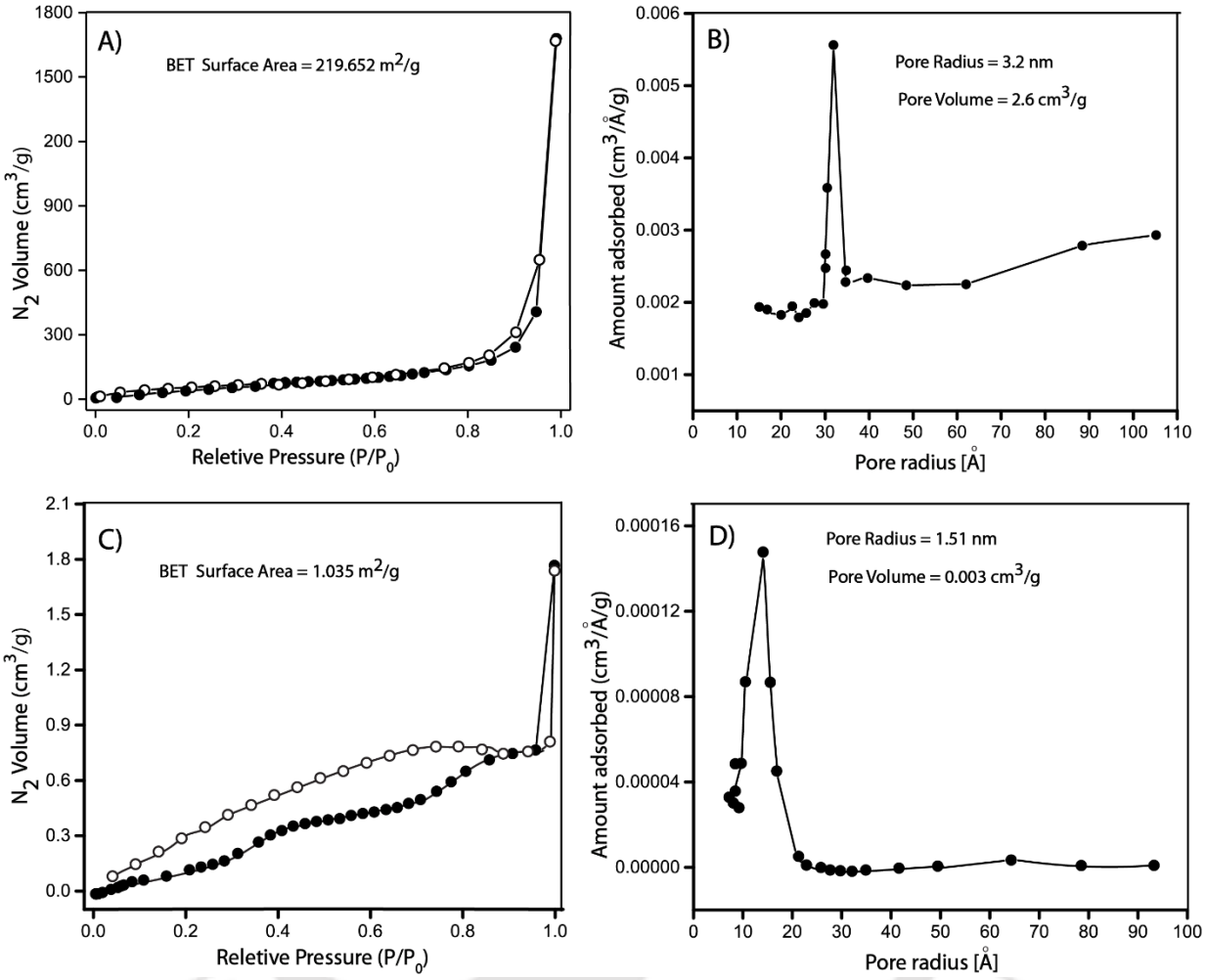

Figure 5.7 A) Nitrogen adsorption–desorption isotherms and B) Pore size distribution of Hydrophilic silica nanotubes; C) Nitrogen adsorption–desorption isotherms and D) Pore size distribution of Hydrophobic Silica nanotubes.

In summary, self-assembled peptide nanofibers have been used as template for the fabrication of different types of silica nanotubes. These nanotubes have been well characterized using different microscopic, spectroscopic techniques. Using N_2 adsorption desorption method, it has been shown that different types of synthesized silica nanotube have different surface character.

5.3 Semi-conducting Behavior of Supramolecular Assemblies

It has been mentioned in chapter 1, that the semiconducting property of PDI based molecules is of immense importance owing to their applications in organic-electronics materials and devices. As it has been shown in chapter 4, a peptide-PDI conjugate self-assembled in different nano-structures with

varying solvent composition, here an approach has been made to correlate the semi-conducting behavior of the material with morphology. However, only few studies has so far been reported to correlate the semi-conducting property with the morphology of these self-assembled n-type semiconductors.[259,260]

In order to evaluate the relation between nano-structures with their conducting ability, the helical nano-fibers and nano-rings were subjected to Conducting – Atomic Force Microscopy (C-AFM).

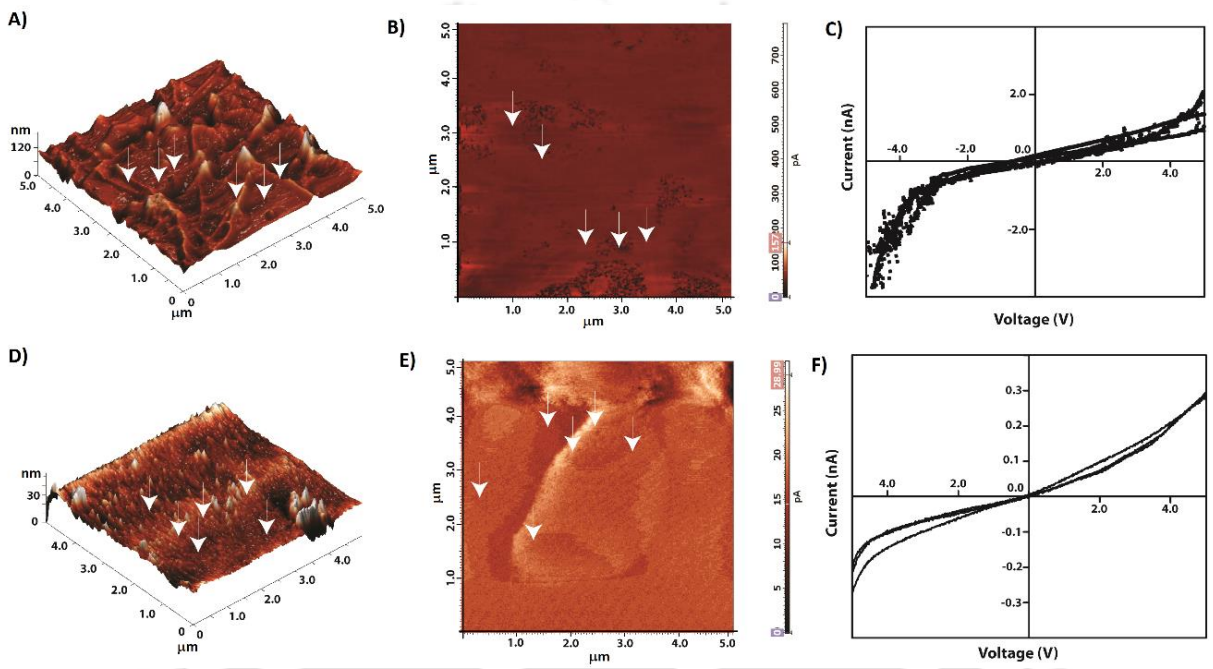

Figure 5.8 C-AFM analyses of thin film of **FFPDIFF** (10 µM) prepared from THF (A-C) and 10% THF (D-F). A) & D) 3D topography of the nanofibers and nano-rings respectively; B) & E) SRI pictures for the films; C) & F) I-V characteristics of nanofiber and nano-rings.

The topography of the nanofibers and nano-rings has been observed in height profile of contact mode AFM images. For THF system, 3-dimensional images of nanofibers were obtained all over the surface (Figure 5.8A). The scanning resistance image (SRI; figure 5.8B) shows higher current at the nano-fiber regions and dark points correspond to low current regions on the substrate. With the set point bias the maximum current recorded is around 150 pA. The current-voltage characteristics were recorded at the probe points (points indicated by arrows, figure 5.8A, B). These probe points were carefully chosen so that the probe can land either on nanofiber or on valley. For current-voltage characterization, a bias sweep from -5 V to +5 V was applied and respective currents were recorded (Figure 5.8C). These characteristics show quite higher current value, whereas an abrupt increase in current can be seen in negative bias after -4 V. This is presumably due to mismatch in work functions of the gold coated tip to

doped Si. However, the characteristics indeed testify that the probed nanostructures are electronically active and semiconducting in nature. This is affirmed from the increasing conductivity and the nature of the characteristics – which signify there should be a band gap to facilitate charge flow through them. A similar treatment with the sample from 10% THF system revealed the formation of nano-rings on the surface as can be seen from figure 5.8D. A higher valley, distinctive of the lower back-ground was observed which might apparently be formed by coalescing the nano-rings side-by-side. The SRI also has confirmed the same where this structure seems as a brighter patch. Though the nano-rings are formed by the aggregation of **FFPDIFF**, the conductivity is much lesser than that of the nanofibers as the maximum current recorded at set point condition is 30 pA. In order to differentiate the conducting property of the nanostructures from the back ground of the Si doped surface, the background current was measured as shown in figure 5.9. The background current-voltage characteristics has been observed to be much lower and packed with noises as well as very much similar for both samples. These characteristics also do not have any specific trend. The lower conductivity of the nano-ring is also observable from the current-voltage characteristics (Figure 5.8F). These current-voltage characteristics from the bright section of the SRI have semiconducting nature too, however, they may have higher band gap. Due to this higher band gap, the wave-function mismatch between tip and substrate is not noticeable in the current-voltage characteristics.

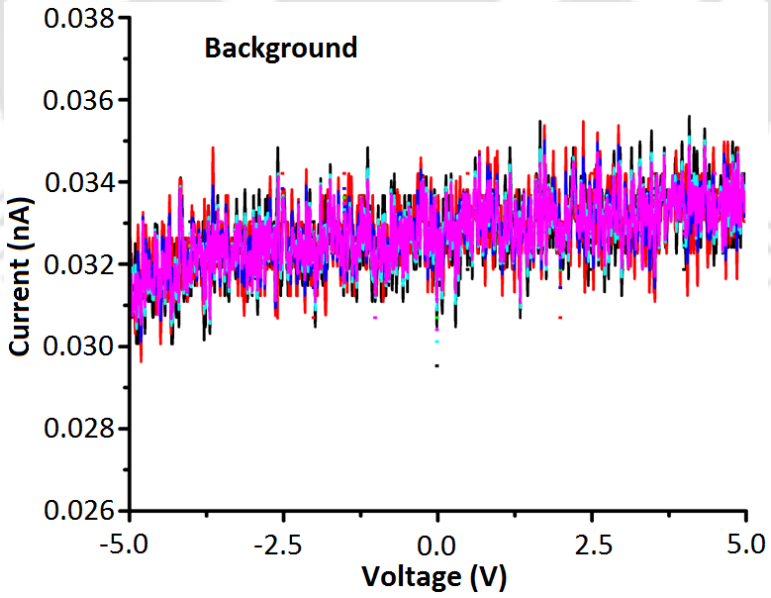

Figure 5.9 Background current-voltage characteristics from the doped Si surface.

Though both the nanostructures are made up of same molecule, the constructional and size difference between them may have resulted higher effective band-gap for nano-rings. It is also plausible that interfaces between nano-rings restraint the charge transport through the nano-rings. The nano-fiber

structures have advantage of percolating path of charge flow whereas charges possibly get localized within the confined structure of nano-rings. While for nano-fibers, charges transmitting transversely *i.e.* across the diameter, in case of planar nano-rings, charges are passing through the core of the molecules. Nevertheless, the current voltage characteristics of the nano-fibers and nano-rings reveal that the aggregation pattern and the morphology play vital role in the semiconducting nature of these materials.

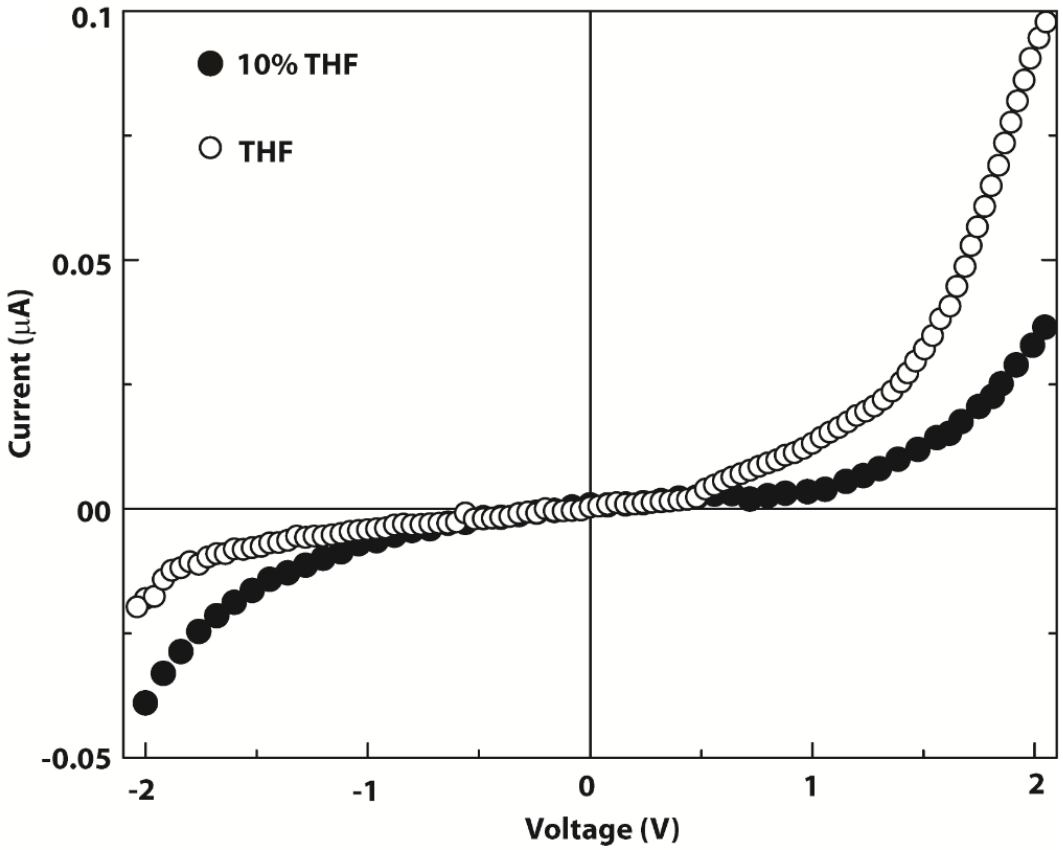

Figure 5.10 Current-voltage characteristics of **FFPDIFF**. The thin films of **FFPDIFF** have been deposited from different solvents as the legends indicate.

For conventional current-voltage (*I-V*) characterization, *I-V* measurements in thin film configuration were carried out. Thin films were deposited from THF or 10% THF-water by slow spin cast method. With the used concentration of **FFPDIFF** in these solvents, the expected thickness of the films could be ~200 nm. These films were sandwiched between two Al electrodes deposited *via* thermal evaporation. Figure 5.10 shows the *I-V* characteristics of thin films within a bias range of -2 V to +2 V. From these measurements it is clearly seen that the thin film from the mixed solvent is semiconducting while that from THF shows current rectifying behavior. These electronic natures of two different types of nanostructures have also been seen in C-AFM study. Here, as the electrodes of on both sides of the film

are of same metal, the effect of built-in potential can be negated. Thus the current rectification behavior may be attributed to conformational changes which has different local energy levels.[261] It must be noted that the charge conduction in nano-fiber network takes place through the delocalized 'PhePhe' groups of the molecules. This is associated with organized hopping sites for charge carriers.[262] Specific orientation of molecules provides preferable direction of charge transmission which may cause the current rectification in nano-fiber network. A detailed investigation correlating the morphology and conducting property of such organic semiconductors is currently under progress.

In summary, self-assembled nanostructures have been tasted for their semi-conducting behavior and an approach has been made to correlate the semi-conducting behavior with the morphology of their self-assembled nanostructures.

5.4 Experimental section

5.4.1 Methods

Synthesis of silica nano-tube

In a typical experiment, 10 mg (16.92 μmol) of **2.1** was taken in 1 mL of HPLC grade water and the sample was heated slowly to 80 °C. It was stirred at that temperature slowly for 5 min before cooling it down to RT and 50 μL of silica precursor (TEOS or APTES or ODTMS) was added to it and slowly stirred for 5 min. The mixture was then allowed to stay undisturbed for 24 h at RT for hydrolysis. The material became viscus and was transferred to a silica crucible and calcined at 550 °C for three hours. A white solid thus obtained was utilized for further studies.

SEM and FESEM sample preparation

The silica nano-tubes, the calcined material (1mg) was dispersed in methanol (0.5 mL) and from that suspension a small drop (~10 μL) was spotted on a glass plate air dried overnight.

TEM sample preparation

The silica nanotubes (1mg) was dispersed in methanol (0.5 mL). A droplet (~20 μL) of the dispersion was deposited on a clean surface. Then a copper TEM grid (300 mesh Cu grid with thick carbon film from Pacific grid Tech, USA) was immersed into the droplet for 15 s. The excess liquid on the grid was removed with filter paper. The attached silica nanotubes on the grid were then air-dried for TEM observation.

Fourier Transformed Infrared (FTIR) Spectroscopy

KBr pellets were prepared using the silica nanotubes and the spectra were recorded on a Nicolet is10 spectrometer. The baseline was subtracted from the obtained absorbance intensity in each case.

N_2 Adsorption/Desorption

N_2 adsorption/desorption isotherm was obtained by using a Quantachrome Autosorb 1-C surface area analyzer at 77 K. The samples were heated at 100 °C overnight to remove all the adsorbed gases prior to the experiment. Pore size distributions were calculated employing the NLDFT (Non Localized Density Functional Theory) and BHJ (Barrett-Joyner-Halenda) model.

Conductive AFM

The C-AFM had been carried out with drop casted film on doped Si substrates. The films were dried in closed ambient condition for a day and then dusted off by slow N_2 gas blowing. C-AFM characteristics were measured using a NT-MDT NTEGRA Aura Atomic Force Microscope. A gold coated highly conductive tip was used to probe at 10 kHz. The C-AFM has a gold coated tip as biasing electrode. Doped Si substrate is highly conducting and could serve the purpose of ground electrode. The set point bias and current were fixed at 300 mV and 0.1 nA respectively.

Electrical characterization

Thin films were prepared from solutions of **FFPDIFF** in appropriate solvent(s). Spin-coating at 1000 rpm was applied to fabricate the thin films on Aluminum coated glass substrates. Top electrode was thermally evaporated Al on the thin films. I-V characteristics were taken by Keithley 2450 source measure unit.

Postlude

Nature is the biggest puzzle to break! It is amazing to realize how complex yet simple the nature is. It is the continuous effort of the entire scientific fraternity to realize, understand and utilize the natural phenomenon. Century after century, scientists are devoting their life to understand the underlying processes behind every natural processes. The effort is to protect the nature and not to overpower it. In this continuous process, understanding the chemical and bio-chemical processes demands high priority as they are directly related to the betterment of the mankind and progress. Self-assembly of peptide molecules is the first step of any proteins to function properly and it is thus of immense importance to realize how they assemble and where can they be utilized. In this Thesis, a small effort is made to contribute to the fundamental understanding of the self-assembly processes. Though very little, the effort will certainly contribute to the advancement of this continuous process.

References

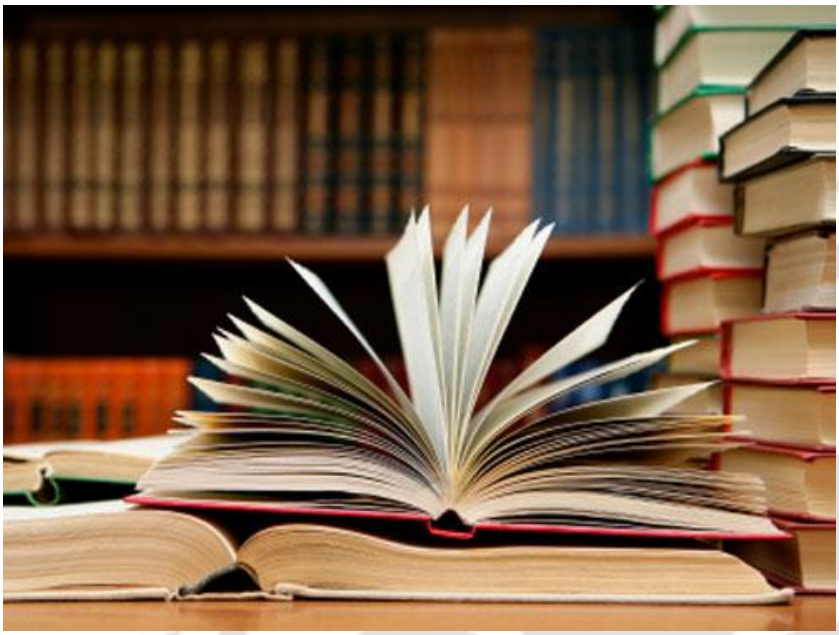

1. van der Waals, J. D. (1873) *Over de Continuiteit van den Gas-en Vloeistoftoestand (on the continuity of the gas and liquid state)*. PhD thesis (excerpt), Leiden, The Netherlands.
2. Lehn, J.-M. Supramolecular Chemistry—Scope and Perspectives Molecules, Supermolecules, and Molecular Devices (Nobel Lecture). *Angew. Chem., Int. Ed.* **1988**, *27*, 89-112.
3. Drury, J. L.; Mooney, D. J. Hydrogels for Tissue Engineering: Scaffold Design Variables and Applications Hydrogels for Tissue Engineering: Scaffold Design Variables and Applications. *Biomaterials* **2003**, *24*, 4337–4351.
4. Collier, J. H.; Rudra, J. S.; Gasiorowski, J. Z.; Jung, J. P. Multi-Component Extracellular Matrices Based on Peptide Self-Assembly. *Chem. Soc. Rev.* **2010**, *39*, 3413–3424.
5. Vermonden, T.; Censi, R.; Hennink, W. E. Hydrogels for Protein Delivery. *Chem. Rev.* **2012**, *112*, 2853–2888.
6. Darbre, T.; Reymond J.-L. Peptide Dendrimers as Artificial Enzymes, Receptors, and Drug-Delivery. *Acc. Chem. Res.* **2006**, *39*, 925-934.
7. Kim, J. H.; Lim, S. Y.; Nam, D. H.; Ryu, J.; Ku, S. H.; Park, C. B. Self-Assembled, Photoluminescent Peptide Hydrogel as a Versatile Platform for Enzyme-Based Optical Biosensors. *Biosensors and Bioelectronics* **2011**, *26*, 1860–1865.
8. Galler, K. M.; Aulisa, L.; Regan, K. R.; D'Souza, R. N.; Hartgerink, J. D. Self-Assembling Multidomain Peptide Hydrogels: Designed Susceptibility to Enzymatic Cleavage Allows Enhanced Cell Migration and Spreading. *J. Am. Chem. Soc.* **2010**, *132*, 3217–3223.
9. Zhang, S.; Holmes, T.; Lockshin, C.; Rich, A. Spontaneous Assembly of a Self-Complementary Oligopeptide to Form a Stable Macroscopic Membrane. *Proc. Natl. Acad. Sci. U. S. A.* **1993**, *90*, 3334–3338.
10. Han, T. H.; Kim, J.; Park, J. S.; Park, C. B.; Ihee, H.; Kim, S. O. Liquid Crystalline Peptide Nanowires. *Adv. Mater.* **2007**, *19*, 3924–3927.
11. Ryu, J.; Park, C. B. Synthesis of Diphenylalanine/Polyaniline Core/Shell Conducting Nanowires by Peptide Self-Assembly. *Angew. Chem., Int. Ed.* **2009**, *48*, 4820–4823.
12. Cui, H.; Muraoka, T.; Cheetham, A. G. Self- Assembly of Giant Peptide Nanobelts. *Nano Lett.* **2009**, *9*, 945–951.
13. Aggeli, A.; Bell, M.; Boden, N.; Keen, J. N.; Knowles, P. F.; McLeish, T. C. B.; Pitkeathly, M.; Radford, S. E. Responsive Gel Formed by the Spontaneous Self-Assembly of Peptides into Polymeric Beta-Sheet Tapes. *Nature* **1997**, *386*, 259–262.
14. Estroff, L. A.; Hamilton, A. D. Water Gelation by Small Organic Molecules. *Chem. Rev.* **2004**, *104*, 1201–1217.
15. Molecular gels: Materials with Self-Assembled Fibrillar Networks; Weiss, R. G.; Terech, P., Eds.; Springer-Verlag: Dordrecht, 2006.
16. Dasgupta, A.; Mondal, J. H.; Das, D. Peptide Hydrogels. *RSC Adv.* **2013**, *3*, 9117–9149.
17. Jonker, A. M.; Löwik, D. W. P. M.; van Hest, J. C. M. Peptide and Protein-Based Hydrogels. *Chem. Mater.* **2012**, *24*, 759–773.
18. Du, X.; Zhou J.; Shi, J.; Xu, B. Supramolecular Hydrogelators and Hydrogels: From Soft Matters to Molecular Biomaterials. *Chem. Rev.* **2015**, *115*, 13165–13307.
19. Tao, K.; Wang, J.; Zhou, P.; Wang, C.; Xu, H.; Zhao, X.; Lu, J. R. Self-Assembly of Short Aβ(16-22) Peptides: Effect of Terminal Capping and the Role of Electrostatic Interaction. *Langmuir* **2011**, 27, 2723-2730.
20. Gotner, R. A.; Hoffman, W. F. *J. Am. Chem. Soc.* **1921**, *43*, 2199–2202.
21. Shi, J.; Gao, Y.; Yang, Z.; Xu, B. Exceptionally Small Supramolecular Hydrogelators Based on Aromatic-Aromatic interaction. *Beilstein J. Org. Chem.* **2011**, *7*, 167–172.
22. Yang, Z.; Xu, B. A Simple Visual Assay Based on Small Molecule Hydrogels for Detecting Inhibitors of Enzymes. *Chem. Commun.* **2004**, 2424–2425.
23. Reches, M.; Gazit, E. Self-Assembly of Peptide Nanotubes and Amyloid-Like Structures by Charged-Termini-Capped Diphenylalanine Peptide Analogues. *Isr. J. Chem.* **2005**, *45*, 363–371.
24. Seebach, D.; Matthews, J. L. β–Peptide: A Surprise at Every Turn. *Chem. Commun.* **1997**, 2015–2022
25. Yang, Z.; Lianga, G.; Xu, B. Supramolecular Hydrogels Based on β-Amino Acid Derivatives. *Chem. Commun.* **2006**, 738–740.
26. Ikeda, M.; Tanida, T.; Yoshii, T.; Hamachi, I. Rational Molecular Design of Stimulus-Responsive Supramolecular Hydrogels Based on dipeptides. *Adv. Mater.* **2011**, *23*, 2819–2822.
27. Adhikari, B.; Palui, G.; Banerjee, A. Self-Assembling Tripeptide Based Hydrogels and Their Use in Removal of Dyes from Waste-Water. *Soft Matter* **2009**, *5*, 3452–3460.
28. Palui, G.; Nanda, J.; Ray, S.; Banerjee, A. Fabrication of Luminescent CdS Nanoparticles on Short-Peptide-Based Hydrogel Nanofibers: Tuning of Optoelectronic Properties. *Chem.–Eur. J.* **2009**, *15*, 6902–6909.
29. Deming, T. J. Polypeptide Hydrogels *via* a Unique Assembly Mechanism. *Soft Matter* **2005**, *1*, 28–35.
30. Nowak, A. P.; Breedveld, V.; Pakstis, L.; Ozbas, B.; Pine, D. J.; Pochan, D.; Deming, T. J. Rapidly Recovering Hydrogel Scaffolds From Self-Assembling Diblock Copolypeptide Amphiphiles. *Nature*, **2002**, *417*, 424–428.
31. Nowak, A. P.; Breedveld, V.; Nowak, A. P.; Breedveld, V.; Deming, T. J. Unusual Salt Stability in Highly Charged Diblock Co-Polypeptide Hydrogels. *J. Am. Chem. Soc.* **2003**, *125*, 15666–15670.
32. Schneider, J. P.; Pochan, D. J; Ozbas, B.; Rajagopal, K.; Pakstis, L.; Kretsinger, J. Responsive Hydrogels from the Intramolecular Folding and Self-Assembly of a Designed Peptide. *J. Am. Chem. Soc.* **2002**, *124*, 15030–15037.
33. Ozbas, B.; Kretsinger, J.; Rajagopal, K.; Schneider, J. P.; Pochan, D. J. Salt-Triggered Peptide Folding and Consequent Self-Assembly into Hydrogels with Tunable Modulus. *Macromolecules* **2004**, *37*, 7331–7337.

34. Pochan, D. J.; Schneider, J. P.; Kretsinger, J.; Ozbas, B.; Rajagopal, K.; Haines, L. Thermally reversible Hydrogels via Intramolecular Folding and Consequent Self-Assembly of a *de Novo* Designed Peptide. *J. Am. Chem. Soc.* **2003**, *125*, 11802–11803.
35. Pochan, D. J.; Pakstis, L.; Ozbas, B.; Nowak, A. P.; Deming, T. J. SANS and Cryo-TEM Study of Self-Assembled Diblock Copolypeptide Hydrogels with Rich Nano- through Microscale Morphology. *Macromolecules*, **2002**, *35*, 5358–5360.
36. Holowka, E. P.; Pochan, D. J.; Deming, T. J. Charged Polypeptide Vesicles with Controllable Diameter. *J. Am. Chem. Soc.* **2005**, *127*, 12423–12428
37. Nowak, A. P.; Sato, J.; Breedveld V.; Deming, T. J. Hydrogel Formation in Amphiphilic Triblock Copolypeptides. *Supramol. Chem.* **2006**, *18*, 423–427.
38. Li, Z.; Deming, T. J. Tunable Hydrogel Morphology *via* Self-Assembly of Amphiphilic Pentablock Copolypeptides. *Soft Matter* **2010**, *6*, 2546–2551.
39. Breedveld V.; Nowak, A. P.; Sato, J.; Deming T. J.; Pine, D. J. Rheology of Block Copolypeptide Solutions: Hydrogels with Tunable Properties. *Macromolecules* **2004**, *37*, 3943–3953.
40. Katchalski E.; Sela, M. Synthesis and Chemical Properties of Poly-Alpha-Amino Acids. *Adv. Protein Chem.* **1958**, *13*, 243–492.
41. Ruana, L.; Zhanga, H.; Luoa, H.; Liua, J.; Tanga, F.; Shib, Y.-K.; Zhao, X. Designed Amphiphilic Peptide forms Stable Nanoweb, Slowly Releases Encapsulated Hydrophobic Drug, and Accelerates Animal Hemostasis. *Proc. Natl. Acad. Sci. U. S. A.* **2009**, *106*, 5105–5110.
42. Hinterding, K.; Alonso-Dı´az. D.; Waldmann. H. Organic Synthesis and Biological Signal Transduction. *Angew. Chem., Int. Ed.* **1998**, *37*, 688–749.
43. Claussen, R. C.; Rabatic. B. M.; Stupp. S. I. Aqueous Self-Assembly of Unsymmetric Peptide Bolaamphiphiles into Nanofibers with Hydrophilic Cores and Surfaces. *J. Am. Chem. Soc.* **2003**, *125*, 12680–12681.
44. Das, D.; Dasgupta. A.; Roy. S.; Mitra. R. N.; Debnath. S.; Das. P. K. Water Gelation of an Amino Acid-Based Amphiphile. *Chem.–Eur. J.* **2006**, *12*, 5068–5074.
45. Mitra, R. N.; Das, P. K. In situ Preparation of Gold Nanoparticles of Varying Shape in Molecular Hydrogel of Peptide Amphiphiles *J. Phys. Chem. C* **2008**, *112*, 8159–8166.
46. Roy S.; and Das, P. K. Antibacterial Hydrogels of Amino Acid-Based Cationic Amphiphiles. *Biotechnol. Bioeng.* **2008**, *100*, 756–764.
47. Shome, A.; Debnath, S.; Das, P. K. Head Group Modulated pH-Responsive Hydrogel of Amino Acid-Based Amphiphiles: Entrapment and Release of Cytochrome *c* and Vitamin B_{12}. *Langmuir* **2008**, *24*, 4280–4288.
48. Mitra, R. N.; Das, D.; Roy, S.; Das, P. K. Structure and Properties of Low Molecular Weight Amphiphilic Peptide Hydrogelators, *J. Phys. Chem. B.* **2007**, *111*, 14107–14113.
49. Mitra, R. N.; Shome, A.; Paul, P.; Das, P. K. Antimicrobial Activity, Biocompatibility and Hydrogelation Ability of Dipeptide-Based Amphiphiles. *Org. Biomol. Chem.* **2009**, *7*, 94–102.
50. Suzuki, M.; Yumoto, M.; Kimura, M.; Shirai, H.; Hanabusa, K. A Family of Low-Molecular-Weight Hydrogelators Based on L-Lysine Derivatives with a Positively Charged Terminal Group. *Chem.–Eur. J.* **2003**, *9*, 348–354.
51. Suzuki, M.; Yumoto, M.; Kimura, M.; Shirai, H.; Hanabusa, K. Novel family of low molecular weight hydrogelators based on L-lysine derivatives. *Chem. Commun.* **2002**, 884–885.
52. Langer, R.; Vacanti, J. P. Tissue Engineering. *Science* **1993**, *260*, 920–926.
53. Zhou, M.; Smith, A. M.; Das. A. K.; Hodson, N. W.; Collins. R. F.; Ulijn. R. V.; Gough. J. E, Self-assembled Peptide-Based Hydrogels as Scaffolds for Anchorage-Dependent Cells. *Biomaterials*, **2009**, *30*, 2523–2530.
54. Silva, G. A.; Czeisler, C.; Niece. K. L.; Beniash, E.; Harrington, D. A.; Kessler, J. A.; Stupp, S. I. Selective Differentiation of Neural Progenitor Cells by High-Epitope Density Nanofibers. *Science* **2004**, *303*, 1352–1355.
55. Nagai, Y.; Unsworth, L. D.; Koutsopoulos, S.; Zhang, S. Slow Release of Molecules in Self-assembling Peptide Nanofiber Scaffold. *J. Controlled Release*, **2006**, *115*, 18–25.
56. Zarhitsky, S.; Rapaport, H. The Interactions between Doxorubicin and Amphiphilic and Acidic β-sheet Peptides towards Drug Delivery Hydrogels. *J. Colloid Interface Sci.* **2011**, *360*, 525–531.
57. Mao, L.; Wang, H.; Tan, M.; Ou, L.; Kong, D.; Yang, Z. Conjugation of Two Complementary Anti-cancer Drugs Confers Molecular Hydrogels as a Co-delivery System. *Chem. Commun.* 2**012**, *48*, 395–397.
58. Dutta, S.; Shome, A.; Kar T.; Das, P. K. Counterion-Induced Modulation in the Antimicrobial Activity and Biocompatibility of Amphiphilic Hydrogelators: Influence of in-Situ-Synthesized Ag−Nanoparticle on the Bactericidal Property. *Langmuir* **2011**, *27*, 5000–5008.
59. Hatgerink, J. D.; Beniash, E.; Stupp, S. I. Self-Assembly and Mineralization of Peptide-Amphiphile Nanofibers. *Science* **2001**, *294*, 1684–1688.
60. Yan, X.; Zhu, P.; Li, J. Self-Assembly and Application of Diphenylalanine-Based Nanostructures. *Chem. Soc. Rev.* **2010**, *39*, 1877-1890.
61. Lakshmanan, A.; Zhang, S.; Hauser, C. A. E. Short Self-Assembling Peptides as Building Blocks for Modern Nanodevices. *Trends Biotechnol.* **2012**, *30*, 155–165.

62. Reches, M.; Gazit, E. Casting Metal Nanowires With in Discrete Self-Assembled Peptide Nanotubes. *Science* **2003**, *300*, 625-627.
63. Gazit, E. Self-Assembled Peptide Nanostructures: The Design of Molecular Building Blocks and their Technological Utilization. *Chem. Soc. Rev.* **2007**, *36*, 1263-1269.
64. Niu, L.; Chen, X.; Allen S.; Tendler, S. J. B. Using the Bending Beam Model to Estimate the Elasticity of Diphenylalanine Nanotubes. *Langmuir* **2007**, *23*, 7443–7446.
65. Yemini, M.; Reches, M.; Gazit, E.; Rishpon, J. Peptide Nanotube-Modified Electrodes for Enzyme–Biosensor Applications. *Anal. Chem.* **2005**, *77*, 5155–5159.
66. Yemini, M.; Rishpon, J.; Gazit, E. Novel Electrochemical Biosensing Platform Using Self-Assembled Peptide Nanotubes. *Nano Lett.* **2005**, *5*, 183–186.
67. Adler-Abramovich, L. Gazit, E. Controlled Patterning of Peptide Nanotubes and Nanospheres Using Inkjet Printing Technology. *J. Pept. Sci.* **2008**, *14*, 217–223.
68. Sedman, V. L.; Allen, S.; Chen, X.; Roberts, C. J.; Tendler, S. J. B. Thermomechanical Manipulation of Aromatic Peptide Nanotubes. *Langmuir* **2009**, 25, 7256–7259.
69. Castillo, J.; Tanzi, S.; Dimaki, M.; Svendsen, W. Manipulation of Self-Assembly Amyloid Peptide Nanotube by Dielectrophoresis. *Electrophoresis* **2008**, *29*, 5026–5032.
70. Adler-Abramovich, L.; Aronov, D.; Gazit, E.; Rosenman, G. Patterened Arrays of Ordered Peptide Nanostuctures. *J. Nanosci. Nanotechnol.* **2009**, *9*, 1701–1708.
71. M. B. Larsen, K. B. Andersen, W. E. Svendsen and J. Castillo, Self-Assembled Peptide Nanotubes as an Etching Material for the Rapid Fabrication of Silicon Wires. *BioNanoScience* **2011**, *1*, 31–37.
72. Dutta, S.; Shome, A.; Debnath, S.; Das, P. K. Counterion Dependent Hydrogelation of Amino Acid Based Amphiphiles: Switching from Non-Gelators to Gelators and Facile Synthesis of Silver Nanoparticles. *Soft Matter* **2009**, *5*, 1607–1620.
73. Kar, T.; Mandal, S. K.; Das, P. K. Influence of Pristine SWNTs in Supramolecular Hydrogelation: Scaffold for Superior Peroxidase Activity of Cytochrome c. *Chem. Commun.* **2012**, *48*, 8389–8391.
74. Maity, I.; Rasale, D. B.; Das, A. K. Sonication Induced Peptide-Appended Bolaamphiphile Hydrogels for *in situ* Generation and Catalytic Activity of Pt Nanoparticles. *Soft Matter* **2012**, *8,* 5301–5308.
75. Rodriguez-Llansola, F.; Miravet, J. F.; Escuder, B. Supramolecular hydrogel as reusable Heretogeneous Catalyst for the Direct Aldol Reaction. *Chem. Commun.* **2009**, 7303–7305.
76. Pederson, C. J. Cyclic Polyethers and Their Complexes with Metal Salts. *J. Am. Chem. Soc.* **1967**, *89*, 7017–7036.
77. Pedersen, C. J. The Discovery of Crown Ethers (Noble Lecture). *Angew. Chem., Int. Ed.* **1988**, 27, 1021-1027.
78. Cram, D. J. The Design of Molecular Hosts, Guests, and their Complexes (Nobel Lecture). *Angew. Chem., Int. Ed.* **1988**, 27, 1009-1020.
79. Gale, P. A. Supramolecular Chemistry Anniversary. *J. Chem. Soc. Rev.* **2007**, *36*, 141-142.
80. Crini, G. Review: A History of Cyclodextrins. *Chem. Rev.* **2014**, *114*, 10940–10975.
81. Kim, H. J.; Lee, M. H.; Mutihac, L.; Vicens, J.; Kim, J. S. Host Guest Sensing by Calixarenes on the Surfaces. *Chem. Soc. Rev.* **2012**, *41*, 1173–1190.
82. Xue, M.; Yang, Y.; Chi, X.; Zhang, Z.; Huang, F. Pillararenes, a New Class of Macrocycles for Supramolecular Chemistry. *Acc. Chem. Res.* **2012**, *45*, 1294–1308,
83. Hu, X.-B.; Chen, Z.; Chen, L.; Zhang, L.; Hou, J.-L.; Lia, Z.-T. Pillar[*n*]arenes (*n* = 8-10) with Two Cavities: Synthesis, Structures and Complexing Properties. *Chem. Commun.* **2012**, *48*, 10999–11001.
84. Lagona, J.; Mukhopadhyay, P.; Chakrabarti, S.; Isaacs, L. The Cucurbit[n]uril Family. *Angew. Chem., Int. Ed.* **2005**, *44*, 4844–4870.
85. Lee, J. W.; Samal, S.; Selvapalam, N.; Kim, H.-J.; Kim, K. Cucurbituril Homologues and Derivatives: New Opportunities in Supramolecular Chemistry. *Acc. Chem. Res.* **2003**, *36*, 621-630.
86. Das, D.; Scherman, O. Cucurbituril: At the Interface of Small Molecule Host–Guest Chemistry and Dynamic Aggregates. *Isr. J. Chem.* **2011**, *51*, 537–550.
87. Rekharsky, M. V.; Mori, T.; Yang, C.; Ko, Y. H.; Selvapalam, N.; Kim, H.; Sobransingh, D.; Kaifer, A. E.; Liu, S.; Isaacs, L.; Chen, W;. Moghaddam, S.; Gilson, M. K.; Kim, K.; Inoue, Y. A synthetic Host-Guest System Achieves Avidin-Biotin Affinity by Overcoming Enthalpy–Entropy Compensation. *Proc. Natl. Acad. Sci. USA* **2007**, *104*, 20737–20742.
88. Freeman, W. A.; Mock, W. L.; Shih, N.-Y. Cucurbituril. *J. Am. Chem. Soc.* **1981**, *103*, 7367–7368.
89. Behrend, R.; Meyer, E.; Rusche, F. I. Ueber Condensationsproducte aus Glycoluril und Formaldehyd. *Justus Liebigs Ann. Chem.* **1905**, *339*, 1–37.
90. Kim, J.; Jung, I.-S.; Kim, S.-Y.; Lee, E.; Kang, J.-K.; Sakamoto, S.; Yamaguchi, K.; Kim, K. New Cucurbituril Homologues: Syntheses, Isolation, Characterization, and X-ray Crystal Structures of Cucurbit[*n*]uril (*n* = 5, 7, and 8). *J. Am. Chem. Soc.* **2000**, *122*, 540–541.
91. Day, A. I.; Arnold, A. P.; Blanch, R. J.; Snushall, B. Controlling Factors in the Synthesis of Cucurbituril and Its Homologues. *J. Org. Chem.* **2001**, *66*, 8094 –8100.
92. Day, A. I. Blanch, R. J. Arnold, A. P. Lorenzo, S. Lewis, G. R. Dance, I. A Cucurbituril-Based Gyroscane: A New Supramolecular Form. *Angew. Chem., Int. Ed.* **2002**, *41*, 275–277.

93. Liu, S.; Zavalij, P. Y.; Isaacs, L. Cucurbit[10]uril. *J. Am. Chem. Soc.* **2005**, *127*, 16798 –16799.
94. Buschmann, H.-J.; Cleve, E.; Jansen, K.; Wego, A.; Schollmeyer, E. The Determination of Complex Stabilities Between Different Cyclodextrins and Dibenzo-18-Crown-6, Cucurbit[6]uril, Decamethylcucurbit[5]uril, Cucurbit[5]uril, p-tert-butylcalix[4]arene and p-tert-butylcalix[6]arene in Aqueous Solutions using a Spectrophotometric Method. *Mater. Sci. Eng. C* **2001**, *14*, 35 – 39.
95. Germain, P.; Letoffe, J. M.; Merlin, M. P.; Buschmann, H.-J. Thermal behaviour of hydrated and anhydrous Cucurbituril: A DSC, T.G. and calorimetric study in temperature range from 100 to 800 K. *Thermochim. Acta* **1998**, *315*, 87 – 92.
96. Buschmann, H.-J.; Cleve, E.; Schollmeyer, E. Cucurbituril as a ligand for the complexation of cations in aqueous solutions. *Inorg. Chim. Acta* **1992**, *193*, 93 – 97.
97. Masson, E.; Ling, X.; Joseph, R.; Kyeremeh-Mensah, L.; Lu, X. Cucurbituril Chemistry: A Tale of Supramolecular Success. *RSC Advances* **2012**, *2*, 1213–1247.
98. Urbach A. R.; Ramalingam, V. Molecular Recognition of Amino Acids, Peptides, and Proteins by Cucurbit[n]uril Receptors *Isr. J. Chem.* **2011**, *51*, 537–550.
99. Kaifer, A. E.; Li, W.; Yi, S. Cucurbiturils as Versatile Receptors for Redox Active Substrates. *Isr. J. Chem.* **2011**, *51*, 496–505.
100. Zhang, X. X.; Krakowiak, K. E.; Xue, G.; Bradshaw, J. S.; Izatt, R. M. A Highly Selective Compound for Lead: Complexation Studies of Decamethylcucurbit[5]uril with Metal Ions. *Ind. Eng. Chem. Res.* **2000**, *39*, 3516-3520.
101. Heo, J.; Kim, J.; Whang, D.; Kim, K. Columnar One-Dimensional Coordination Polymer Formed with a Metal ion and a Host-Guest complex as Building Blocks: Potassium Ion Complexed Cucurbituril. *Inorg. Chim. Acta* **2000**, *279*, 307-312.
102. Sokolov, M. N.; Virovets, A. V.; Dybtsev, D. N.; Gerasko, O. A.; Fedin, V. P.; Hernandez-Molina, R.; Clegg, W.; Sykes, A. G. Metal Incorporation into and Dimerization of M3E4 Clusters (M=Mo, W; E=S, Se) in Supramolecular Assemblies with Cucurbituril: A Molecular Model of Intercalation *Angew. Chem., Int. Ed.* **2000**, *39*, 1659-1661.
103. Jeon, Y.-M.; Kim, J.; Whang, D.; Kim, K. Molecular Container Assembly Capable of Controlling Binding and Release of Its Guest Molecules: Reversible Encapsulation of Organic Molecules in Sodium Ion Complexed Cucurbituril. *J. Am. Chem. Soc.* **1996**, *118*, 9790-9791.
104. Whang, D.; Heo, J.; Park, J. H.; Kim, K. A Molecular Bowl with Metal Ion as Bottom: Reversible Inclusion of Organic Molecules in Cesium Ion Complexed Cucurbituril. *Angew. Chem., Int. Ed.* **1998**, *37*, 78-80.
105. U.S. Patent: Kim, K.; Kim, J.; Jung, I.-S.; Kim, S.-Y.; Lee, E.; Kang, J.-K. Pohang University of Science and Technology Foundation, 2000.
106. Bush, M, E.; Bouley, N. D.; Urbach, A. R. Charge-Mediated Recognition of N-Terminal Tryptophan in Aqueous Solution by a Synthetic Host. *J. Am. Chem. Soc.* **2005**, *127*, 14511-14517.
107. Heitmann, L. M.; Taylor, A. B.; Hart, P. J.; Urbach, A. R. Sequence-Specific Recognition and Cooperative Dimerization of N-Terminal Aromatic Peptides in Aqueous Solution by a Synthetic Host. *J. Am. Chem. Soc.* **2006**, *128*, 12574-12581.
108. Kim, H-J.; Heo, J.; Jeon, W. S.; Lee, E.; Kim, J.; Sakamoto, S.; Yamaguchi, K.; Kim, K. Selective Inclusion of a Hetero-Guest Pair in a Molecular Host: Formation of Stable Charge-Transfer Complexes in Cucurbit[8]uril. *Angew. Chem., Int. Ed.* **2001**, *40*, 1526-1529.
109. Jeon, W. S.; Kim, H.-J.; Lee, C.; K. Kim, Control of the Stoichiometry in Host-guest Complexation by Redox Chemistry of Guests: Inclusion of Methyl-viologen in Cucurbit[8]uril. *Chem. Commun.* **2002**, 1828-1829.
110. Deroo, S.; Rauwald, U.; Robinson, C. V.; Scherman, O. A. Discrete, Multi-Component Complexes Cucurbit[8]uril in the Gas- Phase. *Chem. Commun.* **2009**, 644 –646.
111. Rauwald, U.; Scherman, O. A.; Supramolecular Block Copolymers with Cucurbit[8]uril in Water. *Angew. Chem., Int. Ed.* **2008**, 47, 3950–3953.
112. Appel, E. A.; Biedermann, F.; Rauwald, U.; Jones, S. T.; Zayed, J. M.; Scherman, O. A. *J. Am. Chem. Soc.* **2010**, *132*, 14251 – 14260.
113. Liu, Y.; Yu, Y.; Gao, J.; Wang, Z.; Zhang, X. Water-Soluble Supramolecular Polymerization Driven by Multiple Host-Stabilized Charge-Transfer Interactions, *Angew. Chem., Int. Ed.* **2010**, *49*, 6576–6579.
114. Liu, Y.; Liu, K.; Wang, Z.; Zhang, X. Host-Enhanced π–π Interaction for Water Soluble Supramolecular Polymerization. *Chem.–Eur. J.* **2011**, *17*, 9930–9935.
115. Liu, Y.; Fang, R.; Tan, X.; Wang, Z.; Zhang, X. Supramolecular Polymerization at Low Monomer Concentrations: Enhancing Intermolecular Interactions and Suppressing Cyclization by Rational Molecular Design. *Chem.–Eur. J.* **2012**, *18*, 15650-15654.
116. Tan, X.; Yang, L.; Liu, Y.; Huang, Z.; Yang, H.; Wang, Z.; Zhang, X. Water Soluble Supramolecular Polymers Fabricated Through Specific Interactions Between Cucurbit[8]uril and a Tripeptide of Phe-Gly-Gly. *Polym. Chem.*, **2013**, *4*, 5378–5381.
117. Yang, L.; Liu, X.; Tan, X.; Yang, H.; Wang, Z.; Zhang, X. Supramolecular Polymer Fabricated by Click Polymerization from Supra-monomer. *Polym. Chem.* **2014**, *5*, 323-326.
118. Yang, H.; Bai, Y.; Yu, B.; Wang, Z.; Zhang, X. Supramolecular Polymers Bearing Disulfide Bonds. *Polym. Chem.* **2014**, *5*, 6439–6443.
119. Tan, X.; Yang, L.; Huang, Z.; Yu, Y.; Wang, Z.; Zhang, X. Amphiphilic Diselenide-Containing Supramolecular polymers. *Polym. Chem.* **2015**, *6*, 681–685.

120. Song, Q.; Li, F.; Yang, L.; Wang, Z.; Zhang, X. Supramolecular Polymers Synthesized by Thiol-Ene Click Polymerization from Supra-monomers. *Polym. Chem.* **2015**, *6*, 369-372.
121. Yang, L.; Bai, Y.; Tan, X.; Wang, Z.; Zhang, X. Controllable Supramolecular Polymerization through Host–Guest Interaction and Photo Chemistry. *ACS Macro Lett.* **2015**, *4*, 611−615.
122. Fang, R.; Liu, Y.; Wang, Z.; Zhang, X. Water Soluble Supramolecular Hyperbranched Polymers Based on Host-Enhanced π–π Interaction. *Polym. Chem.* **2013**, *4*, 900–903.
123. Yang, H.; Ma, Z.; Wang, Z.; Zhang, X. Fabricating Covalently Attached Hyperbranched Polymers by Combining Photochemistry with Supramolecular Polymerization. *Polym. Chem.* **2014**, *5*, 1471 –1476.
124. Del Barrio, J.; Horton, P. N.; Lairez, D.; Lloyd, G. O.; Toprakcioglu, C.; Scherman, O. A. Photocontrol over Cucurbit[8]uril Complexes: Stoichiometry and Supramolecular Polymers. *J. Am. Chem. Soc.* **2013**, *135*, 11760−11763.
125. Barrow, S. J.; Kasera, S.; Rowland, M. J.; Barrio, J. Del.; Scherman, O. A. Cucurbituril-Based Molecular Recognition, *Chem. Rev.* **2015**, *115*, 12320-12406.
126. Hagen Klauk (Ed.) "Organic "Electronics: Materials, Manufacturing and Applications" 2006, Wiley-VCH, Weinheim. Print ISBN 9783527312641.
127. Hagen Klauk (Ed.) "Organic electronics. More materials and applications" 2010, Wiley-VCH, Weinheim. ISBN 9783527640218 electronic bk.
128. McNeill, R.; Siudak, R.; Wardlaw, J. H.; Weiss, D. E. Electronic Conduction in Polymers. I. The Chemical Structure of Polypyrrole. *Aust. J. Chem.* **1963**, *16*, 1056–1075.
129. *"The Nobel Prize in Chemistry 2000". Nobelprize.org. Nobel Media.*
130. Jones, B. A.; Antonio, F.; Wasielewski, M. R.; Marks, T. J. Tuning Orbital Energetics in Arylene Diimide Semiconductors. Materials Design for Ambient Stability of n-Type Charge Transport. *J. Am. Chem. Soc.* **2007**, *129*, 15259-15278.
131. Ling, M.-M.; Erk, P.; Gomez, M.; Koenemann, M.; Bao, Z. N. Air Stable n-Channel Organic Semiconductors Based on Perylene Diimide Derivatives without Strong Electron Withdrawing Groups. *Adv. Mater.* **2007**, *19*, 1123-1127.
132. Schmide, R.; Ling, M. M.; Oh, J. H.; Winkler, M.; Könemann, M.; Bao, Z. N.; Würthner, F. *Adv. Mater.* **2007**, *19*, 3692-3695.
133. Zang, L.; Che, Y. K.; Moore, J. S. One-Dimensional Self- Assembly of Planar π-Conjugated Molecules: Adaptable Building Blocks for Organic Nanodevices. *Acc. Chem. Res.* **2008**, *41*, 1596– 1608.
134. Würthner, F. Perylene Bisimide Dyes as Versatile Building Blocks for Functional Supramolecular Architectures. *Chem. Commun.* **2004**, 1564–1579.
135. Elemans, J. A. A. W.; van Hameren, R.; Nolte, R. J. M.; Rowan, A. E. Molecular Materials by Self-Assembly of Porphyrins, Phthalocyanines, and Perylenes. *Adv. Mater.* **2006**, *18*, 1251–1266.
136. Görl, D.; Zhang, X.; Würthner, F. Molecular Assemblies of Perylene Bisimide Dyes in Water. *Angew. Chem., Int. Ed.* **2012**, *51*, 6328–6348.
137. Hasegawa, M.; Iyoda, M. Conducting Supramolecular Nanofibers and Nanorods. *Chem. Soc. Rev.* **2010**, *39*, 2420–2427.
138. Yao, W.; Zhao, Y. S. Tailoring The Self-Assembled Structures and Photonic Properties of Organic Nanomaterials. *Nanoscale* **2014**, *6*, 3467−3473.
139. Supura, M.; Fukuzumi, S. Energy and Electron Transfer of One- Dimensional Nanomaterials of Perylene Diimides. *ECS J. Solid State Sci. Technol.* **2013**, *2*, M3051−M3062.
140. Li, C.; Wonneberger, H. Perylene Imides for Organic Photovoltaics: Yesterday, Today, and Tomorrow. Adv. *Mater.* **2012**, *24*, 613–636.
141. Huang, C.; Barlow, S.; Marder, S. R. Perylene-3,4,9,10- Tetracarboxylic Acid Diimides: Synthesis, Physical Properties, and Use in Organic Electronics. *J. Org. Chem.* **2011**, *76*, 2386–2407.
142. Zhao, Q. L.; Zhang, S.; Liu, Y.; Mei, J.; Chen, S. J.; Lu, P.; Qin, A. J.; Ma, Y. G.; Sun, J. Z.; Tang, B. Z. Tetraphenylethenyl-Modified Perylene Bisimide: Aggregation-Induced Red Emission, Electrochemical Properties and Ordered Microstructures. *J. Mater. Chem.* **2012**, *22*, 7387–7394.
143. Wang, W.; Wang, L.; Palmer, B. J.; Exarhos, G. J.; Li, A. D. Q. Cyclization and Catenation Directed by Molecular Self-Assembly. *J. Am. Chem. Soc.* **2006**, *128*, 11150-11159.
144. Han, J. J.; Shaller, A. D.; Wang, W.; Li, A. D. Q. Architecturally Diverse Nanostructured Foldamers Reveal Insightful Photoinduced Single-Molecule Dynamics. *J. Am. Chem. Soc.* **2008**, *130*, 6974-6982.
145. Backes, C.; Schunk, T.; Hauke, F.; Hirsch, A. Counterion Effect on the Aggregation of Anionic Perylene Dyes and the Influence on Carbon Nanotube Dispersion Efficiencies. *J. Mater. Chem.* **2011**, *21*, 3554-3557.
146. Chen, Z.; Stepanenko, V.; Dehm, V.; Prins, P.; Siebbeles, L. D. A.; Seibt, J.; Marquetand, P.; Engel, V.; Würthner, F. Photoluminescence and Conductivity of Self-Assembled π–π Stacks of Perylene Bisimide Dyes. *Chem.–Eur. J.* **2007**, *13*, 436-449.
147. Kaiser, T. E.; Wang, H.; Stepanenko, V.; Würthner, F. Supramolecular Construction of Fluorescent J-Aggregates Based on Hydrogen-Bonded Perylene Dyes. *Angew. Chem. Int. Ed.* **2007**, *46,* 5541-5544.
148. Liu, R. C.; Holman, M. W.; Zang, L.; Adams, D. M. Single Molecule Spectroscopy of Intramolecular Electron Transfer in Donor- Bridge-Acceptor Systems. *J. Phys. Chem. A* **2003**, *107*, 6522–6526.
149. Datar, A.; Balakrishnan, K.; Yang, X. M.; Zuo, X. B.; Huang, J. L.; Oitker, R.; Yen, M.; Zhao, J. C.; Tiede, D. M.; Zang, L. Linearly Polarized Emission of an Organic Semiconductor Nanobelt. *J. Phys.Chem. B* **2006**, *110*, 12327−12332.

150. Tidhar, Y.; Weissman, H.; Wolf, S. G.; Gulino, A.; Rybtchinski, B. Pathway-Dependent Self-Assembly of Perylene Diimide/Peptide Conjugates in Aqueous Medium. *Chem.–Eur. J.* **2011**, *17*, 6068-6075.
151. Sun, Y.; He, C.; Sun, K.; Li, Y.; Dong, H.; Wang, Z.; Li, Z. Fine-Tuned Nanostructures Assembled from L-Lysine-Functionalized Perylene Biimides. *Langmuir* **2011**, *7*, 11364-11371.
152. Lu, X.; Guo, Z.; Sun, C.; Tian, H.; Zhu, W. Helical Assembly Induced by Hydrogen Bonding from Chiral Carboxylic Acids Based on Perylene Bisimides *J. Phys. Chem. B* **2011**, *115*, 10871-10876.
153. Schmidt, C. D.; Böttcher, C.; Hirsch, A. Chiral Water Soluble Perylenediimides. *Eur. J. Org. Chem.* **2009**, 5337-5349.
154. Xu, Y.; Leng, S.; Xue, C.; Sun, R.; Pan, J.; Ford, J.; Jin, S. A Room-Temperature Liquid-Crystalline Phase with Crystalline π Stacks. *Angew. Chem., Int. Ed.* **2007**, *46*, 3896-3899.
155. Xue, C.; Chen, M.; Jin, S. Synthesis and Characterization of the First Soluble Nonracemic Chiral Main-Chain Perylene tetracarboxylic Diimide Polymers. *Polymer* **2008**, *49*, 5314-5321.
156. Datar, A.; Balakrishnan, K.; Zang, L. One-Dimensional Self- Assembly of a Water Soluble Perylene Diimide Molecule by pH Triggered Hydrogelation. *Chem. Commun.* **2013**, *49*, 6894–6896.
157. Draper, E. R.; Walsh, J. J.; McDonald, T. O.; Zwijnenburg, M. A.; Cameron, P. J.; Cowan, A. J.; Adams, D. J. Air-Stable Photoconductive Films Formed from Perylene Bisimide Gelators. *J. Mater. Chem. C* **2014**, *2*, 5570–5575.
158. Sukul, P. K.; Singh, P. K.; Majib, S. K.; Malik, S.; Aggregation Induced Chirality in a Self-Assembled Perylene Based Hydrogel: Application of the Intracellular pH Measurement. *J. Mater. Chem. B* **2013**, *1*, 153–156.
159. Irima-Vladu, M. "Green" Electronics: Biodegradable and Biocompatible materials and devices for sustainable Future. *Chem. Soc. Rev.* **2014**, *43*, 588-610.
160. Cipriano, T.; Knotts, G.; Laudari, A.; Bianchi, R. C.; Alves, W. A.; Guha, S. Bioinspired Peptide Nanostructures for Organic Field-Effect Transistors. *ACS Appl. Mater. Interfaces* **2014**, *6*, 21408-21415.
161. Chang, J.-W.; Wang, C.-G.; Huang, C.-Y.; Tsai, T.-D.; Guo, T.-F.; Wen, T.-C. Chicken Albumen Dielectrics in Organic Field-Effect Transistors. *Adv. Mater.* **2011**, *23*, 4077-4081.
162. Singh, T.; Sariciftci, N.; Grote, J. in Organic Electronics SE-6, Advancesin Polymer Science, Vol. 223, Springer, Berlin–Heidelberg, Germany 2010 pp. 73.
163. Xia, Y.; Yang, P.; Sun, Y.; Wu, Y.; Mayers, B.; Gates, B.; Yin, Y.; Kim, F.; Yan, H. One Dimensional Nanostructures: Synthesis, Characterization, and Applications. *Adv. Mater.* **2003**, *15*, 353-389.
164. Zhao, X.; Pan, F.; Xu, H.; Yaseen, M.; Shan, H.; Hauser, C. A. E.; Zhang, S.; Lu, J. R. Molecular Self-Assembly and Applications of Designer Peptide Amphiphiles. *Chem. Soc. Rev.* **2010**, *39*, 3480-3498.
165. Löwik, D. W. P. M.; van Hest, J. C. M. Peptide Based Amphiphiles. *Chem. Soc. Rev.* **2004**, *33*, 234-245.
166. Duan, P.; Qin, L.; Zhu, X.; Liu, M. Hierarchical Self-Assembly of Amphiphilic Peptide Dendrons: Evolution of Diverse Chiral Nanostructures through Hydrogel Formation over a wide pH range. *Chem.–Eur. J.* **2011**, *17*, 6389-6395.
167. Bowerman, C. J.; Nilsson, B. L. A Reductive Trigger for Peptide Self-Assembly and Hydrogelation. *J. Am. Chem. Soc.* **2010**, *132*, 9526-9527.
168. Shome, A.; Dutta, S.; Maiti, S.; Das, P. K. *In situ* Synthesized Ag Nanoparticle in Self-Assemblies of Amino Acid based Amphiphilic Hydrogelators: Development of Antibacterial Soft Nanocomposites. *Soft Matter* **2011**, *7*, 3011-3022.
169. Salick, D. A.; Kretsinger, J. K.; Pochan, D. J.; Schneider, J. P. Inherent Antibacterial Activity of a Peptide-Based β-hairpin Hydrogel. *J. Am. Chem. Soc.* **2007**, *129*, 14793-14799.
170. Ghosh, A.; Dey, J. pH-Responsive and Thermo-reversible Hydrogels of N-(2-hydroxyalkyl)-l-valine Amphiphiles. *Langmuir* **2009**, *25*, 8466-8472.
171. Sone, E. D.; Stupp, S. I. Semiconductor-Encapsulated Peptide–Amphiphile Nanofibers. *J. Am. Chem. Soc.* **2004**, *126*, 12756-12757.
172. Fenniri, H.; Mathivanan, P.; Vidale, K. L.; Sherman, D. M.; Hallenga, K.; Wood, K. V.; Stowell, J. G. Helical Rosette Nanotubes: Design, Self-Assembly, and Characterization. *J. Am. Chem. Soc.* **2001**, *123*, 3854-3855.
173. Israelachvili, J. N. In Intermolecular and Surface Forces, 2nd ed.; Academic Press: New York, **1991**.
174. Cao, H.; Yuan, Q.; Zhu, X.; Zhao, Y-P.; Liu, M. Hierarchical Self-Assembly of Achiral Amino Acid Derivatives into Dendritic Chiral Nanotwists. *Langmuir* **2012**, *28*, 15410-15417.
175. Chang, C.-D.; Waki, M.; Ahmad, M.; Meienhofer, J.; Lundell, E. O.; Haug, J. D. Preparation and Properties of Nalpha-9-fluorenylmethyloxycarbonylamino Acids bearing tert.-butyl side chain Protection. *Int. J. Pept. Protein Res.* **1980**, *15*, 59-66.
176. Harrison, J. L.; Petrie, G. M.; Noble, R. L.; Beilan, H. S.; McCurdy, S. N.; Culwell A. R.; In *Fmoc Chemtstry' Synthesis, Kinetics, Cleavage, and Deprotection of Arginine-Containing Peptides, in Techniques in Protein Chemistry,* Hugli, T. E. Ed.; Academic, San Diego, **1989**, pp 506-516.
177. Froster, T. Excimers. *Angew. Chem., Int. Ed.* **1969**, *8*, 333-343.
178. Schulman, S.; In *Fluorescence and Phosphorescence Spectroscopy: Physicochemical Principles and Practice*, Belcher, R., Freiser, H. Eds.; Pergamon Press, **1977**.
179. Yang, Z.; Gu, H.; Zhang, Y.; Wanga, L.; Xu, B. Small Molecule Hydrogels Based on a Class of Antiinflammatory Agents. *Chem. Commun.* **2004**, 208-209.
180. Berova, N.; Nakanishi K.; Woody, R. W. *Circular Dichroism: Principles and Applications*, Wiley-VCH, New York, **2000**.

181. Zhang, J.; Coulston, R. J.; Jones, S. T.; Geng, J.; Scherman, O. A.; Abell, C. One-Step Fabrication of Supramolecular Microcapsules from Microfluidic Droplets. *Science* **2012**, *335*, 690-694.
182. Biedermann, F.; Hathazi, D.; Nau, W. M. Associative Chemosensing by Fluorescent Macrocycle–Dye Complexes – a Versatile Enzyme Assay Platform beyond Indicator Displacement. *Chem. Commun.* **2015**, *51*, 4977-4980.
183. Ramalingam, V.; Urbach, A. R. Cucurbit[8]uril Rotaxanes. *Org. Lett.* **2011**, *13*, 4898-4901.
184. Jones, S. T.; Zayed, J. M.; Scherman, O. A. Supramolecular Alignment of Gold Nanorods *via* Cucurbit[8]uril Ternary Complex Formation. *Nanoscale*, **2013**, *5*, 5299-5302.
185. Barooah, N.; Pemberton, B. C.; Sivaguru, J. Manipulating Photochemical Reactivity of Coumarins within Cucurbituril Nanocavities. *Org. Lett.* **2008**, *10*, 3339-3342.
186. Mondal, J. H.; Ahmed, S.; Ghosh, T.; Das, D. Reversible Deformation–Formation of a Multistimuli Responsive Vesicle by a Supramolecular Peptide Amphiphile. *Soft. Matter* **2014**, *11*, 4912-4920.
187. Zhang, Q.; Qu, D.-H.; Wu, J.; Ma, X.; Wang, Q.; Tian, H. A Dual-Modality Photoswitchable Supramolecular Polymer. *Langmuir* **2013**, *29*, 5345−5350.
188. Stoffelen, C.; Voskuhl, J.; Jonkheijm, P.; Huskens, J. Optical Control over Bioactive Ligands at Supramolecular Surfaces. *Angew. Chem., Int. Ed.* **2014**, *53*, 3400–3404.
189. Qian, H.; Guo, D.-S.; Liu, Y. Cucurbituril-Modulated Supramolecular Assemblies: From Cyclic Oligomers to Linear Polymers. *Chem.–Eur. J.* **2012**, *18*, 5087-5095.
190. Stoffelen, C.; Staltari-Ferraro, E.; Huskens, J. Effects of the Molecular Weight and the Valency of Guest-Modified Poly(ethylene glycol)s on the Stability, Size and Dynamics of Supramolecular Nanoparticles. *J. Mater. Chem. B* **2015**, *3*, 6945-6952.
191. Petka, W. A.; Harden, J. L.; McGrath, K. P.; Wirtz, D.; Tirrell, D. A. Reversible Hydrogels from Self-Assembling Artificial Proteins. *Science* **1998**, *281*, 389–392.
192. Micklitsch, C. M.; Knerr, P. J.; Branco, M. C.; Nagarkar, R.; Pochan, D. J.; Schneider, J. P. Zinc-Triggered Hydrogelation of a Self-Assembling β-Hairpin Peptide. *Angew. Chem., Int. Ed.* **2011**, *50*, 1577–1579.
193. Ahmed, S.; Mondal, J. H.; Behera, N.; Das, D. Self-Assembly of a Peptide-Amphiphile Forming Helical Nano-Fibres and in-situ Template Synthesis of Uniform Mesoporous Single Wall Silica Nano-tubes. *Langmuir* **2013**, *29*, 14274-14283.
194. Oshaben, K. M.; Horne, W. S. Tuning Assembly Size in Peptide-Based Supramolecular Polymers by Modulation of Subunit Association Affinity. *Biomacromolecules* **2014**, *15*, 1436−1442.
195. Haino, T. Molecular-recognition-directed Formation of Supramolecular Polymers. *Polym. J.* **2013**, *45*, 363-383.
196. Rowland, M. J.; Atgie, M.; Hoogland, D.; Scherman, O. A. Preparation and Supramolecular Recognition of Multivalent Peptide–Polysaccharide Conjugates by Cucurbit[8]uril in Hydrogel Formation. *Biomacromolecules* **2015**, *16*, 2436–2443.
197. de Borba, E. B.; Amaral, C. L. C.; Politi, M. J.; Villalobos, R.; Baptista, M. S. Photophysical and Photochemical Properties of Pyranine/Methyl Viologen Complexes in Solution and in Supramolecular Aggregates: A Switchable Complex. *Langmuir* **2000**, *16*, 5900−5907.
198. Harris, C.; Kamat, P. V. Photocatalytic Events of CdSe Quantum Dots in Confined Media. Electrodic Behavior of Coupled Platinum Nanoparticles. *ACS Nano* **2010**, *4*, 7321−7330.
199. Zhang, T.; Sun, S.; L. F.; Fan, J.; Pang, Y.; Sun, L.; Peng, X. Redox-Induced Partner Radical Formation and its Dynamic Balance with Radical Dimer in Cucurbit[8]uril. *Phys. Chem. Chem. Phys.* **2009**, *11*, 11134-11139.
200. Jeon, W. S.; Kim, E.; Ko, H.; Hwang, I.; Lee, J. W.; Kim, S.-Y.; Kim, H.-J.; Kim, K. Molecular Loop Lock: A Redox-Driven Molecular Machine Based on a Host-Stabilized Charge-Transfer Complex. *Angew. Chem., Int. Ed.* **2005**, *44*, 87–89.
201. Zhang, L.; Zhou, T.-Y.; Tian, J.; Wang, H.; Zhang, D-W.; Zhao, X.; Liu, Y.; Li, Z-T. A Two-Dimensional Single-Layer Supramolecular Organic Framework that is Driven by Viologen Radical Cation Dimerization and Further Promoted by Cucurbit[8]uril. *Polym. Chem.* **2014**, *5*, 4715–4721.
202. Moon, K.; Grindstaff, J.; Sobransingh, D.; Kaifer, A. E. Cucurbit[8]uril-Mediated Redox-Controlled Self-Assembly of Viologen-Containing Dendrimers. *Angew. Chem., Int. Ed.* **2004**, *43*, 5496 –5499.
203. Schimdt, R.; Stolte, M.; Grune, M.; Wurthner, F. Hydrogen-Bond-Directed Formation of Supramolecular Polymers Incorporating Head-to-Tail Oriented Dipolar Merocyanine Dyes. *Macromolecules* **2011**, *44*, 3766-3776.
204. Liu, Y.; Wang, Z.; Zhang, X. Characterization of Supramolecular Polymers. *Chem. Soc. Rev.* **2012**, *41*, 5922−5932.
205. Haino, T.; Watanabe, A.; Hirao, T.; Ikeda, T. Supramolecular Polymerization Triggered by Molecular Recognition between Bisporphyrin and Trinitrofluorenone. *Angew. Chem., Int. Ed.* **2012**, *51*, 1473-1476.
206. Buck, A. T.; Paletta, J. T.; Khindurangala, S. A.;Beck, C. L.; Winter, A. H. A Noncovalently Reversible Paramagnetic Switch in Water. *J. Am. Chem. Soc.* **2013**, *135*, 10594−10597.
207. Juetten, M. J.; Buck, A. T.; Winter, A. H. A Radical Spin on Viologen Polymers: Organic Spin Crossover Materials in Water, *Chem. Commun.* **2015**, *51*, 5516-5519.
208. Yamauchi, M.; Ohba, T.; Karatsu, T.; Yagai, S. Photoreactive Helical Nanoaggregates Exhibiting Morphology Transition on Thermal Reconstruction. *Nat. Commun.* **2015**, *6*, No. 8936.

209. Merg, A. D.; Boatz, J. C.; Mandal, A.; Zhao, G.; Mokashi-Punekar, S.; Liu, C.; Wang, X.; Zhang, P.; van der Wel, P. C. A.; Rosi, N. L. Peptide-Directed Assembly of Single-Helical Gold Nanoparticle Superstructures Exhibiting Intense Chiroptical Activity. *J. Am. Chem. Soc.* **2016**, *138*, 13655-13663.
210. Lee, C. L.; Grenier, C.; Meijer, E. W.; Schenning, A. P. H. Preparation and Characterization of Helical Self-Assembled Nanofibers. *J. Chem. Soc. Rev.* **2009**, *38*, 671-683.
211. Yang, M.; Kotov, N. A. Nanoscale Helices from Inorganic Materials. *J. Mater. Chem.* **2011**, *21*, 6775-6792.
212. Araoka, F.; Sugiyama, G.; Ishikawa, K.; Takezoe, H. Highly Ordered Helical Nanofilament Assembly Aligned by a Nematic Director Field. *Adv. Funct. Mater.* **2013**, *23*, 2701-2707.
213. Zhang, L.; Wang, T.; Shen, Z.; Liu, M. Chiral Nanoarchitectonics: Towards the Design, Self-Assembly, and Function of Nanoscale Chiral Twists and Helices. *Adv. Mater.* **2016**, *28*, 1044-1059.
214. Kulkarni, C.; Bejagam, K. K.; Senanayak, S. P.; Narayan, K. S.; Balasubramanian, S.; George, S. J. Dipole-Moment-Driven Cooperative Supramolecular Polymerization. *J. Am. Chem. Soc.* **2015**, *137*, 3924-3932.
215. Cui, J.; Liu, A.; Guan, Y.; Zhang, J.; Shen, Z.; Wan, X. Tuning the Helicity of Self-Assembled Structure of a Sugar-Based Organogelator by the Proper Choice of Cooling Rate. *Langmuir* **2010**, *26*, 3615-3622.
216. Brizard, A.; Aimé, C.; Labrot, T.; Huc, I.; Berthier, D.; Artzner, F.; Desbat, B.; Oda, R. Counterion, Temperature, and Time Modulation of Nanometric Chiral Ribbons from Gemini-Tartrate Amphiphiles. *J. Am. Chem. Soc.* **2007**, *129*, 3754-3762.
217. Hu, J.; Kuang, W.; Deng, K.; Zou, W.; Huang, Y.; Wei, Z.; Faul, C. F. J. Self-Assembled Sugar-Substituted Perylene Diimide Nanostructures with Homochirality and High Gas Sensitivity. *Adv. Funct. Mater.* **2012**, *22*, 4149-4158.
218. Pashuck, E. T.; Stupp, S. I. Direct Observation of Morphological Tranformation from Twisted Ribbons into Helical Ribbons. *J. Am. Chem. Soc.* **2010**, *132*, 8819-8821.
219. Singh, N.; Kumar, M.; Miravet, J. F.; Ulijn, R. V.; Escuder, B. Peptide-Based Molecular Hydrogels as Supramolecular Protein Mimics. *Chem.-Eur. J.* **2017**, *23*, 981-993.
220. Banwell, E. F.; Abelardo, E. S.; Adams, D. J.; Birchall, M. A.; Corrigan, A.; Donald, A. M.; Kirkland, M.; Serpell, L. C.; Butler, M. F.; Woolfson, D. N. Rational Design and Application of Responsive α–helical Peptide Hydrogels. *Nat. Mater.* **2009**, *8*, 596-600.
221. Adler-Abramovich, L.; Gazit, E. The Physical Properties of Supramolecular Peptide Assemblies: From Building Block Association to Technological applications. *Chem. Soc. Rev.* **2014**, *43*, 6881-6893.
222. Scanlon, S.; Aggeli, A. Self-Assembling Peptide Nanotubes. *Nanotoday* **2008**, *3*, 22-30.
223. Guo, C.; Arnon, Z. A.; Qi, R.; Zhang, Q.; Adler-Abramovich, L.; Ehud Gazit, Wei, G. Expanding the Nanoarchitectural Diversity Through Aromatic Di- and Tri-Peptide Coassembly: Nanostructures and Molecular Mechanisms. *ACS Nano* **2016**, *10*, 8316-8324.
224. Engelkamp, H.; Middlebeek, S.; Nolte, R. J. M. Self-Assembly of Disk-Shaped Molecules to Coiled-Coil Aggregates with Tunable Helicity. *Science* **1999**, *284*, 785-788.
225. Li, W.; Aida, T. Dendrimer Porphyrins and Phthalocyanines. *Chem. Rev.* **2009**, *109*, 6047-6076.
226. Adachi, M.; Murata, Y.; Nakamura, S. Spectral Similarity and Difference of Naphthalenetetracarboxylic Dianhydride, Perylenetetracarboxylic Dianhydride, and Their Derivatives. *J. Phys. Chem.* **1995**, *99*, 14240-14246.
227. Huang, Y.; Yan, Y.; Smarsly, B. M.; Wei, Z.; Faul, C. F. J. Helical Supramolecular Aggregates, Mesoscopic Organisation and Nanofibers of a Perylenebisimide–Chiral Surfactant Complex *via* Ionic Self-Assembly. *J. Mater. Chem.* **2009**,*19*,2356 – 2362.
228. Würthner, F.; Kaiser, T. E.; Saha-Möller, C. R. J-aggregates: From Serendipitous Discovery to Supramolecular Engineering of Functional Dye Materials. *Angew. Chem., Int. Ed.* **2011**, *50*, 3376-3410.
229. Würthner, F.; Chen, Z.; Hoeben, F. J. M.; Osswald, P.; You, C. C.; Jonkheijm, P.; Herrikhuyzen, J. V.; Schenning, A. P. H. J.; van derSchoot,P. P. A. M.; Meijer, E. W.; Beckers, E. H. A.; Meskers, S. C. J.; Janssen, R. A. J. Supramolecular p–n-Heterojunctions by Co-Self-Organization of Oligo(p-phenylene Vinylene) and Perylene Bisimide Dyes. *J. Am. Chem. Soc.* **2004**, *126*, 10611-10618.
230. Würthner, F.; Thalacker, C.; Diele, S.; Tschierske, C. Fluorescent J-type Aggregates and Thermotropic Columnar Mesophases of Perylene Bisimide Dyes. *Chem.–Eur. J.* **2001**, *7*, 2245-2253.
231. Manchineella, S.; Prathyusha, V.; Priyakumar, U. D.; Govindaraju, T. Solvent-Induced Helical Assembly and Reversible Chiroptical Switching of Chiral Cyclic-Dipeptide Functionalized Naphthalenediimides. *Chem.–Eur. J.* **2013**, *19*, 16615-16624.
232. Sakajiri, K.; Hirama, T.; Yasuda, K.; Kutsumizu, S.; Watanabe, J. Supramolecular Helical Columnar Structures Formed by Hydrogen-Bonded Disk-Like (Phenylethynul)benzene Derivatives with L-Alanine Pendant Groups: Helix Stability and Supramolecular Helical Sense Inversion. *Bull. Chem. Soc. Jpn.* **2013**, *86*, 940-946.
233. Pan, L.; Lu, S.; Xiao, X.; He, Z.; Zeng, C.; Gao, J.; Yu, J. Enhanced Mechanical and Thermal Properties of Epoxy with Hyperbranched Polyester Grafted Perylenediimide. *RSC Adv.* **2015**, *5*, 3177-3186.
234. Green, M. M.; Reidy, M. P. Macromolecular Stereochemistry: The Out-Of-Proportion Influence of Optically Active Comonomers on the Conformational Characteristics of Polyisocyanates. The Sergeants and Soldiers Experiment. *J. Am. Chem. Soc.* **1989**, *111*, 6452-6454.
235. Delley, B. From Molecules to Solids with the DMol3DMol3 Approach. *J. Chem. Phys.* **2000**, *113*, 7756-7764.

236. Delly, B. An All-Electron Numerical Method for Solving the Local Density Functional for Polyatomic Molecules. *J. Chem. Phys.* **1990**, *92*, 508-517.
237. Foresman, J. B.; Frisch, A.; Exploring Chemistry with Electronic Structure Methods, 2nd ed., Gaussian Inc., Pittsburg, PA, 1996.
238. Dewar, M. J. S.; Zoebisch, E. G.; Healy, E. F.; Stewart, J. J. P. Development and Use of Quantum Mechanical Molecular Models. 76. AM1: a new General Purpose Quantum Mechanical Molecular Model. *J. Am. Chem. Soc.* **1985**, *107*, 3902-3909.
239. Kim, K.; Jordan, K. D. Comparison of Density Functional and MP2 Calculations on the Water Monomer and Dimer. *J. Phys. Chem.* **1994**, *98*, 10089-10094.
240. Becke, A. D. Density-Functional Exchange-Energy Approximation with Correct Asymptotic Behavior. *Phys. Rev. A* **1988**, *38*, 3098-3100.
241. Becke, A. D. Density-Functional Thermochemistry. III. The role of exact Exchange. *J. Chem. Phys.* **1993**, *98*, 5648-5652.
242. Porezag, D.; Frauenheim, T.; Köhler, T.; Seifert, G.; Kaschner, R. Construction of Tight-Binding-Like Potentials on the Basis of Density-Functional Theory: Application to Carbon. *Phys. Rev. B* **1995**, 51, 12947-12951.
243. Seifert, G.; Porezag, D.; Frauenheim, T. Calculations of Molecules, Clusters, and Solids with a Simplified LCAO-DFT-LDA Scheme. *Int. J. Quantum Chemistry* **1996**, 58, 185-192.
244. Eder, D. *Carbon Nanotube–Inorganic Hybrids. Chem. Rev.* **2010**, *110*, 1348–1385.
245. Teo, B. K.; Sun, X. H. Silicon-Based Low-Dimensional Nanomaterials and Nanodevices. *Chem. Rev.* **2007**, *107*, 1454–1532.
246. Liu, Y.; Goebla, J.; Yin, Y. Templated Synthesis of Nanostructured Materials. *Chem. Soc. Rev.* **2013**, *42*, 2610–2653.
247. Shimizu, T.; Masuda, M.; Minamikawa, H. Supramolecular Nanotube Architectures Based on Amphiphilic Molecules. *Chem. Rev.* **2005**, *105*, 1401–1444.
248. Nan, A.; Bai, X. S.; Son, J.; Lee, S. B.; Ghandehari, H. Cellular Uptake and Cytotoxicity of Silica Nanotubes. *Nano Lett.* **2008**, *8*, 2150– 2154.
249. Mitchell, D. T.; Lee, S. B.; Trofin, L.; Li, N.; Nevanen, T. K.; Söderlund, H.; Martin, C. R. Smart Nanotubes for Bio-separations and Bio-catalysis. *J. Am. Chem. Soc.* **2002**, *124*, 11864–11865.
250. Ben-Ishai, M.; Patolsky, F. Wall-Selective Chemical Alteration of Silicon Nanotube Molecular Carriers. *J. Am. Chem. Soc.* **2011**, *133*, 1545–1552.
251. Chen, X.; Berger, A.; Ge, M.; Hopfe, S.; Dai, N.; Göosele, U.; Schlecht, S.; Steinhart, M. Silica Nanotubes by Templated Thermolysis of Silicon tetraacetate. *Chem. Mater.* **2011**, *23*, 3129–3131.
252. Martin, C. R. Nanomaterials: a Membrane-Based Synthetic Approach. *Science* **1994**, *266*, 1961–1966.
253. Li, D.; Qu, X.; Newton, S. M. C.; Klebba, P, E.; Mao, C. Morphology-Controlled Synthesis of Silica Nanotubes through pH- and Sequence-Responsive Morphological Change of Bacterial Flagellar Bio-templates. *J. Mater. Chem.* **2012**, *22*, 15702–15709.
254. Yildirim, A.; Acar, H.; Erkal, T. S.; Bayindir, M.; Guler, M. O. Template-Directed Synthesis of Silica Nanotubes for Explosive Detection. *ACS Appl. Mater. Interfaces* **2011**, *3*, 4159–4164.
255. Jiang, J.; Wang, T.; Liu, M. Creating Chirality in the Inner Walls of Silica Nanotubes through a Hydrogel Template: Chiral Transcription and Chiroptical Switch. *Chem. Commun.* **2010**, *46*, 7178–7180.
256. Lu, H.-T. Synthesis and Characterization of Amino-Functionalized Silica Nanoparticles. *Colloid Journal* **2013**, *75*, 311–318.
257. Hu, J.-L.; Luo, L-B.; Yang, X-Z.; Yao, R-S.; Zhang, H-B.; Qian, H-S. Silica-Based Hybrid Microspheres: Synthesis, Characterization and Wastewater Treatment. *RSC Adv.* **2013**, *3*, 25620-25626.
258. Nistor, C. L.; Ianchis, R.; Ghiurea, M.; Nicolae, C.-A.; Spataru, C. -I.; Culita, D. C.; Cusu, J. P.; Fruth, V.; Oancea, F.; Donescu, D. Aqueous Dispersions of Silica Stabilized with Oleic Acid Obtained by Green Chemistry. *Nanomaterials* **2016**, *6*, 9.
259. Avinash, M. B.; Govindaraju, T. Engineering Molecular Organization of Naphthalenediimides: Large Nanosheets with Metallic Conductivity and Attoliter Containers. *Adv. Funct. Mater.* **2011**, *21*, 3875-3882.
260. Eakins, G. L.; Pandey, R.; Wojciechowski, J. P.; Zheng, H. Y.; Webb, J. E. A.; Valéry, C.; Thordarson, P.; Plank, N. O. V.; Gerrard, J. A.; Hodgkiss, J. M. Functional Organic Semiconductors Assembled *via* Natural Aggregating Peptides. *Adv. Funct. Mater.* **2015**, *25*, 5640-5649.
261. Chabinyc, M. L.; Chen, X.; Holmlin, R. E.; Jacobs, H.; Skulason, H.; Frisbie, C. D.; Mujica, V.; Ratner, M. A.; Rampi, M. A.; Whitesides, G. M. Molecular Rectification in a Metal-Hnsulator-Metal Junction Based on Self-Assembled Monolayers. *J. Am. Chem. Soc.* **2002**, *124*, 11730-11736.
262. Mujica, V.; Ratner, M. A.; Nitzan, A. Molecular Rectification: Why is it so Rare? *Chem. Phys.* **2002**, *281*, 147–150.

List of Publications

1. **Sahnawaz Ahmed**, K. N. Amba Sankar, Bapan Pramanik, Nilotpal Singha, Kallol Mohanta, and Debapratim Das, *Solvent dependent aggregation of a peptide-perylenediimide conjugate and their differential semi-conducting behavior.* (Manuscript under review)
2. Bapan Pramanik, **Sahnawaz Ahmed**, Rupam Roy, Basab Kanti Das, Nilotpal Singha, and Debapratim Das, *A DNA-NDI hybrid to efficiently detect histone in parts per trillion (ppt) level.* (Manuscript under review)
3. Nilotpal Singha, Purnima Gupta, Bapan Pramanik, **Sahnawaz Ahmed**, Antara Dasgupta, Anindita Ukil, and Debapratim Das, *Hydrogelation of a naphthalene diimide appended peptide amphiphile and its application in cell-imaging and intracellular pH sensing.* (Manuscript under review)
4. Bapan Pramanik, **Sahnawaz Ahmed,** Nilotpal Singha, and Debapratim Das, *Self-assembly assisted tandem sensing of Pd^{2+} and CN^- by a perylenediimide-peptide conjugate.* (Manuscript under review)
5. **Sahnawaz Ahmed**, Bapan Pramanik, K. N. Amba Sankar, Abhinav Srivastava, Nilotpal Singha, Payel Dowari, Arpita Srivastava, Kallol Mohanta, Ananya Debnath, and Debapratim Das, *Solvent assisted tuning of helicity and morphology of a peptide-perylenediimide conjugate: Helical fibers to nano-rings and their differential* semi-conductivity. *Scientific Reports* **2017**, *7*, 9485
6. Bapan Pramanik, Julfikar Hassan Mondal, Nilotpal Singha, **Sahnawaz Ahmed**, Jyotirmayee Mohanty, and Debapratim Das, *A viologen–perylenediimide conjugate as an efficient base sensor with solvatochromic property. ChemPhysChem.* **2017**, *18*, 245 – 252.
7. **Sahnawaz Ahmed**, Nilotpal Singha, Bapan Pramanik, Julfikar Hassan Mondal and Debapratim Das, *Redox controlled reversible transformation of a supramolecular alternating copolymer to a radical cation containing homo-polymer. Polym. Chem.* **2016**, *7*, 4393–4401.
8. Julfikar Hassan Mondal, **Sahnawaz Ahmed**, Titli Ghosh, and Debapratim Das, *Reversible deformation–formation of a multistimuli responsive vesicle by a supramolecular peptide amphiphile. Soft Matter* **2015**, *11*, 4912-4920.
9. Julfikar Hassan Mondal, Titli Ghosh, **Sahnawaz Ahmed**, Debapratim Das, *Dual self-sorting by cucurbit[8]uril to transform a mixed micelle to vesicle. Langmuir* **2014**, *30,* 11528-11534.
10. Julfikar Hassan Mondal, **Sahnawaz Ahmed**, and Debapratim Das, *Physicochemical analysis of mixed micelles of a viologen surfactant: extended to water-in-oil (w/o) microemulsion, and cucurbit[8]uril assisted vesicle formation. Langmuir* **2014**, *30*, 8290-8299.

11. **Sahnawaz Ahmed**, Julfikar Hassan Mondal, Nibedita Behera, and Debapratim Das, *Self-assembly of a peptide-amphiphile forming helical nano-fibres and in-situ template synthesis of uniform mesoporous single wall silica nano-tubes. Langmuir* **2013**, *29*, 14274–14283.